ESA-SCI-DIR-RP-003
November 2023

EnVision

Understanding why Earth's closest neighbour is so different

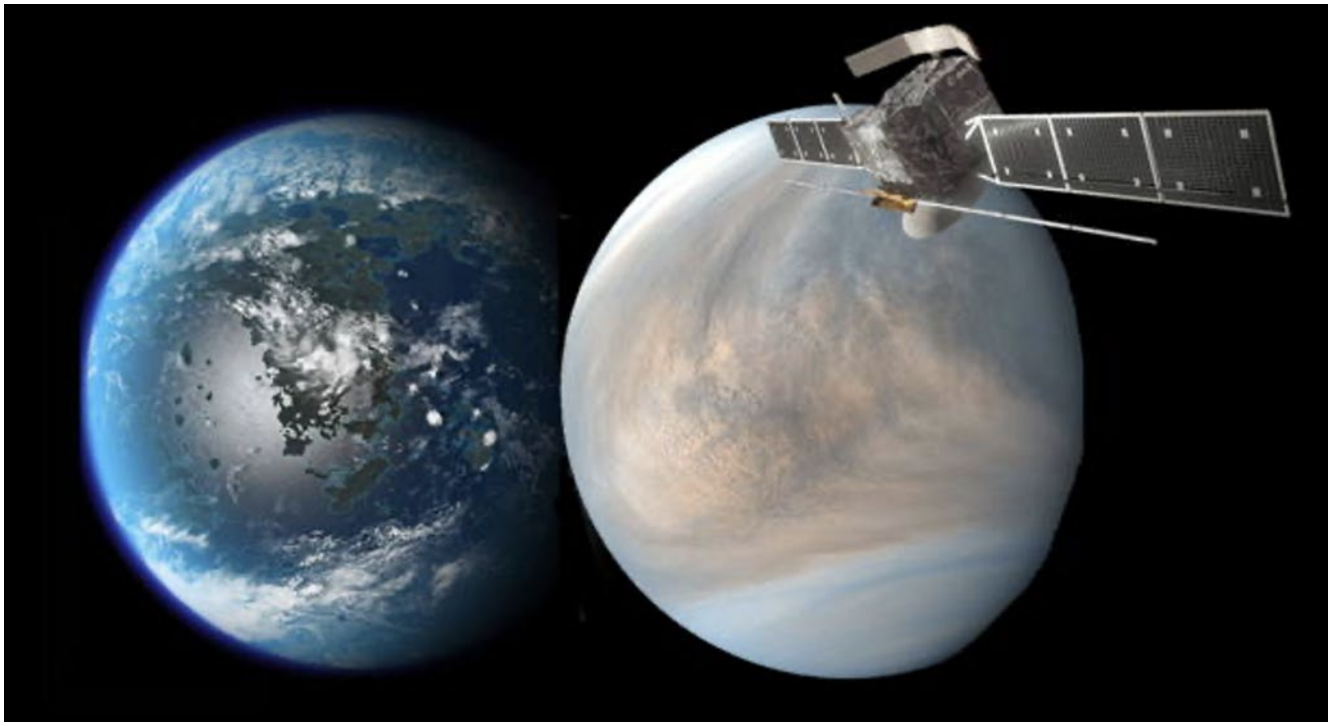

Definition Study Report

MISSION OVERVIEW

EnVision Mission Summary	
EnVision Science Themes (Section 2.1)	EnVision will address the following overall science themes, in no particular order of priority: • History - How have the surface and interior of Venus evolved? • Activity - How geologically active is Venus? • Climate - How are Venus' atmosphere and climate shaped by geological processes?
EnVision Science Objectives (Section 2.2)	EnVision's Science Objectives, in no particular order of priority are: • Understanding Venus' magmatic history; • Understanding Venus' tectonic history; • Assessing Venus' surface modification processes; • Understanding how Venus' interior and surface have evolved; • Understanding Venus' volcanic activity in the present era; • Assessing Venus' aeolian activity and mass wasting; • Understanding the role of geological activity in Venus' climate evolution; • Assessing temporal variations of the Venus atmosphere.
Strategy and Science Observation Requirements (Section 2.3)	EnVision's Science Observation strategy, in no particular order of priority are: • Establish the magmatic history of Venus: changes in style and volume with time, range of magma compositions; • Establish the tectonic history of Venus: magnitude of deformation, implications for lithospheric thickness and heat flow; • Characterize surface modification processes: impact crater modification, low emissivity/radar bright highlands; • Constrain the size of the major internal layers (crust/lithosphere, mantle, core), and the physical state of the core; • Constrain styles and occurrence of recent volcanism on Venus; • Characterize geomorphological changes by mass-wasting and aeolian processes; • Assess tropospheric trace gases spatial and temporal variability; • Measure variability of clouds and cloud droplets, and map the variability of the mesospheric composition.
Payload (Chapter 4)	• VenSAR, a reflectarray, dual polarization S-band Synthetic Aperture Radar, will map the surface using a range of modes including imaging at spatial resolutions of 10 m to 30 m, altimetry, dual polarimetry and radiometry; • A Subsurface Sounding Radar (SRS) will penetrate into the top hundreds of metres of the subsurface, and search for underground layering and buried boundaries; • Three spectrometers VenSpec-U, VenSpec-H and VenSpec-M, operating in the UV and Infrared, will map trace gasses, including volcanic gas plume searches, above and below the clouds, and map surface composition and emissivity; • A Radio Science Experiment (RSE) will use the satellite radio link to map the planet's gravity field, constraining internal structure, and to measure atmospheric properties through radio occultation.
Spacecraft (Section 5.2)	• EnVision will be a three-axis stabilized orbiter, ~2m x 2m x 3m in stowed configuration. • The launch dry mass is 1.7 t, and the max power, including system margins, is 2.8 kW; • EnVision will be in a low Venus quasi-polar orbit, with an inclination between 87° and 89°, and an altitude varying from 220 to 510 km. The orbital period is about 92 min; • • EnVision will downlink 189 Tbits of science data, using a Ka-/X-band comms system with a 2.5 m diameter fixed high-gain antenna.
Launch and Operations (Section 5.1 and Chapter 6)	• EnVision will launch with an Ariane 62 from Kourou in November 2031 (back-up launch window November 2032), into a Highly Elliptical Orbit around the Earth. It will arrive at Venus after about 18-months cruise. Following orbit insertion, orbit circularisation achieved by aerobraking over a period of about 16 months, followed by a nominal science phase of 4 Earth years; • The Mission Operations Centre (MOC) will be at ESOC (Darmstadt), the Science Operations Centre (SOC) at ESAC (Madrid), and the instrument operations will be supported by the Instrument Teams.
Data Policy and distribution (Chapters 6 and 9)	• EnVision data follow the PDS4 standard, with telemetry, raw, calibrated, and derived product levels; • EnVision raw and calibrated data products will become publicly available less than 6 months after they become available to the instrument teams; • The raw, calibrated and derived data products will be archived in the ESA Planetary Science Archive (PSA). Data will also be archived in NASA's Planetary Data System (PDS).

1. EnVision Definition Study Overview

1.1. Authorship and acknowledgments

This Definition Study Report has been prepared by:

EnVision Science Study Team (SST)		
Anne Grete Straume (EnVision Study Scientist and SST co-chair)	ESA	Noordwijk, The Netherlands
Mitch Schulte (EnVision Program Scientist and SST co-chair)	NASA	Washington, DC, USA
Lorenzo Bruzzone	Università di Trento	Trento, Italy
Paul Byrne	Washington University in St. Louis	St. Louis, MO, USA
Lynn Carter	LPL, University of Arizona	Tucson, AZ, USA
Caroline Dumoulin	LPG, Nantes Université	Nantes, France
Gabriella Gilli	Instituto de Astrofísica de Andalucía (IAA-CSIC)	Granada, Spain
Jörn Helbert	DLR Institute of Planetary Research	Berlin, Germany
Scott Hensley	Jet Propulsion Laboratory, Caltech	Pasadena, CA, USA
Kandis Lea Jessup	Southwest Research Institute	Boulder, CO, USA
Walter Kiefer (Report lead Editor)	Lunar and Planetary Institute	Houston, TX, USA
Emmanuel Marcq	LATMOS, IPSL, U. Versailles Saint-Quentin	Guyancourt, France
Philippa Mason	Earth Science and Engineering, Imperial College	London, UK
Alberto Moreira	DLR Microwaves and Radar Institute	Oberpfaffenhofen, Germany
Ann Carine Vandaele	Royal Belgian Institute for Space Aeronomy	Brussels, Belgium
Thomas Widemann (Report lead Editor)	LESIA, Observatoire de Paris	Meudon, France

ESA Study Team		
Thomas Voirin (Study Manager)	ESA	Noordwijk, The Netherlands
Robert Buchwald (System Manager 2021 and 2022)	ESA	Noordwijk, The Netherlands
Martin Haag (System Manager 2023)	ESA	Noordwijk, The Netherlands
Pierre-Élie Crouzet (Payload Study Manager)	ESA	Noordwijk, The Netherlands
Jayne Lefort (Science Operations Manager)	ESA	Villanueva de la Cañada, Spain
Arno Wielders (Deputy Study Manager)	ESA	Noordwijk, The Netherlands
Coordination Office of the ESA Science Programme		
Luigi Colangeli	ESA	Noordwijk, The Netherlands
NASA EnVision Program and Mission Management		
Ramon De Paula	NASA	Washington, DC, USA
Joshua M. Moore	NASA Marshall	Huntsville, AL, USA

The national EnVision mission payload and ESA and NASA team members are thanked for their invaluable contributions.

The EnVision mission payload teams would also like to thank their respective funding agencies in the ESA member states and NASA for their support during the Study Definition Phases.

We also acknowledge the contributions by the competing industrial prime contractor teams from:

- Airbus Defence and Space, UK, and their partners;
- Thales Alenia Space, Italy, and their partners.

1.2. Foreword / Document Scope

Venus has been an object of fascination for centuries, and throughout the space age. It was the site of the first planetary flyby in 1962 (Mariner-2), first entry probe in 1967 (Venera-4), first soft landing in Dec. 1970 (Venera-7), first image from the surface of another planet in 1975 (Venera-9), first orbiter and radar in 1978 (Pioneer). The Soviet series of Venera and VeGa missions were phenomenally successful, with their technologically advanced landers taking pictures of Venus' surface and analysing drill samples, despite the high temperature and pressure conditions. The VeGa missions also included successfully deployed balloons in the atmosphere in 1985. Global studies of the surface have been achieved using cloud-penetrating radars, firstly from Earth using large radio antennas like those at Goldstone, California, and then from spacecraft orbiting the planet, beginning with Pioneer Venus' operations in 1980. Far more detail was revealed by the synthetic aperture radars (SARs) on Venera-15 and 16 in 1983, followed by Magellan in 1989.

From 2006 to 2014, ESA's Venus Express, a landmark in Venus exploration, answered many questions about our nearest planetary neighbour and established European excellence in Venus research. Focussed on atmospheric research, some of the enigmatic results from Venus Express nonetheless concerned its surface: hints of current volcanic activity including a tenfold change in mesospheric sulphur dioxide, anomalously dark lava surrounding volcanoes, and surface temperature changes, all pointed towards a geologically active planet. Many significant questions remain on the current state of Venus, suggesting major gaps in our understanding of how and when Venus's evolutionary pathway diverged from Earth's. Furthermore, recent climate modelling has found that Venus might have been cool enough to maintain liquid water for up to billions of years.

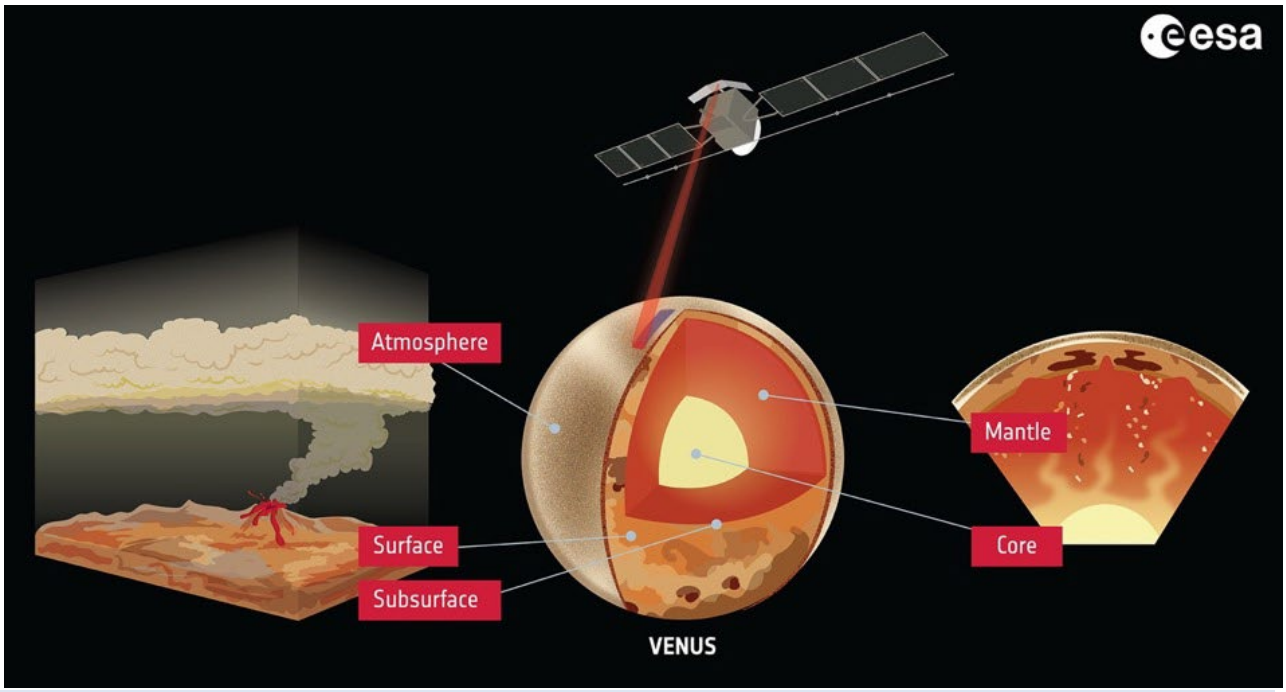

Figure 1.2.1 – *EnVision will be the first mission to investigate simultaneously Venus from its inner core to its upper atmosphere at an unprecedented scale of resolution, characterising the interaction between its different envelopes: its upper and lower atmosphere, surface/subsurface and interior (Credit: ESA).*

To pursue these intriguing observations and other lines of investigation, the EnVision orbiter was proposed and selected as ESA's 5th M-class mission in June 2021, with the concept of bringing Venus geology up to date with a 21st century Synthetic Aperture Radar (SAR) geophysics investigation, heavily informed by Earth observation heritage, in combination with atmospheric (with 3 spectrometers and radio occultations), subsurface (with a sounding radar) and interior (with radio science experiment) investigations built on heritage from across ESA's suite of planetary missions. EnVision is an ESA led mission in partnership with NASA, with NASA providing the Synthetic Aperture Radar (VenSAR), support to the aerobraking phase, and Deep Space Network support for critical mission phases.

During phase B1 (the mission definition phase), the achievability of the EnVision science objectives have been consolidated by the instrument teams through bottom-up (end-to-end) simulations using the updated and more detailed instrument and mission design. All science objectives identified in the phase A "Assessment Study Report" (ESA, 2021) were confirmed to be still achievable, although some acceptable risks still remain as listed in Section 8.5 of this report. Therefore, several parts of this "Definition Report" are identical to the phase A "Assessment Study Report", giving a full overview of the main mission science goals and how they are achieved. New sections describe results obtained during the phase B1 activities. This included amongst others a further consolidation of the mission, spacecraft and instrument technical design and operations, breadboarding, further development and refinements of (end-to-end) performance simulations, cost and schedule analysis. Dedicated workshop between each industrial prime and the instrument teams were organized, to harmonise the interfaces between the spacecraft (S/C) and the payload, and to consolidate the payload accommodation. Finally, the mission was subject to and successfully passed the phase B1 payload requirements and system reviews, and mission adoption review.

This Definition Study Report summarizes the output of the work done by the EnVision Science Study Team, the ESA EnVision Study teams, the instrument teams in the contributing ESA member states, at NASA and NASA JPL, and the compliance of the spacecraft industry consortia to the requirements. Furthermore, the successful EnVision workshop at DLR in Berlin, Germany on 9-11 May 2023 (https://atpi.eventsair.com/2023-envision-workshop/) contributed to a further consolidation of the EnVision science objectives by the worldwide scientific Venus community. At this workshop, also the complementarity and synergies with the further Venus missions by NASA in the coming decade were presented and discussed as reported in Sections 8.1-2.

1.3. Document structure

This EnVision Definition Study Report starts with an overview of the EnVision Science motivation and overarching science questions, and how they are addressed (Chapter 2). This is followed by a description of the science and operations requirements and their tracing to the mission science objectives (Chapter 3). In Chapter 4, the mission payloads are described, and their specifications are traced to the science product requirements. Chapters 5 and 6 present the mission and spacecraft design, and the mission and science operations. Chapter 7 describes how the science objectives will be met, as demonstrated by operations and performance simulations, and science use cases combining observations from multiple instruments. Chapter 8 describes EnVision bonus science that the EnVision Science Study Team foresees to be achievable through the synergetic use of EnVision data with data from upcoming Venus missions. Finally, Chapters 9 and 10 describe the EnVision management and communication planning. The report acronyms, glossary, and references are contained in Chapter 11.

1.4. Table of contents

1.5. Executive Summary

Venus exploration offers unique opportunities to answer fundamental questions about the evolution of terrestrial planets and the habitability within our own solar system. Many significant questions remain on the current state of Venus, suggesting major gaps in our understanding of how Venus's evolutionary pathway diverged from Earth's. Comparing the interior, surface and atmosphere evolution of Earth and Venus is essential to understanding what processes have shaped our planet, and is particularly relevant in an era where we expect thousands of terrestrial exoplanets to be discovered.

EnVision is a Venus orbiter mission that will determine the nature and current state of Venus' geological evolution and its relationship with the atmosphere, to understand how and why Venus and Earth evolved so differently. Perched at the inner edge of the habitable zone, Venus may once have had abundant liquid water and been able to sustain life, before developing a runaway greenhouse warming which rendered it uninhabitable today; thus providing a natural laboratory for understanding planetary conditions for life. Venus is Earth's closest sibling geologically, similar in size to the Earth, it has remained active into the present era, unlike the much smaller Mars and Mercury. Venus today does not have a mechanism to sequester atmospheric CO_2 in carbonate rocks and does not exhibit Earth-like plate tectonics, although both processes may have occurred in the past. With few sinks for volcanically emitted volatiles, Venus is left with its present massive atmosphere and a thick cloud deck covering the entire planet; but again, its past and current state is very poorly constrained. Thus, Venus is essential for understanding the links between planetary geophysical evolution and habitability of terrestrial planets from our own Earth to terrestrial planets and exoplanets everywhere, including those which will be the subject of study by other missions in ESA's Space Science programme. EnVision therefore appeals to – and benefits from – a wide community ranging from geologists, geophysicists and atmospheric scientists working on planetary research and Earth Observation, to astronomers seeking to understand terrestrial exoplanets.

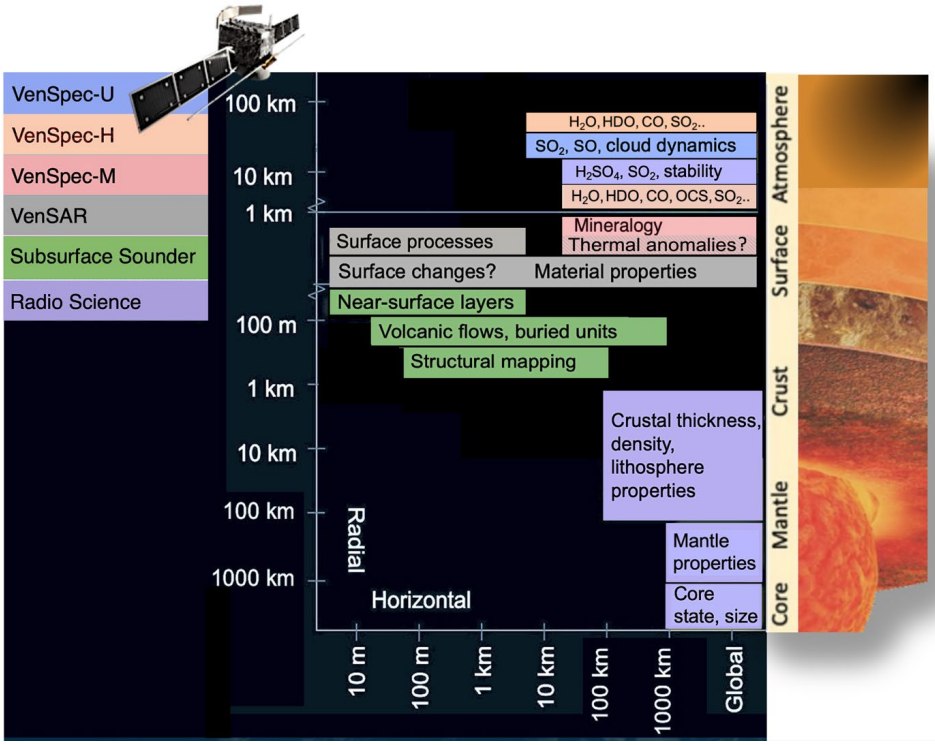

Figure 1.5.2 – *EnVision's multi-messenger strategy combines observations at wavelengths from UV to radio- frequency waves to study geological and atmospheric processes at a range of scales, from the core to the highly variable upper atmosphere.*

Scientific Strategy. – EnVision will deliver new insights into geological history through complementary imagery, polarimetry, radiometry and spectroscopy of the surface coupled with subsurface sounding and gravity mapping; it will search for thermal, morphological, and gaseous signs of volcanic and other geological activity; and it will trace the fate of key volatile species from their sources and sinks at the surface through the clouds up to the mesosphere. Following the same approach through which our understanding of Earth and Mars has been developed, EnVision will combine global observations at low or moderate spatial resolution (e.g. surface emissivity and atmosphere composition) with regionally targeted observations at

higher spatial resolutions from a modern synthetic aperture radar (SAR) and subsurface sounding radar profiles.

Payload. – EnVision's science payload consists of VenSAR, a dual polarization S-band radar also operating as altimeter and microwave radiometer, three spectrometers VenSpec-M, VenSpec-U and VenSpec-H designed to observe the surface and atmosphere of Venus, and the Subsurface Radar Sounder (SRS), a High Frequency (HF) sounding radar to probe the subsurface. These are complemented by the Radio Science Experiment (RSE) which achieves gravity mapping and radio occultation of the atmosphere, for a comprehensive investigation of the Venusian surface, interior and atmosphere and their interactions. This suite of investigations works together to comprehensively assess surface and subsurface geological processes, interior geophysics and geodynamics, and atmospheric pathways of key volcanogenic gases, which together illuminate how and why Venus turned out so differently to Earth. The synergistic and holistic way in which the payload instruments collaborate to investigate processes at different altitudes, depths and spatial scales is graphically illustrated in Figure 1.5.2 and in Chapter 4, Figure 4.1.1.

A **Synthetic Aperture Radar, VenSAR**, will image pre-selected regions of interest at a resolution of 30 m/pixel, and subregions at 10 m/pixel. An order of magnitude better than Magellan and with a better sensitivity, these images are the key to understanding geological processes from the local to global scale, discriminating relationships between units of different age, and identifying the changes caused by geological activity. Topographic information at 300 m spatial and 20 m vertical resolution across these regions, derived from stereo imaging at two different incidence angles, is complemented by a global network of altimetry mode tracks with a vertical resolution of 2.5 m, providing a far better than any previous dataset, essential for resolving the geometry of faults, folds and other features, and enabling the quantitative analysis of geological processes. Surface properties such as roughness will be derived from active imaging in both Horizontal transmit and Horizontal receive (HH) and Horizontal transmit and Vertical receive (HV) linear polarizations (i.e. dual polarized radar system) – a first for a Venus orbiter - and passive radiometry at a range of angles, which also permits the detection of surface temperature anomalies. Repeated observations and comparisons with Magellan imagery allow for the detection of volcanic, tectonic and geomorphic changes over periods of months, years and decades.

A **Subsurface Sounder, SRS**, will characterise the vertical structure and stratigraphy of geological units including volcanic flows. EnVision is the first mission to Venus with a sounding instrument that will perform the direct measurement of subsurface features. Geological inferences from Magellan data point to a range of subsurface structures and geometries that are as yet unquantified. The SRS provides a unique opportunity to sound the great variety in geologic and geomorphic units. It will also provide unprecedented information on the surface in terms of roughness, composition and permittivity (dielectric) properties at wavelengths completely different from those of VenSAR, thus allowing a better understanding of the surface properties. SRS observation will also result in altimetry measurements by providing low-resolution profiles of the topography that can be integrated with the altimetric data of VenSAR.

A **Spectrometer suite, VenSpec**, will obtain global maps of surface emissivity in six wavelength bands using five near-infrared spectral transparency windows in the nightside atmosphere, to constrain surface mineralogy and inform evolutionary scenarios; and measure tropospheric and mesospheric trace gases to link these variations to tropospheric and mesospheric variations and volcanism. **VenSpec-M** is a pushbroom multispectral imager optimised to map thermal emission from Venus' surface using six narrow bands ranging from 0.86 to 1.18 μm, and three bands at 1.195, 1.31, and 1.51 μm to study cloud microphysics and dynamics. This allows mapping of surface composition, by characterising emissivity variations, as well as searching for thermal anomalies associated with volcanic activity. **VenSpec-H** is a high-resolution near-Infrared atmospheric spectrometer. The main objective is to quantify SO_2, H_2O and HDO in the atmosphere, below and above the clouds, characterising gas exchanges from the surface and within the atmosphere, searching for sources such as volcanic plumes. **VenSpec-U**, an ultraviolet spectrometer, will monitor minor sulphur species (mainly SO and SO_2) and investigate the complex and highly variable upper atmosphere and its relationship with the lower atmosphere. In combination, VenSpec will provide unprecedented insights into the current state of Venus and its past evolution. VenSpec will perform a comprehensive search for volcanic activity by targeting atmospheric signatures, thermal signatures and compositional signatures, as well as a global map of surface composition.

A **Radio Science Experiment, RSE,** uses the spacecraft-Earth radio link for gravity mapping and atmospheric profiling. Magellan gravity data are consistent with an organised pattern of mantle convection broadly similar to Earth but lack the resolution necessary to understand its connection with geological-scale features, such as individual coronae or mountain belts. Higher spatial resolution is needed to better constrain the crustal and lithospheric structure variations; EnVision will obtain an unprecedented gravity observation resolution, globally, allowing better constraints on the geodynamic evolution of the planet. EnVision's gravity measurements will also allow calculation of the tidal Love number k_2 with an accuracy better than 0.01. This increased precision will constrain the distribution of internal mass, and the size and state of the core. Furthermore, the refraction and absorption of EnVision's radio signal in the Venus neutral atmosphere will be used in combination with a Master Reference Oscillator (MRO) to obtain high-resolution vertical profiles of temperature, pressure, and sulphuric acid (vapour and liquid) profiles in the neutral atmosphere.

Mission and Spacecraft Design. – EnVision will be launched on an Ariane 62 in November 2031 (with backup date in November 2032) in a Highly Elliptical Orbit (HEO) around the Earth. An interplanetary cruise of 18 months is followed by orbit insertion and then circularisation by aerobraking over a period of about 15 months to achieve the nominal science orbit, a low quasi-polar Venus orbit with an inclination between 87° and 89°, altitudes varying from 220 to 510 km, and an orbital period of about 92 min. The nominal science phase of the mission will last six Venus sidereal days (four Earth years). The choice of science orbit around Venus is mainly driven by the need for global VenSpec, SRS, and VenSAR altimeter and radiometer coverage, stereo topography, polarimetric and repeated VenSAR imaging, and for high-resolution gravity mapping. The spacecraft is approximately rectangular, 3 m in height x 2 m in depth and width in stowed configuration, with chemical propulsion and powered by two deployable solar arrays. EnVision will downlink 189 Tbits of science data (Table 5.1.3), using a Ka-/X-band comms system with a 2.5 m diameter fixed high-gain antenna.

Project, Operations and Science Management. – EnVision is an ESA led mission in partnership with NASA and contributions from individual ESA member states for the provision of payload elements. NASA is contributing the VenSAR instrument and supplies aerobraking support and Deep Space Network (DSN) support during critical mission phases. The other payload instruments are contributed by the ESA member state national agencies ASI, DLR, BelSPO, and CNES, leading the procurement of SRS, VenSpec-M, VenSpec-H, the Ultra Stable Oscillator (USO) and VenSpec-U instruments, respectively. Further mission contributions are provided by the Czech Republic, Portugal, the Netherlands, Spain and Switzerland. The Belgian, Czech Republic, Portugal and Swiss contributions are provided through the ESA PRODEX program. ESA has responsibility for the overall management, the launch segment, spacecraft procurement, some hardware developments, and the mission and science operations.

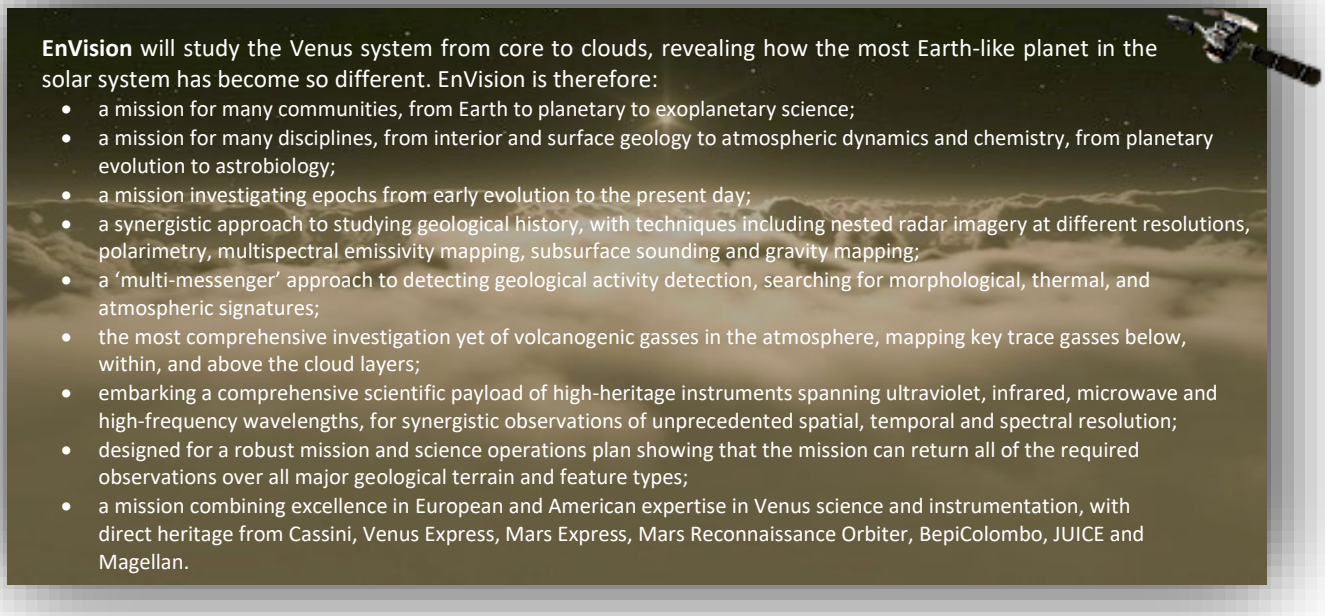

2. Science Themes and Objectives

2.1. EnVision Science themes

2.1.1. ESA's Cosmic Vision objectives addressed by EnVision

The EnVision mission is addressing the following high-level ESA Cosmic Vision objectives (ESA BR-247, 2005):
- What are the conditions for planetary formation and the emergence of life?
- How does the Solar System work?

More specifically, the following questions are formulated and will be addressed by EnVision as follows:

Why are the terrestrial planets so different? – Venus is in many ways the most Earth-like of all our planetary neighbours: its size, bulk composition and distance from the Sun are very similar to those of Earth. Its original atmosphere may have been similar to that of early Earth, with abundant water that might have been liquid at the surface under the young Sun's fainter output, (Hamano et al., 2013; Way et al., 2016; Salvador et al., 2017; Way and Del Genio, 2020). However, there is considerable debate on this topic, and some studies (Turbet et al., 2021; Marchi et al., 2023) suggest that the current nighttime only presence of water vapour in the atmosphere suggests that water never condensed on Venus (Turbet et al., 2021). Even today, with its global cloud cover, the surface of Venus receives less solar energy than Earth, so why did a moderate climate ensue here, whereas a catastrophic runaway greenhouse warming may have occurred on Venus? Which lessons can be learned about the life story of terrestrial planets in general, in this era of discovery of Earth-like exoplanets? Were the radically different evolutionary paths of Earth and Venus driven solely by distance from the Sun, or do internal dynamics, geological activity, volcanic outgassing and weathering also played an important part?

These questions are tied to our general understanding of the universe and lie at the heart of ESA's Cosmic Vision program objectives listed above. Surprisingly little is known about our nearest planetary neighbour, not even the basic sequence and timing of events that formed its dominant surface features. The Magellan mission revealed an enigma: an apparently relatively young surface (~500 Ma), rich in geological activity, yet with an apparently random crater distribution (Phillips et al., 1992; Strom et al., 1994). How can a geologically active surface be reconciled with the global stasis inferred from the apparently random impact crater distribution?

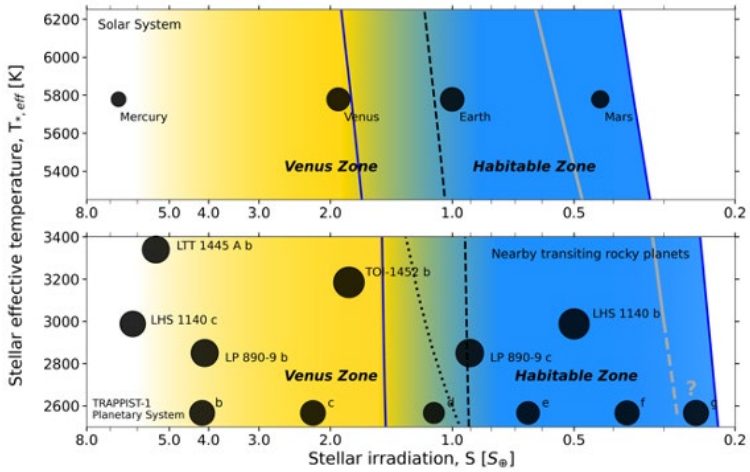

Figure 2.1.1 – *Perched on the inner edge of the habitable zone, ancient Venus might have hosted liquid water for up to billions of years under a faint young sun (Way et al, 2016, Way and Del Genio, 2020). In this figure the Venus zone (Kane et al. 2014) and HZ are clearly indicated, and a number of detected potential Venus Analogues selected as function of stellar irradiation and stellar effective temperature. Revealing the history of its evolution informs not only our understanding of the inner solar system but also of terrestrial exoplanets (Adapted from Fig. 1 in Quirino et al. 2023).*

The EnVision mission's investigations of Venus and the evolution of its geology and climate are highly complementary to other Space Science missions. This is particularly true for PLATO, which focuses on terrestrial planets in the habitable zone around sunlike stars, and ARIEL, which will conduct spectroscopic analyses of exoplanetary atmospheres. Although ideal ARIEL targets are hot and warm giant planets close to their host star, a long-term scientific objective is to characterize the whole range of exoplanets, including potentially habitable ones. One example is the proposed LIFE mission, aiming at observing Earth-like exoplanets (Quanz et al, 2022). In fact, most terrestrial planets discovered within the coming decades are likely to be more Venus-like than Earth-like, given the detection bias towards short orbital periods of transit and radial velocity techniques, so EnVision's focus on understanding the inner edge of the habitable zone is particularly relevant.

Diverging evolutionary paths of Earth-like planets. – The discoveries of many exoplanets, including terrestrial exoplanets, due to increasingly sensitive methods of discovery and characterisation, make exchange between exoplanetary and planetary scientific communities increasingly necessary. The search for exoplanets is largely motivated by the need for answers to the questions: Is our solar system common and is there life beyond it? Answering these questions requires also understanding the habitability of a planet, i.e., the potential of a planet to develop and maintain a living environment. Venus and Earth formed under very similar conditions and may have been supplied with water in the same way, e.g. through inwards scattering of solar outer disk water-rich planetesimal material in the early stage of the solar system formation. The relative amount of incorporated water within Earth and Venus sensitively depends on the delivery mechanism, as well as their relative growth rates and the behaviour of the underlying gaseous disk (Salvador et al., 2023, and references therein). At some point in their history, the evolution of their surfaces and atmospheres diverged dramatically. Earth has been continuously habitable since the end of the Hadean period (-4.6 to -4 Ga), while Venus' surface became uninhabitable at some unknown point in its history (Lammer et al., 2018). Although at the inner edge of the 'habitable zone' (Figure 2.1.1), Venus could be the type of planet that has changed from a habitable and Earth-like state during the early history of the solar system when the sun was less bright, to an uninhabitable one (Way and Del Genio, 2020), thus providing a natural laboratory for studying the evolution of habitability (Kane et al, 2019).

To this end, many fundamental questions about Venus' evolution need to be answered. How did its surface and atmosphere evolved over time? If the planet transitioned from a magma ocean phase to a runaway greenhouse, how did that happen? If there ever was a water-rich surface environment, including the liquid phase, how long was it present and when and why did the surface water disappear (Figure 2.1.2)? How does Venus lose its heat, how volcanically and tectonically active has Venus been over the last billion years? Does Venus really have a 'stagnant lid', has its resurfacing been more episodic, or was a plate tectonics regime present earlier in its history (O'Neill et al., 2007)? Or is the solution more complex, such as the 'plutonic-squishy lid' regime (Lourenco et al., 2020), which would explain its likely thin crust and high heat flow? What is the composition of the highland tessera terrain? Are these regions made from the oldest rocks exposed on the Venus surface? How oxidized are those rocks, and do these surfaces retain evidence of an earlier time when water was more prevalent (Khawja et al., 2020)?

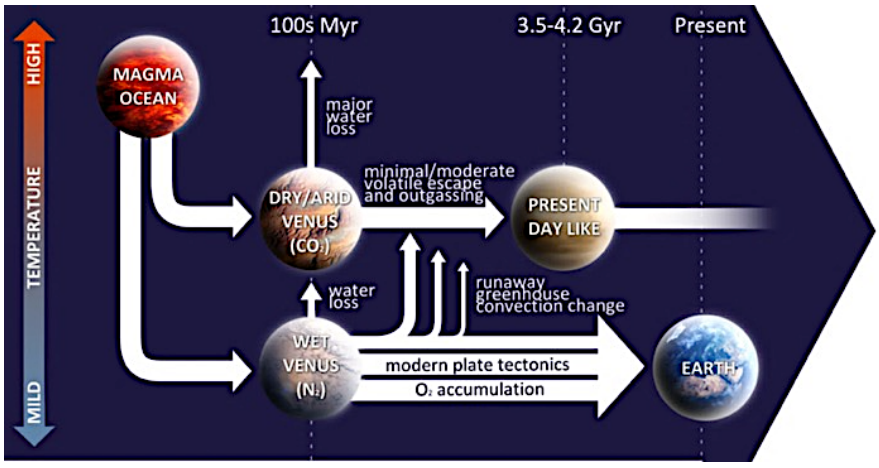

Figure 2.1.2 – *Venus shares some striking similarities with Earth; at the same time, it exhibits characteristics that are widely different from that of our own planet. It is an example of an active planet that may have followed a radically different evolutionary pathway despite the similar mechanisms at work and probably comparable initial conditions. Understanding Venus' evolution might be a key to our comprehension of how a planet can become or cease to be habitable. The evolution of Venus is still poorly constrained, partly due to a lack of relevant measurements. Even existing data can prove inconclusive due to their dependence on many interconnected mechanisms. (Kasting 1988; Way et al., 2016; Way and Del Genio, 2020, Gillmann et al., 2022). As a result, there is currently no consensus on the history of Earth's sister's surface conditions, with some scenarios involving dry evolutionary pathways, while others suggest a wet past (Gillmann et al., 2009; Massol et al., 2016; Salvador et al., 2017, 2023, Way et al., 2023). Figure after Gillmann et al., 2022.*

2.1.2. Overview of EnVision's top level science questions

History – How have the surface and interior of Venus evolved?

EnVision will **characterize** the sequence of events that generated the regional and global surface features of Venus, determine crustal support mechanisms, mantle and core properties, and characterize the geodynamics framework

that controls the release of internal heat over Venus's history. It will: (1) determine the styles of volcanic processes which have occurred on Venus, studying the sources, emplacement styles, magma properties and relative ages of different volcanic flows; (2) determine the styles of tectonic deformation that have operated on Venus by studying their surface structure and gravity signatures, and determining their role in planetary heat loss; (3) characterize surface modification processes (impact crater modification, altitude dependent surface physical properties and signatures such as brightness and emissivity) to improve our understanding of Venus geochronology; (4) constrain Venus' internal structure, through measurements of the gravity field and tidal response, to constrain the properties and thicknesses of Venus' crust, mantle and core.

To reconstruct the history of Venus, we must examine its geological record. The cratering record shows that most of Venus' surface is relatively young (less than 1 billion years old) but some regions (in particular the tessera highlands) may be considerably older (Byrne et al., 2021). Observations from Magellan data imply a variety of age relationships and long-term activity, with at least some activity in the recent past. There is a non-random distribution of topography (the highs particularly are semi-linear features) and an association between geological features and elevation (Stoddard and Jurdy, 2012), such that the uplands are consistently more deformed than the lowlands. The distribution of impact craters is not strictly random either, with recent observations about the degree of crater alteration permitting a wider range of possible recent geological activity (e.g., Herrick and Rumpf, 2011; O'Rourke et al., 2014). How are impact craters modified? Do dark floors form from airfall deposits or magmatism from below?

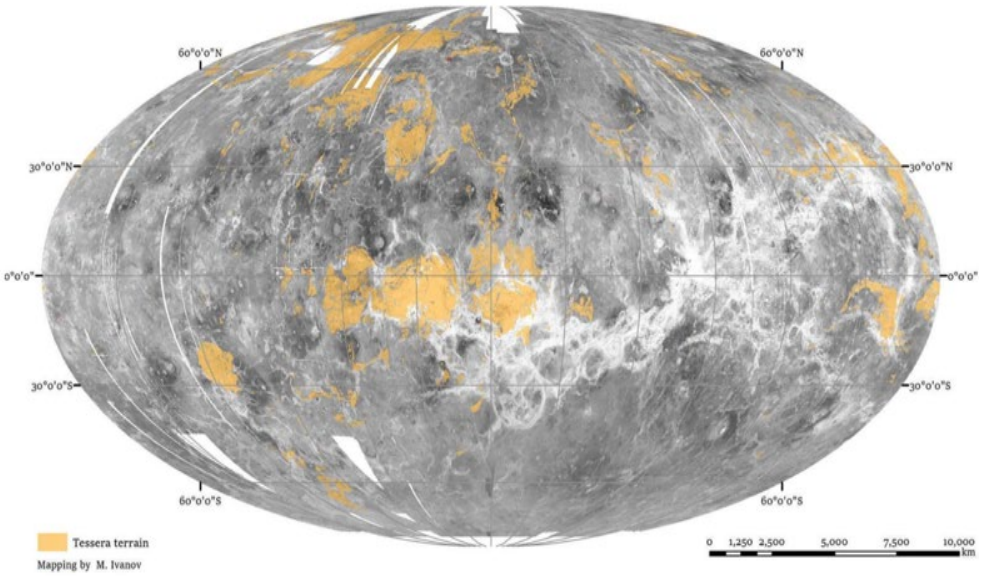

Figure 2.1.3 – *In contrast to the basaltic plains, tessera terrain (in yellow) is heavily modified by tectonic deformation. The primary morphologic characteristics of its precursor materials are not readily seen. Tesserae often occur in large high- standing regions that appear older (embayed) than surrounding plains. In these characteristics, tesserae to some degree resemble terrestrial continents (old, high-standing, tectonized massifs), the bulk of which are made of non-basaltic materials. If a non- basaltic component of the crust indeed exists on Venus, tesserae appear to be one of the best candidates. The image is derived from NASA Magellan data and Tessera classification by M. Ivanov.*

Constraining the history is critical to understanding when and how Venus was resurfaced, but it is also important to know the nature of that activity. Has there been a systematic change in volcanic style, for example, are canali confined to a past regime or still active today? Were the plains formed from a few massive outpourings in a short period of time or from many thousands of small flows over their entire history? Or were they formed, or modified, in an entirely different way? Perhaps Venus exhibits even more tectonic deformation than Earth? What is the role of tectonism in resurfacing the planet? Has the history of tectonic deformation changed over time? How did tesserae, in particular (Figure 2.1.3), accumulate their extraordinary degree of deformation?

Although chemically similar to basalts, the layering observed in the rocky blocks visible in Venera landers images is more akin to sedimentary or pyroclastic bedding, formed by cycles of air fall or ground flow. Based on load carrying capacities derived from the penetrometer and dynamic loads during lander impact, the strength of the surface materials at the Venera 13 site is similar to that of a dense sand or weak rock. At the Venera 14 and Vega 2 sites the recorded strengths are higher but similar to that of a sedimentary sandstone and less than half that of an average basalt (Marov and Grinspoon, 1998). A major problem is that almost the entire area imaged by each Venera lander sits within a single Magellan image pixel, and their landing position is known to only ~150 km, so that it is impossible to correlate features observed in the lander images with those in Magellan images. Do they represent a surface weathering veneer on otherwise intact lava flows, or thick accumulations of aeolian or pyroclastic deposits? This demonstrates the importance of reconstructing the Venus history not just understanding the emplacement of rock units, but their subsequent transport, modification and weathering processes.

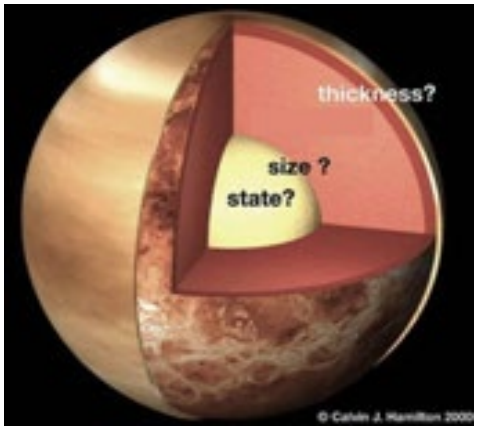

Figure 2.1.4 – *Sketch of the interior of Venus, showing the main open questions on its structure. To a first approximation, Venus' interior is generally held to be* Earth-like*, based on its similar bulk composition and radius. Higher spatial resolution gravity field measurements are needed to better constrain the crustal and lithospheric structure variations, which is essential to understand the geodynamic evolution of the planet. Higher accuracy of the tidal Love number is needed to better constrain the size and state of the core as well as mantle properties. Image copyright: Calvin J Hamilton 2000.*

To a first approximation, Venus' interior is generally held to be 'Earth-like', based on its similar bulk composition and radius. Any differences in their evolutionary histories are likely to be reflected in differences in their internal structure, and Venus' lack of a magnetic field suggests this might be the case. Venus is also less dense than expected if it had Earth's bulk composition, and its moment of inertia (the most powerful way to constrain the first order radial structure of a planet) is unknown (Fig. 2.1.4). Indeed, the shape of the planet appears to be unconnected to its rotational rate, which is too small to explain the observed flattening. The rotation rate itself is variable (Mueller et al., 2012), however only part of the variation is explained with the current knowledge of Venus' solid body and atmosphere and their interactions (Cottereau et al., 2011). The tidal Love number, estimated from Doppler tracking of Magellan and Pioneer Venus Orbiter spacecraft data, is not known with sufficient accuracy to constrain the size or state of the core (Dumoulin et al., 2017). The Venera landers returned a number of K, U and Th measurements that imply bulk ratios, and hence internal radiogenic heating rates, comparable with Earth (Namiki and Solomon, 1998). Magellan gravity data are consistent with an organized pattern of mantle convection broadly similar to Earth (see e.g. Smrekar et al., 2018a) but lack the resolution necessary to understand its connection with geological-scale features, such as individual coronae (Figure 2.1.5) or mountain belts. Higher spatial resolution is needed to better constrain the crustal and lithospheric structure variations, which is essential to understand the geodynamic evolution of the planet.

Activity – *How geologically active is Venus?*

EnVision will **search** for ongoing geological processes and determine where and how active the planet is, in the present era. It will: (1) constrain the style and distribution of ongoing volcanism on Venus, characterizing its morphological, thermal and volatile inventory; (2) assess present era landscape evolution on Venus, on time scales of years to decades, by searching for changes in repeated radar imagery.

It has recently been demonstrated that Venus is geologically active today, by the identification of a volcanic vent or caldera which expanded substantially between Cycles 1 and 2 of Magellan (Herrick and Hensley, 2023). Because Venus is similar in size and composition to Earth, its internal heat is expected to drive mantle convection, and associated volcanic and tectonic activity, to the present day. Venus' geologically young surface, with a mean surface age under 800 My (McKinnon et al. 1997), requires extensive volcanic resurfacing, but it is still not clear whether this happens in occasional episodic global-scale resurfacing events (e.g. Strom et al. 1994; Phillips et al. 1992) or whether a more continuous resurfacing occurs (e.g. Bjonnes et al., 2012; O'Rourke et al., 2014). The nature of volcanic and tectonic activity can be used to help distinguish between these different mechanisms of global heat loss: large-scale lunar mare-style flood lava units would be indicative of episodic global or regional resurfacing events that are concentrated in time, with

little activity between, whereas widespread, interdigitate, small-scale flow units would be indicative of a more equilibrium resurfacing style (Mueller et al., 2017). Near-IR emissivity mapping from Venus Express found anomalously high emissivity near suspected active volcanoes (Smrekar et al., 2010), interpreted as relatively fresh, as-yet unweathered lava flows. Recent lab-based experiments suggest that the timescale of weathering is days to years, implying that the Venus volcanoes have been active very recently, however, the detailed nature of the mineralogy and the weathering processes are still unknown. Further hints of active volcanism were provided by the Venus Monitoring Camera on Venus Express, which observed apparent temporal changes in thermal emission from the surface, consistent with what would be expected from an ongoing volcanic eruption (Shalygin et al., 2005), but this was observed only in one location and, as a monospectral observation, it was not possible to fully discount the possibility of atmospheric influence on the signal.

As well as understanding the nature of geological activity, it is important to understand the tectonic regime associated with this activity. Steep slopes and landslides are common on Venus, implying active uplift, but existing data provide no constraint on current rates of tectonic activity. The surface of Venus is not organized into large plates as on Earth's oceanic plates but appears to be partitioned into areas of low strain bounded by narrow margins of high strain, analogous to continental basins and microplates (Ghail et al., 2019). Are these regions actively created and destroyed, like Earth's oceanic plates, or simply mobilized locally? What is the significance of the global network of elevated rift systems, which are similar in extent to mid-ocean ridges but very different in appearance?

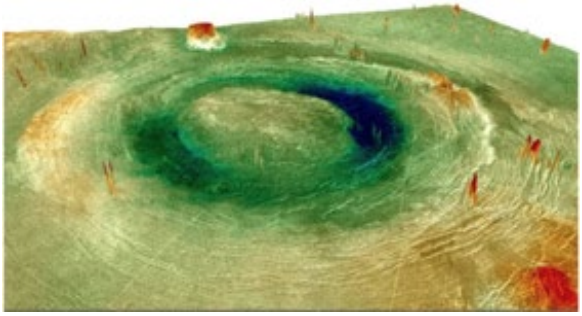

Figure 2.1.5 – *In the absence of global plate tectonics, mantle convection and plume–lithosphere interaction are the main drivers of surface deformation on Venus. Among documented tectonic structures, circular volcano-tectonic features known as coronae may be the clearest surface manifestations of mantle plumes and hold clues to the global Venusian tectonic regime. Yet, the exact processes underlying coronae formation and the reasons for their diverse morphologies remain controversial. This oblique view shows a typical example, located at 082°E, 25°S, is 400 km in diameter across the circumferential fractures, outside a 200 km diameter topographic trough 1100 m below the central high. Magellan SAR image on colourised topography, from -1500 m in blue to +500 m in red.*

Unique to Venus are coronae, quasi-circular tectonic features, typically 100–500 km across, with a range of associated volcanic features (Figure 2.1.5). Are coronae the surface expression of active plumes or magmatic intrusions, as found in recent research (Gülcher et al., 2020), or even subduction zones (Davaille et al., 2017)? There is now growing evidence from new models and experiments, of high heat flow, mantle plume evolution and recent volcanic activity, that suggests Venus is currently geodynamically active (D'Incecco et al., 2020, O'Rourke and Smrekar, 2018, Gülcher et al., 2020, Filiberto et al., 2020). Complementary, repeated, multi-type and multi-scale observations are needed to help detect the characteristics of such activity. After the formation of the surface by volcanic and tectonic processes, it is modified by weathering under Venus' extreme atmospheric conditions (high pressure, temperature), meteorite impacts and gravity-driven slope movements (landslides), all of which favour the fragmentation of surface materials. Along with clastic debris from volcanic activity (e.g. pyroclastic materials, Airey et al., 2015, Campbell et al., 2017, Ghail and Wilson, 2018) these unconsolidated materials would form a layer of regolith subject to further remodelling, transport and deposition by winds. The formation of volcano-sedimentary rocks cannot be excluded locally if these sediments are also subject to compaction by burial, sintering and hypervelocity impacts which favour clast consolidation and accretion (Greeley et al., 1987, Kreslavskly and Bondarenko, 2018). Apparent landslides were observed (Malin, 1992, Greeley et al., 1992) and some evidence for dune fields were found in Magellan data, but these were barely resolved at the 100 m to 200 m spatial resolution of Magellan's imagery. Resolving these features and processes in more detail is critical for understanding Venus' current surface interactions between atmosphere, surface and subsurface and any near-surface activity. Comparative studies on other planetary bodies, combined with analogue and numerical models indicate that a variety of active aeolian bedforms and geomorphological features should be expected on the Venus surface (Claudin, 2006; Lorenz, 2016; Diniega et al., 2017; Neakrase et al., 2017; Bondarenko and Kreslavsly, 2018). Therefore, higher resolution data and more detailed characterisation of the physical properties and mineralogy of the materials are needed to better characterize and understand these processes.

The Magellan radar orbiter revealed snapshots of all of the above processes everywhere on Venus but, without high resolution or repeated same-geometry observations over time, it has been extremely difficult to detect change (Herrick and Hensley, 2023) and impossible to estimate a rate at which these processes might be occurring. As discussed above, Venus Express, despite the atmospheric focus of most of its science goals, provided tantalizing hints of active volcanism, including temporal variations of surface temperatures (Shalygin et al., 2015), temporal variations of potentially volcanic sulphur dioxide gas (Marcq et al., 2013), and emissivity anomalies on the flanks of volcanoes (Smrekar et al., 2010). Repeated observations of the surface with the same viewing geometry, and repeated observations of the atmosphere, are thus crucial for addressing this science question, as will be explained in §2.2 and §2.3. Changes can be detected using a range of techniques, of which repeated imaging is one. Repeated and new observations also provide opportunity for searching for changes since previous missions (Magellan, Venus Express) despite the difficulties imposed by different resolution and viewing geometry. So the time scale for the search for change is larger than the mission duration: EnVision's investigations will seek to address the timescales of months; longer timescales of years to decades can be addressed through comparison between EnVision's map (expected between 2035 and 2039) and those of the Magellan radar orbiter active imaging data obtained in 1990-1992.

Climate – *How are Venus' atmosphere and climate shaped by geological processes?*

EnVision will **characterize** regional and local geological units and the planet's atmosphere, to improve our understanding of the Venus surface and atmosphere coupling, and the Venus cloud and atmospheric variability. It will (1) determine the role of geological activity, including both volcanism and surface-atmosphere chemical reactions, in sustaining the volatile and cloud content of the lower atmosphere; (2) assess intrinsic variability and transport of geophysically important volatile species through the atmosphere and clouds of Venus, through measurements below, within, and above the cloud layer, so as to be able to identify signatures of geophysical activity.

If Venus were a newly discovered exoplanet, it would be arguably one of the most Earth-like ones yet identified. Not only are its size and bulk density similar to those of Earth; its equilibrium temperature of 227 K is remarkably close to Earth's 255 K, and thus gives no clue to the hellish temperatures below the clouds. Transit spectroscopy would reveal its CO_2-rich atmosphere and lack of water but otherwise would suggest a very Earth-like world, perhaps similar to what the Earth itself might look like after a runaway greenhouse warming. Understanding how and why the atmospheres of Venus and Earth have evolved so differently is one of the compelling reasons to study Venus, as it directly addresses the question of how our own planet became habitable.

Understanding the evolution of Venus' atmosphere and climate requires understanding of its exchanges with the interior, with the surface and with space. The latter was studied extensively by the Analyzer of Space Plasmas and Energetic Atoms (ASPERA) instrument onboard Venus Express. EnVision will focus instead on the planet's mesosphere (60-100 km altitude above surface), troposphere (0-65 km altitude above surface) and their exchanges with the surface and interior. The volatile content of Venus' interior is unknown, but the existence of Venus' sulphuric acid cloud deck (Figure 2.1.6) may indicate that it is still outgassing SO_2 and/or water, or has done so within the past tens of millions of years (Bullock and Grinspoon, 2001). The input of H_2O and SO_2, required by the Bullock and Grinspoon model to maintain the cloud deck, corresponds to a magma effusion rate of 0.5 $km^3\ yr^{-1}$ (assuming a saturated magma source). Sulphur dioxide and water are both seen to be highly variable in Venus' atmosphere (Marcq et al., 2013, 2020; Shao et al., 2020; Encrenaz et al., 2020), but this variability has not yet been linked to volcanic emission. The detection of both H_2O and HDO in volcanic plumes is of particular interest; elevated D/H ratios on Venus have been interpreted as indicating escape of large amounts of water (Donahue et al., 1982), but the D/H ratio of mantle outgassing would affect those calculations. In summary, direct detection of the volatile content of volcanic emission would not only be important for understanding volcanism, but also for understanding the evolution of Venus climate.

The geological record may itself contain clues as to the history of Venus' climate. In particular, rocks such as granite can form only in the presence of liquid water (e.g. Campbell and Taylor, 1983); detection of such rocks in tessera highlands, as hinted at by Venus Express, would thus suggest that these terrains contain rocks formed at depth during a time when Venus had extensive liquid water in its mantle, and that the Venus' surface was subjected to strong erosive processes to reveal this rock type at the surface (Khawja et al., 2020), before developing a runaway greenhouse effect. The presence of current mantle water content and its

evolution are not well understood and are the subject of current debate (Rolf et al., 2022). Obtaining compositional data from these areas is therefore critical along with searching for evidence for fluvial or marine processes, including shorelines. Beyond the coupling and interactions discussed above, though, the most important unknown factor in determining the long-term history of Venus' atmosphere and indeed its habitability, is the history of the solid planet, as it represents the all-important lower boundary condition for the atmosphere. Therefore, all of EnVision's results regarding the history of Venus' geological activity will be important inputs for the reconstruction of Venus' atmospheric history.

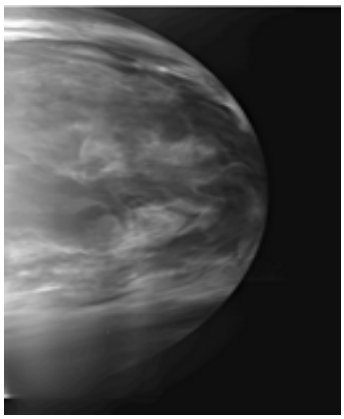

Figure 2.1.6 – *The nightside image of Venus taken by the Akatsuki's IR2 (InfraRed 2 micrometre) camera on April 26, 2016 at 16:03 JST, and the Akatsuki's altitude was 76 000 km at that time. Clouds are illuminated by the thermal radiation from the atmosphere near the Venusian surface. Dark areas represent thicker clouds; some of these could result from volcanic plumes of ash or sulphate particulates of present-era volcanic activity. Understanding the evolution of Venus' climate requires understanding of its exchanges with the interior, with the surface. Volcanic effects cannot be identified without understanding the intrinsic background variability of the atmosphere, which will be addressed by EnVision. Surface- atmosphere interactions are therefore a vital boundary condition on the evolution of Venus and its habitability through time. Credit ISAS/JAXA.*

2.2. EnVision Science Objectives

The following key science questions are addressed by the EnVision Science objectives:

2.2.1: Understanding Venus'magmatic history
What are the **compositions of volcanic rocks**? Are they all basaltic, or are there substantial volumes of more granitic rocks that would indicate magma formation in the presence of liquid water? Has volcanism been continuous or episodic? What are the **styles of magma emplacement**, and what do they imply about the range of magma emplacement rates?
These questions are addressed by EnVision's science objective
R1-H-50: "Determine the morphological characteristics, detailed planform, surface roughness, dielectric properties, infrared emissivity, and range thickness of lava flows/fields and plains units to understand their modes of emplacement, magma properties, dominant sources, composition, and relative age."

2.2.2: Understanding Venus' tectonic history
How did the **various types of tectonic structure form**? What is the nature of the forces that produced these features, and what are the magnitudes of the deformation? What do these structures imply about the **evolution of lithospheric thickness and heat flow as a function of time**?
These questions are addressed by EnVision's science objective
R1-H-60: "Determine the style of tectonic deformation that have operated on Venus in order to understand spatial and temporal variations in the lithospheric and crustal structure, the causes and magnitudes of the forces driving tectonism, and the process of planetary heat loss."

2.2.3: Assessing Venus' surface modification processes
How has the **surface of Venus** been modified since it was formed? In particular, what are the **processes** that have modified and partially filled impact craters? What are the causes of the low emissivity material in some highlands, and what does this imply about weathering processes and possible volatile transport?
These questions are addressed by EnVision's science objective
R1-H-10: "Determine the degree of crater morphological modification and infilling, the surface physical properties and elevation dependence of radar brightness signatures, and the microwave and infrared emissivity of the plains, to understand the processes that modify the surface over different time scales."

2.2.4: Understanding how Venus' interior and surface have evolved
How does the **interior structure of Venus,** with its most important compositional layers, core, mantle and crust, differ from Earth's? What is the **size** and **physical state** of the core? What is the geodynamic and thermochemical evolution of Venus, the crustal and lithospheric structures of the main volcano-tectonic features (coronae, large volcanoes, ridges, tesserae, rifts)?
These questions are addressed by EnVision's science objective
R1-H-70: "Determine the size of the major internal layers (crust/lithosphere, mantle, core), and the state of the core, to better understand Venus' thermo-chemical evolution."

2.2.5: Understanding Venus' volcanic activity in the present era
Is Venus the only other terrestrial planet beside Earth that is still **volcanically active** in the present era? What are or have been the styles and distribution of volcanism? Has volcanism changed over time, and is it localized or global? How does volcanism contribute to the volatile cycles on Venus?
These questions are addressed by EnVision's science objective
R1-A-10: "Constrain style and occurrence rate of current-day volcanism on Venus, by searching for its thermal, morphological and volatile signatures in repeated observations of the surface and of the atmosphere."

2.2.6: Assessing Venus' aeolian activity and mass wasting
What are the mechanisms and processes by which the planet's surface is modified and evolves? Magellan detected **mass-wasting and aeolian features**, such as landslides, dune-fields and wind-streaks; what are their distribution, abundance and geomorphology, and how do they change with time?
These questions are addressed by EnVision's science objective
R1-A-30: "Characterize geomorphological changes over the short time scale (years to decades), focussing on mass wasting and aeolian processes by repeated imaging and detection of surface and geomorphological changes at all scales."

2.2.7: Understanding the role of geological activity in Venus' climate evolution
How are **tropospheric and geological processes** coupled on Venus? Do exchanges take place from direct outgassing of volatiles into the lowermost atmosphere, buffering of atmospheric species with surface reservoirs, or aeolian or chemical alteration of surface minerals?
These questions are addressed by EnVision's science objective
R1-C-10: "Measure the variability of tropospheric composition, and study whether and how this is linked with surface geological processes and atmospheric dynamics."

2.2.8: Assessing temporal variations of the Venus atmosphere
How are volatile species, particularly water and sulfur dioxide, transported through the **cloud layers and upper atmosphere**? How much of the variability in and above the clouds is due to intrinsic dynamic variability, and how much is directly or indirectly caused by volcanic activity?
These questions are addressed by EnVision's science objectives
R1-C-30: "Measure the variability of clouds and cloud droplets, and determine whether and how this is linked with surface geological processes and atmospheric dynamics."
R1-C-20: "Measure the variability of mesospheric composition, and determine whether and how this is linked with surface geological processes and atmospheric dynamics."

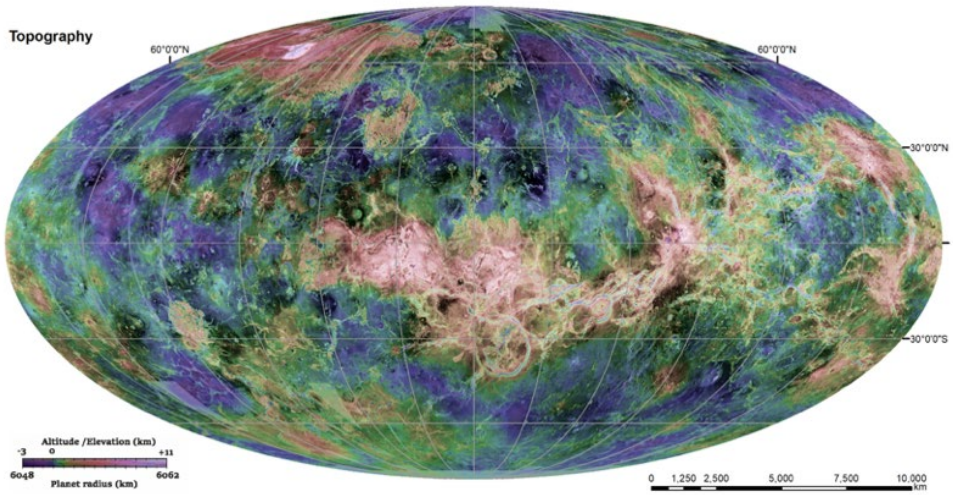

Figure 2.2.1 – *Venus global topographic map from Magellan. Like Earth, Venus hosts continent-like structures, volcanic plains, tectonic rifts and mountains. Altimeter derived color-coded topography is overlain on SAR backscatter image. The majority of what is known about the surface of Venus, its geology and geomorphology, has been derived from this mosaic.*

2.2.1. Understanding Venus' magmatic history

What are the **compositions of volcanic rocks**? Are they all basaltic, or are there substantial volumes of more granitic rocks that would indicate magma formation in the presence of liquid water? Has volcanism been continuous or episodic? What are the **styles of magma emplacement**, and what do they imply about the range of magma emplacement rates?

These questions are addressed by EnVision's science objective **R1-H-50**: "Determine the morphological characteristics, detailed planform, surface roughness, dielectric properties, infrared emissivity, and range thickness of lava flows/fields and plains units to understand their modes of emplacement, magma properties, dominant sources, composition, and relative age."

How were volcanic materials emplaced at the surface of Venus?

Volcanic eruptions form and modify much of the surfaces of terrestrial planets. While virtually all surface volcanism on the smaller planets has ended, it is likely that Venus is similar to the Earth in having continued intrusive and extrusive activity. Flow thickness, length, vent structure, and features like channels have long been used to better understand the composition of the erupted magmas and to model eruption rate and duration. These properties in turn point to the nature of heat flow and lithospheric thickness that control the ascent and eruption of gasses and magma. It is probable that at least 90% of the surface was formed by effusive volcanic materials, so understanding their physical properties is crucial to unravelling the geologic history of Venus.

The scale of the associated landforms spans the range from km-scale domes in the plains (Fink et al., 1993) to shield volcanoes 300-400 km in diameter, vast flow fields up to 1000 km in length (Roberts et al., 1992) and hypothesized lava channels thousands of kilometres long (Komatsu et al., 1993) (Figure 2.2.2). Hybrid volcano-tectonic corona features are also surrounded by flow fields hundreds of km in extent (Stofan et al., 1992). While most of the large volcanic features have terrestrial analogues, evidence of the long-term eruption processes required to form them has often been removed by erosion on Earth. Venus also differs from the Earth in having no plate tectonic mechanism for releasing heat at present, so it is likely that effusive eruptions occur in large pulses from hot, rising mantle plumes, though possibly separated in time by long periods in different locales.

What is the chemical composition of the surface?

The elemental chemical composition of the Venus surface has only been measured in three locations by Soviet Venera and Vega landers. In all three places, the rocks have SiO_2 contents of 45-49 weight %, consistent with a basaltic composition (Treiman et al., 2007). At other landing sites, only K, U, and Th were measured, which is insufficient to chemically classify the rock composition. The presence of basalt on Venus is expected, as basalt is the most common type of volcanic rock on Earth, Mars, and the Moon. An important unanswered question is whether Venus has rocks of more evolved (felsic) composition, such as granites, exposed at its surface ($SiO_2 \geq 56$ weight %). This is an important question, because such rocks on Earth form primarily in the presence of liquid water at subduction zones; finding large volumes of felsic igneous

rocks on Venus would therefore indicate that magmatism once occurred in the presence of abundant liquid water (Campbell and Taylor, 1983). Such a finding would provide an extremely important constraint on the geological and climatological evolution of Venus. Because granite is less dense than basalt, regions with substantial granite in the crust would most likely be topographically elevated. Thus, regions of tesserae, as well as the mountain belts of Ishtar Terra, are widely considered as the most likely places to search for granitic rocks on Venus (Dyar et al., 2020).

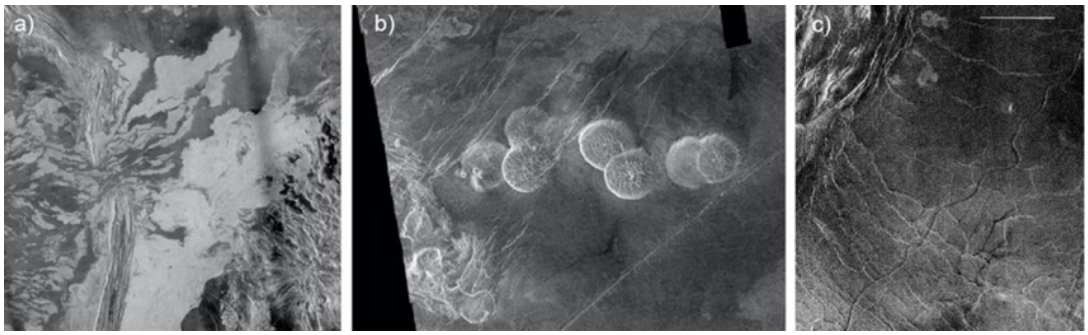

Figure 2.2.2 – *(a, left): Flood lavas in Lada Terra are an example of highly fluid magma emplacement. The image is 550 km across. (b, center): The steep-sided 'pancake domes' near Alpha Regio are about 25 km in diameter and are examples of viscous magma emplacement. (c, right): A portion of sinuous canali-type channel Baltis Vallis, which has a total length of 6800 km. The scale bar is 50 km across. NASA Magellan data.*

Composition of the surface is also essential to understand weathering and oxidation mechanisms that could have an important effect on the evolution of the atmosphere and climate of Venus. At present, those effects may be considered as secondary, due to the purported low diffusion speed of oxygen into solid basaltic material (Wendlandt, 1991). However, the entire mechanism is poorly constrained and a number of parameters (i.e. morphology of lava flows, cooling times, volume of produced lava) can greatly improve our understanding of weathering and oxidation mechanisms (Gillmann et al., 2020).

2.2.2. Understanding Venus' tectonic history

How did the **various types of tectonic structure form**? What is the nature of the forces that produced these features, and what are the magnitudes of the deformation? What do these structures imply about the **evolution of lithospheric thickness and heat flow as a function of time**?

These questions are addressed by EnVision's science objective **R1-H-60**: "Determine the style of tectonic deformation that have operated on Venus in order to understand spatial and temporal variations in the lithospheric and crustal structure, the causes and magnitudes of the forces driving tectonism, and the process of planetary heat loss."

How do tectonic structures form on Venus?

Earth displays three fundamental types of tectonic structure, produced in response to contractional and tensional stresses, and these may be compressional, extensional and transcurrent (or strike-slip). Predominantly vertical motion or deformation may be compressional, forming thrust faults and folds, as exemplified by terrestrial mountain belts. Vertical motions may also be extensional, producing basins and rift systems, such as those of the East African Rift. Finally, predominantly horizontal motions can be extensional but tend to be compressional and may lead to the formation of strike-slip faults at various scales, such as the San Andreas (plate boundary) Fault in California. All three types of structure are observed on Venus. Mountain belts occur in Ishtar Terra and reach elevations of 8-11 km, the highest on Venus. They are likely a product of compressional deformation producing thick crust and reflecting an epoch (possibly in the geologic past) when Venus had a mobile surface. Tesserae are characterized by highly elevated topography, small-scale surface roughness and multiple sets of cross-cutting tectonic structures (Figure 2.2.3), and they appear to represent areas of intense tectonism. The formational models to explain such high, complex and strained terrain are still the subject of much debate and uncertainty: horizontal convergence, extension, mantle upwelling, sub-crustal flow, crustal underplating, sub-crustal rejuvenation, crustal plateau formation, diapiric intrusion, gravitational sliding and relaxation, or all of these? (Hansen and Willis, 1996; Ivanov and Head, 2011).

Lesser amounts of compression can be seen in the ridge belts and wrinkle ridges of the vast plains on Venus. Extension has produced rift systems in several places on Venus, including Guor Linea in Western Eistla Regio and Devana Chasma in Beta Regio and is likely associated with regions of upwelling mantle convection (e.g., Kiefer and Swafford, 2006). Although the Magellan mission provided a first-order overview of the types of tectonic structures on Venus, the limited spatial resolutions of its imagery and topography inhibit our ability to interpret the tectonic evolution of Venus with any confidence. EnVision's much sharper view is the necessary next step to better understanding the geologic evolution of Venus.

How has lithosphere thickness affected tectonism? What does thickness imply about heat flow?

The lithosphere is the outermost physical layer of a planet; it is colder and therefore stronger than deeper layers. The thickness of the lithosphere has a strong effect on the style of tectonic deformation, including the characteristic spacing between tectonic structures. Lithospheric thickness has been proposed as an important control on the evolution of volcanic structures, including defining the evolutionary spectrum between the formation of a coronae and the appearance of a volcanic edifice at the surface. Tesserae are intensely deformed and characterized by closely spaced fault systems (Figure 2.2.3a), suggesting that the lithosphere was thin and that heat flow from Venus's interior was high when the tesserae formed (Brown and Grimm, 1999). Other tectonic units have more broadly spaced tectonic structures, implying a thicker (less easily deformed) lithosphere and lower heat flow.

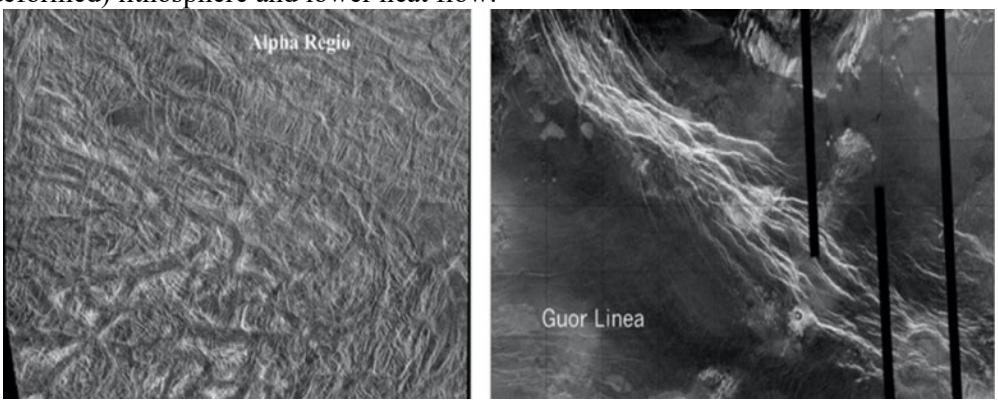

Figure 2.2.3 – *(a, left): A tessera in Alpha Regio. Image is 290 km across. (b, right): Guor Linea in Western Eistla Regio is a rift system formed by extension and stretching of the crust. Image is 900 km across. NASA Magellan data.*

2.2.3. Assessing Venus' surface modification processes

How has the **surface of Venus** been modified since it was formed? In particular, what are the **processes** that have modified and partially filled impact craters? What are the causes of the low emissivity material in some highlands, and what does this imply about weathering processes and possible volatile transport?

These questions are addressed by EnVision's science objective **R1-H-10**: "Determine the degree of crater morphological modification and infilling, the surface physical properties and elevation dependence pf radar brightness signatures, and the microwave and infrared emissivity of the plains, to understand the processes that modify the surface over different time scales."

What processes modify Venus' impact craters?

The impact of asteroids and comets on the surface of Venus, and other planets, produces craters at a range of sizes. Venus has only about 950 recognizable craters on its surface, far fewer than on the Moon or Mars. This small number suggests that Venus has been resurfaced relatively recently in its history, thus concealing evidence of previous impacts. However, there is considerable debate about the timing and nature of this resurfacing process, with proposals ranging from a short, single, catastrophic resurfacing event a few hundred million years ago to gradual, periodic or semi-continuous resurfacing (see review by Herrick et al., 2023). The craters across Venus' surface show a range of morphologies, ranging from pristine to significantly degraded (Figure 2.2.4). More detailed imaging, SRS sounding, and higher resolution topographic data will help constrain the processes that have modified or obliterated craters on Venus as well as the thickness of any material that has apparently filled them.

What do low microwave emissivity/radar-bright terrains reveal about Venus' modern environment?

Magellan's radar imagery revealed that some areas of Venus display anomalously low microwave emissivity and high radar reflectivity. Such regions are primarily located at high elevations (> 2 km) (Pettengill et al.,

1992, 1996), but not all highlands show this anomalous behaviour. The low emissivity may be related with very high dielectric constant, as high as 80 (for comparison, most planetary crusts have dielectric constant from 3 to 10 and Venusian plains, the most extensive geologic unit on the planet, exhibit a dielectric constant in the range 4 to 5, which is consistent with a moderately dense basalt). In the absence of liquid water (which is known for its high dielectric constant) such high values are puzzling; possible explanations for the high-altitude 'snowline' on Venus include cold trapping of exotic volatile species, or yet unidentified weathering reactions. Among the candidate materials, that have unusually high dielectric, are ferroelectric substances (e.g. chlorapatite) (Arvidson et al., 1994; Shepard et al., 1994; Treiman et al., 2016) and 'metallic frosts' (e.g. volatile metal halides and sulphides) transported from the 'hot' plains to the relatively 'cool' highlands, where they condense forming a surficial coating (Brackett et al., 1995).

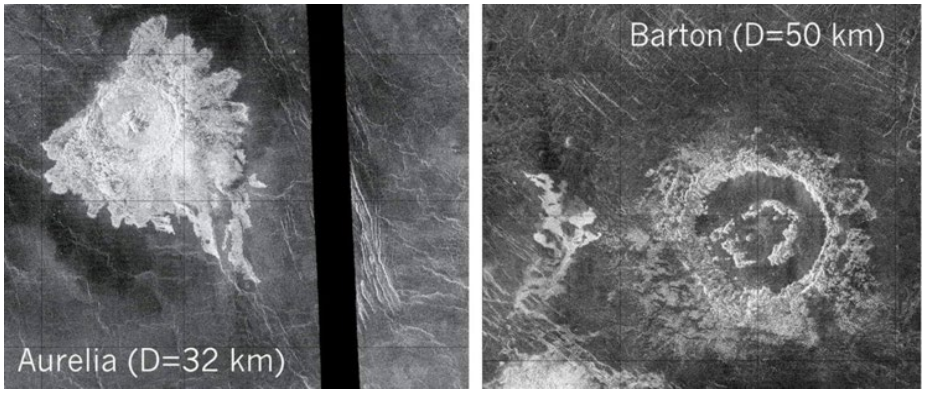

Figure 2.2.4 – *(a, left): Crater Aurelia (diameter 32 km) is interpreted as a pristine impact crater. It has a rough (radar bright) floor and ejecta blanket. (b, right): Crater Barton (diameter 50 km) is interpreted as a modified crater. It has a smooth (radar dark) floor suggestive of post-impact volcanic filling. The ejecta blanket is also embayed with later radar dark material, which is also consistent with post-impact lava flooding outside the crater rim. NASA Magellan data.*

It is important, however, to highlight that the estimation of the dielectric constant of all 'highlands', from the measured backscatter and emissivity, relies on models that do not account well for multiple and volume scattering. While it is true that many arguments are in favour of the dominance of surface scattering in the highlands, volume scattering due to inclusions embedded in a low-loss or low-density substrate could also explain the observed anomalous microwave properties without requiring the presence of a high dielectric constant material. Furthermore, some highlands (e.g. Ishtar, Ovda and Maat) do not display anomalous backscatter and emission properties at all. In particular, some lava flows on Maat Mons (1.5°N, 1.94°E) do not exhibit a clear 'snow-line' (Robinson and Wood, 1993; Campbell, 1994). This lack may reflect different rock or atmosphere compositions, perhaps implying a slow reaction process (or infrequent frosting) that has yet to affect these flows. Better characterization of the highlands and, particularly, improvement in the topographic resolution of the bounding elevations, will provide important insights into mineral genesis and atmospheric sinks in the modern Venus environment.

2.2.4. Understanding how Venus' interior and surface have evolved

How does the **interior structure of Venus,** with its most important compositional layers, core, mantle and crust, differ from Earth's? What is the **size** and **physical state** of the core? What is the geodynamic and thermochemical evolution of Venus, the crustal and lithospheric structures of the main volcano-tectonic features (coronae, large volcanoes, ridges, tesserae, rifts)?

These questions are addressed by EnVision's science objective **R1-H-70**: "Determine the size of the major internal layers (crust/lithosphere, mantle, core), and the state of the core, to better understand Venus' thermo-chemical evolution."

The interior structure of a planet and the driving forces of tectonism and volcanism are connected by its inner thermal 'engine'. The effectiveness of this engine determines the cooling behaviour of a planet and controls its heat budget which, in turn, has a strong influence on the evolution of its magnetic field, atmospheric evolution through volatile outgassing during volcanism and, finally, the timing of volcanic activity. Phases of strong cooling and volcanic activity cause the temperature of a silicate melt to fall below its melting point. There may be a long phase of inactivity until the system can heat up again through radioactive heat sources – or not. Venus' thermal engine seems to be particularly complex, as is evidenced by its great variety of tectonic and volcanic features. A better understanding of the interior structure and dynamic processes will help us to better understand the planetary heat flow as well as how it influences a planet's habitability.

The heat engine in Venus' interior: what are the driving forces for volcanism and tectonism?

In general, rocky planets of similar size and mass, such as Venus and Earth, need to release about the same amount of heat over time. How they do that can vary greatly in time and there are many geodynamic mechanisms and models to explain those changes. On Earth, plate tectonics is the dominant present-day heat loss mechanism but, early in Earth's history, magmatic processes are thought to have played a much more significant part in transferring heat from interior to exterior. In all cases, it is the interior dynamics that essentially governs how a planet cools, and different convection regimes may lead to very different tectonic characteristics. There is a growing number of mantle dynamic models which attempt to better explain the complexity of Venus' tectonic characteristics as visible on its surface. These allow for varying degrees of 'lid mobility' and present different scenarios dominated by extrusive or intrusive magmatic activity, on a continuum in time between a past global magma ocean and a terminal stagnant lid (Rolf et al., 2022). More and better datasets are needed to constrain and refine such models, and thus to better understand the interior structure and processes that govern Venus' volcanism and tectonism.

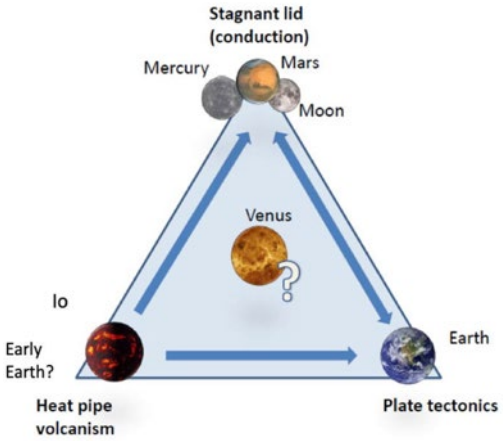

Figure 2.2.5 – *Heat loss on the terrestrial planets occurs in three basic ways. Mars, Mercury, and the Moon lose their heat by thermal conduction through a thick lithosphere. On Earth, mantle convection and plate tectonics is the dominant present-day heat loss mechanism. On Io, and possibly on the early Earth ('Hadean'), heat transport was predominantly caused by magmatic eruptions. On Venus, the mode(s) of heat transport and their possible evolution over time remains poorly known. A better understanding of the interior structure and the dynamic processes will help us to better understand the planetary thermal engine as a whole and how it can influence a planet's habitability.*

On Venus, mode(s) of heat transport and their evolution over time remain very poorly understood (Figure 2.2.5). Venus' surface suggests that its tectonic regime could be far more complex than a simple stagnant lid, and it may have changed significantly over the course of its evolution. Venus' present interior dynamic regime seems to be consistent with convection beneath a 'stagnant lid' but in some areas, this lid does not seem to be entirely 'stable'. Instead, a so-called 'sluggish lid' may exist, which may represent an instability of the lower crust like a delamination, or the onset of a subduction event (akin to plate tectonics), potentially related to upwelling mantle plumes (Gerya et al., 2015; Davaille et al., 2017). Analyses of gravitational and topographic data suggest that Venus has a comparable number of large, active mantle plumes to Earth, as well as many hundreds of smaller active plumes (Smrekar and Phillips, 1991). Such a regime, if existent on Venus, would also support the hypothesis of plume-induced subduction, which has been proposed as the initiator of plate tectonics on early Earth (Gerya et al., 2015).

In addition to these mantle dynamic features, the surface of Venus seems to have been resurfaced by volcanism within the last 500 million to a billion years. The nature and duration of this volcanic activity and the associated tectonic style(s) are however unclear. Currently discussed evolution scenarios in the literature include (i) episodic catastrophic resurfacing (Parmentier and Hess, 1992; Turcotte 1993, 1995; Armann and Tackley, 2012), (ii) gradual decay of volcanism over time in a stagnant lid regime and (iii) mixed forms and transitions between the different tectonic regimes, i.e. stagnant lid, mobile lid, episodic, plutonic-squishy lid and transitional (e.g., Gillmann and Tackley, 2014; Weller and Lenardic, 2018; Weller and Kiefer 2020; Lourenço et al., 2020). In the 'transitional' case, resurfacing is likely limited to certain regions, i.e. it is not global but results in multiple localized resurfacing and melting events (Noack et al., 2012; Weller and Kiefer, 2020). A key parameter controlling the regime may be surface temperature, which is also influenced by atmosphere conditions and thus by the coupling between interior and the atmosphere (Gillmann and Tackley, 2014).

How does the interior structure of Venus differ from Earth's?

Knowledge of the interior structure with its most important compositional layers, i.e. core, mantle and crust, is essential for a better understanding of the formation and evolution of a planet. For one, the size of these layers provides constraints about the bulk composition of Venus. Previous models about the bulk mantle and crust composition are based on cosmochemical assumptions (Fegley, 2014 for review) and show a 500 km uncertainty in the size of the core to fit the observed mass and radius of Venus (Dumoulin et al., 2017). The uncertainty is even greater if one assumes that the core of Venus could also have a different composition than

the Earth's core, in particular in the concentration of its light-alloying elements. The size of the core, however, can influence the convection structure in the mantle and thus also the distribution of volcanism at the surface (Breuer and Moore, 2015). On the other hand, the present-day interior structure with its main chemical layers shows the product of the processes that have shaped the planet so far. This starts from early metal-silicate differentiation to form the iron-rich core and continues with silicate-silicate differentiation to form the silicate crust by magmatism. Core formation is expected to have occurred very early in the first ten million to hundred million years (e.g., Kleine et al., 2002) and provides also the link to an internal magnetic field that can be generated in an iron-rich fluid core. For Venus core, previous measurements do not even allow us to determine the state of the core, i.e. whether it is solid or liquid today (Dumoulin et al., 2017) – an important piece of information for the understanding of both thermal and magnetic field evolution. Crust formation on the other hand is typically a longstanding process that can last throughout the entire planetary evolution as it is observed on Earth or is limited to certain periods during the evolution as suggested for instance for Mercury, Mars and the Moon.

2.2.5. Understanding Venus' volcanic activity in the present era

Is Venus the only other terrestrial planet beside Earth that is still **volcanically active** in the present era? What are or have been the styles and distribution of volcanism? Has volcanism changed over time, and is it localized or global? How does volcanism contribute to the volatile cycles on Venus?

These questions are addressed by EnVision's science objective **R1-A-10:** "Constrain style and occurrence rate of current-day volcanism on Venus, by searching for its thermal, morphological and volatile signatures in repeated observations of the surface and of the atmosphere."

How does volcanic activity contribute to the planetary heat budget?

As on Earth, internal heat is expected to drive mantle convection, and thus the associated volcanism and tectonism, but a lack of understanding of how the driving forces are organized, coupled with a lack of observations over time, makes estimating of the planet's heat budget challenging. Venus' apparently uniformly young surface suggests extensive volcanic resurfacing, although it is not clear whether resurfacing is periodic and catastrophic, or semi-continuous and localized, and this hinders estimation of the levels of activity and volcanic eruption. The detection and better characterisation of current volcanic and tectonic activity should help distinguish between these styles and inform models of heat exchange.

The current rate of volcanic activity on Venus is unknown, with only highly under-constrained estimates proposed. Measurements from VEx/VIRTIS weakly constrained the Venus extrusive volcanism rate to <300 km^3/yr (Mueller et al., 2017); suggesting an improbable factor of more than ten times larger than Earth (*ca* 20 km^3/yr) – chiefly because VEx/VIRTIS coverage was not optimized for detection of volcanic activity. Mueller et al. (2017) estimated that new imaging with similar total coverage to VIRTIS but with higher SNR (x20), would have a high likelihood (> 75%) of observing at least one eruption, at rates of volcanism of 10 km^3/yr, on the basis of conservative assumptions on flow brightness; both these imaging conditions will be satisfied by EnVision's VenSpec-M observations. Magellan's repeat imaging was not optimized for change detection, having widely varying look angles between observations and thus, until very recently, the absence of reported change was interpreted as an indication of a volcanism rate smaller than 10 km^3/yr (Lorenz, 2015). In contrast, the recent discovery of volcanic activity at Maat Mons that occurred between Cycles 1 and 2 of the Magellan mission (Herrick and Hensley, 2023), coupled with new statistical analyses of eruption probabilities, from estimates of rift-related and subduction-related volcanism, suggest we should expect between several 10s and ~120 volcanic eruptions to occur on Venus, every Earth year (Byrne and Krishnamoorthy, 2021; van Zelst, 2022). All these estimates rely on many assumptions, about eruptive magnitude, duration and style, but they provide very useful frameworks within which to interpret any observations of volcanic activity made during EnVision's mission period.

There have also been several studies of transient hotspots in data from Venus Monitoring Camera (VMC) and VIRTIS/VeX data, see Figure 2.2.6 (Smrekar et al., 2010; D'Incecco et al., 2017, 2020, 2022), as well as spectroscopic analyses of Venus surface analogues (Filiberto et al., 2020; Cutler et al., 2020), which also point strongly towards recent activity. Additionally, Magellan imagery of parts of Ganiki Chasma, and Sitwell Crater show parabola of radar-dark (fine grained) material where there are also transient bright spots. These could represent lava flows that have flowed over (thus post-dating) rift fractures and faults, as well as faults which cut across very young lava flows, and lava flows clearly overlying dark parabola materials. At Ozza Mons dark parabola from the Uvaysi Impact, tentatively dated as occurring between 9 – 60 Ma, overly and are overlain by a complex stratigraphy of lavas (Brossier et al, 2021; Klidaras and Mason, 2022). All these observations strongly support the conclusion that Venus is experiencing active volcanism in the modern day.

Improving estimates of the current rate of volcanic effusion, even to an order of magnitude better than current estimates (i.e., to within 1 km^3/yr), would help to address the outstanding question of whether resurfacing on Venus is continuous, or episodic. For instance, in an equilibrium resurfacing model, proposed volcanism rates could vary widely from a minimum of 0.5 km^3/yr to 200 km^3/yr (Turcotte, 1989). If resurfacing instead occurs in episodic, catastrophic events, then periods of much smaller or much greater volcanic activity are possible. Importantly, such assessments of volcanic activity would also help to understand the volatile budget of the Venus atmosphere. Nine large volcanic topographic rises have been studied (Stofan et al., 1995), each typically 1000 km in diameter, and they are thought to be associated with large-scale mantle upwellings; such rises are expected to have increased rates of volcanism, and this makes them important focal points in the search for evidence of active volcanism. Several studies have presented compelling evidence that volcanism (and tectonic) processes, at Imdr, Themis, Dione and Atla Regio, are geologically recent, possibly as young as 250,000 yr (D'Incecco et al. 2020, Filiberto et al. 2020, Smrekar et al., 2010).

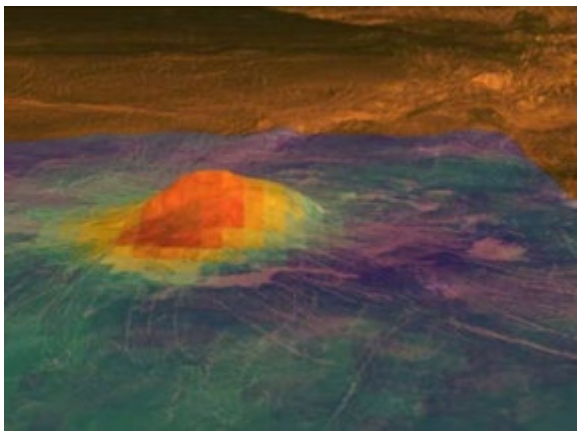

Figure 2.2.6 – *Surface brightness temperature measured by VIRTIS/Venus Express on the volcanic peak Idunn Mons in the Imdr Regio area of Venus. High emissivity (in red-orange) corresponds to compositional variations possibly caused by less-weathered lava flows, which appear against the blue-purple background of lower emissivity rocks.*
Image: © NASA/JPL-Caltech/ESA.

Near InfraRed (NIR) thermal emissivity mapping, from Venus Express, detected anomalously high emissivities near suspected active volcanoes, and these were interpreted as relatively fresh, as-yet unweathered lava flows, but the nature of the mineralogy and the nature and rates of weathering processes are still unknown. However, recent laboratory analysis in Venus-like conditions reveal that chemical weathering of fresh surface rocks could occur on a scale of days to weeks (Santos et al., 2023). Other thermorheological lava flow modelling suggests that for the effective effusion rate and topography, a freshly erupting lava on Venus travels further than an equivalent flow on Earth and that its cooling should be detectable by future orbital instruments (Flynn et al., 2023); suggesting that emissivity anomalies detected by VIRTIS over lavas and volcanic rises were very fresh indeed (Figure 2.2.6). All such areas (and possibly others) are also expected to be active today. Repeat imaging and emissivity measurements, and high-resolution imaging, are needed across such key sites to assist in constraining levels of activity and informing current models of the Venus heat budget. EnVision will obtain repeated radar imagery either with the same look angle, or with a small look angle difference of typically 5° between stereo pairs for extraction of topography. This repeated imagery, at much higher spatial resolution, even with small look angle difference, will offer far better sensitivity to surface change than was achievable with Magellan data.

Evidence suggests that Venus lacks a system of plate tectonics comparable to Earth and, therefore, it must have a thick lithosphere to support its range of topography. If Venus has a similar radiogenic heat production rate to Earth, the heat would require either a transport mechanism other than plate tectonics and conduction, or accumulation in the interior. The rate of magmatism required to transport this heat through the lithosphere is on the order of 200 km^3/yr. Fractionation of heat producing elements into the crust may reduce the required rate of magmatism to 90 km^3/yr (Spohn, 1991). Armann and Tackley (2012) included the heat budget in a

numerical model of mantle dynamics allowing for episodic behaviour; they found rates of magmatism on the order of 10^3 km^3 /yr, in 150 Myr long episodes of foundering lithosphere, and rates on the order of 50 km^3 /yr in periods of stable lithosphere lasting approximately 0.5 Gyr. It is unclear how much of this predicted magmatism would contribute to extrusive, directly observable volcanism. The ratio of intrusive to extrusive volcanism is estimated to be 5 to 1 for basaltic crust on Earth, but this might be different and possibly much higher for the higher temperature and less mobile lithosphere of Venus, since the hot, dry climate may inhibit volcanism (Mikhail and Heap, 2017).

How does active volcanism contribute to the volatile cycle on Venus?

The presence of CO_2, N_2, SO_2, HCl and HF gasses in the Venus atmosphere is taken as key evidence of active volcanism and degassing (Figure 2.2.7). The cycling of such volatiles, between interior and Venusian atmosphere, may be episodic and is thought to be closely related to resurfacing events. Some volatiles (S, Cl) may decline in content over time, through weathering and escape from the upper atmosphere, until the next resurfacing event. Others that do not react with surface materials (C, N, and Ne), or are not lost from the clouds, may accumulate over time. Multi-temporal and detailed atmospheric characterisation carried out by instruments of the VenSpec suite, will provide better understanding of Venusian volatile cycles, including the potential link to volcanism.

The main obstacle in the search for active volcanism with the Venus Express VIRTIS imaging instrument was the low signal-to-noise ratio. In improved signal-to-noise ratio means higher sensitivity and detection to eruptions of lower intensity, because the signature is proportional to the effusion rate. Thus, increasing the signal-to-noise ratio from 16 (VIRTIS) to at least 20, could enable the detection of flow rates down to 50 m^{3}s^{-1}, a value more frequently seen during eruptions on Earth. Multiple (repeated) observations of the same surface per day will allow for detection of short-lived thermal signatures, and thereby greatly increasing the detection reliability.

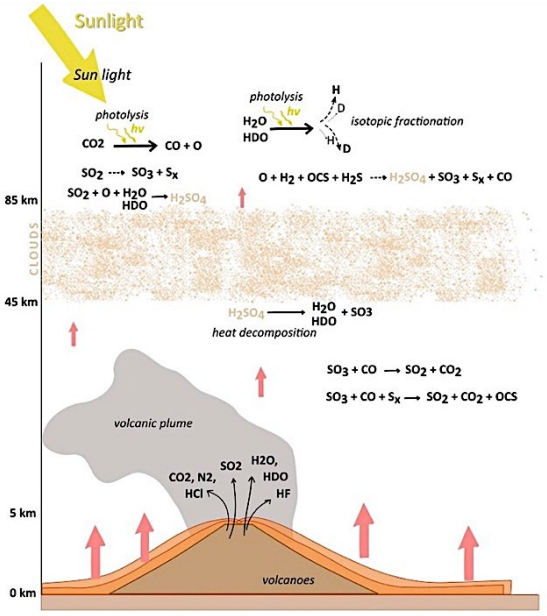

Figure 2.2.7 – *Chemical cycling of volatiles in the Venus system between interior, surface, atmosphere and clouds (graphic by Enora Moisan, Oxford University).*

2.2.6. Assessing Venus' aeolian activity and mass wasting

What are the mechanisms and processes by which the planet's surface is modified and evolves? Magellan detected **mass-wasting and aeolian features**, such as landslides, dune-fields and wind-streaks; what are their distribution, abundance and geomorphology, and how do they change with time?

These questions are addressed by EnVision's science objective **R1-A-30:** "Characterize geomorphological changes over the short time scale (years to decades), focussing on mass wasting and aeolian processes by repeated imaging and detection of surface and geomorphological changes at all scales."

After formation, any terrestrial planet's surface interacts with the atmosphere (and other volatiles present) and responds to a variety of stresses; it is then modified by a range of processes, such as gravity-driven mass-movements (e.g., landslides and slumps), erosion and deposition, and by active chemical weathering, and evolves over time. Providing constraints on the distribution, scales and effects of these processes is vital to understanding the mechanisms and rates of interior, surface and atmospheric interactions on any planet, and is critical for understanding Venus' geological timeline.

What evidence is there of active physical and chemical landscape change?

Landscape evolution refers to geodynamic processes which modify the morphology of a planet's surface, in particular gravity-driven mass-wasting processes such as landslides and slumps, often in response to uplift.

Mass-wasting is a ubiquitous gravity-driven geomorphological process operating on all hill slopes, and such features are thus observed on Earth and its Moon, Mercury, Venus, Mars, icy satellites, comets and asteroids. Even Magellan's low-resolution radar imagery provided the first glimpses of mass-movements on Venus, in the form of large-scale slope failures: "rock slumps, rock and/or block slides, rock avalanches, debris avalanches, and possibly debris flows are seen in areas of high relief and steep slope gradients" (Malin, 1992; Figure 2.2.8a) and often on the steep flanks of volcanoes which are commonly unstable on short and long time scales (Hahn and Byrne, 2023; Figure 2.2.9). However, the different view angles of Magellan's repeat pass imagery made correlation difficult and such slope change detections are in some cases tenuous. Multi-temporal observations are essential for constraining the frequency of mass wasting occurrence but these are limited to Earth and a handful of cases on Mars. This lack prevents the understanding of the rates, frequencies and triggers of mass-wasting occurrences in our Solar System. Repeated imaging at higher resolution, over short time-scales (years to decades) is needed to improve understanding of the scales and character of geodynamism on Venus.

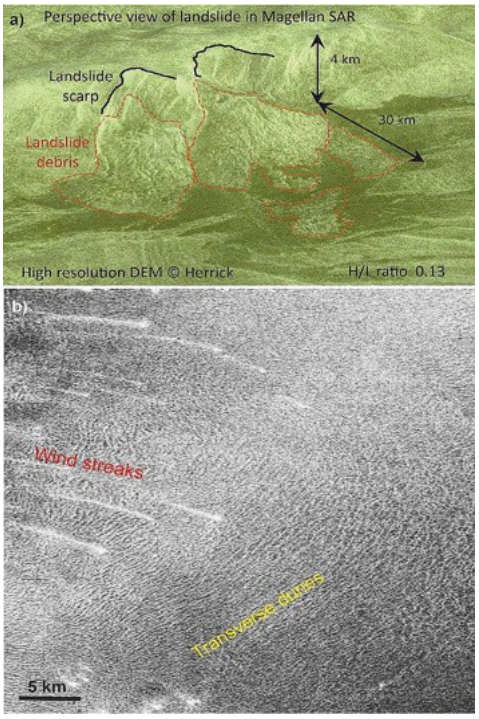

Figure 2.2.8 – *Surface geomorphological features imaged by Magellan. (a, top): Perspective view of two large landslides or rock/block avalanches projected on DEM data generated by R. Herrick, Malin (1992); and (b, bottom): lowlands of Al-Uzza Undae showing subtle NE-SW-trending curvilinear features interpreted as transverse dunes, and bright SE-NW-trending wind-streaks. Kreslavsly and Bondarenko (2017).*

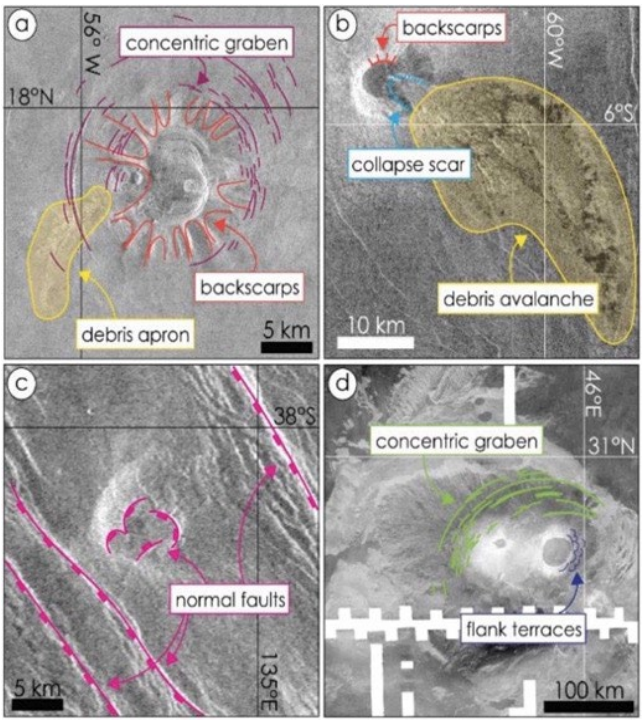

Figure 2.2.9 – *Examples of ground deformation features associated with volcanic edifices: a) landslides; b) sector collapse; c) volcano spreading; and d) volcano sagging. Radar images conform to an equirectangular project and the look direction is from the left in each image.*

Magellan's imagery also provided evidence for two dune fields (Greeley et al., 1992; 1995) and indirect evidence for putative 'micro-dunes' (Weitz et al., 1994) that were not resolved by the 100 – 200 m spatial resolution of Magellan's imagery. The surface winds evidenced by these dune fields and by wind streaks and debris fans (downwind of impact craters) are likely to be important agents of aeolian geomorphological change, but data of higher spatial and temporal resolution, and the ability to distinguish loose from consolidated surface materials, are needed to characterize them. Furthermore, the availability and production of fine-grained sediment necessary for aeolian activity and its genesis are completely unknown on the Venusian surface, and a dedicated investigation with improved data sets will be required to reveal evidence of the sources and transport and deposition of such materials. Planetary bodies (Earth, Mars, Titan and Venus), including those with extremely tenuous atmosphere, such as Pluto and comet 67P, have been shown to exhibit many aeolian landforms, such as dunes and wind-streaks (see Figure 2.2.8b) but the significance of aeolian landscape change in planetary sciences has, until recently, been under-appreciated. In particular, comparison of dune migration rates on Earth and Mars, made possible by multi-temporal, very high-

resolution imagery (cm to m), has revealed that these are, in general, lower by up to 1 m yr^{-1} on Mars than on Earth (Bridges et al., 2012)

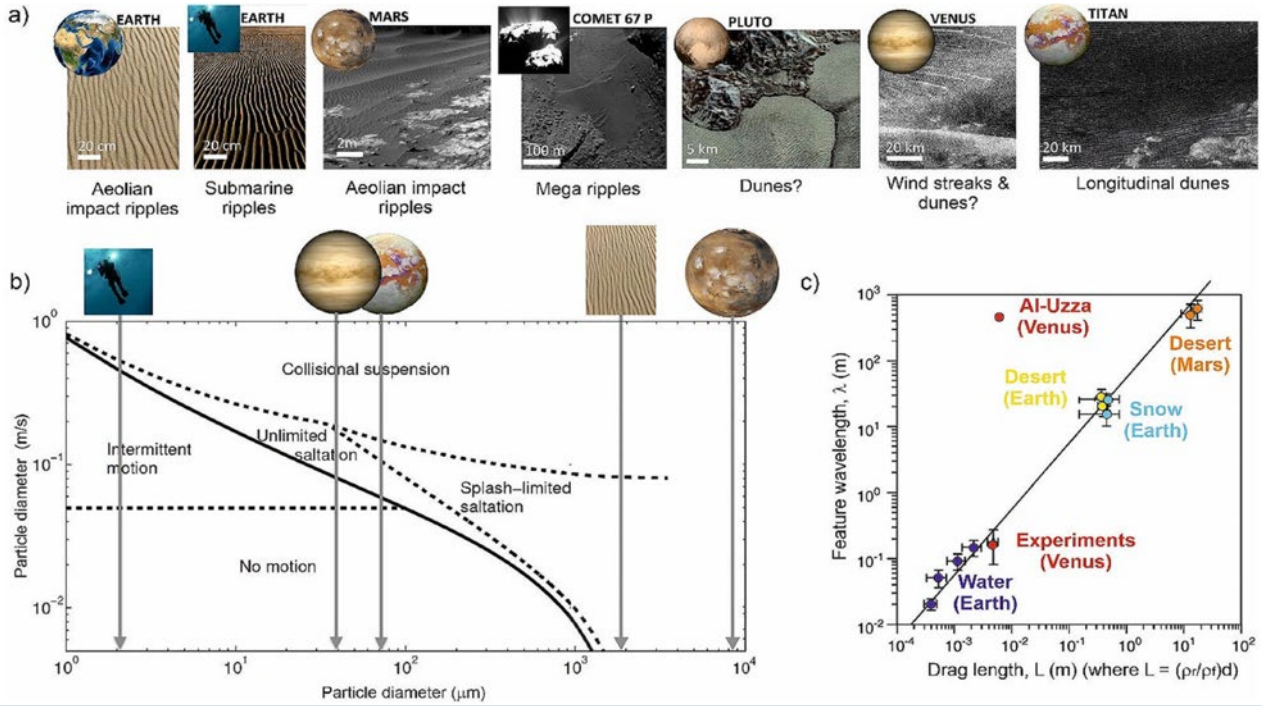

Figure 2.2.10 – *(a, top): Examples of sedimentary bedforms on various planetary bodies; (b, bottom left): Regimes and processes of sedimentary transport placing likely Venus aeolian environment in its context between submarine Earth and aeolian Earth and Mars; and (c, bottom right): scales of various sedimentary transport regimes in operation, showing expected scales of dune formation on Venus. Modified after Duran Vinent et al., (2019), Claudin and Andreotti (2006), Greeley et al. (1984), Neakrase et al. (2017) and Carpy et al. (2020).*

What are the nature, distribution and range of sedimentary surface modification processes?

On Venus, fine-grained sediments are likely produced by impact cratering and weathering. Even if these are not volumetrically large, sediments are likely widespread, covering a large fraction of the surface; aeolian erosion and deposition may be important processes at the Venus surface.

Indeed, despite low surface wind velocities (0.25-1.0 ms^{-1}), as recorded by probes (Lorenz, 2016), and thanks to the high atmospheric pressure (~90 bars), the transport of clastic material is possible by creep and saltation processes (e.g. Marshall and Greeley, 1992; Greeley and Arvidson, 1990), and thus dunes may be widespread on Venus but with typical feature sizes < 100 m, below the limit of Magellan's SAR image resolution. From experimental modelling, Venus' aeolian landforms are expected to form under conditions which lie between the regimes characteristic of 'submarine' and 'desert' environments on Earth (Figures 2.2.10b and 2.2.10c) (Claudin et al., 2006, Neakrase et al., 2017). Venus' plains may also harbour many 'micro-dunes' or small-scale ripple-like aeolian landforms. Fine grained material may also be trapped behind topographic obstacles, forming wind-streaks, and may also cause abrasion leading to wind-faceted pebbles or ventifacts. Wind-streaks and debris-fans (downwind of impact craters) are relatively large-scale features on Venus (km to tens of km in length) and they are commonly observed in Magellan images (Figure 2.2.8b; Greeley et al., 1992, 1995; Kreslavsly and Bondarenko, 2017).

Whilst impact cratering is likely the main process behind sediment production on Venus, the planet's hot, dense and highly oxidizing atmospheric conditions are likely to cause intense chemical weathering of surface materials, making them vulnerable (Santos et al, 2023). Associated with impacts, landslides and tectonic activity, these fragmented and unconsolidated weathered materials are seen to accumulate at the bases of slopes and are locally redistributed by winds into lowlands where they may form dune-fields, for example.

Lastly, the existence of sedimentary or volcano-sedimentary (i.e. pyroclastic) rocks is not excluded on the Venusian surface; a small number of volcanic deposits with bright, diffuse appearance in Magellan imagery have been proposed to have been formed by pyroclastic density currents (Ganesh et al., 2022). We would assume that potentially large accumulations of clastic material, derived from impact ejecta, explosive volcanism, landslides and potentially during early periods of water-rich environment, are subject to

diagenesis due to burial or by sintering of fines under the high temperatures at the Venus surface. Many of the Venera landers images indicate a planetary surface of flat-lying, layered rocks. *In-situ* Unconfined Compressive Stress (UCS) testing measurements from Venera 13 and 14 and Vega 2 suggest strengths of less than half of an average basalt and more like those of a sandstone (Basilevsky et al., 1985). Active research on the Venus weathering environment (Marshall et al. 1991, Waltham et al., 2008, Treiman et Schwenzer, 2009; Aveline et al., 2011; Nealley et al., 2017; Port et al., 2020) leads us to expect that the lava flows of the Venus plains are accompanied by sedimentary deposits, and that these are likely to be in various states of consolidation.

2.2.7. Understanding the role of geological activity in Venus' climate evolution

How are **tropospheric and geological processes** coupled on Venus? Do exchanges take place from direct outgassing of volatiles into the lowermost atmosphere, buffering of atmospheric species with surface reservoirs, or aeolian or chemical alteration of surface minerals?

These questions are addressed by EnVision's science objective **R1-C-10:** "Measure the variability of tropospheric composition, and study whether and how this is linked with surface geological processes and atmospheric dynamics."

Venus, Earth and Mars started life as siblings, born at around the same time in similar parts of the protoplanetary disk. After accretion, during the magma ocean phase, they would have acquired a dense proto-atmosphere dominated by carbon dioxide and steam (Figure 2.1.2). Venus has a highly enriched D/H ratio, which suggests that it has lost much of its primordial water (Donahue et al, 1982), but it is not clear whether this water was lost from a steam atmosphere phase or from a liquid ocean phase.

To understand the long-term climate evolution of Venus we need to establish (1) whether there is any morphological and compositional evidence of an epoch with abundant liquid water on the surface; (2) how geologically active Venus is now, and whether this is continuous or episodic in style, to constrain interior-atmosphere exchange throughout history; (3) search for atmospheric evidence of present day volatile sources and sinks at the atmosphere of Venus, including potential active volcanic sources; (4) determine how volatiles, in particular sulphur- and water-related, are transported through the atmosphere and how they interact with cloud layers (Figure 2.2.11). The first two investigations above – the search for morphological or compositional evidence of a water-rich epoch and the study of Venus' geological activity – have already been discussed in §2.2.5; here we will discuss the other two points below.

How do volatile delivery and loss couple tropospheric and geological processes over geological time scales?
The most variable species in the atmosphere of Venus are sulphur dioxide and water vapour. Both play a crucial role in determining climate on Venus as on Earth or Mars, and are key magmatic volatile species. Therefore, they will be a particular target of investigation for EnVision. On a geological timescale, SO_2 is thought to originate from volcanism and to be lost through reactions with surface minerals (Fegley et al., 1997; Hashimoto and Abe, 2005). Data from Vega 1 and 2 probes suggest SO_2 in the lower atmosphere of Venus is present at abundances significantly higher than predicted by the thermochemical equilibrium models (Bertaux et al., 1996). Halogen species such as HCl and HF may also play an important role throughout the atmosphere (Krasnopolsky et al., 2013; Wilson et al., 2023, and references therein).

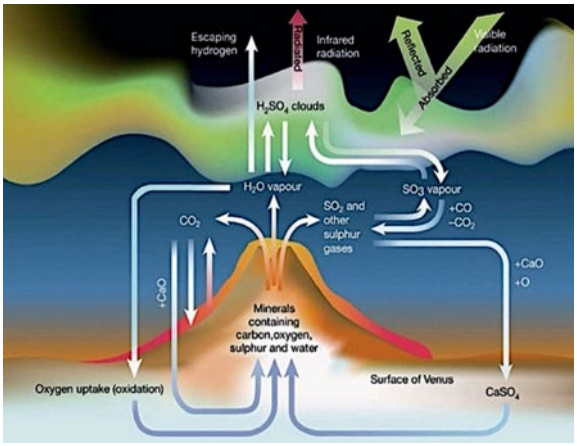

Figure 2.2.11 – *Venus has an atmosphere of 96.5% CO_2 which is primarily responsible for its greenhouse effect and high surface temperature. Venus also has a thick layer of sulphuric acid (H_2SO_4) clouds that reflect sunlight away from its surface, helping to cool it. The greenhouse warming is greater than the cooling effect of the clouds, making the surface of Venus much warmer than of Earth. Numerical models suggest that over the past 1 billion years the climate on Venus has experienced periods of both cooling and warming, largely triggered by global volcanic activity spewing out large amounts of sulphur dioxide (SO_2) and water vapour (H_2O) (Bullock and Grinspoon, 2001).*

There may be high-temperature condensate clouds of exotic composition only 1-2 km above the surface, at temperatures in excess of 400°C. This is hinted at by the radar-bright/low emissivity deposits found consistently at high altitude regions around the planet, and by particulate layers detected by Venera 13 and

14 descent probes (Grieger et al, 2003). These could be explained by condensing metal halides and chalcogenides – similar to those found emitted from volcanic vents on Earth (Brackett et al., 1995; Port et al., 2020). Searching for variations in deep atmospheric species will help constrain geophysical sources and sinks including potential active volcanic sources.

What drives present day sulphur and water chemical cycles, and what are their links to active volcanism?
Sulphur dioxide is the third most abundant gas in the atmosphere of Venus after CO_2 and N_2, with an abundance of some 150 ppm below the clouds, but its mesospheric abundance above the clouds is highly variable, ranging from < 1 to > 1000 ppbv (Encrenaz et al., 2012, 2016, 2019, 2020; Esposito et al., 1988; Marcq et al., 2013, 2020; Vandaele et al., 2017a, 2017b). The proximate cause for these variations is related to spatial and temporal fluctuations of the SO_2 supply through vertical mixing within the cloud region, since (i) SO_2 is more than three orders of magnitude more abundant below the clouds compared to cloud top level, so that the lower atmosphere acts as a large reservoir; and (ii) SO_2 exhibits, at least on the day side, a very short photochemical lifetime that allows for large horizontal and temporal contrasts to occur. However, the origin of these vertical mixing fluctuations is barely understood. Purely atmospheric phenomena such as momentum deposition from upward propagating atmospheric gravity waves, induced e.g. by topography (Kitahara et al., 2019), or diurnal variations of cloud top convection through solar absorption (Lefèvre et al., 2022), certainly play a role; but thermal destabilization of the atmospheric column through hot volcanic outgassing has also been suggested (Esposito 1984). In the region around the clouds top, photochemical reactions between CO_2, SO_2, H_2O, and chlorine compounds lead to the formation of sulfuric acid, which is the main component of the cloud particles. The chemistry of the lower atmosphere is dominated by thermal decomposition of sulfuric acid, and thermochemical cycles that include sulphur and carbon species and water vapour.

Water vapour exhibits a similar, albeit less dramatic behaviour, with abundance of ~ 30 ppmv in the lower atmosphere (Marcq et al., 2018) and variable abundance of 1 to 10 ppmv above the clouds (Cottini et al., 2015, Fedorova et al., 2016, Chamberlain et al., 2020). Water vapour also plays an important role in the transfer of heat and energy, which helps to maintain the massive greenhouse effect and drives the atmospheric super-rotation (Lee et al., 2007; Lebonnois et al., 2010, 2015; Horinouchi et al., 2020). The latter is also the key element of chemical models through the release, transport and sequestering of volatiles that drive climate changes (Bullock and Grinspoon, 2001).

2.2.8. Assessing temporal variations of the Venus atmosphere

How are volatile species, particularly water and sulphur dioxide, transported through the **cloud layers and upper atmosphere**? How much of the variability in and above the clouds is due to intrinsic dynamic variability, and how much is directly or indirectly caused by volcanic activity?

These questions are addressed by EnVision's science objectives
R1-C-30: "Measure the variability of clouds and cloud droplets, and determine whether and how this is linked with surface geological processes and atmospheric dynamics."
R1-C-20: "Measure the variability of mesospheric composition, and determine whether and how this is linked with surface geological processes and atmospheric dynamics."

What are the relationships between clouds, long-term climatology and active volcanism?
The high-resolution images of Venus' cloud deck acquired a decade ago by the Venus Monitoring Camera on board Venus Express showed, as never before, the details of convective structures and gravity waves, and how crucial those small-scale phenomena are for understanding the Venusian climate (Markiewicz et al., 2007). Our current understanding of the clouds suffers from the limitations of the available data (very few in-situ observations are available within the cloud layers), and from the lack of complete models to interpret the observations. One- and two-dimensional modelling studies on Venus clouds have been published since late 1990s (James et al., 1997; Imamura and Hashimoto, 1998, 2002), one advanced cloud model has been extensively used and developed further to study the clouds and interpret the data (McGouldrick and Toon, 2007, 2008a, 2008b). Three-dimensional simulations of the Venus photochemistry and cloud from the ground to the bottom of the thermosphere (Stolzenbach et al., 2023) are in overall agreement with most vertical profiles of minor species measured between 30 and 100 km, and cloud characteristics. In particular they reproduce the steep decrease of H_2O and SO_2 mixing ratio inside the cloud layer. Latest microphysical models

include all the main microphysical processes: homogeneous nucleation of sulfuric acid solution particles (Määttänen et al., 2018), heterogeneous nucleation through a simple parameterisation (James et al., 1997), condensation/evaporation processes and Brownian coagulation (Pruppacher and Klett, 1997). The clouds of Venus play a large role in atmospheric chemistry (serving as reservoirs of water and sulphur in the form of sulphuric acid), radiative balance (reflecting away 70% of the light falling on Venus, and absorbing much of the rest), and therefore also in the atmospheric dynamics. In the 45-65 km altitude range, sulphur and water chemical cycles are coupled through the formation of H_2SO_4-rich cloud droplets. EnVision's investigation will focus on understanding the chemical cycles and transport of SO_2, H_2O and H_2SO_4 involved in cloud forming processes.

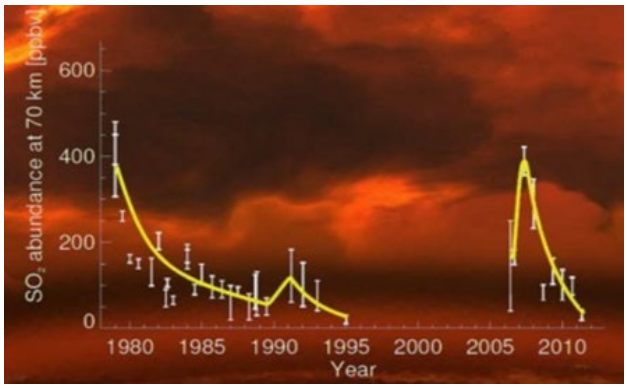

Figure 2.2.12 – *Sulphur dioxide above Venus' clouds shows episodic variations which may indicate active volcanism – but proving this link conclusively requires further data on chemical abundances in and below the clouds. This graph indicates the variation of the abundance of sulphur dioxide (SO_2) in the upper atmosphere of Venus over 40 years, expressed in units of parts per billion by volume (ppbv). A clear rise in the concentration of the SO_2 concentration was observed at the start of the Venus Express mission (2006), with a subsequent decrease. The increase in SO_2 can be interpreted as evidence for volcanic activity or for decadal-scale variations in the circulation of Venus' vast atmosphere (after Marcq et al., 2013).*

How are interannual variations of mesospheric SO_2 linked to volcanic processes?

The interannual variations of mesospheric SO_2 – sharp rises followed by gradual declines in following years – are suspected as one of the potential signs of active volcanism (Esposito, 1984, Marcq et al., 2013; Figure 2.2.12). As previously mentioned, these enhancements are associated with increased vertical mixing rather than direct volcanic injection. EnVision will carry out mapping of SO_2, H_2O and related compounds both below and above the clouds, to characterize as extensively as possible (w.r.t. latitude, local solar time, longitude) their spatial and temporal distribution, and thus help in determining whether at least some of these increases in vertical mixing are caused by transient thermally buoyant volcanic plumes.

2.3. Strategy and Science Observation Requirements to Achieve the Science Objectives

In order to achieve the EnVision science objectives outlined in the previous section, a top-down analysis has been performed, resulting in a set of science observation requirements and investigation strategies. The resulting science observation requirements specify the data products and their accuracy and sampling. In this section, this top-down analysis and the resulting requirements are described.

2.3.1. Establish the magmatic history of Venus: changes in style and volume with time, range of magma compositions (R1-H-50)

Geologic mapping of volcanic features, their surface morphology and dielectric constant

Geologic mapping of volcanic features and their surface morphology and dielectric constant is a cornerstone of Magellan data interpretation (Campbell and Campbell, 1992; Campbell, 1994). There is a need to carry this work to finer spatial scales and into the subsurface to answer fundamental questions of localized stratigraphy (from subsurface profiles and geologic mapping from images), magma composition (from morphology, roughness, and dielectric properties), surface mineralogy, order-of-magnitude eruption rates and volumes (from morphologic features and subsurface profiles), and post-emplacement weathering (from morphologic features and dielectric properties). EnVision will accomplish this objective in part through SAR imaging at 30 m and 10 m resolutions and polarimetric imaging at 30 m resolution, along with VenSpec-M surface temperature and emissivity observations.

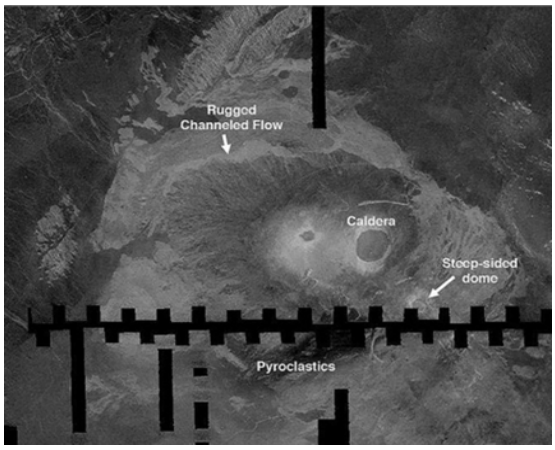

Figure 2.3.1 – *Magellan radar image of Tepev Mons, showing the range of volcanic features and eruption history within one major shield volcano.*

EnVision 30m SAR imagery will dramatically enhance our understanding of volcanic surface features. At the >120 m resolution of Magellan (120 m azimuth resolution and 93 m best case range resolution), features like flow channels are visible only where they are at the highest end of those typically seen in terrestrial flow fields, vent locations and associated ash or rugged clinkers are too small to observe, and collapsed tubes or skylights are unseen. Within any single major shield volcano, there are often a wide range of features indicative of magma storage beneath calderas, rapid eruptions that form rugged, channelised flows, fine-grained pyroclastic ash from volatile-rich eruptions, and steep-sided constructs linked with higher-viscosity magma (Campbell and Rogers, 1994; Figure 2.3.1). Targeted VenSAR imagery at 10 m resolution will bring out crucial details in the stratigraphic relationship between flows, their likely thickness, and the range of scales in flow fields (i.e., short high-volume eruptions or long-term, tube-fed complexes).

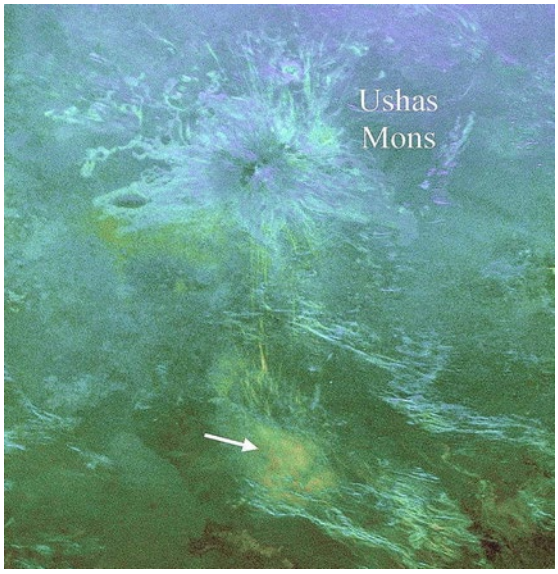

Figure 2.3.2 – *Surface roughness mapping from Earth-based polarimetric 12.6-cm radar image of Ushas Mons (400 km across) and ridge belts to the south. The color overlay is similar to the HV/HH ratio to be obtained with EnVision. Warmer colors and higher brightness represent rougher surfaces, showing differences among flow fields on Ushas. White arrow is rough debris associated with an explosive event during a geologically recent period of renewed volcanism.*

Radar backscatter is sensitive to surface roughness on horizontal and vertical scales comparable to or larger than one tenth of incoming wavelength. For the primary VenSAR HH-polarization mode of EnVision, both small-scale roughness and larger-scale topography play a role, with surfaces tilted toward the radar returning a much stronger echo than those areas which slope away from the sensor. VenSAR also collects data in HV polarization mode, which is much less sensitive to local slopes. Taking the two polarizations together, often as a ratio value, to complement the HH image, will yield significant information on surface texture not available from the HH- and VV-polarized Magellan data. The proof of concept for these observations comes from Earth-based polarimetric mapping using the Arecibo radar, which shows that information on small-scale roughness correlates Venus's lava flows with those in terrestrial settings (Campbell and Campbell, 1992), and can reveal deposits formed during recent, volatile-rich eruptions (Campbell et al., 2017; Figure 2.3.2). While ~7 km resolution Arecibo data collect same-sense (SC) and opposite-sense (OC) circular echoes, there is a high degree of correlation between the HV-to-SC and HH-to-OC power. Radiometry performed at a nadir but also off-nadir, in H and V polarizations, will also bring insights on the composition and surface roughness.

Rock Composition: Does Venus Have Granitic Rocks?

The Venus atmosphere is semi-transparent across a series of narrow atmospheric windows near 1 micron wavelength in the near infrared. Spectral analysis, using emissivity measured at these wavelengths, can be used to detect and map the composition of exposed surface materials (Figure 2.3.3). A variety of iron-bearing minerals in various oxidation states are expected in Venus's surface materials, either in fresh basalt or as chemically weathered products of basaltic rocks. Basalts on Venus are likely subject to rapid chemical weathering on exposure to the atmosphere, transforming pristine igneous silicate minerals such as pyroxene and olivine with ferrous iron (Fe^{2+}) to oxide minerals such as hematite and magnetite containing ferric iron (Fe^{3+}) (Filiberto et al., 2020). VenSpec-M emissivity spectral mapping allows effective discrimination of these minerals (Gilmore et al., 2015; Ferrari et al., 2020).

In contrast, rocks exposed at the surface which lack iron-bearing minerals are interpreted to have a felsic composition (SiO_2-rich rocks such as granite). These point to a more evolved magma source and, importantly, to the presence of water in the mantle where melting occurred which, in turn, hints at the potential presence of water at or near the planet's surface, and its likely influence in chemical and physical processes there. Mapping the distribution of felsic rocks across the surface of Venus will help reveal whether and how Venus was different in the past; whether liquid water was capable of condensing on the surface or near-surface, or whether Venus was even hotter, and once experienced a steam-atmosphere phase (Dyar et al., 2020).

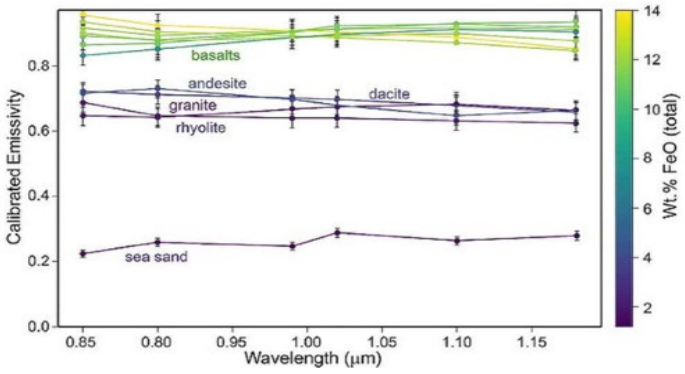

Figure 2.3.3 – *Emissivity data from high-temperature laboratory experiments performed at the Planetary Spectroscopy Laboratory of DLR in Berlin (Germany) down-sampled to the resolution of surface filters used by the VenSpec-M. Error bars represent a conservative estimate of the uncertainty of ±4% for the retrieval of emissivity from orbit including instrumental and atmospheric effects, and show that VenSpec-M can determine variations in rock composition from orbit.*

Variations in morphologic characteristics, stratigraphic relationships, and dielectric properties of plains

The volcanic plains cover around 80% of Venus. Far from being uniform, they exhibit signs of extensive geological activity, from volcanic (R1-H-50) and tectonic (R1-H-60) to aeolian and weathering (R1-A-30) processes. Did the plains form rapidly, with few flow boundaries (like lunar mare) or are they constantly reformed by small-scale volcanism, below the resolution of Magellan? Understanding and mapping stratigraphic boundaries is important in distinguishing geologically old and young units, and between directional and equilibrium surface histories. Because of the huge area covered by the plains units (> 300 million km^2, more than twice the land area on Earth), it is not planned to target all of the plains for detailed characterisation. Global coverage will be obtained for those data types which have not been obtained before at Venus (multispectral near-IR spectroscopy, and subsurface sounding). However, as we already have global imagery maps from the Magellan radar mission at low resolution (> 120 m resolution), EnVision VenSAR 30 m imagery needs only target a subset (~10%) of the plains, chosen to include representative samples of all known features and terrain types. The targeting strategy is explained in Section 3.2.

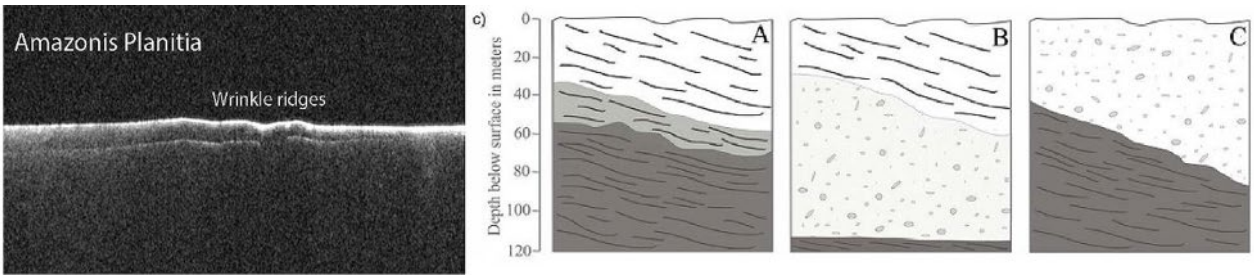

Figure 2.3.4 – *(a, left): A SHARAD radargram showing layering about 100 meters thick in Amazonis Planitia warped by wrinkle ridges. The image is 400 km across (Campbell et al., 2008). (b, right): Schematic representation of the three potential scenarios of subsurface stratigraphy interpreted from SHARAD radar sounding of volcanic layering in the Arsia Mons caldera; A – stacked lava flows with vesiculated and less dense flows overlying very dense lava; B – less dense lava-flow and a thick tephra deposit overlying denser bedrock; C – pyroclastic or other low-density material deposited over dense lava-flows in the southern part of the caldera, adjacent to the wall (Ganesh et al., 2020; Watters et al., 2006).*

The Subsurface Radar Sounder will be used to look for layering in the plains and elsewhere on Venus, as has been successfully done on both the Moon and Mars. Indeed, Lunar Radar Sounder (LRS) has successfully revealed and mapped several periods of flood basalts in the Lunar subsurface (Ono et al., 2009; Kobayashi et al., 2014). The sub-horizontal parallel layers of materials of differing densities, at multiple depths and different thicknesses, observed at several locations, have allowed the establishment of a series of volcano-stratigraphic units related to distinct flood-basal eruption periods. The SHAllow RADar (SHARAD) instrument has been used to similar effect on Mars (Ganesh et al., 2020; Watters et al., 2006), to interpret the organization of stacked lava flows and pyroclastic deposits, from their differing densities and 3-dimensional organization (Figure 2.3.4). Analyses of this type enable a far better understanding of Venus's recent geological past and reveal vital information about the character, thickness and mode of resurfacing on Venus. As illustrated in the figure, layers to be investigated are typically a few tenths up to 100 m in thickness, and

reach down to several hundred meters into the planet crust. For example, catastrophic resurfacing models for Venus (Strom et al., 1994) predict that the plains were resurfaced in a brief epoch several hundred million years ago. In such a model, there might not be sufficient time between lava flows to develop thick weathering layers that would produce discrete layered returns in SRS data. If SRS does detect clear layering in the plains, it would tend to favour more gradual resurfacing models for Venus.

This investigation will be carried out using VenSAR imaging, polarimetry and radiometry, working closely with Surface composition from VenSpec-M, subsurface structures from SRS, to understand the magmatic history of Venus.

On the basis of the top-down analysis above, the science observation requirements defined to address this EnVision science objective R1-H-50 are listed in Table 2.3.1

Table 2.3.1 – *EnVision science observation requirements addressing Venus magmatic history.*

R2-H-10	Obtain **regional SAR imagery surface mapping**, resolving features at a **spatial resolution < 100 m** and a **geographical coverage >100s km**.
R2-H-20	Obtain **targeted SAR imagery surface mapping**, resolving features at a **horizontal resolution ≤ 10 m** and a **geographical coverage > 10s km**.
R2-H-30	Measure **surface topography** (1) **regionally** (at least 20% of the planet) by means of **stereo radar imaging** on **selected RoIs** (yielding an elevation **accuracy less than ≤ 80 m for 85% of the data** and **horizontal resolution ≤ 300 m**); and (2) **globally** (**at least 65%** of the planet) by means of **nadir altimetry** (**vertical resolution < 10 m** and **along-track resolution ≤ 6 km**).
R2-H-35	**Map locally** (over selected **Regions of Interest and at least 1% of the planet**) the **microwave emissivity in V and H polarization** using passive off-nadir (incidence angle > 25°) radiometry, with an **accuracy < 2 K** and **a horizontal resolution < 50 km**.
R2-H-40	Characterize **surface polarimetric reflection properties** for **selected SAR regions** at a **horizontal resolution < 30 m**.
R2-H-50	Obtain a global (**≥75% of the planet) map** of the **microwave emissivity** using passive radiometry with a **precision < 1.0 K** and an absolute radiometric **accuracy < 2.0 K**.
R2-H-60	Characterize **near-IR emissivity** of surface targets **over 60% of the planet surface** with a **relative emissivity uncertainty < 4% at a spatial resolution < 100 km**.
R2-H-70	Search for **subsurface material boundaries down to 1000 m** of the crust over **at least 65% of the planet surface**, with a **vertical resolution of ~20 m, an across-track resolution of ≤11 km , and an along-track resolution of ≤ 3 km**.
R2-A-20	Detect and characterize **changes in surface radar imagery** in selected **Regions of Interest (RoI)** that include the areas with high probability of volcanic and seismic activity with a **horizontal resolution < 100 m**.

2.3.2. Establish the tectonic history of Venus: magnitude of deformation, implications for lithospheric thickness and heat flow (R1-H-60)

Mapping of tectonic structures

Magellan observations provide a valuable overview of tectonic processes on Venus (Solomon et al., 1992), but are limited by the resolution of the radar images and especially the topography (10-30 km). VenSAR's much higher horizontal resolution: 10-30 m imagery, 300 m horizontal resolution of the SAR stereo Digital Elevation Model (DEM) will enable much clearer definition of the styles of tectonic deformation and of the superposition and cross-cutting relationships used by geologists to map the sequence of deformation in a given region.

The high-resolution radar data is particularly essential in understanding the tesserae of Venus, which contain fine-scale, complex patterns of deformation (Figures 2.1.3, 2.2.3). We need to understand whether the tesserae represent thick, ancient remnants of deformed and deep-rooted continental crust. The tesserae may also hold clues to the nature of past resurfacing; particularly whether there have been periods of enhanced crustal mobility, or whether Venus has been in its current state for most of its history. We expect that tesserae represent the oldest terrain, locally, but they may not have all formed at the same time; better understanding of their structure and arrangement, their relationship with volcanic terrains and their correlation from one place to another would help to unravel these temporal and structural conundrums. Magellan imagery revealed very varied tesserae interiors often with complex arrangement of solid and deformed rocks, blanketed by finer grained or smoother materials (Hansen and Willis, 1996, Ivanov and Head, 2011) but without greater spatial resolution and better topographic detail, the nature of the materials and their origins could not be resolved. Multi-polarimetry observations (HH and HV) are needed to better understand their surface textures and physical structures, to reveal emissivity variations of solid lithologies and to discriminate them from unconsolidated materials.

Relative age dating is particularly important and helpful, in the absence of independent absolute age data, in understanding the mode and sequence of formation of near-surface layers and structures. We ask whether the tesserae are always the oldest terrain, overlapped and overlain by plains materials, for instance? Or, what are the stratigraphic relationships between all the terrain types? Does Venus have a global stratigraphic, sequential organization, or many different sequences in different regions? This science objective thus has significance across many of the other objectives because the relationships between terrain types are poorly constrained. To assist this effort, high-resolution imagery is placed within the context of larger contiguous areas imaged at medium resolution. This approach is known to be successful in establishing the morphological details of inter-relationships between spatially separated strata and other geological units. These goals will be achieved by VenSAR regional mapping at 30 m (to resolving features < 100 m in scale over >100s km in extent), targeted mapping at 10 m (resolving features > 30 m in scale), measurement of surface topography (through stereo radar imaging and near-global nadir altimetry), characterizing of polarimetric reflection properties of surface materials, near-infrared spectral surface imaging by VenSpec-M, and SRS subsurface imaging of material boundaries (within upper few hundred meters of the crust). Since this science objective focuses on the boundaries and physical, chronological relationships between terrain types, attention will be aimed at regions where multiple terrain types are in close association.

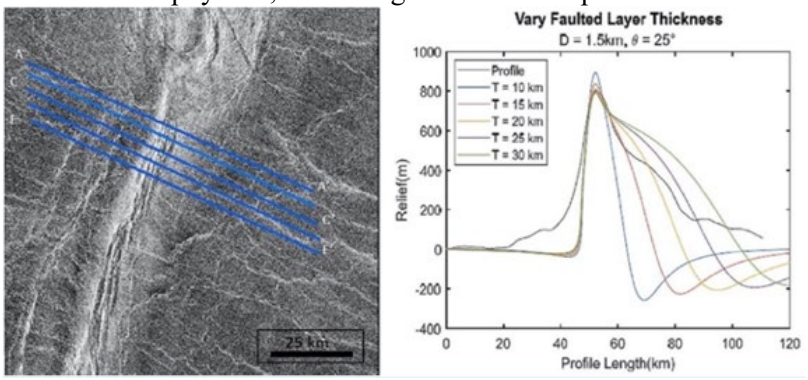

Figure 2.3.5 – *(a, left): A Magellan radar image across the Vedma Dorsa ridge belt. (b, right): Elastic dislocation modelling of thrust faulting in Vedma Dorsa. The black line is the observed topography (averaged for the 5 profile lines on the left image). The various colour lines represent the topography produced by thrust faulting terminating at various depths below the surface (Moruzzi and Kiefer, 2023).*

Quantitative modelling of deformation caused by faulting and folding and determining litospheric thickness and heat flow

It is generally assumed that highly deformed crustal plateaux are In the isostasy regime, where the weight of the topography is balanced by a crustal root floating over a higher-density mantle, and that the geologic processes responsible for their formation are no longer taking place. However, their origin, structure, and evolution are still topics of great debate (Maia and Wieczorek, 2022). The combination of high-resolution VenSAR radar imagery for mapping structural geology and VenSAR high-resolution topography for quantitative modelling of tectonic processes will be particularly valuable to improve the mapping and modelling of the Venus surface and crust. Quantitative modelling of deformation caused by faulting and folding can constrain the physical processes that produced the observed landforms, the magnitude of the deformation, the orientation of the stress field that created the deformation, and the mechanical structure of the crust and lithosphere in the vicinity of the tectonic structure. In turn, mechanical structure can be interpreted in terms of chemical layering (crust and mantle) and temperature (thermal gradient and heat flow). Figure 2.3.5 shows an example of such modelling (Moruzzi and Kiefer, 2023), which is only possible in a limited number of regions of Venus using Magellan topography. Higher resolution VenSAR imaging data will permit such modelling for representative examples of all major types of tectonic structures. This will be supplemented by RSE gravity observations, which give information needed to constrain the thickness and size of major surface and internal layers of the planet.

This investigation will be carried out using VenSAR imaging, polarimetry and radiometry, working closely with surface composition from VenSpec-M, subsurface structures from SRS and gravity mapping from RSE, in order to understand the evolution of lithospheric thickness and planetary heat flow with time.

On the basis of the top-down analysis above, the science observation requirements defined to address this EnVision science objective R1-H-60 are listed in Table 2.3.2.

Table 2.3.2 – *EnVision science observation requirements addressing Venus tectonic history.*

R2-H-10	Obtain **regional SAR imagery surface mapping**, resolving features at a **spatial resolution < 100 m** and a **geographical coverage >100s km**.
R2-H-20	Obtain **targeted SAR imagery surface mapping**, resolving features at a **horizontal resolution ≤ 10 m** and a **geographical coverage > 10s km**.

R2-H-30	Measure **surface topography** (1) **regionally** (at least 20% of the planet) by means of **stereo radar imaging** on **selected RoIs** (yielding an elevation **accuracy less than ≤ 80 m for 85% of the data** and **horizontal resolution ≤ 300 m**); and (2) **globally** (**at least 65%** of the planet) by means of **nadir altimetry** (**vertical resolution < 10 m** and **along-track resolution ≤ 6 km**).
R2-H-35	**Map locally** (over selected **Regions of Interest and at least 1% of the planet**) the **microwave emissivity in V and H polarization** using passive off-nadir (incidence angle > 25°) radiometry, with an **accuracy < 2 K** and **a horizontal resolution < 50 km**.
R2-H-40	Characterize **surface polarimetric reflection properties** for **selected SAR regions** at a **horizontal resolution < 30 m**.
R2-H-50	Obtain a global (**≥75% of the planet) map** of the **microwave emissivity** using passive radiometry with a **precision < 1.0 K** and an absolute radiometric **accuracy < 2.0 K**.
R2-H-60	Characterize **near-IR emissivity** of surface targets **over 60% of the planet surface** with a **relative emissivity uncertainty < 4% at a spatial resolution < 100 km**.
R2-H-70	Search for **subsurface material boundaries down to 1000 m** of the crust over **at least 65% of the planet surface**, with a **vertical resolution of ~20 m, an across-track resolution of ≤11 km , and an along-track resolution of ≤ 3 km**.
R2-H-80	Measure the **gravity field** of the planet with **spatial resolution of < 270 km**; **accuracy of < 0.2 mm/s² globally**; improved **higher spatial resolution of < 200 km**; **accuracy of < 0.1mm/s² over >40% of the planet;** and the **k2 Love number** with an accuracy of **0.01**.

2.3.3. Characterize surface modification processes: impact crater modification, low emissivity/radar-bright highlands (R1-H-10)

Impact crater modification

The only method for determining the absolute age of a surface, in the absence of measurement of radioactive isotopes, is through the use of crater counts. Because Venus has so few craters it is difficult, or impossible, to reliably distinguish the age of different geological units using craters alone. However, craters on Venus are modified to varying degrees, first by loss of radar-dark halo, and then by infilling, causing dark floors. Some are also modified volcanically or tectonically (Izenberg et al., 1994). Because initial crater depth depends on crater diameter, the extent to which a particular crater deviates from the expected depth-diameter relationship provides a guide to post-impact infilling by lava or sediments at that crater. The height of the crater's rim above the surrounding terrain similarly provides a guide to the thickness of post-impact fill in the crater's ejecta blanket. Initial estimates of crater fill with Magellan data (Herrick and Rumpf, 2012) was limited by the accuracy of the available stereo topography digital elevation model. In contrast, VenSAR stereo observations will be optimized to produce high resolution DEMs (Section 3.3.2), and VenSAR and SRS nadir altimetry profiling will provide global topographic data. Possible direct measurements of crater infilling with the SRS sounding radar will be complementary to topography-based estimates of crater fill thickness. Craters are globally distributed, so such measurements can provide important new information about the global resurfacing history of Venus.

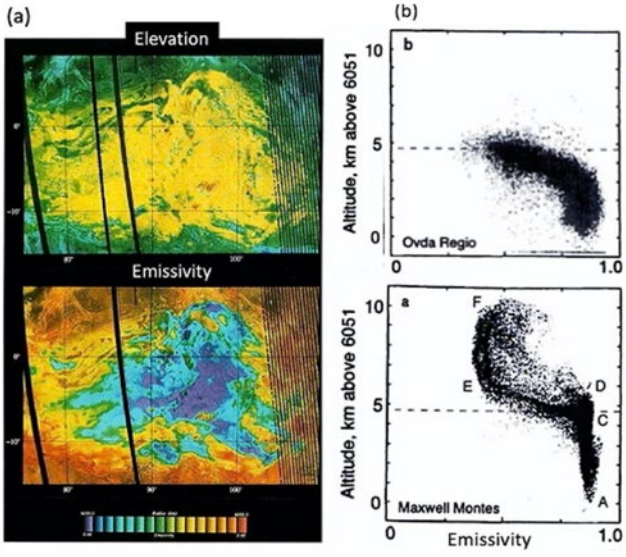

Figure 2.3.6 – *(a, left): Magellan SAR image of Ovda Regio, overlain (in false color) with the relief (top) and the emissivity (bottom). Odva Regio displays anomalously low values of emissivity. Figure from Pettingill et al. (1992). (b, right): Scatterplots of emissivity vs altitude for two mountainous regions on Venus (Maxwell Montes and Ovda Regio). Adapted from Klose et al. (1992).*

Low emissivity/radar-bright highlands

The low microwave emissivity and high radar brightness of some highlands is an enduring puzzle about Venus. It is not yet established whether these anomalous microwave properties are due to a locally extremely high dielectric constant or to volume scattering in the subsurface. It is even less clear whether they are due to rock chemistry or the deposition of atmospheric precipitates made possible by the cooler temperatures of the highlands. These anomalous radar properties have a strong dependence on altitude (Figure 2.3.6), suggesting a possible relationship to atmospheric temperature.

Two possible explanations for the unexpected low emissivity values (and concurrent high radar reflectivity) of Venusian highlands have been advanced (Pettengill et al., 1992): (1) emission from a highly reflective surface having a bulk dielectric permittivity of the order of 80; or (2) emission from a low-loss medium having a usual permittivity (of order 5) but containing many voids and/or heterogeneities responsible for efficient scattering in the subsurface volume and therefore for the observed decrease in emissivity. The EnVision mission will distinguish between these hypotheses thanks to the VenSAR radar polarimetry, both active and passive. Polarimetry radiometry, in particular, will provide a direct measurement of the effective dielectric constant of a set of Venus highlands that are included in the RoIs of the mission. Associated with active polarimetry, it will bring key insights into the surface roughness and degree of volume scattering in the subsurface of these regions. The composition of the highlands will also be globally characterized in terms of VenSpec-M near-IR and microwave emissivities; their variations will be investigated as a function of topography, which will be available nearly globally by means of VenSAR and SRS nadir altimetry and/or regionally with VenSAR stereo radar imaging. All these measurements together will help identify the alteration mechanism(s) at play at high altitudes on Venus.

This investigation will be carried out using VenSAR imaging, polarimetry, radiometry and altimetry/SAR stereo, working closely with surface composition from VenSpec-M, and surface and subsurface properties from SRS. Detailed imaging, SRS sounding and higher resolution topography data will constrain the processes that have modified or obliterated craters on Venus and the thickness of material that have apparently filled them.

On the basis of the top-down analysis above, the science observation requirements defined to address this EnVision science objective R1-H-10 are listed in Table 2.3.3.

Table 2.3.3 – *EnVision science observation requirements addressing Venus's surface modification processes.*

R2-H-10	Obtain **regional SAR imagery surface mapping**, resolving features at a **spatial resolution < 100 m** and a **geographical coverage >100s km**.
R2-H-20	Obtain **targeted SAR imagery surface mapping**, resolving features at a **horizontal resolution ≤ 10 m** and a **geographical coverage > 10s km**.
R2-H-30	Measure **surface topography** (1) **regionally** (at least 20% of the planet) by means of **stereo radar imaging** on **selected RoIs** (yielding an elevation **accuracy less than ≤ 80 m for 85% of the data** and **horizontal resolution ≤ 300 m**); and (2) **globally** (**at least 65%** of the planet) by means of **nadir altimetry** (**vertical resolution < 10 m** and **along-track resolution ≤ 6 km**).
R2-H-35	**Map locally** (over selected **Regions of Interest and at least 1% of the planet**) the **microwave emissivity in V and H polarization** using passive off-nadir (incidence angle > 25°) radiometry, with an **accuracy < 2 K** and **a horizontal resolution < 50 km**.
R2-H-40	Characterize **surface polarimetric reflection properties** for **selected SAR regions** at a **horizontal resolution < 30 m**.
R2-H-50	Obtain a global (**≥75% of the planet) map** of the **microwave emissivity** using passive radiometry with a **precision < 1.0 K** and an absolute radiometric **accuracy < 2.0 K**.
R2-H-60	Characterize **near-IR emissivity** of surface targets **over 60% of the planet surface** with a **relative emissivity uncertainty < 4% at a spatial resolution < 100 km**.
R2-H-70	Search for **subsurface material boundaries down to 1000 m** of the crust over **at least 65% of the planet surface**, with a **vertical resolution of ~20 m, an across-track resolution of ≤11 km , and an along-track resolution of ≤ 3 km**.

2.3.4. Constrain the size of the major internal layers (crust/lithosphere, mantle, core), and the physical state of the core (R1-H-70)

The Lithosphere and Crust thickness

Measurements of the lateral variations in the strength of a planet's gravity field is an important tool in probing the subsurface structure of a planet. Regional differences in elevation can be supported by differences in crustal thickness, by flexure of the elastic lithosphere, and/or by convective flow in the mantle. These mechanisms can in turn be distinguished by their expected gravity signatures, resulting in estimates of the thickness of the crust and elastic lithosphere in different regions of Venus.

Crustal thickness variations can measure the integrated amount of volcanism over time and thus provide tests of thermo-chemical evolution models, but can also sometimes be the product of extensional or compressional tectonism. Crustal thickness also affects the stratification of mechanical strength in the lithosphere and thus can also affect the style of tectonic deformation. *Elastic thickness* is related to the thermal state of the lithosphere, and its estimate allows to compute a value of local heat flow prevailing during the relief

formation, assuming a crustal composition and strain rate (see McNutt, 1984). The analysis of the lithosphere thickness and its lateral variation is therefore an important component to understand the mechanism of heat transfer.

Crustal and elastic thicknesses are evaluated using joint gravity and topography field analysis. As shown in a recent study over major crustal plateaus (Maia and Wieczorek (2022)), the outcomes vary with the employed analysis techniques (see Figure 2.3.7). The resolution of Magellan gravity field induces large error bars and over some regions even prevents to use these techniques.

Determining lithospheric thickness with gravity data is particularly sensitive to data at wavelengths of less than 500 km. Unfortunately, the Magellan solution of the Venus gravity field is poorly resolved in large areas, in particular in the Southern hemisphere (Figure 3.3.12), which has limited our ability to assess the thermal evolution of Venus. Combining Magellan and EnVision RSE gravity data would allow determination of the gravity field over at least 95% of the planet, with an average spatial resolution better than 200 km, and an accuracy better than 20 mGal. Such spatial resolution and global coverage are required to better understand the crustal and lithospheric structure of the main volcano-tectonic features of Venus (coronae, large volcanoes, ridges, tesserae, rifts etc), using both RSE gravity and VenSAR topography fields (Figure 2.3.7).

The Deep Interior

Understanding the thermo-chemical evolution of Venus requires knowledge of its internal structure and thermal state. Our current knowledge of the internal structure of Venus is based on a limited set of data such as mass, radius, gravity and topography. A directly existing constraint on the internal structure and thermal state is provided by the tidal Love number k_2 estimated from the Doppler tracking of Magellan and Pioneer Venus Orbiter ($k_2 = 0.295 \pm 0.066$ after Konopliv and Yoder, 1996). Due to uncertainties, however, even the distinction between a liquid and solid core cannot be determined (Dumoulin et al., 2017). The absence of a current internal magnetic field is not a limitation, since both a liquid and a solid core are compatible with this observation (Stevenson, 2003). Most current models of internal structure therefore consider Venus to be only a rescaled Earth, although these two planets have followed very different geological and climatic evolution.

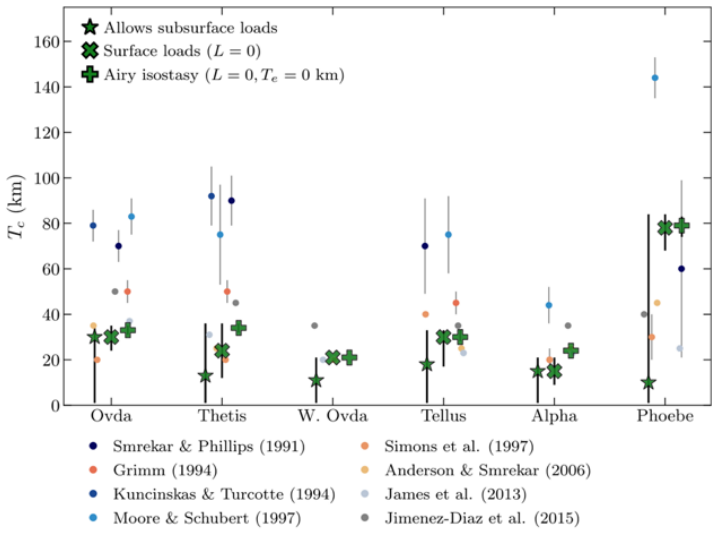

Figure 2.3.7 – *Estimates of crustal thickness over major crustal plateaus by different authors, assuming various topographic support and using different techniques and/or data sets (figure from Maia and Wieczorek, 2022).*

For the thermal state, estimates of the current temperature distribution in the interior of Venus vary widely and the published temperature profiles for the interior of Venus differ by up to 500 K in the upper mantle and 1000 K in the lower mantle (e.g., Steinberger et al., 2010; Armann and Tackley, 2012) with different implications for cooling and volcanic history (see Figure 2.2.4). Indirect information about the thermal state of Venus is obtained from its volcanic activity or when it has subsided – today's high temperatures mean a greater probability of ongoing volcanism, while low temperatures may suggest that Venus is not volcanically active. This relationship is ambiguous, since the volatile content in planetary interiors strongly influences the melting temperature. A further independent indication is given by the mantle viscosity, which is strongly related to the temperature and water content in the mantle (both of which reduce viscosity).

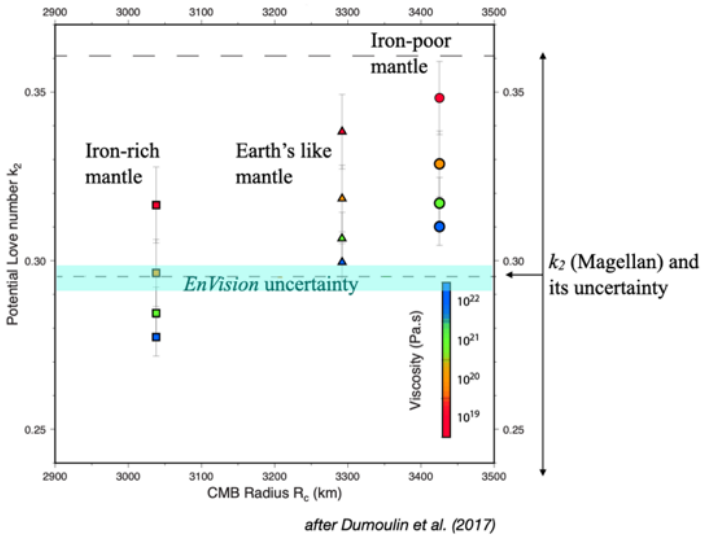

Figure 2.3.8 – *Expected k_2 Love number in function of core radius for different models of mantle composition and viscosity. The actual value with its uncertainty is displayed on the right side. The expected accuracy for EnVision (1%) is shown with the blue area, assuming the same k_2 value (Dumoulin et al., 2017).*

EnVision will provide accurate RSE gravity measurements (Figure 2.3.8). The potential Love number, related to the deformation response to the tidal force of the Sun, helps to determine the state of the core and, in the case of a liquid core, also its size. On other space missions to Mercury, Mars and the Moon, these parameters have already been determined with varying degrees of accuracy, and it has been shown that they can be used to delimit the internal structure: the measured k_2 is an indicator of a liquid (or partially liquid) core for Moon (Williams et al., 2014), Mercury (Margot et al., 2018) and Mars (Yoder et al., 2004). Furthermore, for Mars the core size and the amount of volatile components such as sulphur were restricted (Rivoldini et al., 2011) and via the phase lag also the viscosity profile in its mantle (Plesa et al., 2018).

The estimate of k_2 is important for the state of the core and its size. Dumoulin et al. (2017) investigated the viscoelastic tidal response of Venus, taking into account different compositional, temperature and viscosity profiles for the interior. They show that the determination of k_2 with an error of less than 0.01 allows us to distinguish between different classes of interior conditions. Love numbers higher than 0.27-0.28 would indicate that the core is partially or completely liquid. A high value of k_2 (> 0.34) indicates the existence of a large core (Rc > 3300 km) and favours an Earth-like composition or a low FeO content.

The investigation of the interior relies largely on gravity mapping, achieved using precise radio tracking of the spacecraft, combined with high accuracy altimetry achieved with SAR and SRS instruments. EnVision will better constrain the interior structure and the state of the core by measuring the k_2 Love number.

On the basis of the top-down analysis above, the science observation requirements defined to address this EnVision science objective R1-H-70 are listed in Table 2.3.4.

Table 2.3.4 – *EnVision science observation requirements addressing the size of the major internal layers (crust/lithosphere, mantle, core), and the physical state of the core.*

R2-H-30	Measure **surface topography** (1) **regionally** (at least 20% of the planet) by means of **stereo radar imaging** on **selected RoIs** (yielding an elevation **accuracy less than ≤ 80 m for 85% of the data** and **horizontal resolution ≤ 300 m**); and (2) **globally** (**at least 65%** of the planet) by means of **nadir altimetry** (**vertical resolution < 10 m** and **along-track resolution ≤ 6 km**).
R2-H-80	Measure the **gravity field** of the planet with **spatial resolution of < 270 km**; **accuracy of < 0.2 mm/s² globally**; improved **higher spatial resolution of < 200 km**; **accuracy of < 0.1mm/s² over >40% of the planet;** and the **k2 Love number** with an accuracy of **0.01**.

2.3.5. Constrain styles and occurrence of recent volcanism on Venus (R1-A-10)

The EnVision mission's activity investigations will seek to address changes on the timescale of months, as well as changes over longer timescales from years to decades, by comparison between EnVision's feature mapping (expected to be obtained 2035-2039) and those of the Magellan radar orbiter active imaging data (obtained 1990-1992). Answers will be provided by searching for its morphological, thermal and volatile signatures in repeated observations of the surface and of the atmosphere.

Detecting volcanic activity in repeated SAR images (change detection)

Detection and characterization of relatively large eruptions over the past 40 years will be achieved in three ways; i) any new, large lava flows (> 200 m wide and 100s m long) erupted since the Magellan mission and lying within EnVision's mapped area will likely be revealed in the first imaging of that area, ii) any large scale changes to the morphology of volcanic edifices will also be revealed within EnVision cycles, and iii)

any new, small lava flows (> 60 m wide and at least a few hundred meters long) erupted in the 4-year duration of the EnVision mission. Detected changes (and 'non-detections') will be used to place bounds on the volcanic activity rate, as described in Lorenz et al. (2015). The recent discovery of intra-Magellan volcanic change (Herrick and Hensley, 2023) and the estimation of likely rates of volcanism based on Earth examples and Earth-Venus scaling (Byrne and Krishnamoorthy, 2023; van Zelst, 2023) suggest we should expect to detect a significant number of changes to volcanic features since the time of Magellan, as well as 10s to 100s of eruptions during the period of the mission.

Searching for surface and near-surface temperature anomalies and/or changes

In addition to VenSAR imaging, temperature signatures associated with volcanic activity from both hot lava and hot volatile gasses will be detected and monitored in the infrared (VenSpec-M) and microwave (VenSAR radiometry) domains. Temperatures associated with volcanic eruptions can range from only 500°C, for low viscosity carbonatite lava, to well over 1000°C, for ultramafic lavas. Such young, hot lavas will be directly detectable by their signature in IR emissivity data (provided lava outflows cover an area of at least 0.1 km^3). Cooling rates at the surface are estimated to be on the order of hours (Mueller et al., 2017), but microwaves offer the prospect of sensing the shallow subsurface and thus may detect warmth from old lava flows, i.e. lava flows which have cooled at the surface possibly years ago and thus have no more IR emission signature but are still hundreds of K above ambient at depth (Lorenz et al., 2016). VenSAR polarimetric radiometry measurements (used to determine whether candidate areas have anomalous emissivity rather than high physical temperature) and a better knowledge of the topography (and therefore of the altitude-dependence of the surface physical temperature) will greatly enhance the reliability of the volcanic detection and monitoring. Hotspots may also be revealed through the detection of temporal changes in the surface IR or microwave brightness temperature, either at decadal (Magellan-EnVision comparison over 40 years) or yearly (EnVision inter-cycle comparison) time scales.

Detection of volcanogenic gas and particulate plumes

Sulphur dioxide variations in the mesosphere have been attributed as possible evidence of volcanic activity (Esposito, 1984), but they also could be due to intrinsic dynamic variability of the atmosphere, associated with temporal changes in transport of SO_2 from troposphere (where it is highly abundant) to mesosphere (where it is detected). On the other hand, volcanic gas plumes in the troposphere (below the clouds) would have quite a distinct signature, with distinct plumes advecting with the prevailing East-to-West winds. Water vapour is likely to be a better tracer of volcanic activity than sulphur dioxide, because it is less abundant in the Venus atmosphere than SO_2, and because it can be mapped by VenSpec-H at three different altitudes in the troposphere using different spectral bands on the nightside.

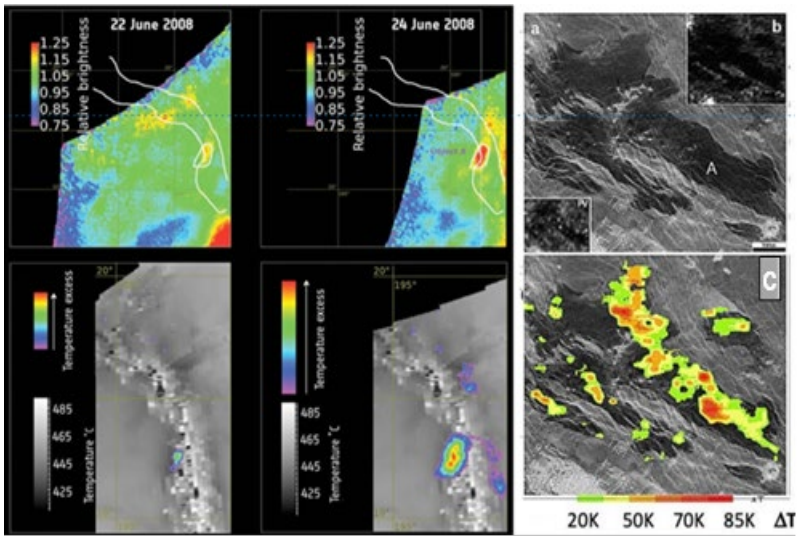

Figure 2.3.9 – *(a, left): Four transient hotspots were detected by Venus Express in the Ganiki Chasma rift zone in Atla Regio. Changes in relative brightness (top row) and changes in temperature (bottom row) are shown between 22 and 24 June 2008. The bottom row shows the temperature excess compared with the average surface background temperature. Taking into account atmospheric effects, the hotspot is likely about 1 square km with a temperature of 830°C (Shalygin et al., 2015). (b, top right): Magellan SAR image of Bereghinia Planitia. (c, bottom right): calculated DT overlaid on Magellan SAR image, using Magellan microwave radiometry observations (Bondarenko et al., (2010). Bondarenko et al. identified a large lava flow in Bereghinia Planitia, which is 60–80 K warmer than its surroundings, suggesting that this flow was already present in Pioneer Venus data, acquired around 15 years before Magellan. However, this detection is still debated as it could be due to regionally high emissivity.*

Analyses of Venus Express data found no evidence of tropospheric water vapour variations (Bézard et al., 2009, 2011), but these analyses represent data only from a few days and, due to low spectral resolution, could only determine water vapour to a fairly wide range of 25 – 40 ppmv. The nominal column mass of volcanic gasses in the Venus atmosphere, integrated from surface to space, is ~200 kg m^{-2} for SO_2, ~10 kg m^{-2} for H_2O

and ~0.1 kg m^{-2} for HDO. If the composition of Venus volcanic gasses is the same as on Earth, provided that plume dispersion does not exceed 10^4 km^2, the limiting spatial resolution induced by cloud scattering, then a large, Pinatubo-size eruption (a 2.5 km caldera, and ash plume reaching up to above 30 km altitude on Earth) would change H_2O abundance, D/H ratio, and SO_2 abundance, respectively, by ~+30%, -30%, and +1%. The latter effect may be underestimated with respect to the others, both because the Venusian interior may be much drier than Earth's, and because the outgassed SO_2/H_2O ratio is expected to be higher for a given magma volatile content due to Venus' high atmospheric pressure (Gaillard and Scaillet, 2014). Furthermore, for more typical size volcanic eruptions, the delta H_2O abundances are expected to be on the order of 10% (Realmuto and Worden, 2000; Sioris et al. 2016).

Search for volcanic activity will be carried out using a combination of repeated VenSAR imaging, repeated VenSAR (polarimetric) microwave and VenSpec-M infrared temperatures and thermal emission mapping, and repeated VenSpec-H tropospheric gas. Non-detections as well as detections will narrow the possible volcanism rates for Venus.

On the basis of the top-down analysis above, the science observation requirements defined to address this EnVision science objective R1-A-10 are listed in Table 2.3.5.

Table 2.3.5 – *EnVision science observation requirements addressing the style and occurrence rate of current day volcanism on Venus.*

R2-H-60	Characterize **near-IR emissivity** of surface targets **over 60% of the planet surface** with a **relative emissivity uncertainty < 4% at a spatial resolution < 100 km**.
R2-A-10	Detect and characterize spatial and temporal anomalies of the **surface and near-surface temperature** with a precision of **1 K** over time scales **from hours to years** and **spatial resolution < 100 km**.
R2-A-20	Detect and characterize **changes in surface radar imagery** in selected **Regions of Interest (RoI)** that include the areas with high probability of volcanic and seismic activity with a **horizontal resolution < 100 m**.
R2-C-10	Map **tropospheric gases** at **0-45 km altitude**: (1) H_2O partial column random accuracy: < 10% (and < 20% below 15 km altitude) (2) HDO partial column random accuracy: < 20% (and < 30% below 15 km altitude) (3) CO partial column ratio: < 14% (4) OCS partial column ratio: < 18% (5) SO_2 partial column ratio: < 30% at a **horizontal resolution of < 100 km (and < 200 km for H2O and HDO below 15 km altitude)**, to detect gradients related to surface-atmosphere and cloud interaction processes.

2.3.6. Characterize geomorphological changes by mass-wasting and aeolian processes (R1-A-30)

Understanding the range and scope of mass-wasting processes (landslides)

Though Magellan imagery showed us evidence of mass-wasting and aeolian features, it was not able to reveal their temporal changes during the mission's lifetime, so their geomorphological and temporal properties remain unknown, and we have almost no information about weathering, surface alteration or other aeolian processes. Since there is currently no constraint on the mechanisms and rates at which these processes might be occurring, better topography and nested imaging at multiple resolutions, and repeated imaging during the mission, are needed.

Malin (1992) estimated that at least one large landslide (5–10 km runout distance) should, somewhere on the planet, occur per year if activity rates on Venus are comparable to those on Earth. That such activity was not detected in Magellan data may be a consequence of differing imaging geometries and limited spatial resolution from each cycle, and not a lack of landslides. Higher resolution, VenSAR SAR imagery observations, with consistent geometry, should reveal many smaller features and better resolve the morphology of features that were not resolved by Magellan. Repeated VenSAR SAR imagery observations of regions expected to be active, e.g. along rifts, will help to characterize processes operating at decadal (Magellan-EnVision comparison over 40 yrs) and yearly (EnVision inter-cycle comparison) time scales.

In the absence of near-surface water which, on Earth, affects material bulk density, shear strength and pore-pressure, and thus lead to slope instability. The mechanisms of slope instability and failure on Venus are unclear, and it is likely that landslides require triggering by external forces, such as earthquakes. Magellan imagery revealed a very strong spatial relationships between the locations of large-scale mass-wasting features and steep slopes related to rift zones and volcanic edifices, which may in turn point to them being geodynamically active in the recent geological past. EnVision's proposed Regions of Interest (RoIs, see also §3.2) and higher resolution VenSAR SAR imaging offer excellent coverage of known mass-wasting features and increase the likelihood of imaging new or previously undetected smaller features. The planned VenSAR

investigations will include detailed characterisation of mass-wasting geomorphological properties and features with VenSAR stereo imagery, and of their surface conditions with VenSAR polarimetry.

Detecting and characterizing aeolian activity

Evidence of dune-fields, debris fans and large ripples are scarcely resolvable in the > 120 m spatial resolution Magellan imagery. The surface winds evidenced by these features, downwind of impact craters, are likely to be important agents of geomorphological change, but higher resolution repeated imagery, and improved surface investigation to distinguish loose from consolidated materials (from polarimetry) are needed to characterize them.

Wind-streaks are widespread across Venus' surface and the locations of two dune-fields and possible fields of micro dunes are also known (Greeley et al., 1992). Detection of aeolian processes, via features of erosion, transport and deposition (sedimentation), will be attempted by repeated imagery at high spatial resolution (decametre scale), and will help to constrain rates of such processes on decadal (Magellan- EnVision comparison over 40 yrs) and yearly (EnVision inter-cycle comparison) time scales. Planned VenSAR investigations will also include detailed characterisation of geomorphological features with stereo images, and of their surface material properties using multi-polarimetric observations. EnVision will search for features of aeolian activity beyond what we know from Magellan and will attempt to detect any temporal changes to these features for the first time.

The search for geomorphological changes will be carried out by searching for changes in repeated VenSAR SAR imagery at 30 m and 10 m resolution. The analysis will be complemented by SAR polarimetry physical properties.

On the basis of the top-down analysis above, the science observation requirements defined to address this EnVision science objective R1-A-30 are listed in Table 2.3.6

Table 2.3.6 – *EnVision science observation requirements addressing Venus surface geomorphological changes.*

R2-H-10	Obtain **regional SAR imagery surface mapping**, resolving features at a **spatial resolution < 100 m** and a **geographical coverage >100s km**.
R2-H-20	Obtain **targeted SAR imagery surface mapping**, resolving features at a **horizontal resolution ≤ 10 m** and a **geographical coverage > 10s km**.
R2-H-30	Measure **surface topography** (1) **regionally** (at least 20% of the planet) by means of **stereo radar imaging** on **selected RoIs** (yielding an elevation **accuracy less than ≤ 80 m for 85% of the data** and **horizontal resolution ≤ 300 m**); and (2) **globally** (**at least 65%** of the planet) by means of **nadir altimetry** (**vertical resolution < 10 m** and **along-track resolution ≤ 6 km**).
R2-H-40	Characterize **surface polarimetric reflection properties** for **selected SAR regions** at a **horizontal resolution < 30 m**.
R2-A-20	Detect and characterize **changes in surface radar imagery** in selected **Regions of Interest (RoI)** that include the areas with high probability of volcanic and seismic activity with a **horizontal resolution < 100 m**.

2.3.7. Assess tropospheric trace gasses spatial and temporal variability (R1-C-10)

The established most variable atmospheric species on Venus – SO_2, SO, H_2O, CO, COS, H_2SO_4 – are often associated with volcanic emissions on Earth. The goal of EnVision is to understand the intrinsic atmospheric variability, and to establish to what extent it can be associated with extrinsic inputs such as geological activity. Several key gasses can be mapped below the cloud deck, at 0-50 km altitude: water vapour (H_2O and HDO) (Bézard et al., 2009), sulphur compounds (SO_2, COS) and carbon monoxide (CO) (Tsang et al., 2009; Marcq et al., 2008, 2023; Arney et al., 2014) – these are all potential volcanic volatile gasses. In particular, discovering spatial variability of the D/H ratio – whether associated with volcanic plumes or other fractionating processes – would be fundamental for understanding the history of the water on Venus. The atmosphere is known to be variable on a range of time scales from minutes to years, so measurements over a wide range of timescales are required.

The high surface pressure of Venus is maintained through surface-atmosphere chemical buffering reactions, which are as yet unidentified. Buffer systems proposed have included Calcite-Anhydrite and Pyrite-Magnetite systems, but there is little evidence constraining these claims, and several of the relevant minerals including pyrite are not stable in Venus surface conditions (Hashimoto and Abe, 2005). Latitudinal gradients have already been observed in CO and OCS (Marcq et al., 2018) so these species act as tracers for the meridional circulation and provide a glimpse into some of the chemical cycles of the troposphere. The water vapour vertical gradient in the deep atmosphere is not known and may exhibit a steep gradient due to surface-

atmosphere reactions (Ignatiev et al., 1997). Studying how trace gas abundances change over terrain of different compositions and/or elevations may yield insight into the surface-atmosphere exchange occurring.

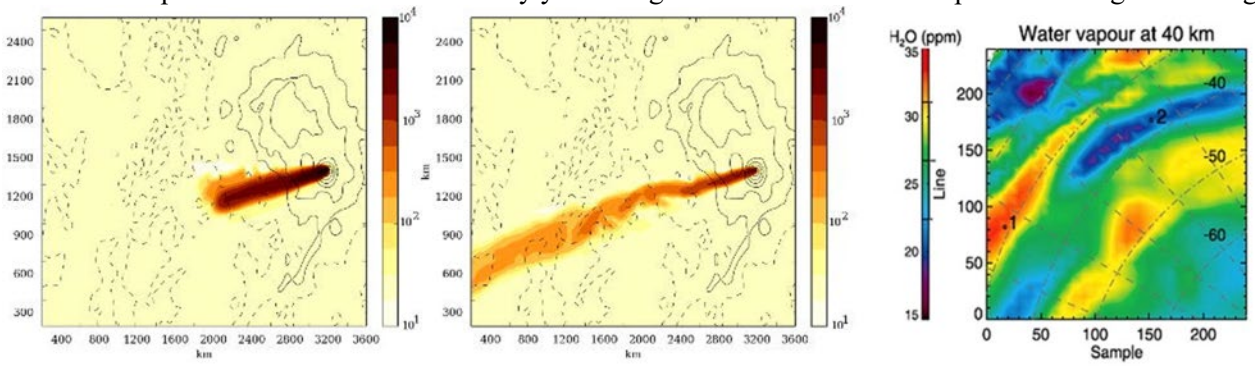

Figure 2.3.10 – *Simulated advection of a volatile gas plume emitted from Imdr Regio. Black contours represent topography. Colors show excess water vapour (in arbitrary units) after 72 hours of outgassing, at (a, left:) 10 km altitude and (b, center:) 35 km altitude. (Wilson and Lefèvre, 2020). (c, right): Variations of water vapour at 40 km altitude (Tsang et al., 2010). This result was later found to be potentially attributed to degeneracies between cloud and water vapour retrieval. The higher spectral resolution of VenSpec-H, compared to VIRTIS-M, will enable unambiguous disentangling of these signals.*

Radar-bright highland regions may occur due to deposition of airborne particulates or volatiles, or may indicate chemical interaction between surface and atmosphere. Observation of the composition and physical properties of these terrains, along with mapping of tropospheric gasses and particulates, are necessary to study this phenomenon. The atmospheric observations required for this are global in scope, and not targeted to particular volcanic regions, because an understanding of global atmospheric variability is needed. The only technique available for mapping tropospheric gasses from orbit is to exploit spectral windows on the nightside of Venus, centred near 1.18 μm, 1.74 μm and 2.3 μm; these spectral windows probe gasses at ~5 – 25 km, 20 – 30 km, and 30 – 40 km respectively. Water vapour can be mapped in all three of these windows, allowing mapping at three different heights, making it an ideal candidate for 3-D volcanic plume mapping. Further gasses in one or more of the spectral windows include HDO, SO_2, OCS, CO, HCl and HF – see Table 4.5.1 below.

The only previous orbiter equipped with spectrometers capable of probing these spectral windows was Venus Express; its observations demonstrated the viability of mapping gasses at these wavelengths but their relatively low spectral resolution (VIRTIS-M, with resolving power $\lambda/\Delta\lambda$~70, and SPICAV-IR with resolving power $\lambda/\Delta\lambda$~1700) led to low retrieval precision, of typically 5 – 10 ppm for water vapour (Bézard et al., 2009, 2011). Water vapour variations were tentatively reported in the 2.3 μm band (Tsang et al., 2010), as shown in Figure 2.3.10 right panel. It was later shown that, due to low spectral resolution, there was a degeneracy between water vapour and liquid water content in the cloud (Barstow et al., 2012). The EnVision VenSpec-H IR spectrometer will repeat these measurements, but with higher spectral resolution, in order to allow much higher sensitivity to these key trace gas species and with a much greater temporal and spatial coverage. EnVision's investigations will be discussed in greater detail in Section 3.4. The VenSpec-M instrument will provide contextual observations of surface lower atmosphere H_2O and cloud opacity variability observations. The VenSAR instrument will provide contextual observations of surface brightness temperatures. The RSE radio occultation observations of the upper troposphere, cloud and mesosphere sulphuric compounds and atmospheric stability will provide further context information.

The principal instrument for trace gas mapping is **VenSpec-H**, designed to map key gasses including water vapour at three different altitude ranges in the troposphere at high spectral resolution, as will be described in Section 3.4.1. These observations also provide validation for simultaneous and co-located VenSpec-M multispectral observations that provide wider mapping of H_2O variability at 5-25 km altitude, as well as cloud optical density variability information. These will be supported by upper tropospheric and mesospheric mapping of sulphuric acid vapour and atmospheric stability and dynamics by RSE radio occultation.

On the basis of the top-down analysis above, the science observation requirements defined to address this EnVision science objective R1-C-10 are listed in Table 2.3.7.

Table 2.3.7 – *EnVision science observation requirements addressing Venus tropospheric composition spatial and temporal variability*

R2-A-10	Detect and characterize spatial and temporal anomalies of the **surface and near-surface temperature** with a precision of **1 K** over time scales **from hours to years** and **spatial resolution < 100 km**.

R2-C-10	Map **tropospheric gases** at **0-45 km altitude**: (1) H_2O partial column random accuracy: < 10% (and < 20% below 15 km altitude) (2) HDO partial column random accuracy: < 20% (and < 30% below 15 km altitude) (3) CO partial column ratio: < 14% (4) OCS partial column ratio: < 18% (5) SO_2 partial column ratio: < 30% at a **horizontal resolution of < 100 km (and < 200 km for H_2O and HDO below 15 km altitude)**, to detect gradients related to surface-atmosphere and cloud interaction processes.
R2-C-30	**Map** the **relative variability** of the **Venus cloud opacity** at a **resolution of < 100x100 km²** for atmospheric correction of the VenSpec-M surface emissivity product.
R2-C-50	Measure **vertical profiles of H_2SO_4 liquid** (from **45-55 km altitude**) and **vapour** (from **35-55 km altitude**) and **SO_2 profiles** (from **45-55 km altitude**) with: (1) H_2SO_4 concentration **accuracy of <30 mg/m³** and **vertical resolution of < 300 m**; (2) H_2SO_4 vapour **accuracy of <3 ppm** and a **vertical resolution < 300 m**; (3) SO_2 **accuracy <30 ppm** and a **vertical resolution < 300m.**
R2-C-60	Measure **vertical profiles of atmospheric density, temperature and pressure** from **45-90 km altitude**. (1) **Density profile accuracy**: **10% at 100 km**, ~1*10^{19} m^{-3} at lower boundary, vertical resolution: 100 m; (2) **Temperature profile accuracy**: **10% at 100 km**, 0.1K at lower boundary, vertical resolution:100 m; (3) **Pressure profile accuracy**: **10% at 100 km**, ~1-2 Pa at lower boundary, vertical resolution: 100 m.

2.3.8. Measure variability of cloud and cloud droplets (R1-C-30), and map the variability of the mesospheric composition (R1-C-20)

Explore the main constituent of the cloud and cloud tops, and H_2SO_4 in both vapour and liquid form
The main constituent of the clouds, H_2SO_4, in both vapour and liquid form, can be monitored near the cloud base altitude, yielding clues as to cloud formation and convection processes. Geological activity can affect clouds in several ways: (1) volcanic ash can contribute to cloud and haze layers; (2) volcanic sulphur dioxide emissions can contribute to formation of sulphate cloud and haze layers and to the as-yet unidentified UV absorber seen at cloud-tops; (3) volcanically emitted volatiles can form condensate layers, as discussed in Section 2.3.5; (4) heat from volcanic activity can cause changes in atmospheric circulation (Esposito et al., 1984); (5) near-surface winds in Venus' dense atmosphere can lift dust and other particulates from the surface into airborne suspension. Understanding the dependence of the cloud layer on outgassed mantle volatiles is critical for understanding the long-term climate evolution of the planet. All of these effects can be studied by monitoring the spatial and temporal variations of clouds and hazes. Characteristic timescales of cloud formation and dissipation have been measured to be of the order of hours to days, therefore observations on such timescales are required.

Measurements of the vertical profile of temperature, pressure and number density in the troposphere and mesosphere (35-90 km) of Venus will help to understand the processes driving the short and long-term variability of the cloud-level composition, as well as convection and global circulation (Figures 2.2.7, 2.2.11, 2.3.11). These processes are fundamental to understanding the transport of momentum and the variable distribution of atmospheric constituents in the Venus atmosphere. Measurements of vertical atmospheric profiles with the required high vertical resolution are only possible through radio occultations. Coverage at a wide range of latitudes and local solar times is needed to parameterise cloud-level convective as well as dynamical processes. Measurements in consecutive orbits allow us to monitor the short-term variability caused e.g., by atmospheric waves. Observations should be as widely spread in latitude, longitude and local solar time, to build up a climatology of atmospheric observations. Measurement of sulfuric acid *vapour* abundance profiles by exploiting the absorption of X-band radio signals has been demonstrated from previous Venus orbiters (Oschlisniok et al., 2021, and references therein). EnVision will repeat these measurements, with more frequent RSE radio occultations due to its lower orbital period (94 minutes for EnVision, compared to 24 hours for VEx and 10 days for Akatsuki), allowing shorter-period variability to be studied. Furthermore, EnVision will also measure sulphuric acid *liquid* abundance, for the first time, using its Ka band radio signals. Further information is given in Section 4.8.

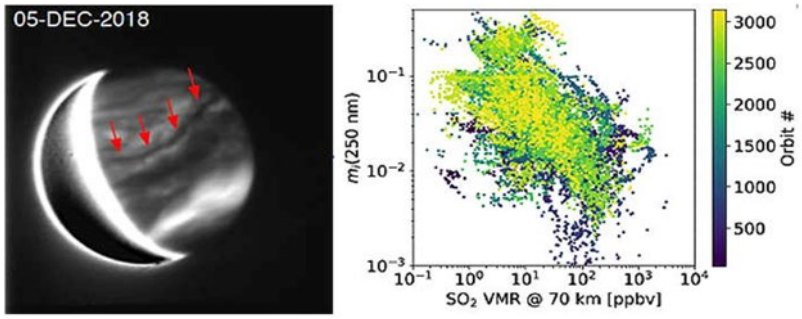

Figure 2.3.11 – *(left): Dark streak of thicker cloud or particulates, imaged on the nightside of Venus using IRTF/SPEX. Could this be a volcanic plume? (Young et al., EPSC, 2019). (right): Scatter plot between imaginary index of mode 1 particles at 250 nm and SO_2 mixing ratio at 70 km as measured by SPICAV-UV, hinting at a conversion between SO_2 and a sulphur-bearing UV absorber. Figure from Marcq et al. (2020).*

Spatial variations of the unknown UV absorber, possibly made of sulphur material, produce contrasts in daytime images peaking near 365 nm, and are a means of inferring bulk motions in the cloud top atmosphere (e.g., Travis 1975, Bertaux et al., 1996, Titov et al., 2008). It is unclear whether the cloud-level abundance of the absorber is solely the result of material upwelling from below, or whether it depends on chemical reactions between upwelling and downwelling species (Figure 2.3.11). The EnVision VenSpec-U spectral imager contains dedicated UV spectral coverage for the investigation and monitoring of the unknown UV absorber.

Constrain mesospheric composition and its variability

EnVision will measure gas abundances in the mesosphere (70-100 km altitude) above the clouds. Mesospheric abundances of carbon monoxide (CO), sulphur dioxide (SO_2), sulphur monoxide (SO), and water (H_2O) have been shown to be highly variable (Vandaele et al., 2015, 2016; Marcq et al., 2013, 2020; Chamberlain et al., 2020; Mahieux et al., 2021, 2023a,b). Mesospheric variability may be driven by variations in vertical transport, temperature, local solar flux, and coupling among components of the SO_2-H_2O-H_2SO_4-aerosol system. Previous measurements of these species could not constrain the physical origin of this variability. Ground-based observations by e.g., Encrenaz et al. (2019, 2020) are global, low spatial resolution 'snapshots' acquired only during maximal elongations of Venus as seen from Earth, large scale images from Venus orbiters (e.g. VMC/VEx, UVI/Akatsuki) lacked spectroscopic capabilities, whereas orbiter-borne spectrographs (e.g. VIRTIS-H/VEx, SPICAV-UV/VEx) lacked extensive spatial coverage (Figure 2.3.12). As the mesospheric composition is variable on a range of time scales from hours to years, measurements over a wide range of latitude, local time, longitude and timescales are required. According to known spatial variability in cloud top albedo and sulphurous gasses (Titov et al., 2012; Piccialli et al., 2015; Vandaele et al., 2017a,b), the investigated spatial scales should range from about 10 km to several thousand km (local to planetary scale).

EnVision will resume the observations of trace gasses in the mesosphere conducted by these previous missions, in both UV (VenSpec-U) and IR (VenSpec-H) wavelengths, but with higher spectral resolution. In the UV range, this will allow separate retrieval of SO and SO_2 species, as was demonstrated using HST observations (Jessup et al., 2015); simultaneous and co-located IR observations will allow simultaneous retrieval of water vapour, carbon monoxide and further key tracer species. Together, these observations will give an unprecedented view of transport and chemical processes at the cloud-top, in order to provide a better understanding of volatile transport through the atmosphere.

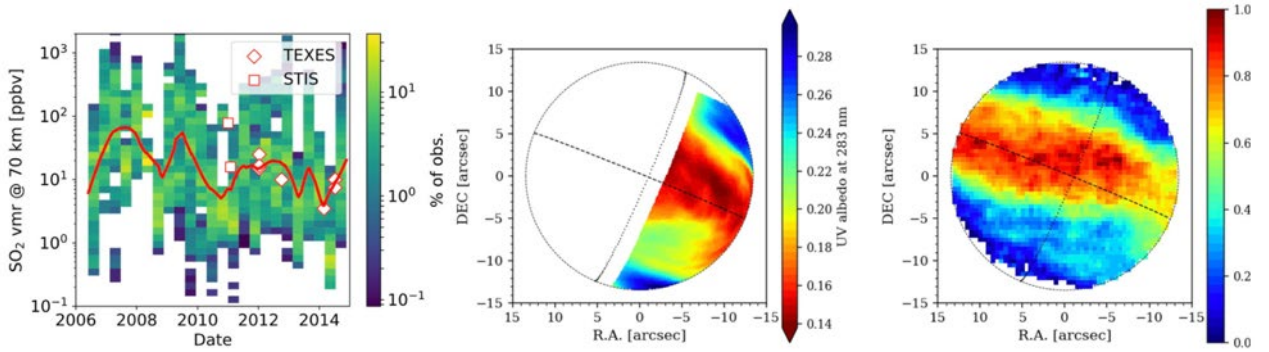

Figure 2.3.12 – *(left): Temporal evolution of SO_2 mixing ratio at 70 km for latitudes lower than 30° as measured by SPICAV-UV. The red line stands for the moving median value, and white diamonds/squares show other SO_2 measurements in the same time interval. Figure from Marcq et al. (2020). (center): UV albedo map derived from the Akatsuki UVI data recorded on January 21, 2017, at 01:46 UT. Dashed lines represent the equator and the evening terminator. (right): TEXES map of the SO_2 volume mixing ratio at the cloud top, inferred from the SO_2/CO_2 line depth ratio at 7.4 µm on January 21, 2017, at 03:43–04:18 UT. Figure from Encrenaz et al. (2019).*

This investigation relies on dual-band **RSE** radio occultation to obtain vertical profiles of sulphuric acid liquid and vapor in the clouds, as well as temperature profiles to assess where convective transport is occurring. Lower cloud distribution and properties are monitored by **VenSpec-M** nightside near-IR multispectral imager, and cloud-top properties and mesospheric gas abundances are monitored using **VenSpec-U** UV and **VenSpec-H** IR dayside spectroscopy.

On the basis of the top-down analysis above, the science observation requirements defined to address this EnVision science objectives R1-C-30 and R1-C-20 are listed in Table 2.3.8.

Table 2.3.8 – *EnVision science observation requirements addressing Venus cloud and mesospheric variability.*

R2-A-10	Detect and characterize spatial and temporal anomalies of the **surface and near-surface temperature** with a precision of **1 K** over time scales **from hours to years** and **spatial resolution < 100 km**.
R2-C-20	Map **mesospheric gases** at **65-80 km altitude**: (1) SO_2 partial column random error: < 20% (2) SO:SO_2 partial column random error: < 25% at a **spatial resolution of 5 (small-scale convection and vertical mixing) to 50 km at UV wavelength** (3) H_2O partial column random error: < 20% (4) HDO partial column random error: < 20% (5) H_2O:HDO partial column random error: < 25% (6) SO_2 partial column random error: < 20% (7) CO partial column random error: < 20% (8) OCS partial column random error: < 20% at a **spatial resolution of <50 km at IR wavelength** in order to assess coupling between surface (volcanic activity, topographic features), cloud and mesospheric measurements.
R2-C-30	**Map** the **relative variability** of the **Venus cloud opacity** at a **resolution of < 100x100 km²** for atmospheric correction of the VenSpec-M surface emissivity product.
R2-C-40	Map **upper cloud properties and their variations** (i.e. cloud top altitude, UV absorber) from **65-80 km altitude**: (1) **Cloud top altitude random error**: 1 km (2) **UV absorber accuracy**: 10% in radiance factor at 365 nm (3) **Temporal resolution** of features to be observed: hours to years (4) **Horizontal scale** of features to be observed: 5 to >1000 km
R2-C-50	Measure **vertical profiles of H_2SO_4 liquid** (from **45-55 km altitude**) and **vapour** (from **35-55 km altitude**) and **SO_2 profiles** (from **45-55 km altitude**) with: (1) H_2SO_4 concentration **accuracy of <30 mg/m³** and **vertical resolution of <300 m**; (2) H_2SO_4 vapour **accuracy of <3 ppm** and a **vertical resolution <300 m**; (3) SO_2 **accuracy <30 ppm** and a **vertical resolution < 300m.**
R2-C-60	Measure **vertical profiles of atmospheric density, temperature and pressure** from **45-90 km altitude**. (1) **Density profile accuracy**: **10% at 100 km**, ~$1*10^{19}$ m^{-3} at lower boundary, vertical resolution: 100 m; (2) **Temperature profile accuracy**: **10% at 100 km**, 0.1K at lower boundary, vertical resolution:100 m; (3) **Pressure profile accuracy**: **10% at 100 km**, ~1-2 Pa at lower boundary, vertical resolution: 100 m.

3. Scientific Requirements

The EnVision science observation requirements have been derived in phase A from the mission science themes and objectives, as described in Chapter 2 and ESA (2023c). In this chapter, the science observation requirements and the resulting data products are summarized in Section 3.1, and the associated observation strategy to ensure that the objectives are met is outlined in Section 3.2. This is followed by descriptions of how the science objectives are met by applying the intended Science Observation Reference Scenario (SORS) (Chapter 3, Sections 3.2-3.6 and Chapter 5, Section 5.4) and the mission and payload (also called measurement) requirements (Chapter 4). The mission and payload requirements were defined top-down from the science observation requirements, and based on specifications from earlier relevant Venus missions. These have then been verified to be appropriate and to meet the science observation requirements through performance simulations, as described in Chapters 4 and 7. Finally, a summary requirements traceability matrix is provided (Section 3.6).

During phase B1, the maturing of the instrument and S/C design led to the need to review and update the science requirements in a few instances (ESA, 2023c). This concerned in particular the product accuracy and coverage requirements, e.g. in the troposphere. These updates are summarized in Section 3.6 and consolidated in Chapter 7 summarizing the end-to-end performance simulations performed in the definition phase. Further science goal requirements could also be added in phase B1 (see e.g., Tables 8.5.1-2 in Section 8.5). These are not part of the mission baseline requirements and hence will be achieved on a best-effort basis only (not driving the mission design). These are further addressed in Chapter 8.

3.1. EnVision Science Observation Requirements

Table 3.1.1 provides an overview of the EnVision science observation requirements derived in Chapter 2. Based on the Science observation requirements, the list of data products and their specifications are defined in Table 3.1.2 (see next page).

Table 3.1.1 – *EnVision Science observation requirements summary (see also ESA, 2023c). In the left-hand column, the EnVision requirements number is noted, together with a reference to the sections describing further the requirement flow-down and how the science objectives are met applying the intended observation strategy and mission payloads.*

Requirement number and §	Description
R2-H-10 (Sect. 3.3.1)	Obtain **regional SAR imagery surface mapping**, resolving features at a **spatial resolution < 100 m** and a **geographical coverage >100s km (>20% of the planet)**.
R2-H-20 (Sect. 3.3.1)	Obtain **targeted SAR imagery surface mapping**, resolving features at a **horizontal resolution ≤ 10 m** and a **geographical coverage > 10s km (>2% of the planet)**.
R2-H-30 (Sect. 3.3.2)	Measure **surface topography** (1) **regionally** (at least 18% of the planet) by means of **stereo radar imaging** on **selected RoIs** (yielding an elevation **accuracy less than ≤ 80 m for 85% of the data** and **horizontal resolution ≤ 300 m**); and (2) **globally** (**at least 65%** of the planet) by means of **nadir altimetry** (**vertical resolution < 10 m** and **along-track resolution ≤ 6 km**).
R2-H-35 (Sect. 3.3.3)	**Map locally** (over selected **Regions of Interest and at least 1% of the planet**) the **microwave emissivity in V and H polarization** using passive off-nadir (incidence angle > 25°) radiometry, with an **accuracy < 2 K** and **a horizontal resolution <50 km**.
R2-H-40 (Sect. 3.3.3)	Characterize **surface polarimetric reflection properties** for **selected SAR regions** (**≥5% of the planet**) at a **horizontal resolution < 30 m**.
R2-H-50 (Sect. 3.3.3)	Obtain a global (**≥75% of the planet) map** of the **microwave emissivity** using passive radiometry with a **precision < 1.0 K** and an absolute radiometric **accuracy < 2.0 K**.
R2-H-60 (Sect. 3.3.3)	Characterize **near-IR emissivity** of surface targets **over 60% of the planet surface** with a **relative emissivity accuracy < 4% at a spatial resolution < 100 km**.
R2-H-70 (Sect. 3.3.4)	Search for **subsurface material boundaries down to 1000 m** of the crust over **at least 65% of the planet surface**, with a **vertical resolution of ~20 m, an across-track resolution of ≤11 km , and an along-track resolution of ≤ 3 km**.
R2-H-80 (Sect. 3.3.5)	Measure the **gravity field** of the planet with **spatial resolution of < 270 km**; **accuracy of < 0.2 mm/s² globally**; improved **higher spatial resolution of < 200 km**; **accuracy of < 0.1mm/s² over >40% of the planet;** and the **k2 Love number** with an accuracy of **0.01**.
R2-A-10 (Sect. 3.4.1)	Detect and characterize spatial and temporal anomalies of the **surface and near-surface temperature** with a precision of **1 K** over time scales **from hours to years** and **spatial resolution < 100 km**.
R2-A-20 (Sect. 3.4.2)	Detect and characterize **changes in surface radar imagery** in selected **Regions of Interest (RoI)** that include the areas with high probability of volcanic and seismic activity with a **horizontal resolution < 100 m**.
R2-C-10 (Sect. 3.5.1)	Map **tropospheric gases** at **0-45 km altitude**: (1) H_2O partial column random error: < 10% (and < 20% below 15 km altitude) (2) HDO partial column random error: < 20% (and < 30% below 15 km altitude) (3) CO partial column random error: < 14% (4) OCS partial column random error: < 18% (5) SO_2 partial column random error: < 30% at a **horizontal resolution of < 100 km (and < 200 km for H_2O and HDO below 15 km altitude)**, to detect gradients related to surface-atmosphere and cloud interaction processes.
R2-C-20 (Sect. 3.5.3)	Map **mesospheric gases** at **65-80 km altitude**: (1) SO_2 partial column random error: < 20% (2) SO:SO_2 partial column random error: < 25% at a **spatial resolution of 5 (small-scale convection and vertical mixing) to 50 km at UV wavelength** (3) H_2O partial column random error: < 20% (4) HDO partial column random error: < 20% (5) H_2O:HDO partial column random error: < 25% (6) SO_2 partial column random error: < 20% (7) CO partial column random error: < 20% (8) OCS partial column random error: < 20% at a **spatial resolution of <50 km at IR wavelength** in order to assess coupling between surface (volcanic activity, topographic features), cloud and mesospheric measurements.
R2-C-30 (Sect. 3.5.1)	**Map** the **relative variability** of the **Venus cloud opacity** at a **resolution of < 100x100 km²** for atmospheric correction of the VenSpec-M surface emissivity product.
R2-C-40 (Sect. 3.5.3)	Map **upper cloud properties and their variations** (i.e. cloud top altitude, UV absorber) from **65-80 km altitude**: (1) **Cloud top altitude random error**: 1 km (2) **UV absorber accuracy**: 10% in radiance factor at 365 nm (3) **Temporal resolution** of features to be observed: hours to years (4) **Horizontal scale** of features to be observed: 5 to >1000 km
R2-C-50 (Sect. 3.5.2)	Measure **vertical profiles of H_2SO_4 liquid** and **vapour** and **SO_2 vapour profiles** with: (1) H_2SO_4 concentration **accuracy of <30 mg/m³** and **vertical resolution of <300 m** from **49 to 55 km at the poles and 50 to 55 km at the equator**; (2) H_2SO_4 vapour **accuracy of <3 ppm** and a **vertical resolution <300 m, from 36 - 55 km at the poles and from 35 - 55 km at the equator;** (3) SO_2 **accuracy <40 ppm** and a **vertical resolution < 300m, from 45 - 55 km.**
R2-C-60 (Sect. 3.5.2)	Measure **vertical profiles of atmospheric density, temperature and pressure** from **35-100 km altitude**. (1) **Density profile accuracy**: **2% at 70 km altitude**, ~$1*10^{19}$ m^{-3} at lower boundary, vertical resolution: 100 m; (2) **Temperature profile accuracy**: **2% at 70 km altitude**, 0.1K at lower boundary, vertical resolution:100 m; (3) **Pressure profile accuracy**: **2% at 70 km altitude**, ~1-2 Pa at lower boundary, vertical resolution: 100 m.

Table 3.1.2 – *EnVision data product specifications. Raw and calibrated data will be publicly available as soon as they are processed, validated and calibrated, and no later than 6 months after the data are available to the instrument teams (see Section 6.3.2, 6.3.3, and Section 9.4).*

Instrument/ Experiment	Data product description	Required accuracy	Required horizontal resolution	Req. vertical resolution	Required coverage (% of planet surface)
VenSpec-M	Near-Infrared surface and near-surface temperatures	< 1K	< 100 km^2	-	60 %
VenSpec-M	Near-Infrared emissivity maps	< 4 %	< 100 km^2	-	60 %
VenSAR	Repeat SAR imagery (change detection)	-	< 100 m	-	Regions of Interest, >2 % of the planet
VenSAR	SAR imagery maps	-	< 100 m	-	> 100s km^2, Regions of Interest, > 20 % of the planet
VenSAR	High resolution SAR imagery maps	-	< 10 m	-	> 10s km^2, over selected Regions of Interest
VenSAR	Surface topography maps (SAR stereo imaging)	-	< 300 m	< 80 m	>20 % of the planet
VenSAR	Surface topography maps (radar altimetry)	-	< 6 km along-track	< 10 m	> 65 % of the planet
VenSAR	Microwave emissivity imaging in off-nadir geometry in V and H polarization (radar)	< 2 K	< 30 m	-	> 1 % of the planet
VenSAR	Dual polarization SAR imagery	-	< 30 m	-	> 5 % of the surface for selected Regions of Interest
VenSAR	Microwave emissivity maps (radiometry, S-band)	< 1 K precision < 2.0 K radiometric accuracy	-	-	> 75 % of the planet
SRS	Sub-surface material boundaries	-	< 3 km along-track	~20 m	> 65 % of the planet
RSE	Gravity field	< 0.2 mm/s^2	< 270 km	-	global
RSE	Gravity field observations	< 0.1 mm/s^2	< 200 km	-	> 40 % of the planet
RSE	k_2 Love number	< 0.01	-	-	
VenSpec-H	Tropospheric H_2O	< 10% rms	< 100 km	-	> 60 %
VenSpec-H	Tropospheric HDO	< 20% rms	< 100 km	-	> 60 %
VenSpec-H	Tropospheric CO	< 14% rms	< 100 km	-	> 60 %
VenSpec-H	Tropospheric OCS	< 18% rms	< 100 km	-	> 60 %
VenSpec-H	Tropospheric SO_2	< 30% rms	< 100 km	-	> 60 %
VenSpec-H	Mesospheric H_2O	< 20% rms	< 50 km	-	> 60 %
VenSpec-H	Mesospheric HDO	< 20% rms	< 50 km	-	> 60 %
VenSpec-H	Mesospheric H_2O:HDO	< 25% rms	< 50 km	-	> 60 %
VenSpec-H	Mesospheric CO	< 20% rms	< 50 km	-	> 60 %
VenSpec-H	Mesospheric OCS	< 20% rms	< 50 km	-	> 60 %
VenSpec-U VenSpec-H	Mesospheric SO_2	< 20% rms	< 5-50 km < 50 km	-	> 60 %
VenSpec-U	Mesospheric SO:SO_2	< 25% rms	< 5-50 km	-	> 60 %
VenSpec-M	Maps of Venus cloud opacity relative variability	-	< 100 km^2	-	> 60 %
VenSpec-U	Cloud top altitude	< 1 km	5-100 km (goal: 3 km)	-	
VenSpec-U	Cloud UV absorption	< 10% at 365 nm	5-100 km (goal: 3 km)	-	
RSE	Profiles of liquid H_2SO_4 (radio occultation)	<30 mg/m^3	-	< 300 m	49-55 km altitude
RSE	Profiles of H_2SO_4 vapour (radio occultation)	<3 ppm	-	< 300 m	35-55 km altitude
RSE	Profiles of SO_2 (radio occultation)	<40 ppm	-	< 300 m	45-55 km altitude
RSE	Profiles of atmospheric density (radio occultation)	< 2% at 70 km altitude, ~1*10^{19} m^{-3} at lower boundary	-	100 m	35-100 km altitude
RSE	Profiles of atmospheric temperature (radio occultation)	< 2% at 70 km altitude, 0.1K at lower boundary	-	100 m	35-100 km altitude
RSE	Profiles of atmospheric pressure (radio occultation)	< 2% at 70 km altitude, 1-2 Pa at lower boundary	-	100 m	35-100 km altitude

3.2. Requirements for the EnVision Observation Strategy

Overview. - Our current understanding of Venus' geology comes almost entirely from the Magellan orbiter's near global SAR image dataset, at > 120 m to 300 m spatial resolution (gridded to 75 m pixel size), and its topographic data, at 10 – 30 km (horizontal) and 50 – 100 m (vertical) resolution (Figure 2.1.7). Ground-based radar observations from Arecibo have added polarimetric information at spatial resolutions of ~1 – 2 km, which has yielded some broad diagnostic surface properties and surface roughness. Near-IR emissivity mapping has also been achieved, at ~50 km spatial resolution, using the VIRTIS mapping spectrometer onboard Venus Express, but this mapping was performed at one wavelength only, and it covers only around 40% of the planet, all in the southern hemisphere. These datasets have enabled a very broad classification of the Venus surface into different regions and terrain types; and have allowed, for example, the identification of some 900 impact craters and almost two thousand large volcanoes. These important datasets have provided a global geological context and a rich catalogue of targets, which now need studying in greater detail.

Table 3.2.1 – *Required scales of surface observations for VenSAR imagery. It is not necessary to repeat Magellan's global low-resolution imagery, thus EnVision will instead focus on obtaining higher-resolution regional and targeted VenSAR observations with spatial resolutions ranging from 30 m down to 10 m. Context for these observations is also provided by VenSpec M's surface spectroscopy, Subsurface Radar Sounder investigations and from radar altimetry.*

Mapping scales:	Global	**Regional**	**Targeted**
EnVision coverage (% of global)	> 65% or all longitudes (altimetry)	> 20% (Req.)	> 2% (10s of km²) (Req.)
VenSAR SAR imaging spatial resolution	150 m	30 m (Standard)	10 m (High Resolution)
Approximate feature extents	1 – 100s km	100s -1000s m	10 – 100s m
Examples of observable geomorphological features at these scales:			
Structures	Terra 'continents', Planitia	Chasmata, Dorsa	Folds, graben
Volcanoes	Volcanic rises (Regio)	Volcanic edifices	Lava Flows
Sediments	'Featureless' plains	Parabolas, halos	Landslides
		EnVision SAR observations	

Following similar strategies adopted on Earth and Mars, what is needed now is a more focused and nested observation strategy; collecting imagery at increasing spatial resolution, to enable holistic interpretations, from global down to local scales, and from the cloud-tops down to the subsurface. Hence EnVision's focused investigative approach is broadly twofold: for observation types not obtained before at Venus (i.e. spectroscopic characterisation of large-scale surface composition and subsurface sounding), a global (or near-global) mapping strategy will be employed; and secondly, VenSAR's observations will focus on a series of targeted Regions of Interest (RoIs) which provide a representative sample of all major geologic terrain types and the boundaries between them, as well as many key locations of interest as identified by the Venus science community over many years (Table 3.2.1, Figure 3.2.1).

Coverage requirements. Specifically, coverage requirements for each EnVision instrument and instrument mode have been defined, based on a top-down analysis, to ensure that the mission science objectives (Chapter 2) and science requirements (Chapter 3) are met. In the following, a brief summary of the rational for the coverage requirements are provided (see Chapter 3, Table 3.6.1 Science Traceability Matrix for a summary of Science data products and coverage requirements; Chapter 7, Figure 7.2.2 and Table 7.2.1 for performance analysis results).

- for the VenSAR regional 30 m imaging mode, multiple images of all major Venus surface and terrain types are needed for understanding the planet's history and activity. A careful study of the Venus geological map derived from the Magellan data resulted in a requirement to observe at least 20 % of the planet to achieve this (see Chapter 2, Chapter 3, Section 3.1);
- for the VenSAR 'targeted' 10 m imaging mode, images at key locations are needed; sites where maximum spatial detail is needed to resolve surface morphology and texture, and structure. For this rich, high-resolution dataset, the surface coverage requirement is decreased by an order of magnitude compared to the 30 m mode, and this corresponds to an increased focus on process and morphology rather than large scale variability. For example, nearly half the 20 % regional coverage is dedicated to imaging of the upland areas (~10 % of the surface) that may contain the oldest (and perhaps also

the youngest) terrains on Venus, but the small-scale processes which modify them (e.g. landslides, faults, material transport) are likely to be similar across all uplands - thus it is unnecessary to image them all. This analysis results in a requirement to observe at least 2 % of the surface (~10s of km^2) in this mode (see Chapter 2; Chapter 3, Section 3.1; and Chapter 4);

- VenSAR repeat imaging of Regions of Interest, to detect surface activity, requires that at least 3 images are acquired with the same look direction. The analysis of areas where change is expected results in the requirement to image at least 2% of the surface three times during the mission.
- VenSAR Dual polarization SAR imagery at 30 m resolution is required over certain Regions of Interest, where we expect active surface processes and different material types and densities, equivalent to >5% of the Venus Surface.
- VenSAR regional stereo SAR imaging mode requires >20% of the planet, which should include a selection of tesserae, of areas thought to be active, and as broad a selection of terrain types and geological features as is achievable. The figure of 20% is a compromise largely driven by mission data downlink prioritization and capabilities.
- VenSAR's altimetry mode provides a global topography dataset that will provide an important reference frame to assist the VenSpec-M and SRS observations. In-line with the VenSpec-M and SRS coverage requirements described below, the VenSAR altimetry mode coverage requirement is >65% of all longitudes of the planet.
- VenSAR's near-global microwave emissivity mapping (of brightness temperature) in nadir or near-nadir, by means of radiometry, requires evenly distributed observations throughout the mission covering all local times. This allows the search for surface temperature anomalies. To achieve this, coverage of at least 75% of the Venus surface is required.
- VenSAR microwave emissivity observations, in V and H polarization and with off-nadir geometry, are needed for targeted observations of specific regions for which active SAR polarimetry will be also available. The requirement is to image at least 1% of Venus surface, corresponding to 6 SAR imaging units, and at least 2 of these should cover at least 50% of highlands (i.e., terrains with altitude >2 km). Plains represent a secondary target for these emissivity observations. Off-nadir measurements must be orbit-to-orbit observations (rather than cycle-to-cycle observations) to avoid a large temporal gap between observations;
- for VenSpec-M, VenSpec-H, and VenSpec-U, a requirement for coverage of 60% of the surface of Venus was defined in Phase A; 100% coverage remains a goal for all instruments. This compromise was necessary due to the similarity between the day and year lengths on Venus, meaning that approximately 40% of longitudes cannot be imaged on the nightside by a polar-orbiting satellite during a four-year mission, and this is especially the case for the narrow Field of View of VenSpec-H. To allow VenSpec-M to observe all major landforms, and to test the hypothesis that tessera highlands contain more felsic crust (similar to Earth's continental crust) which formed in a water-rich past, at least half the planet needs to be observed (ESA, 2023c). Furthermore, this would also be sufficient coverage to evaluate estimates of global activity rates. It is anticipated that coverage of 60% of longitudes will allows enough volcanoes to be observed to allow characterization of the volcanism rate;
- for SRS, a requirement for global coverage of 65% of all longitudes and all latitudes up to 80 degrees has been defined. A goal of 100% global coverage is desirable but is not possible for a polar orbiting satellite optimized for multiple science goals and the slow Venus rotation speed. This coverage will permit SRS to observe all major types of terrain and surface feature, as addressed by the RSR science objectives, e.g., ancient and recent volcanoes, impact craters and surface modification areas. Similarly, the VenSAR and SRS altimetry coverage requirement is also 65% of all longitudes, with the same need to observe all major types of landforms such as (ancient and recent) volcanoes, impact craters and surface modification areas;
- the RSE gravity observation coverage requirement is formulated such that the periapsis latitude spread should be greater than 80˚. In this way, a global gravity field can be derived from the

observations over all mission cycles. To ensure a sufficient number of radio occultation observations for the mapping of Venus cloud and mesosphere variability, at least 2 radio occultation ingress + egress campaigns should be performed every 20 hours, and during 50% of the days in each cycle. This allows almost all latitudes to be covered during the mission.

These requirements and how they are achieved are described in further detail in the next sections of this chapter; please see also Table 3.6.1 (Science Traceability Matrix).

VenSAR targeted observation strategy. - VenSAR will provide imaging at 'Regional' scales (30 m resolution) across its RoIs which could cover *about* 30% of the planet's surface (compared to the 20% coverage requirement), and at 'Targeted' scales (10 m resolution) across about 2% of planet's surface within those RoIs (Table 3.2.1, see also Figures 7.1.2 and 7.2.1), thus high resolution observations will be placed in their spatial context, with all other types of observation. The RoIs will also be used to target more frequent subsurface sounding passes, thus to obtain smaller track-to-track spacing, in 'high density' sounding mode. VenSAR will also image at different angles (for stereoscopic construction of topography) and at multiple times during the mission (for change detection). The RoIs have thus been arranged to cover areas where we would like to understand information from polarimetry, where we expect that change may be occurring and/or where the highest spatial resolution will be needed to resolve the geology and geomorphology. In all cases, more accurate topographic data will be vital to understand surface morphology and structure, to declutter the SRS observations, to calibrate VenSpec-M surface emissivity observations, and to facilitate terrain correction of Magellan imagery and thus reliable change detection with EnVision's image products. Analysis of these complementary, multi-scale datasets, and their placement in the context of Magellan's global image framework, will allow a far better understanding of large-scale geological processes at work.

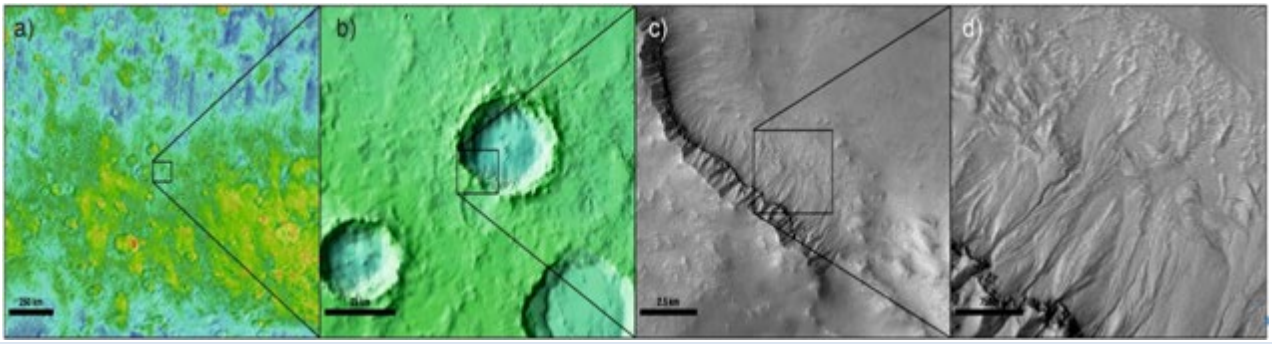

Figure 3.2.1 – *An example from Mars showing the power of nested imaging: a) Thermal Inertia data at ~50 km/pixel (similar to spatial resolution of VenSpec-M); b) MOLA topography (232 m/px) overlain on 100 m THEMIS mosaic (equivalent to EnVision's stereo-derived global topography; c) CTX data (29 m/px), equivalent to EnVision's 30 m standard SAR; and d) CTX data (7 m/px), equivalent to EnVision's high resolution SAR. These illustrate how the progression from global coverage towards targeted imaging will allow EnVision's observations to make a significant leap forward from the understanding we have gained from Magellan data.*

To illustrate this targeted imaging concept at Venus, a SAR imaging scenario has been developed and is illustrated in Figures 3.3.1. This was developed to illustrate the kind of science return that will be possible while satisfying all mission requirements and constraints. As illustrated in Figure 3.3.1 and Table 3.2.1, the RoIs in this baseline imaging scenario will sample approximately 36% of coronae thought to be active by Gülcher et al., 2020, 67% of known dune fields, 69% of identified landslides, 43% of the probes/landers, 14% of volcanic rises, 26% of mapped large volcanoes and 19% of small volcanoes. The list of targets used as input to the SAR imaging scenario shown, are included in the science requirements document (ESA, 2023c). Such metrics will be used to further refine the RoI selection in coming years, and will be finalized by the EnVision Science Working Group by the start of the science operations. Table 3.3.1 also shows that this approach allows prioritization of different types of observations – for example, a prioritization of polarimetric observation for regions of suspected anomalous dielectric properties – for different target regions, as will be discussed in further subsection below.

Selection of targets for the final mission operation strategy will continue to evolve depending on inputs from the science team up to and during the mission. The mission design offers enough flexibility to adapt the observation plan to potential future changes in the mission objectives within its 6 months long-term planning cycles. This could include changes in the ratio of different radar modes, for example, or changes of surface targets in response to discoveries made before or during the mission. EnVision will employ the same strategy

that has proved so successful on Mars and on Earth, and that has enabled great leaps forward in the understanding of surface and subsurface processes and their control on geomorphology and geology, as illustrated in Figure 3.2.1. Every time Mars has been observed at roughly an order of magnitude higher resolution, entirely new and often unexpected features and processes have been observed. The global context of these discoveries provides immensely important insights on a planet's evolution. This philosophy of nested, Regional and Targeted imaging is explained more fully in the following sections.

3.3. Requirements tracing for History: EnVision investigation how the Venus surface and interior evolved to their current state

3.3.1. Regional and Targeted Surface Mapping

This section demonstrates how the requirements for regional and targeted surface mapping (R2-H-10, R2-H-20, and R2-A-20, Table 3.1.1) are traced down and met applying a Science Operations Reference Scenario and the instrument and mission requirements provided in Chapters 4 and 5.

The surface of Venus hosts a large variety of different geological and geomorphic features, e.g. volcanoes, coronae, rift zones, mountain belts, impact craters, that range in scale from tens to millions of square kilometres, set in globally extensive regional lowland plains. For example, it is thought there may be about 85,000 small volcanoes are ≤ 5km in diameter (Hahn and Byrne, 2023), the Halle impact crater is 22 km in diameter, major lava flows can be < 750 km in length, and Artemis corona covers an area of about 3 million sq km. While each of these features will undoubtedly have unique characteristics, experience from Earth, Mars and the Moon tells us that each feature type (e.g. shield volcanoes, ridge belts) shares common causal processes that can be understood from a representative selection of a few key examples. Therefore, to understand the key global controls on Venus' geology, it is necessary only to obtain data from a fraction of the surface provided that fraction samples all the major terrain and feature types.

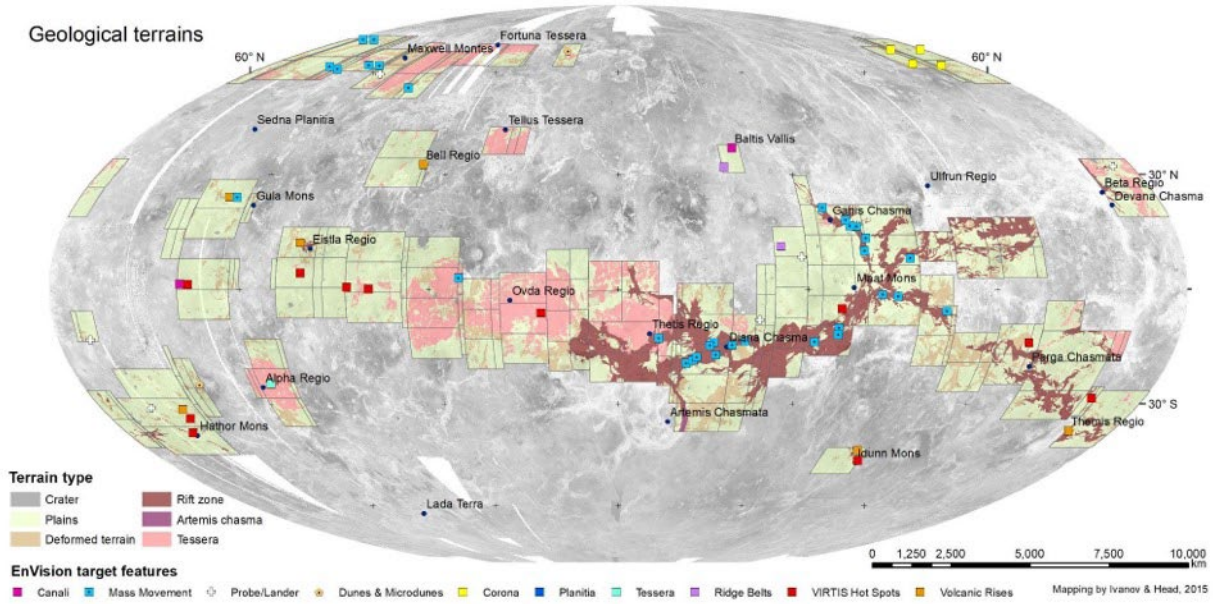

Figure 3.3.1 – *Mapped geological terrains and named features of interest (targets) that will be imaged within the Regions of Interest (RoIs) defined in EnVision's Science Operations Reference Scenario (SORS, see Section 5.4). The baseline science observations planning strategy is based on this distribution of geological target terrains. The RoIs are chosen to include representative samples of all major geological terrain and feature types. Definitions of geological terrain types are as mapped by Ivanov and Head (2015).*

EnVision's observation strategy in achieving that, is to focus VenSAR's imaging within a series of Regions of Interest (RoIs), which are required to cover at least 20% of the planet's surface in order to get a significant set of all surface types to be studied. The RoIs are distributed to capture key locations of interest and a representative sample of all the major terrain types (highland tesserae, rift zones, impact craters and lowland plains); imaging coverage of these will gradually build up during the course of the mission. An illustration of the geological terrains that will have been imaged by the end of the mission appears in Figure 3.3.1, where

RoIs used as input to EnVision Science Operations Reference Scenario (SORS) are shown. The SORS is used as input to simulations determining the EnVision geographical observation coverage during the mission science operation phase. A corresponding representative coverage metrics is shown in Table 3.3.3, where the VenSAR imaging RoI coverage requirement is met by the simulations, and the RoI coverage is ~26%. SAR operations permit an area with latitude extent of between 23 and 47 degrees to be imaged per orbit (between 2500 and 3300 km), and imaging is possible at every longitude around Venus during the mission period, but not in every mode in every RoI, at every longitude, in every cycle; these limitations drive the extents and locations of the RoIs, as well as the observation type(s) made in any given RoI.

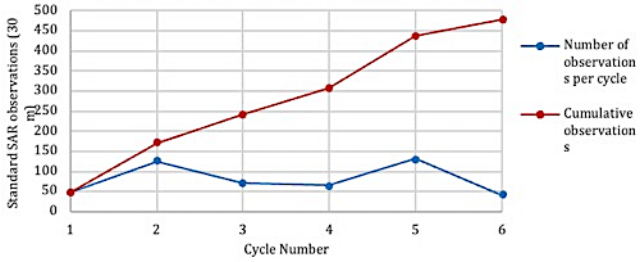

Figure 3.3.2 – *VenSAR 30 m observations (standard SAR, stereo SAR and dual-polarimetry) per cycle and cumulatively during the mission.*

For instance, high resolution SAR and dual-polarization modes are achievable within some of the RoIs, but not necessarily in the same RoIs nor in the same cycle, but these observations will always be coincident with standard SAR imaging so that the different types of observation are always nested to give context within observations of lower resolution. In the EnVision SORS, there are 210 RoIs defined, of which 68 can be imaged three times during the 6 cycles of the mission, and 142 can be imaged twice (in 53 of these, one of the observations will be at dual-polarisation), all at 30 m resolution. In each RoI, imaging at a second, different, look angle, to enable stereoscopy, is achievable at some point during the 6 mission cycles. VenSAR 30 m data acquisition per cycle, and cumulatively, is illustrated in Figure 3.3.2. Global maps showing the evolution of VenSAR data collection across its RoIs through the cycles of the mission, for all observation types, are shown in Chapter 7, Figure 7.1.1.

Table 3.3.1 – *Estimates of the VenSAR 30-m imaging coverage as specified in the Science Operations Reference Scenario with respect to global areal extents of geological terrain types (as mapped by Ivanov and Head, 2015). This should be compared with the coverage requirements listed in Table 3.2.1.*

		Imaging at 30m resolution				Imaging at 10m resolution
Terrain Types	**Fraction of global areal extent**	**All observations within ROIs †**	**Triple observations (change detection) †**	**Double observations (with polarimetry) †**	**Double observations (no polarimetry) †**	**High resolution observations ‡**
Tessera highlands	7%	45%	14%	14%	17%	17%
Tectonically active zones	4%	68%	33%	15%	20%	25%
Impact craters	1%	18%	6%	6%	7%	5%
Lowland plains	80%	18%	6%	5%	8%	5%

Fractions of the global areal extent of each terrain type that can be imaged by VenSAR at 30 m (†) and at 10 m (‡) within the ROIs. Geological terrains as mapped by Ivanov and Head 2015

We now have strong evidence that Venus is the only other geologically active planet in our solar system, thanks to the detection of an expanded caldera and a potential new lava flow at Maat Mons which occurred between Cycles 1 and 2 of Magellan (Herrick and Hensley, 2023). This presents forthcoming missions with the important task of detecting and characterising any other changes that may have occurred since the time of Magellan, as well as optimising their imaging strategies to detect changes during the new mission, especially at the key areas expected to be currently or recently active, e.g. Atla Regio and Imdr Regio.

To help visualise how EnVision will achieve its science goals, the simulated baseline imaging coverage achievable at two key locations, Alpha Regio and Maat Mons, is illustrated in Figure 3.3.3. Contiguous imagery will be collected across their RoIs but not all desirable imaging modes are achievable everywhere in the baseline observation planning. For instance, imaging twice at 30 m resolution (stereo in Cycle 3 and with dual-polarimetry in C5) and once at high resolution (C5) is achievable across the central part of Alpha Regio (Figure 3.3.3a). Conversely, while the summit of Maat Mons and its western flank can be imaged three times at 30 m resolution (C2 and C6, and stereo in C5), neither high resolution nor dual-polarimetry imaging is achievable at these longitudes in this baseline simulation (Figure 3.3.3b); thus observations in those modes would need to be tasked, at the expense of observations elsewhere, in one of the cycles ahead.

This nested VenSAR imaging approach, at distributed RoIs, simplifies targeting and ensures that key features of interest are not imaged in isolation but within their local and regional context. In many areas, RoIs are adjacent to one another, and this will enable seamless image mosaics of extensive regions to be generated,

such as across Aphrodite and Ishtar Terrae. EnVision's complementary, holistic surface science strategy can then be achieved by integration of VenSAR's image products, using stereo-topography, with high density subsurface radar soundings and VenSpec-M data, within and across RoIs. This will enable the semi-automated generation of geomorphology products, classification maps of surface materials and features, as well as change detection datasets. To illustrate how this staggered data acquisition and processing pipeline might function for a change-detection target, Table 3.3.2 illustrates a scenario where a new eruption is detected by VenSpec-M, at Maat Mons, early in the mission.

Table 3.3.2 – *A simulation of a VenSAR image acquisition sequence at Maat Mons and the case of a new eruption detected by VenSpec-M very early in the mission, including some of the likely integrated processing activities that will be enabled as various data are returned during the mission cycles, and some of the desired image products that are not scheduled in the baseline mission, but which would need to be tasked, e.g. high resolution SAR.*

<1994	~2015	2035+ ---------->						
Magellan SAR	**VEx VIRTIS**	**C1**	**C2**	**C3**	**C4**	**C5**	**C6**	**Extended mission**
Maat Mons: Massive shield volcano on western Atla Regio.	Glimpsed only the southern-most part of Maat Mons:	**VenSpec-M anomaly** detected	**1st scheduled 30m VenSAR. VenSpec-M & SRS profiling Tasked High Res 10m VenSAR (if possible)**	**2nd scheduled 30m VenSAR** Enables **Stereo DEM generation** & VenSpec-M	**Tasked High Res 10m VenSAR** & VenSpec-M **Tasked 4th 30m VenSAR at Dual Polarisation (if possible**	**3rd scheduled 30m VenSAR** for intra-mission change detection & VenSpec-M	**Tasked 4th 30m VenSAR at Dual Polarisation** & VenSpec-M	**Tasked** SAR image pairs with suitable baselines for **Repeat Pass Interferometry**
Radar bright. Topographic & emissivity high. Elev. 8 km (5 km above plains). Now proven to be active at the present day.	Emissivity high		Visual comparison of VenSAR with Magellan (& SRS)	**Orthorectification** of Magellan & C3 images. Enables **feature matching** with respect to Magellan	Orthorectification of High-Resolution SAR image	Orthorectification & feature matching	Orthorectification & feature matching	Interferograms and coherence mapping
			Orthorectification & feature matching if VERITAS DEMs available	**Auto-detection of change enabled.** Declutter of SRS using DEM	**Detailed surface & subsurface mapping. Detailed change in small areas**	**Auto-detection of change**	**Automated classification of surface materials, weathering & change detection**	**Quantitative change detection at cm-scale**

Of particular interest is the ~8% of the surface currently classified as 'tessera' highlands, about which little is currently known. These, often highly deformed, terrains appear to be ancient, and they may hold vital clues to Venus' conditions more than a billion years ago – perhaps to a time when conditions permitted liquid water to condense on the planet's surface. Maximizing EnVision's opportunities to understand the planet's past history requires high resolution and dual-polarimetric imaging, detailed topography, and spectral mapping by VenSpec-M, across some of these highlands, to understand their geometry, as well as their physical and chemical or compositional properties, as illustrated by the planned coverage at Alpha Regio in Figure 3.3.3a.

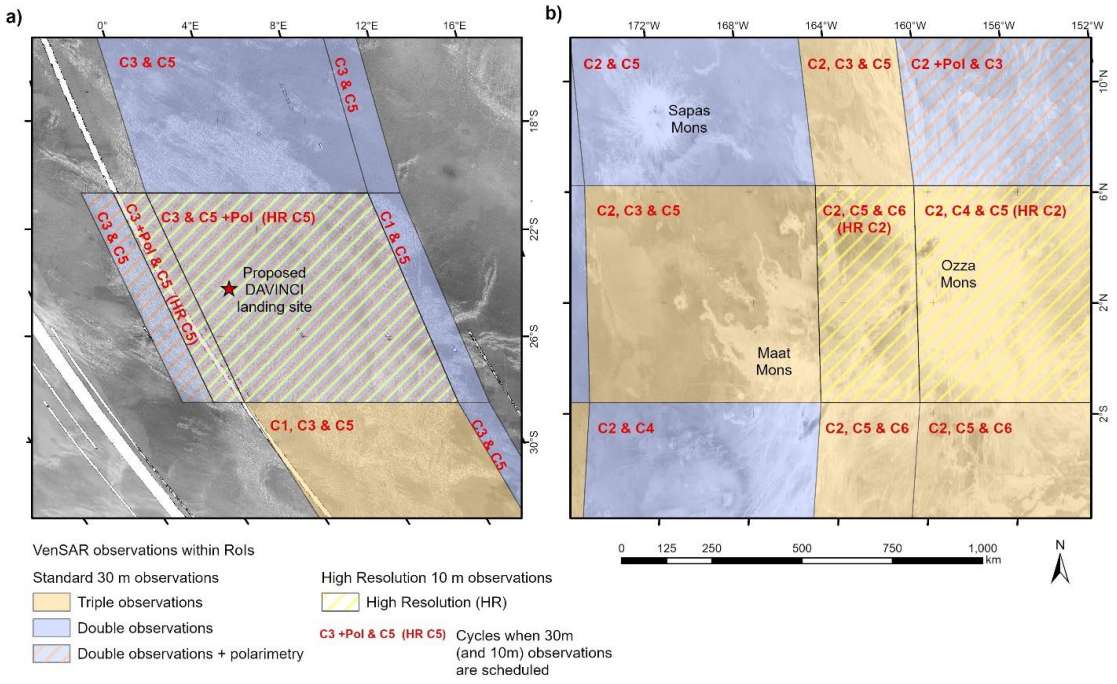

Figure 3.3.3 – *Illustrations of VenSAR targeted observation types and the cycles in which they occur, at a) Alpha Regio and b) Maat Mons, which are history and activity targets respectively.*

VenSAR is the only EnVision instrument which operates in this targeted manor. VenSAR is a far more capable instrument than the Magellan radar, offering not just improved spatial resolution but also superior performance in many other key metrics. A brief comparison of the characteristics of the VenSAR capabilities (based on the aforementioned SORS simulations and the VenSAR instrument measurement and mission requirements), and the Magellan datasets, is given in Table 3.3.3. A full technical presentation of the VenSAR instrument is provided in Section 4.2.

Table 3.3.3 – *EnVision's VenSAR instrument will exhibit markedly superior performance to the Magellan SAR for all of its data products, as shown in this table. A technical description of the VenSAR instrument is given in §4 below. The colours correspond to the different VenSAR modes, as summarized in Table 4.2.1 and Table 4.2.2.. See also Table 7.2.1 for all EnVision instrument coverage numbers resulting from the SORS.*

Parameter	VenSAR Req/ Capability	Magellan
SAR Imaging Modes		
Coverage of planet	20 / 26.4%	99%
SAR imaging spatial resolution	30 and 10 m	120 – 300 m
SAR imaging Swath Width	57 and 20 km	~25 km
Radiometric Resolution	1.1 dB	1.5 dB
Polarimetric SAR		
Dual-pol imaging coverage of planet	5 / 6.5%	<< 1% *
Dual-pol imaging polarizations	HH and HV	HH and VV*
Topography by stereo SAR		
Stereo imaging coverage of planet	18 / 24.3%	20%
Stereo DEM horizontal resolution	300 m	1 – 2 km
Stereo DEM vertical resolution	33 m	50 – 100 m
Altimeter Mode		
Coverage of planet	65 / 69,5%	100%
Vertical Resolution	2.5 m	66 m
Along-track Resolution	3 – 4 km	15-20 km
Radiometer Modes		
Coverage of planet	75 / 96.9%	100%
Along-track resolution	~ 5 km	~ 20 – 80 km
Brightness Temp. Accuracy	1.7 K	15 K
Brightness Temp. Precision	0.7 K	2 K
Radiometry polarization observations	H and V	H and V*

*VV SAR imagery and V radiometry were obtained, in only 12 of Magellan's orbits, by rotating the spacecraft by 90°

3.3.2. Surface Topography

This section demonstrates how the requirement for surface topography (R2-H-30, Table 3.1.1) is traced down and met applying a Science Operations Reference Scenario and the instrument and mission requirements provided in Chapters 4 and 5.

Higher resolution topography products are essential for quantitative modelling of surface geologic processes, like faulting and folding, and for the orthorectification of SAR image products. Thus topography is vital for change detection since this relies on accurate feature matching between VenSAR's repeated images. Surface topography is thus integral to many of EnVision's science investigations, either as the primary data source for understanding the geologic processes that shape the surface, or in providing ancillary information to support the interpretation of other data. The spatial resolution and vertical accuracies required are variable and depend on the investigation; they range between *ca* 250 m to several kilometres spatially and provide vertical accuracies of 10s of metres. Magellan global topographic data with its 15 – 20 km resolution and vertical accuracy of 50 – 100 m is insufficient to support these investigations (Ford, 1992).

Quantitative modelling of faulting and folding requires knowledge of topography with a vertical resolution of 25 – 50 m. Such models can constrain the physical processes that produce the observed tectonic landforms, the magnitude of the deformation, and the mechanical structure of the crust and lithosphere in the vicinity of the tectonic feature. High resolution stereoscopically derived topography data will be vital for the estimation of the post-impact crater fill thicknesses, and spatial resolutions of < 1 km and vertical accuracies of < 20 m will likely be required. Such fine spatial and vertical accuracies will reduce the uncertainty in crater depth-diameter measurements and provide better crater fill thickness estimates (Figure 3.3.4).

Moreover, the globally extensive plains of Venus are under-represented in the RoIs, and thus a globally distributed set of topographic measurements will be particularly important for understanding the plains resurfacing history.

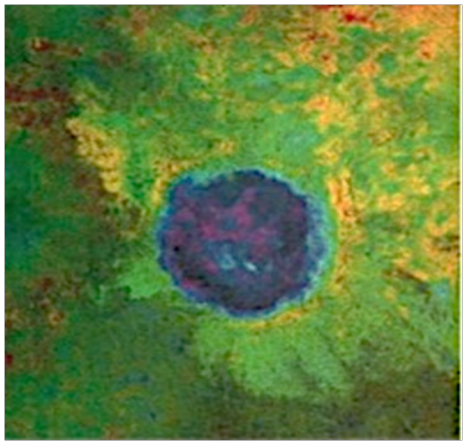

Figure 3.3.4 – *Stereo-derived topography of Markham crater overlain on radar imagery shows that the western portion has no elevated rim and appears embayed by the corona to the west (Herrick, 2000).*

High resolution topography data are also needed for investigations other than those of the SAR itself. Such data are needed to identify likely off-nadir echoes ('clutter') that may confuse feature identification in Subsurface Radar Sounder (SRS) data. High resolution topography is also needed to correct for topographically induced atmospheric effects in VenSpec-M emissivity data, thus topography is also vital in enabling reliable surface rock type determinations and investigation of microwave emissivity as a function of altitude. Variation in surface temperature is primarily dependent on surface altitude; increasing the accuracy of the surface altitude determination to ≤ 10 m would also reduce the uncertainty in the absolute determination of surface emissivity from near-IR nightside observations.

In order to address these science objectives and instrument synergy needs, EnVision has three primary means for topography measurements. Firstly, near-global topographic measurements at low spatial resolution will be made by the VenSAR altimeter and by SRS. These instruments make spot measurements at 2.5 and 15 m vertical resolution, with along-track (spatial) sampling of 3 and 9 km respectively – all of which represent a marked improvement over Magellan topography products, as shown in Table 3.3.3. According to the SORS simulations described earlier and in Section 7.2, the spacing between EnVision's orbital tracks at the equator will be roughly 40 km, and so these data will support a variety of science investigations, such as the aforementioned craters and plains resurfacing, and they will provide an accurate global topographic reference (Fig. 3.3.5). Higher resolution topography will be acquired through radargrammetry or stereoscopy, over roughly 24 % of the surface (18% is required) within the ROIs. By acquiring repeated SAR observations at slightly different look angles, on the order of 5˚ difference, surface elevation or topography can be mapped at about 300 m spatial resolution and 20 – 30 m vertical accuracy, in areas with sufficient scene contrast.

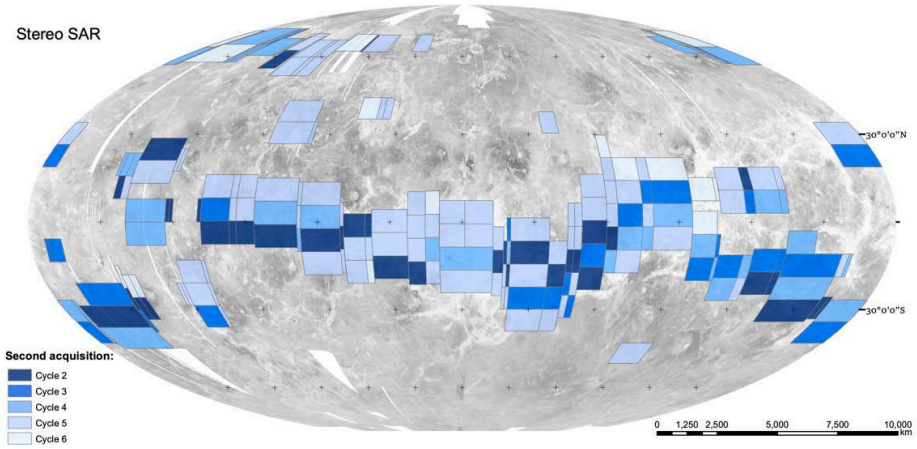

Fig. 3.3.5 – *A Mollweide projection showing the timing of the 2nd acquisitionfor VenSAR stereo at each Region of Interest (RoI). The map is as a measure of how quickly EnVision's VenSAR will acquire stereo topography during the 4-year, 6-cycle nominal mission (see also Figure 3.3.1, Table 3.3.3, Table 4.2.2).*

3.3.3. Surface properties: passive off-nadir radiometry, surface polarimetry, microwave emissivity and Near-IR emissivity

This section demonstrates how the requirements for passive off-nadir radiometry (R2-H-35, Table 3.1.1), surface polarimetry (R2-H-40, Table 3.1.1), microwave emissivity (R2-H-50, Table 3.1.1) and Near-IR emissivity (R2-H-60, Table 3.1.1) are traced down and met applying the Science Operations Reference Scenario simulations and the instrument and mission requirements provided in Chapters 4 and 5.

Used as a passive radiometer, VenSAR has been specified to map the thermal emission emanating from Venus's surface with significantly better precision and accuracy than Magellan's radar (1.0 K against 1-2 K

and 2.0 K against 15 K, respectively, see Table 3.1.1 and Table 3.3.3). These surface brightness temperature (emissivity) maps will then be used to search for thermal anomalies and to infer the composition (via dielectric constant) and physical properties (roughness and density) of the surface materials.

As a baseline, passive radiometry will be carried out in a near-nadir (with a look angle of 14°) or nadir viewing geometry, in parallel with other EnVision instruments. The EnVision SORS simulations confirm that surface microwave brightness temperature will be recorded globally with repeated observations (at least 3 times) and a final resolution likely better than 10 km when using all overlapping near-nadir observations.

Nadir and near-nadir radiometry are primarily designed for the search of thermal anomalies (Section 3.4.1) but they will also be used, based on assumptions on the physical temperature, to build a mosaic of the surface emissivity at 9.5 cm by dividing the measured brightness temperatures by an estimate of the surface temperature. At nadir or near-nadir the microwave emissivity of a surface is largely controlled by its dielectric constant; the surface roughness only has a second order effect. In turn, the dielectric constant is related to the bulk composition and density of the surface material, thus the dielectric map inferred from radiometry measurements can be used to distinguish surface unit material type (Fig. 3.3.6). More specifically, for dry materials, the relationship between dielectric constant and density is generally well described by a power-law function and, with some assumptions, the dielectric map can be readily converted into a global near-surface density map (Campbell et al., 1992).

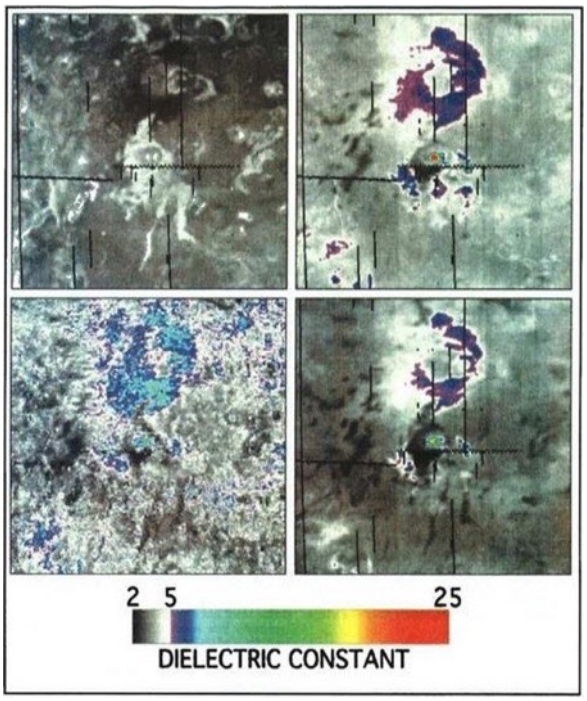

Figure 3.3.6 – *Example of roughness and dielectric mapping from radar and radiometry data for Bell Regio, centred on the 250-km diameter volcano Tepev Mons (Campbell and Rogers, 1994). Clockwise from upper left is (1) roughness map; (2) roughness-corrected dielectric constant; (3) dielectric constant not corrected for roughness; (4) dielectric constant from Magellan radar altimeter data.*

Additionally, polarized radiometry measurements will be acquired in an off-nadir geometry (with a look angle of 25-30°) in selected regions. Additionally, polarized radiometry measurements will be acquired in an off-nadir geometry (with a look angle of 25-30°) in selected regions (>1% of the surface). The main advantage of nadir radiometry is lower sensitivity to roughness than off-nadir radiometry. However, the average of two orthogonally polarized emissivity values (or the polarization ratio) is also less sensitive to roughness than either individual component, and it can be used to provide an independent estimate of the dielectric constant, requiring no assumption on the physical temperature. Such measurements will be primarily performed in Venus's highlands to confirm or infirm their unusually high dielectric constant and put new constraints on their composition candidates. Indeed, recording of both H and V polarization in an off-nadir geometry will distinguish between the effects of dielectric constant and roughness/volume scattering, thus offering an additional powerful tool for surface characterization.

EnVision will also acquire dual-polarization SAR imagery at 30 m resolution for about 6.5% of the surface after 6 cycles (Table 7.2.1) according to the EnVision SORS simulations. As reported in Section 3.1 and Table 7.2.1, at least 5% of the surface is required to be covered. Dual-polarized observations will aid surface characterisation by exploiting the variable polarimetric reflection properties of the surface and its materials. SAR polarimetry is sensitive to surface roughness and structure (e.g. consolidated vs fine-grained material). EnVision employs a dual polarization mode, i.e. transmitting Horizontal (H) and recording H and Vertical (V) polarizations, to enable differentiation of terrain types and to make first-order characterisation of surface properties. Dual-polarization (as opposed to tri- or quad-polarization) was chosen for data-rate and swath-width considerations, and H polarization was selected to match the Magellan data thus enhancing the chance of successful inter-mission change detection.

VenSAR will collect emissivity data at a higher spatial resolution than Magellan, with better precision and accuracy (by a factor ~10) and at geometries (targeted off-nadir polarized measurements) relevant to the science objectives. The VenSAR radiometer data, combined with high-resolution stereo-topography and dual-polarimetric imaging, will improve and refine the mapping of Venus' surface in terms of both composition and physical properties. It will thus provide key information to retrieve the geological history and relative ages of its terrains. In particular, it will help unravel the nature and rate of chemical alteration in Venus high-altitude low-emissivity regions, investigate impact modification in crater ejecta and potentially characterize deeply weathered regions, thick sedimentary layers or signatures of recent resurfacing. By the end of the EnVision mission (after 6 cycles), the EnVision SORS simulation estimate that the radiometry map will cover > 90% of the surface, with a resolution of about 10 km, using all overlapping measurements. As described in Section 3.2, at least 75% of the surface is required to be covered.

The active and passive VenSAR observations described here are complemented also by Near-IR emissivity measurements from VenSpec-M. As discussed in Section 2.3.1 and Section 4.5, the Near-IR spectroscopy takes advantage of narrow atmospheric windows on Venus' nightside to map surface emissivity in six spectral bands at wavelengths between 0.86 and 1.18 μm. This spectral region is particularly sensitive to iron-oxide content. The emissivity maps will be crucial not just in the search for felsic rocks in tesserae highlands (as described in Section 2.3.1), but also as a constraint for the surface material composition studies across all of the EnVision surface investigation domains. Examples include the characterisation of volcanic flows (e.g. d'Incecco et al., 2017) and volcanic highlands, and the investigation of composition changes associated with wind streaks and other aeolian geomorphological features. The VenSpec-M investigation includes eight further spectral bands, most of which are used to compensate for atmospheric variability which otherwise would affect the surface emissivity retrievals. Further details of the instrumental approach is described in Section 4.4. As described in Section 3.1, the VenSpec-M near-IR emissivity maps are required to cover at least 60% of the Venus surface in order to cover all relevant surface types multiple times. VenSpec-M emissivity measurements shall also cover the SAR Regions of Interest where the observations shall be used for synergetic observations as outlined e.g. in Section 3.3.1.

3.3.4. Subsurface material boundaries

This section demonstrates how the requirement for the search for surface material boundaries (R2-H-70, Table 3.1.1) is traced down and met applying the Science Operations Reference Scenario simulations and the instrument and mission requirements provided in Chapters 4 and 5.

EnVision will be the first mission to Venus with a radar sounding instrument onboard[1], and thus the Subsurface Radar Sounder (SRS) will provide the first direct measurements of subsurface features and structures. In this context, SRS provides a unique opportunity to detect, through ground-penetrating 'sounding', the great variety of geologic boundaries and geomorphic units (Figure 3.3.7). SRS will investigate buried stratigraphic and structural patterns, to test hypotheses related to the origin of structures at the surface and in the shallow subsurface and their relationships (Thakur et al., 2022; Figure 3.3.8). This will also enable investigation of processes of interaction between surface features, as well as the detection of 'blind' subsurface structures not directly linked with the surface or surface features.

[1] ISRO's proposed Venus mission Shukrayaan, which is currently expected to launch in 2031, is also considering a sounder, see Section 8 of Widemann et al. (2023)

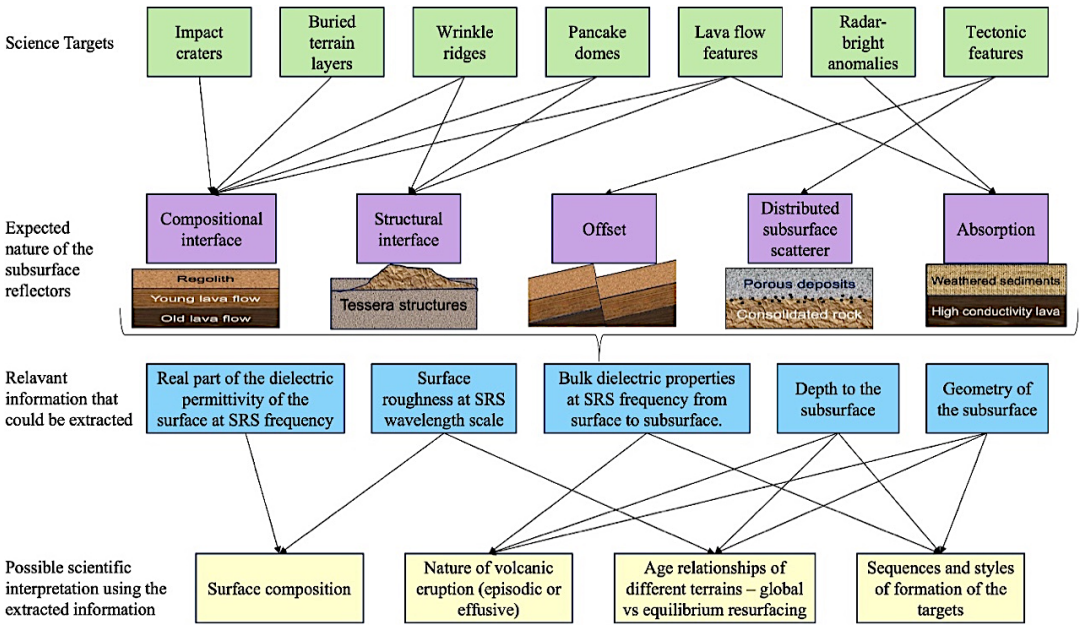

Figure 3.3.7 – *Interlinking between the SRS science targets and the expected nature of the subsurface reflectors. From the radar profiles of SRS, inversion techniques can be applied to extract relevant scientific information, which can be further interpreted (in combination with other ancillary data) to support the understanding of Venus' geological history (Thakur et al., 2023).*

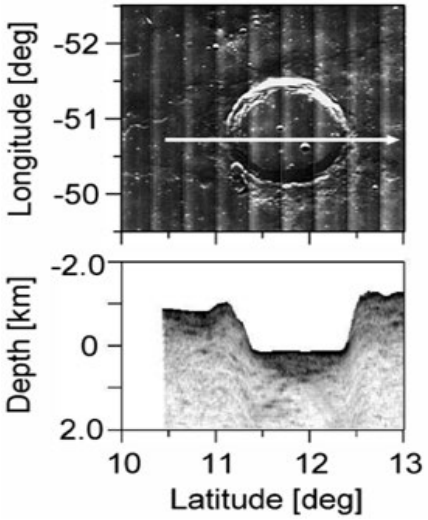

Figure 3.3.8 – *Example of stratigraphic relationships between near-surface layers detected by LRS on the Lunar maria on the Moon (Oceanus Procellarum; depth in m., latitude in deg. (Kobayashi et al., 2014).*

There are many geological investigations for which the detection of subsurface boundaries may provide invaluable constraints. These include understanding infilled or buried impact craters (Figure 3.3.9), the margins of tesserae and their relationship with the plains materials, the margins and 'stratigraphy' of lava flows, and any intersecting tectonic and volcanic features. For any of those features, resolving subsurface characteristics is crucial for the relative dating of surfaces and features by superposition and cross-cutting relationships, the modelling of three-dimensional structure, and the identification of boundaries between units. Delineation of subsurface material boundaries, through sounding, will improve the understanding of Venus resurfacing history and geologic evolution.

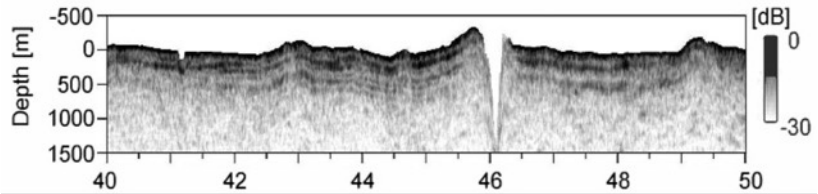

Figure 3.3.9 – *Example of filled crater detected by the LRS on the Moon. Lunar orbiter image of Marius crater (upper) and LRS processed image (lower). LRS ground track is indicated as a white arrow. LRS image clearly shows the basalt filling the inside of the crater to completely cover its original bottom (Kobayashi et al., 2014).*

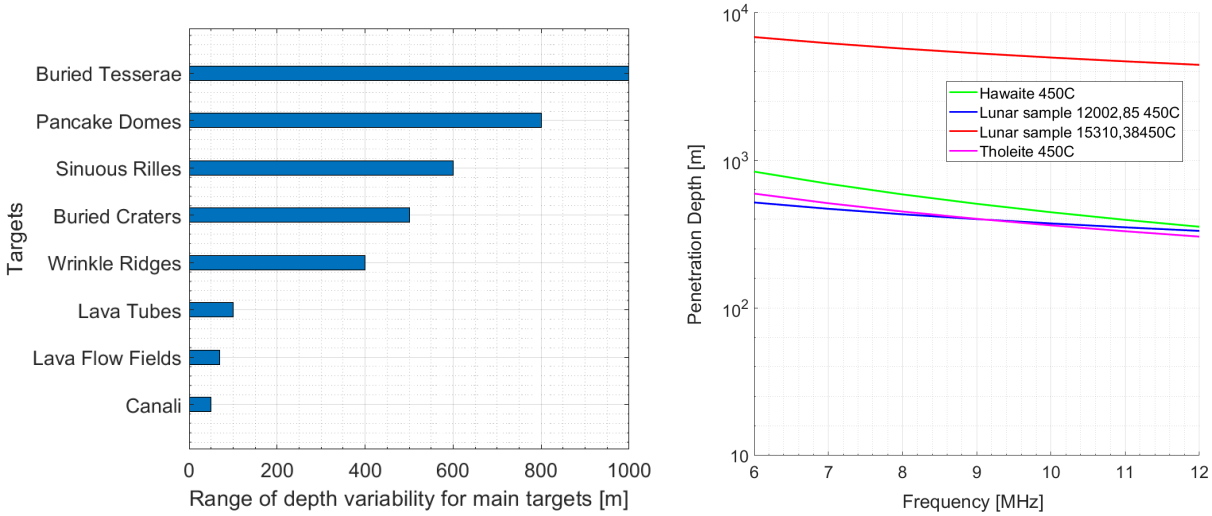

Figure 3.3.10 – *(a, left): Typical range of subsurface depths in which different geological targets can be identified; (b, right:) SRS average penetration depth calculated for different Venus-like samples (from measurements on Moon and Earth analogue materials at Venus temperature) in the SRS bandwidth.*

These investigations will be conducted across the surface of Venus with a required average observation density of 2 per degree of longitude at Equator and a coverage of >65% of the planet, where 75% of the covered area shall be observed from an altitude fulfilling the SNR requirement. This allows for the investigation of a significant number and types of surface targets. In selected RoIs, where these features are also encountered,, a higher average observation density of 10 per degree of longitude at Equator is required. This results in a coverage of ~7% of the planet. The scientific investigations described in Chapter 2 (and summarized in the science traceability matrix, Section 3.6) call for a penetration depth of a few hundreds of metres (up to a maximum of 1000 m) and about 20 metres of vertical resolution (typical ranges of depths in which different subsurface feature types be found are summarized in Figure 3.3.10a). Calculations of penetration depths (shown in Figure 3.3.10b and explained in Section 4.3), confirm that the SRS will be able to investigate a wide variety of geological targets, rock types and surface typologies. To illustrate what might be expected at Venus surface conditions, an example sounder profile through lava at > 600 °C, on the floor of a volcanic crater at Piton de la Fournaise, is shown in Figure 3.2.11. Further information on expected SRS performance is given in Section 4.3.

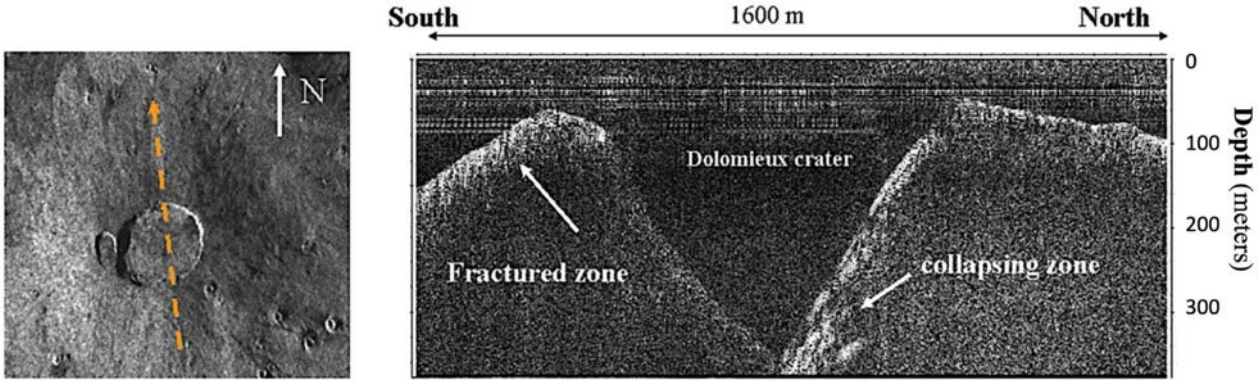

Figure 3.3.11 – *Airborne radar sounder profile at 40 MHz central frequency (more than four times higher than the SRS one) over the Dolomieu Crater on the top of the Piton de la Fournaise Volcano in the Reunion Island in the Indian Ocean. Piton de la Fournaise is a hot spot effusive volcano with geomorphological features and magma dynamic very similar to several Venusian volcanoes (Anderson 2005). The radargram crossing from South to North the main crater on the top of the volcano shows the fractured areas (white areas before and after the crater) that are materialized by the strong signal scattering resulting from the fractures. Inside the crater the radargrams shows the layering that is on the crater's northern wall arising from the succession of debris flowing from the collapsing northern part. The crater depth is approximately 100 m and its width 1 km. The lava temperature ranges from 40 C at the surface to 600 C beyond the 10 m level, demonstrating the viability of HF sounding through rocks at these elevated temperatures (Widemann et al., 2023, adapted from Anderson 2005).*

An important stage in SRS data pre-processing is 'decluttering', which refers to the detection of off-nadir return echoes caused by topography (Ferro et al., 2013; Carrer and Bruzzone, 2017). Therefore, the best quality SRS analysis will be possible within the RoIs, where high-resolution stereo topography will be available. Within the RoIs, SRS sounding will be performed with 'high density' (10 observations per degree of longitude at Equator). The phase B1 SORS simulations yield an SRS high density mode coverage of about

15% of the planet, meeting the requirement of 7% (see Table 7.2.1). Beyond the RoIs, 'low density' SRS investigations (2 observations per degree of longitude at Equator) will be performed over the majority of the rest of the planet, using both topography from VenSAR altimetry, and techniques that do not require a DEM (Carrer and Bruzzone, 2017) for clutter detection. The phase B1 SORS simulations yield an SRS low-density mode coverage of about 70% of the planet, meeting the requirement of 65% (see Table 7.2.1) and with 75% of the covered area observed from an altitude below 350 km fulfilling the SNR requirement.

The SRS will also return valuable information about the surface itself. Echoes from the surface provide information material composition and near-surface reflectivity that can be inverted to help constrain surface permittivity (Watters et al., 2006) at high frequency band. This information can be exploited for reducing ambiguities in VenSAR-derived surface roughness. Moreover, the SRS off-nadir surface (clutter) echoes, when coupled with topography, can both produce high frequency (HF) roughness images of the surface and highlight otherwise undetected shallow subsurface features (Carrer et al., 2021).

3.3.5. Gravity Field

This section demonstrates how the requirement for the observation of the Venus interior and gravity field (R2-H-80, Table 3.1.1) is an improvement compared to our current knowledge, and met applying the Science Operations Reference Scenario simulations and the instrument and mission requirements provided in Chapters 4 and 5.

The current gravity field of Venus is, over large portions of the planet, insufficiently well resolved to allow detection of regional variations that could be related to variations in the lithosphere and crust thicknesses. Indeed, the spatial resolution of the Magellan/Pioneer Venus Orbiter (PVO) gravity solution varies from degree 110 down to 30 (170 km down to 620 km spatial resolution) (Figure 3.3.12). Furthermore, the error on the current solution of the k_2 Love number is 22%, which does not allow determination of the mantle composition, nor the state and size of the core. The EnVision gravity experiment requirement is to obtain a gravity field spatial resolution of < 270 km and an accuracy of < 0.2 mm/s^2 globally, and an improved higher spatial resolution of < 200 km with an accuracy of < 0.1mm/s2 over ≥40% of the planet. Furthermore, the k_2 Love number solution shall be provided with an accuracy of 0.01 (i.e. ~3%). Both gravity field and k_2 Love number are determined from the precise reconstruction of the orbit of the EnVision spacecraft. This Precise Orbit Determination (POD) process relies on the 2-way mode Doppler tracking data and the a priori knowledge of the forces driving the spacecraft motion. Numerical simulations of the POD and gravity reconstruction process including modelling of forces impacting the orbit e.g. gravitational, solar pressure and atmospheric drag show that the EnVision gravity objectives are met with 3.5 hours of effective Doppler tracking per day, using the dual X-Ka band downlink to reduce the solar plasma effect on the Doppler measurements. Simulations show that the error on the k_2 Love number is currently estimated to be better than 1%.

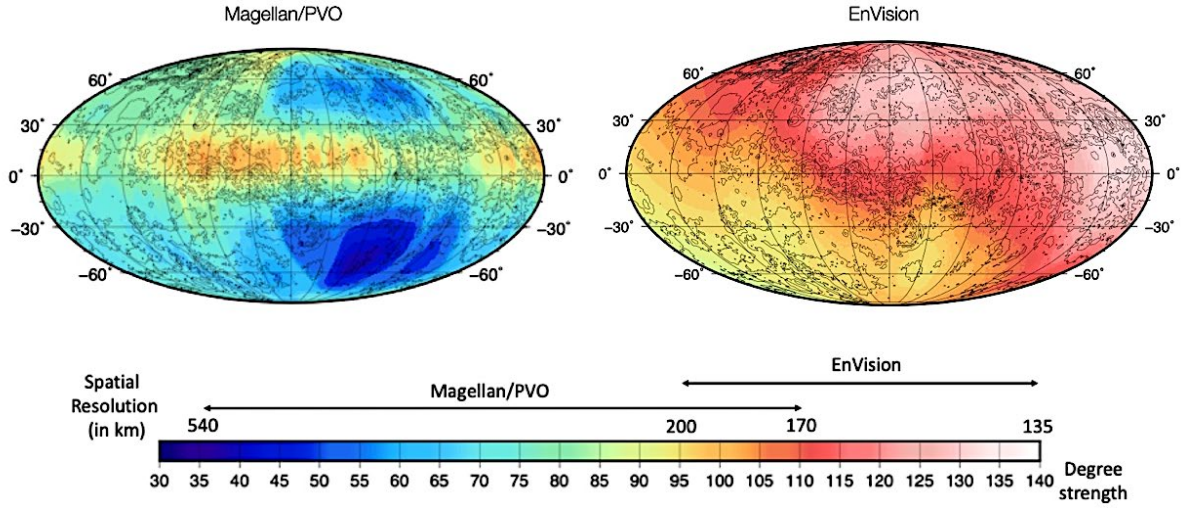

Figure 3.3.12 – *Degree strength map (at 3-sigma) expected after 6 cycles from EnVision (right) vs Magellan/PVO results (left). Maps are in Mollweide projection, centred at 120°.*

The control of the pericentre altitude (at around 220 km) and the mission duration over 6 cycles greatly helps to reach the required resolution and accuracy of the gravity field and k_2 Love number. The Phase B1 SORS simulations also confirmed that the gravity observation coverage requirement is met (see Table 7.2.1).

3.4. Requirements tracing for Activity: EnVision will investigate how geologically active Venus is in the present era

3.4.1. Search for surface temperature anomalies

This section demonstrates how the requirement for the search for surface temperature anomalies (R2-A-10, Table 3.1.1) is an improvement compared to our current knowledge and met applying the Science Operations Reference Scenario simulations and the instrument and mission requirements provided in Chapters 4 and 5.

Currently it is estimated that present volcanic activity can be manifested in anomalously hot surface temperatures due to lava flows, as high as 1200 K. The EnVision mission will search for and monitor spatial and temporal thermal anomalies at the surface with VenSpec-M, and in the near subsurface (with VenSAR operating as a radiometer) over time scales from hours to years and with an effective spatial resolution (including cloud scattering) < 100 km for VenSpec-M and <100 km with VenSAR used in radiometer mode. More specifically, the VenSpec-M IR emissivity mapper will inspect the surface while, depending on the surface composition and therefore on the depth to which the instrument is sensitive, VenSAR operating as a microwave radiometer should be able to probe the near subsurface and detect the thermal signature of an Etna-type eruption (producing 0.1 km^3 or 6 km^2 lava flow at six year intervals) from months to a few decades after it occurred. The eruptions are expected to be detectable in the near-subsurface observations even if the surface itself has cooled to ambient temperature (Lorenz et al., 2016).

A search for thermal anomalies can either include spatial anomalies (regions of unusually high thermal emission) or temporal anomalies (evolution of surface temperatures in repeat temperature measurements within the mission or with respect to Magellan, Venus Express or Akatsuki indicative of volcanic activity). IR observations will be performed on the nightside while microwave observations will be evenly distributed throughout the mission, to obtain coverage at all local times of day. As a start, measurements will be compared to the physical surface temperatures calculated using the adiabatic model of Seiff et al. (1985). The radiometer accuracy will be < 2 K (see Section 3.3.3) to be compared to the 15 K accuracy of the Magellan radiometer. The required precision of 1 K on the recorded brightness temperatures – both in IR and microwave – will guarantee capturing the day-to-night temperature difference at the surface, which latest models estimate to be as much as 3 K at the Equator.

The microwave radiometer will measure the surface brightness temperature at a wavelength of 9.5 cm with a typical footprint on the ground of dimension 5 km x 55 km and an expected final resolution (from overlapping footprints) better than 10 km^2, which represents a significant improvement over Magellan. Venus surface thermal emission at 12.6 cm from Magellan has a resolution of 15 km x 23 km at periapsis (10°N) to about 85 km at the north pole (Pettengill et al., 1991, 1992). It will, as a baseline, operate in a nadir-and near-nadir (14° look angle) viewing geometry which is less sensitive to roughness than Magellan off-nadir observations (for reference Magellan data were collected primarily in H-polarization at look angles of 15-45°) and therefore more appropriate to assess the surface temperature. SORS simulations show that by the end of the EnVision science phase (6 Venus cycles, 4 years), ~76% (VenSpec-M) and ~97% (microwave radiometry) of the Venus surface will have been inspected at least 3 times in search of thermal anomalies (see Chapter 7, Table 7.2.1). If a thermal anomaly is detected in an area not yet included in the RoIs, the mission has the flexibility to observe it at later passes.

3.4.2. Search for changes in surface radar imagery

This section demonstrates how the requirement for surface changes by means of radar imagery (R2-A-20, Table 3.1.1), is an improvement compared to our current knowledge and met applying the Science Operations Reference Scenario simulations and the instrument and mission requirements provided in Chapters 4 and 5.

EnVision employs multiple methods for detecting present data geologic activity on Venus. Changes in radar imagery provide a means of detecting surface changes occurring at the kilometre scale or larger over times spans of 9 months (between cycles of EnVision mapping, see Table 3.3.2) to 45 years (EnVision-to-Magellan). Change detection in radar images is complicated by radar speckle noise and by changes in the imaging geometry. Unlike Magellan, EnVision has planned repeat observations with the same imaging geometry, greatly facilitating more reliable and semi-automated change detection. As outlined in Table 3.3.3, EnVision's SAR will have lower noise levels than Magellan SAR despite its much higher spatial resolution. VenSAR is designed to use at least 8 looks (spatial averaging of radar pixels) for all its radar image products and shall have a Noise Equivalent Sigma Zero (NES0) <-20dB. The speckle/thermal noise will allow more sensitivity to change detection for surface changes like new lava flows or large landslides with the same imaging geometry. Moreover, algorithms exist to efficiently reduce the speckle noise and they proved to be very valuable on the Cassini radar dataset (Lucas et al., 2014).

Decadal time-scale surface modifications will be assessed by comparing EnVision images to Magellan images acquired 45 years before. EnVision uses a radar wavelength very similar to Magellan (9.5 cm versus 12.6 cm) and hence will have similar radar backscatter characteristics. EnVision also plans to acquire its imagery looking to the east to have maximal overlap to that acquired by Magellan. However, as Magellan acquired imagery with a wide range of incidence angle (15˚– 45˚) and at lower resolution than EnVision, reliable comparison demands terrain correction of the imagery using topography data and will necessitate greater care to avoid false detections. By looking for changes exceeding a lower areal threshold, developing robust detection algorithms and by employing the geologic interpretation expertise of the science team we expect to eliminate most false detections.
In order to allow for change detection of regions where active volcanism is expected, and also considering the overall mission constraints, SAR Standard (30 m) third pass observations are required over selected RoIs for about 2% of the planet surface. As shown in Chapter 7, Table 7.2.1, this is achieved according to the Phase B1 SORS simulations.

3.4.3. Search for atmospheric changes

This section demonstrates how the requirements for the observation of atmospheric spatial and temporal variability (R2-A-10, R2-C-10, R2-C-20, R2-C-30, R2-C-40, R2-C-50, R2-C-60, Table 3.1.1) are traced down and met applying the Science Operations Reference Scenario simulations and the instrument and mission requirements provided in Chapters 4 and 5.

As discussed in Section 2.3.5, the search for volcanic activity is conducted not only by surface changes but also by monitoring atmospheric changes such as water vapour, other relevant trace gases or volcanic ash plumes. EnVision will detect such anomalies below the clouds, by searching for water vapour and other relevant trace gas anomalies in three different VenSpec-H altitude regions (0-15 km, 15-30 km and 30-40 km) and with the VenSpec-M low atmosphere water vapour band. The VenSpec-M instrument will furthermore monitor the attenuation in the clouds of the thermal emission from the low atmosphere, which will be applied for the atmospheric correction of the surface thermal emission product. In and above the clouds, the VenSpec-U and -H instrument and the RSE radio occultation observations will allow investigating variations of sulphur and water vapour species and related cloud properties as well as atmospheric dynamics. For a detailed discussion of the atmospheric observation requirements and strategy, the reader is referred to Section 3.5.

3.5. Requirements tracing for Climate: EnVision will investigate how are Venus' atmosphere and climate shaped by geological processes

EnVision's atmospheric science observation requirements have been defined mainly based on the experience from precursor instruments on Venus Express. That experience has been used in a top-down scientific assessment to create a suite of instruments with spectral ranges and resolutions tailor-made for high sensitivity to track key volatile species in the Venus atmosphere from the surface up to the mesosphere. The improved gas sensitivity of EnVision's atmospheric measurement requirements compared to their precursors on Venus Express is summarized in Tables 3.5.1 – 3.5.3. The achievement of these requirements is confirmed through bottom-up end-to-end performance simulations taking the instrument and mission requirements into

account for defined reference atmosphere and surface scenarios, as described in Chapters 4 and 7. EnVision's observations, from low circular orbit, will be very different in spatial coverage than those from Venus Express, offering coverage with higher spatial resolution and more symmetrical latitude coverage than was obtained from Venus Express.

3.5.1. Near-IR nightside spectroscopy to measure tropospheric trace gasses and lower cloud properties

This section demonstrates how the requirements for the observation of the Venus troposphere and lower cloud deck (R2-C-10, R2-C-30,Table 3.1.1) are an improvement compared to our current knowledge and met applying the Science Operations Reference Scenario simulations and the instrument and mission requirements provided in Chapters 4 and 5.

Measurement of gaseous species below the clouds at altitudes of 0 – 50 km will be achieved thanks to several IR spectral transparency 'windows' around 1 μm, at 1.17 μm and 2.3 μm (Table 3.5.1).

Table 3.5.1 – *The EnVision nightside atmospheric gas measurements are informed by, but surpass in sensitivity, equivalent precursor measurements from Venus Express. The requirements for the VenSpec-M, -H and -U spectrometers listed here shows the improvement to similar instrumentation on Venus Express. In §4 and 7, the simulated performances of the instruments are reported.*

Parameter	EnVision	Venus Express
nIR maps: H_2O@ 10-20 km	**VenSpec-M**	**VIRTIS-M-IR**
H_2O relative variability accuracy	10%	~25%
nIR spectra: H_2O @ 10-20 km	**VenSpec-H**	**SPICAV-IR**
Spectral resolving power λ/dλ	~8000	~1700
H_2O random errors	20%	~25%
HDO random errors	30%	Not possible
nIR - gasses @30-40 km	**VenSpec-H**	**VIRTIS-H**
Spectral resolving power λ/dλ	~8000	~2000
H_2O random error	10%	~10%
CO random error	14%	~10%
SO_2 retrieval accuracy	30%	~50%

Through these windows, in-orbit instruments can peer below the clouds down to the lower atmosphere and surface. The thermal radiation emitted by the planet's surface is attenuated as it passes upward through the clouds and the atmosphere. This attenuation arises both because of absorption by cloud particles themselves (nonconservative scattering), and by gaseous absorption. Because the particles are liquid and approximately spherical, and because the wavelength of the light is of the same order as the radius of the particles, one can assume Mie scattering for the calculation of their scattering properties. These measurements can only be performed during the night, when the solar radiation scattered by the clouds does not overwhelm the less intense signal from the surface. EnVision will sound the lower layers of the atmosphere close to the surface to gain information on a series of trace gasses which can be related to volcanism or geological activities on Venus. EnVision will also investigate the lower cloud region to map vertically integrated total cloud opacity, cloud properties and their variations which will be investigated on time scales from hours to years and spatial resolution of ~100 km. The detailed windows into the nightside atmosphere, and the corresponding trace gas species and the altitudes at which they can be measured, are as follows: (1) 1.16–1.19 μm (H_2O, HDO at 0 – 15 km); (2) 1.72–1.75 μm (H_2O, HCl at 15–25 km); (3) 2.29–2.48 μm (H_2O, HDO, HF, CO, COS, SO_2 at 30–40 km). The high spectral resolution (R ~ 8000) coupled to the high sensitivity of the VenSpec-H instrument will be sufficient to clearly identify the absorption features of the targeted species. The full set of observation, measurement and mission requirements are reported in Section 3.1; Chapters 4 and 5.
In order to monitor the major part of the planet for the assessing of the tropospheric spatial variability, also considering the overall mission constraints, VenSpec-H and VenSpec-M observations should cover >60% of the planet. As shown in Chapter 7, Table 7.2.1, this is achieved according to the Phase B1 SORS simulations.

3.5.2. Radio occultation to measure sulphuric species and atmospheric structure

This section demonstrates how the requirements for the observation of the upper troposphere and cloud sulphuric species and cloud and mesosphere atmospheric temperature, pressure and density (R2-C-50 and R2-C-60, Table 3.1.1) are an improvement compared to our current knowledge and met applying the Science Operations Reference Scenario simulations and the instrument and mission requirements provided in Chapters 4 and 5.

EnVision's communication system and an onboard Master Reference Oscillator (MRO, see §4.8.2) will be used by the Radio Science Experiment (RSE) for sounding the neutral atmosphere of Venus, during the occultations that occur during communications links. As the spacecraft starts to be occulted (or after, when reappearing from behind the planet during egress) the spacecraft carrier signal probes the layers of the planet's atmosphere, causing changes in the frequency and amplitude of the carrier waves (at X- and Ka-bands). The bending of the radio-link signal, derived from the frequency shift, allows derivation of profiles of the neutral atmosphere (density, temperature and pressure) and its absorption allows estimation of sulfuric acid concentration, as well as SO_2.

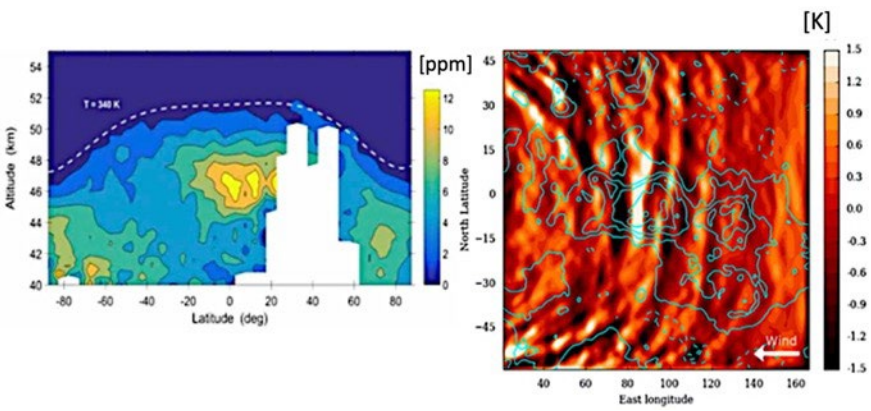

Figure 3.5.1 – *(a, left): Gaseous H_2SO_4 content in function of latitude and altitude derived from radio-occultations by VeRa (Oschlisniok et al.,; 2020). (b, right): Expected temperature anomalies in a gravity wave at 70 km above Aphrodite Terra (Lefèvre et al., 2020).*

The radio-occultation experiment will then determine the atmospheric structure from 35 to 90 km by deriving vertical profiles of neutral mass density, temperature, and pressure as a function of local time and season, with a vertical resolution of a few 100s of meters and an accuracy of 0.1 K at 35 km. Such an accuracy will inform studies of the atmospheric dynamics (gravity waves for instance, see Figure 3.5.1b). Thanks to the use of the dual X-Ka band, the content in liquid phase of the sulfuric acid will be estimated for the first time. The spatial and temporal behaviour of the H_2SO_4 absorbing layer (gaseous and liquid) below the cloud deck will be also investigated (at 35-55 km, with a required accuracy of 3 ppm for the gaseous phase and 30 mg/m^3 for the liquid one with a vertical resolution of 300 m). As shown by Figure 3.4.1a, the H_2SO_4 content varies with depth and latitude. Such an accuracy and vertical resolution, together with the frequent radio-occultations, will allow us to better understand the sulphur cycle.

Table 3.5.2 – *The EnVision radio occultation measurements are informed by, but surpass in sensitivity, equivalent precursor measurements from Venus Express. The requirements listed here shows the improvement to similar instrumentation on Venus Express. In §4 and 7, the simulated performances of the instruments are reported.*

Parameter	EnVision	Venus Express
Radio Occultation	**Radio science**	**VeRa****
Altitude range probed	35 – 90 km	40 – 90 km
H_2SO_4 vapour sensitivity	3 ppm	1 – 3 ppm
H_2SO_4 liquid sensitivity	30 mg/m^3	n/a
Number of profiles per year	~ 720	~100

**Akatsuki also conducted radio occultation, with broadly similar performance to VeRa.

As mentioned in §2.3.7, measurements of the vertical profile of temperature, pressure and number density in the troposphere and mesosphere (35-90 km) of Venus will help to understand the processes driving the short -term as well as the long-term variability of the atmosphere, the cloud-level convection, and the global circulation. As abundance of sulphuric acid in the atmosphere of Venus is linked to a) the present-day volcanic activity and b) the influence of the sulphur cycle, monitoring spatial and temporal variations of H_2SO_4 (gaseous and liquid), on time scales from hours to years with a vertical resolution of ~300 m, will therefore increase the understanding of both, a) and b). Observations should be as widely spread in latitude, longitude and local solar time, and throughout the nominal mission to understand both global circulation processes and transport of atmospheric constituents. The full set of observation, measurement and mission requirements are described in Section 3.1; Chapters 4 and 5.

In order to monitor the major part of the planet for the assessing of the upper troposphere and mesosphere spatial variability, also considering the overall mission constraints, RSE radio occultation observations should cover >50% of the planet. As shown in Chapter 7, Table 7.2.1, this is achieved according to the Phase B1 SORS simulations.

3.5.3. Dayside UV and Near-IR spectroscopy to measure mesospheric trace gasses and cloud-top properties

This section demonstrates how the requirements for the observation of the Venus mesosphere and cloud top (R2-C-20, R2-C-40, Table 3.1.1) are an improvement compared to our current knowledge and met applying the Science Operations Reference Scenario simulations and the instrument and mission requirements provided in Chapters 4 and 5.

The main objective of the EnVision mesospheric investigations is to map the variability of trace species, cloud and aerosol properties and to distinguish intrinsic from extrinsic (e.g. volcanic emissions) variabilities. Sensitive to the UV sunlight scattered by Venus' cloud top, absorption bands allow the detection of ($SO+SO_2$) near 215 nm and SO_2 at 280 nm. Similarly, different IR bands permit the observation of H_2O, HDO, CO, COS, SO_2 at 70–90 km. Observations will provide insight on the spatial distribution of trace gasses essential for the understanding of the main chemical cycles on Venus. Typical spatial resolution of 100 km will help resolve most of the features, but UV monitoring will be able to reach a spatial sampling of ~ 25 km. Moreover, some campaigns with spatial sampling down to 3 km will be used for studying small-scale convection and vertical mixing processes, in particular above specific regions of interest. Typical measurement accuracy should be improved at least by a factor of two compared to previous measurements: total SO_x column density from SPICAV-UV/VEx (Marcq et al., 2013, 2020, 2021), SO:SO_2 ratio from STIS/HST (Jessup et al., 2015). Spatial coverage will also be dramatically improved compared with SPICAV-UV thanks to the much larger FOV of VenSpec-U.

EnVision will investigate the upper atmosphere using the following wavelength ranges and resolutions: (1) 205-235 nm at 0.3 nm spectral resolution (SO_2 and SO separately at 70-80 km); (2) 190-380 nm at 2 nm spectral resolution (UV absorber, total $SO+SO_2$at 70-80 km); (3) 1.36–1.409 μm (H_2O, HDO at 70-90 km); (4) 2.29–2.48 μm (H_2O, HDO, CO, COS, SO_2 at 70–90 km). In the IR range, the high spectral resolution (R ~ 8000) along with the high sensitivity of the instrument will be sufficient to clearly identify the absorption features of the targeted species. In UV, a FOV>20° is required to have 4-5 successive observations over the same ground spot and assess coupling between surface (volcanic activity, topographic features) and cloud top level measurements.

Table 3.5.3 – *The EnVision dayside atmospheric gas measurement requirements are informed by, but surpass in sensitivity, equivalent precursor measurements from Venus Express. The requirements for the VenSpec-H and -U spectrometers listed here shows the improvement to similar instrumentation on Venus Express. In §4 and 7, the simulated performances of the instruments are reported.*

Parameter	EnVision	Venus Express
nIR – gasses @ 70 – 90 km	**VenSpec-H**	**SPICAV-IR***
Spectral resolving power λ/dλ	8000	~1400
H_2O random error	20%	10 – 20%
UV - gasses @ 70 – 90 km	**VenSpec-U**	**SPICAV-UV**
Spectral resolving power λ/dλ	~750 (HR ch)	~200
SO_2 retrieval accuracy	20%	25-50%
SO:SO_2 retrieval accuracy	25%	n/a
Cloud top altitude accuracy	1 km	1 – 2 km

*Both VIRTIS-H and SPICAV-IR measured this; here we have listed the latter instrument.

The full set of observation, measurement and mission requirements are reported in Section 3.1; Chapters 4 and 5.

In order to monitor the major part of the planet for the assessing of the mesospheric spatial variability, also considering the overall mission constraints, the VenSpec-U and VenSpec-H observations should cover >60% of the planet. As shown in Chapter 7, Table 7.2.1, this is achieved according to the Phase B1 SORS simulations.

3.6. Science Traceability Matrix

Table 3.6.1 – *EnVision Science Traceability Matrix. The table traces how top-level science questions are realized through scientific objectives, observation requirements R1 (first two columns) and Science Data products and coverage requirements R2 (H: History; A: Activity; C: Climate).*

Science Objectives	Observation requirements	Science Data product and coverage requirements
R1-H-50: Understanding Venus magmatic history • Change in style and volume of volcanic features • Magma composition range • Volcanic feature variations in morphological characteristics, stratigraphic relationships, and dielectric constant properties • Searching for granite	**R1-H-50:** • Regional and targeted surface mapping of volcanic features • Regional and global topography • Global and local microwave emissivity (nadir and off-nadir) • Polarimetric reflection and emission • Near-Infrared surface thermal mapping • Near-infrared surface spectral emissivity mapping • Sub-surface material boundaries	**R2-H-10:** VenSAR SAR imaging of Regions of Interest (RoIs) • 30 m over 100s km^2, 10 m over 10s km^2 **R2-H-30:** VenSAR stereo imaging • < 300 m horiz., < 80 m vert., 18 % of planet VenSAR altimetry • < 6 km horiz., < 10 m vert., > 65 % of planet **R2-H-50:** VenSAR emissivity maps (radiometry) • < 1 K precision, > 75 % of planet **R2-H-35:** VenSAR emissivity H and V polariz. • < 2 K, < 30 m horiz., > 1 % of planet **R2-H-40:** VenSAR polarimetry • 30 m horiz., Regions of Interest **R2-H-60:** VenSpec-M spectral thermal and emissivity (mapping) • < 4 % accuracy, 60 % coverage **R2-H-70:** SRS sub-surface material boundaries and altimetry • < 3 km horiz along track (2 per longitude at Equator), 20 m vert, 1000 m depth, 65 % coverage
R1-H-60: Understanding Venus tectonic history • Tectonic structure formation • Magnitude of deformation • Lithosphere thickness and heat flow	**R1-H-60:** • Regional and targeted surface imaging mapping • Regional and global topography • Polarimetric reflection and emission • Global microwave emissivity (nadir) • Near-infrared surface spectral mapping • Sub-surface material boundaries • Global and regional gravity field	**R2-H-10:** VenSAR SAR imaging of Regions of Interest (RoIs) • 30 m over 100s km^2, 10 m over 10s km^2 **R2-H-30:** VenSAR stereo imaging • < 300 m horiz., < 80 m vert., 18 % of planet VenSAR altimetry • < 6 km horiz., <10 m vert., > 65 % of planet **R2-H-50:** VenSAR emissivity maps (radiometry) • < 1 K precision, > 75% of planet **R2-H-40:** VenSAR polarimetry • 30 m horiz., Regions of Interest **R2-H-60:** VenSpec-M spectral thermal and emissivity (mapping) • < 4 % accuracy, 60 % coverage **R2-H-70:** SRS sub-surface material boundaries and altimetry • < 3 km horiz along track (2 per longitude at Equator), 20 m vert, 1000 m depth, 65 % coverage **R2-H-80:** RSE gravity field • <20 mGal @ 270 km horiz. res. >95% planet, < 10 mGal @ < 200 km horiz. > 40 % of planet, k_2 Love number > 0.01
R1-H-10: Assess Venus surface modification processes • Highlands brightness and emissivity characteristics • Impact crater modification • Aeolean processes	**R1-H-10:** • Regional and targeted surface mapping • Regional and global topography • Global and local microwave emissivity (nadir and off-nadir) • Polarimetric reflection and emission • Near-Infrared surface thermal mapping • Near-Infrared surface spectral mapping	**R2-H-10:** VenSAR SAR imaging of Regions of Interest (RoIs) • 30 m over 100s km^2, 10 m over 10s km^2 **R2-H-30:** VenSAR stereo imaging • < 300 m horiz., < 80 m vert., 18 % of planet VenSAR altimetry • < 6 km horiz., < 10 m vert., > 65% of planet **R2-H-50:** VenSAR emissivity maps (radiometry) • < 1K precision, > 75 % of planet **R2-H-40:** VenSAR polarimetry • 30 m horiz., Regions of Interest

	• Sub-surface material boundaries	**R2-H-60:** VenSpec-M spectral thermal and emissivity (mapping) • < 4% accuracy, 60 % coverage **R2-H-70:** SRS sub-surface material boundaries and altimetry • < 3 km horiz along track (2 per longitude at Equator), 20 m vert, 1000 m depth, 65 % coverage
R1-H-70: Understanding how Venus interior and surface evolved • Constrain thickness and size of major surface and internal layers (crust/litosphere, mantle, core) • Physical state of the core	**R1-H-70:** • Global gravity observations • Regional gravity observations • Topographic maps	**R2-H-80:** RSE gravity field • <20 mGal @ 270 km horiz. res. > 95 % planet, < 10 mGal @ < 200 km horiz. > 40% of planet, k_2 Love number > 0.01 **R2-H-30:** VenSAR stereo imaging • < 300 m horiz., < 80 m vert., 18 % of planet VenSAR altimetry • < 6 km horiz., < 10 m vert., > 65% of planet **R2-H-70:** SRS altimetry • < 3 km horiz along track (2 per longitude at Equator), 20 m vert, 1000 m depth, 65 % coverage
R1-A-10: Understanding Venus volcanic activity today • Styles of volcanism • Frequency of volcanism • Link to atmosphere and climate	**R1-A-10:** • Spatial and temporal surface and near-surface temperature anomaly mapping over large parts of the planet • Mapping of morphological changes • Variability in tropospheric trace gases originating from volcanic activities	**R2-A-10 and R2-H-60:** VenSpec-M surface temperature and emissivity • T < 1K, <100 km horiz. res., >6 0% of planet • Emissivity: < 4% uncertainty, < 100 km horiz. res., > 60% of planet **R2-A-10:** VenSAR surface brightness temperature observations • < 1K, <100 km horiz. res., >75% of planet **R2-A-20:** VenSAR SAR repeated imaging of Regions of Interest (RoIs) • 30 m over 100s km^2 **R2-C-10:** VenSpec-H high spectral resolution near-IR observations of • H_2O: < 10 % (< 20 % below 15 km), HDO: < 20% (< 30 % below 15 km), CO: < 14%, OCS: < 18%, SO_2: < 30% @ 100-200 km, > 60% of planet (nightside)
R1-A-30: Assessing Venus geomorphological changes • Mass wasting • Aeolian processes	**R1-A-30:** • Spatial and temporal mapping of regional/local regions of interest • Sensing of sub-surface boundaries	**R2-A-20:** VenSAR SAR repeated imaging of Regions of Interest (RoIs) • 30 m over 100s km^2 (>2% of the surface) **R2-H-10, R2-H-20:** VenSAR SAR imaging of Regions of Interest (RoIs) • 30 m over 100s km^2, > 20% of the Venus surface • 10 m, > 2% of the surface **R2-H-30:** VenSAR SAR stereo imaging of RoIs • 30 m at two different incidence angles, > 18% of the surface VenSAR altimetry • < 6 km horiz., < 10 m vert., > 65% of planet SRS altimetry • <20m vertical resolution, < 3 km along-track res., <2 degree long. spacing @ equator and > 65% of the lon's, lat's from -80 to 80 **R2-H-40:** VenSAR dual polarization SAR images • 30m horiz. resolution, >5% of the surface
R1-C-10: Assess state and temporal variations of the Venus troposphere (0-45 km) and how it is linked to geological processes • Understanding tropospheric composition	**R1-C-10:** • Map surface emissivity in the infrared • Map tropospheric gases associated with surface activity • Map atmospheric density, temperature and pressure	**R2-C-10:** VenSpec-H high spectral resolution near-IR observations of • H_2O: <10% (<20% below 15 km), HDO: < 20% (<30% below 15 km), CO: <14%, OCS: <18%, SO_2: < 30% @ 100-200 km, >60% of planet (nightside) VenSpec-M lower troposphere relative variability, • H_2O, hor. res. >100 km^2, >60% of planet **R2-C-30:** VenSpec-M cloud optical density (OD) variability • OD relative variability, < 100x100 km^2 horiz. res.

• Understanding the troposphere sulphur cycle • Understanding tropospheric dynamics		**R2-A-10:** VenSpec-M thermal mapping • < 1K, <100 km horiz. res., >60% of planet • (No requirement: H_2O relative variability, hor. res: >100 km^2, >60% of planet) **R2-C-50:** RSE-RO sulphuric acid observations from 35(45)-55 km • H_2SO_4 (liquid): < 30 mg/m3 accuracy @ <300m vert. res. • H_2SO_4 (gas): < 3 ppm accuracy @ < 300m vert. res. • SO_2 (gas): < 40 ppm accuracy @ <300m vert. res. **R2-C-60:** RSE-RO density, temperature and pressure from 35-100 km • Temperature: 2% accuracy @ 70 km alt., 100m vert res. • Pressure: 2% accuracy @ 70 km alt., 100m vert res. • Density: 2% accuracy @ 70 km alt, 100m vertical res.
R1-C-20: Assessing state and temporal variation of the Venus mesosphere and how it is linked to geological processes • Understanding mesospheric composition • Understand the mesospheric sulphur cycle • Understand mesospheric dynamics	**R1-C-20:** • Measure vertical profiles of sulfuric acid vapour and liquid (35-55 km) • Measure atmospheric density, temperature and pressure (35-90 km) • Map mesospheric gases • Map Venus upper cloud properties (unknown UV absorber)	**R2-C-60:** RSE-RO density, temperature and pressure from 35-100 km • Temperature: 2% accuracy @ 70 km alt., 100m vert res. • Pressure: 2% accuracy @ 70 km alt., 100m vert res. • Density: 2% accuracy @ 70 km alt, 100m vertical res. **R2-C-20:** VenSpec-U Venus upper cloud and mesosphere UV spectroscopy • SO_2: < 20%, SO/SO_2: < 25% @ 5x5 and 25x25 km^2, > 60% of planet (day-side) **R2-C-20:** VenSpec-H high spectral resolution near-IR observations of • H_2O: < 20%, HDO: < 20%, CO: < 20%, SO_2: < 20%, CO: < 20%, OCS: < 20%, HDO: < 20%, < 50 km horiz. res., > 60% of planet (day-side) **R2-C-40:** VenSpec-U observations of unknow UV absorber • Unknown UV absorber: 10% accuracy in radiance factor @365 nm, 5 km sampling, >60% of the planet (day-side)
R1-C-30: Assessing cloud variability and how it is impacted by geological processes	**R1-C-30:** • Map upper and lower cloud variability • Map Venus upper cloud properties (unknown UV absorber)	**R2-A-10:** VenSpec-M near-surface temperature • < 1K, <100 km horiz. res., >60% of planet **R2-C-30:** VenSpec-M relative variability of cloud opacity • Relative cloud opacity variability, 60% coverage (nightside) **R2-C-40:** VenSpec-U UV absorber and cloud altitude • Unknown UV absorber: 10% accuracy in radiance factor @365 nm, 5 km sampling, >60% of the planet (day-side) • Cloud top altitude: 1 km random error **R2-C-50:** RSE-RO sulphuric acid observations from 45-55 km • H_2SO_4 (liquid): < 30 mg/m3 accuracy @ <300m vert. res. • H_2SO_4 (gas): < 3 ppm accuracy @ < 300m vert. res. • SO_2 (gas): < 40 ppm accuracy @ <300m vert. res. **R2-C-60:** RSE-RO density, temperature and pressure from 35-200 km • Temperature: 2% accuracy @ 100 km alt., 100m vert res. • Pressure: 2% accuracy @ 100 km alt., 100m vert res. • Density: 2% accuracy @ 100 km akt, 100m vertical res.

4. Payload

4.1. Payload overview

EnVision carries a robust suite of observing instruments including VenSAR, a dual polarization S-band radar, three spectrometers VenSpec-M, VenSpec-U and VenSpec-H designed to observe the surface and atmosphere of Venus, and SRS a high frequency radar sounding instrument to penetrate into the subsurface. Data from this suite of instruments, coupled with gravity science based on tracking data, and radio occultation measurements will support science investigations of the surface, interior and atmosphere and their various interactions.

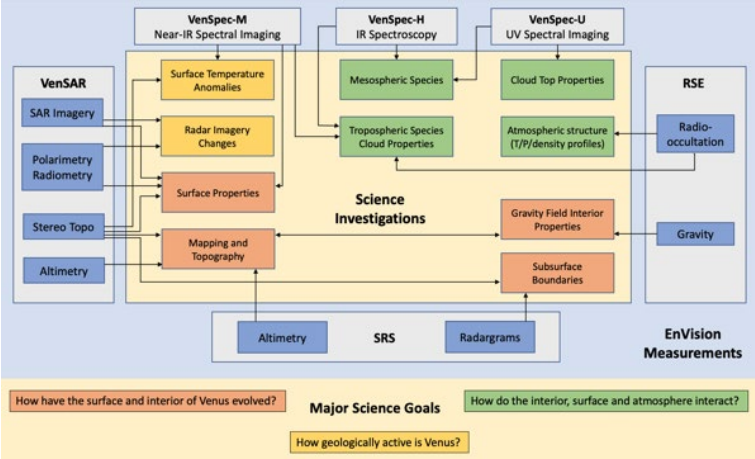

Figure 4.1.1 – *Data flow from EnVision's instrument measurements to science objectives*

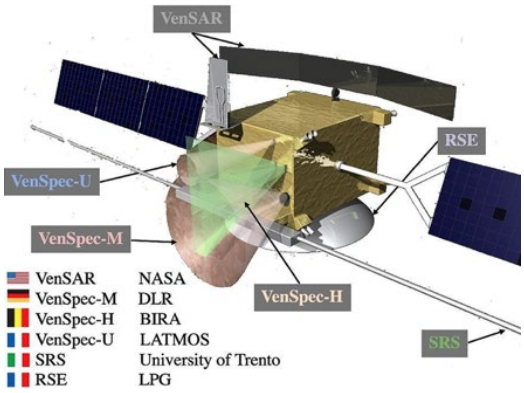

Figure 4.1.2 – *EnVision payload instruments integrated onto spacecraft.*

Each of the payload instruments will be developed and unit tested at the institution responsible for the payload element before being integrated and tested as a combined payload at the spacecraft provider's facility. Figure 4.1.1 illustrates how the suite of measurements address the EnVision science objectives. Figure 4.1.2 shows is an illustration of how the instruments are expected to be mounted on the spacecraft platform. The figure also includes a list of the country and organization responsible for each instrument or experiment. Table 4.1.1 lists the primary science objectives, main characteristics, nominal resources, instrument lead and lead institution for each of the payload subsystems. The EnVision suite of instruments and Radio Science Experiment are described in further detail in the following sections.

Table 4.1.1 – *Instrument and experiment science objectives, main performance characteristics.*

Instrument	Main characteristics	Instrument Lead	Instrument responsibility
VenSAR	SAR Standard Imaging 30 m @ 3.15 GHz, 30 m SAR Stereo Imaging, 10 m SAR High Resolution Imaging, SAR Nadir Altimetry, Dual-Polarimetry 30 m SAR, Radiometric brightness, Off-nadir Microwave Radiometry both H and V polarizations. Repeated 30 m/pix SAR Standard Imaging.	Scott Hensley Jet Propulsion Laboratory, Pasadena, USA	NASA
SRS	Subsurface radar Sounder. Central frequency 9 MHz with 5 MHz bandwidth. Subsurface penetration of up to 1000 m, vertical resolution of 20 m. Low density, High Density, SRS Nadir Altimetry.	Lorenzo Bruzzone Università di Trento, Italy	agenzia spaziale italiana
VenSpec-M	Near-IR spectral / thermal emission from Venus' surface using six narrow bands ranging from 0.86 to 1.18 µm, and three bands to study cloud microphysics and dynamics.	Jörn Helbert DLR Institute of Planetary Research, Berlin, Germany	DLR
VenSpec-H	High-Res. composition and distribution of minor species in the lower atmosphere on the nightside and above the cloud on the dayside. Four spectral bands: 1.165 - 1.180 µm (Band 1), 2.34 - 2.48 µm (Band 2), 1.72 - 1.75 µm (Band 3) and 1.37 - 1.39 µm (Band 4).	Ann Carine Vandaele Royal Belgian Institute for Space Aeronomy (BIRA-IASB), Brussels, Belgium	belspo
VenSpec-U	Distribution and spatial and temporal variations of sulphur bearing gases (SO, SO_2) and unknown particulate absorber at the cloud tops. Dual channel UV spectral imager HR channel 205-235 nm at 0.3 nm spectral resolution; LR channel 190-380 nm at 2 and 5 nm spectral resolution.	Emmanuel Marcq LATMOS, IPSL, Université Versailles Saint-Quentin, Guyancourt, France	cnes
RSE	Tracking using a 2-way coherent carrier Doppler link, X (up) / X-Ka (down); gravity field with a spatial resolution better than 200 km, k_2 Love number accuracy < 1%; USO + 1-way X-Ka coherent downlinks during radio-occultations; H_2SO_4 vapour (at 1 ppm) and liquid (at 1 mg/m^3) content, T and P profiles of the neutral atmosphere.	Caroline Dumoulin LPG,Nantes Université, France	cnes

4.2. Synthetic Aperture Radar VenSAR

4.2.1. Instrument objectives and description

The EnVision VenSAR radar will contribute to addressing the key science objectives of the mission. It will image pre-selected Regions of Interest with resolution of 30 m/pixel and high resolution (10 m/px) across some RoIs. Imaging will be essential for reconstruction of the surface stratigraphy thus revealing geological and chronological relations between surface units. Imaging at two incidence angles will allow reconstruction of surface topography as Digital Elevation Models (DEM) of selected terrains. Quasi-global altimetry would enable quantification of various surface processes. Surface emissivity and roughness will be derived from the imaging in HH and HV polarizations as well as passive radiometry. Comparison to the Magellan images and within the VenSAR data set will allow search for surface changes due to volcanic, tectonic and landscape forming processes from year to decade time scales.

The EnVision VenSAR radar is designed and built by NASA's Jet Propulsion Laboratory, and is a reflectarray antenna concept consisting of a 5.8 m × 0.91 m reflector antenna illuminated by 0.85 m feed separated by a distance of 2.75 m as shown in Figure 4.2.1. Its design was motivated by mass and size considerations, the ability to support multiple modes of operation and a desire to operate with a frequency similar to Magellan thereby facilitating inter comparison of the two datasets. The antenna is a piecewise planar approximation to a parabolic reflector to achieve good sidelobe performance over the entire 60 MHz transmitted bandwidth. The radar supports two bandwidths 15.5 MHz to generate 30 m stripmap imagery with approximately 16 looks, and a 60 MHz mode to generate 10 m stripmap imagery with 8-10 looks and with 2.5 m vertical resolution in the altimetry mode. The radar has a noise equivalent $\sigma_o \leq$-20 dB (where backscatter level equals to the noise power) and operates with incidence angles between 20˚and 40˚ depending on platform altitude (220-540 km depending on latitude, see Table 6.2.2 and Figure 6.2.3). The radar transmits horizontal (H) polarization and can receive both H and vertical (V) polarizations. Additionally, the radar can point to nadir to operate as an altimeter to provide topography and operate passively as a receive-only radiometer to provide brightness temperature measurements with nearly global extent for surface type discrimination and characterization.

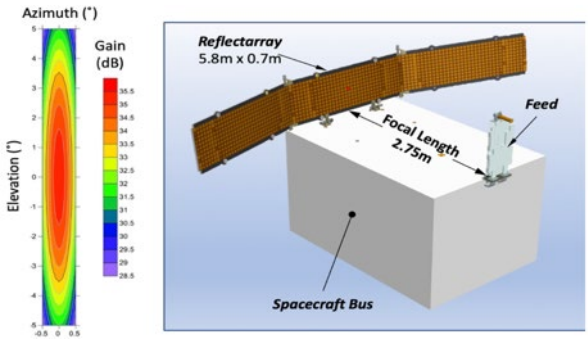

Figure 4.2.1 – *VenSAR is an S-band reflectarray radar designed to image a 57-km swath on the surface with incidence angles from 20° to 40°. The antenna was designed to have side lobes ≤ -20 dB with a short focal length of 2.75 m.*

The VenSAR radar is composed of three primary elements which are the reflectarray antenna, radio frequency (RF) and digital assembly subsystems as shown in Figure 4.2.2. The antenna subsystem consists of the reflectarray, feed, mechanical deployment mechanisms, waveguide choke joints, and interconnect waveguide. The RF subsystem comprises the frequency synthesizer, upconverter, RF receiver, downconverter, solid state power amplifier (SSPA), energy storage subsystem (ESS) and cabling. Control and timing for the radar resides in the Digital Electronics Assembly (DEA) that includes: ADC sampling and signal filtering and decimation; data compression; the command interface from the spacecraft; and the routing of radar science data to the onboard Solid State Mass Memory (SSMM). Key parameters for the radar are shown in Table 4.2.1.

The reflectarray meets key antenna performance requirements with a low mass and power efficient design. This design concept reduces mass and cost by collecting the RF electronics into a single fixed location. A 5.8 m × 0.91 m Folded Panel Reflectarray (FPR) was selected to meet radar antenna requirements. The reflector aperture is partitioned into three 2.0 m × 0.83 m panels that use hinges to stow compactly and deploy shortly after launch.

The reflector is illuminated with a waveguide feed that can handle 2kW peak power and stows compactly against the bus. Beam pointing will be accomplished by physically rotating the spacecraft. Predicted gain is 34.1 dB, including 0.65 dB margin to cover tolerances and other uncertainties. To simplify the feed, the reflectarray separates the V-pol and H-pol focal points by a short distance while keeping the secondary beam peaks co-aligned.

This eliminates the need for a complex dual polarized radiating element. The reflectarray will be thermally isolated from the spacecraft structure.

The RF electronics will be based on the architecture used for SMAP, but at different frequencies and without the chirp generator that will now be replaced with a digital arbitrary waveform generator. The Frequency Synthesizer (FS) will be based on a 10 MHz TCXO from Wenzel that will serve as the radar clock. From this master frequency we will derive a 400 MHz clock signal to serve as the clock for the DAC in the waveform generator. This signal will also be halved to provide a 200 MHz clock to the digitizer used for the H-pol and V-pol receive channels. The ESS will receive 28 VDC (or 50 VDC) from the spacecraft and will provide primary isolation and convert that voltage to the necessary voltages for the SSPA.

Table 4.2.1 – *Key VenSAR Parameters*

Parameter	Value
Center Frequency	3.20 GHz
Antenna Size	5.8 x 0.91 m
Transmit Power	2 kW
Bandwidth	15.5 or 60 MHz
System Noise Temperature	1500˚K
System Losses	-6.5 dB
Atmospheric Losses (2-way)	-1.5 dB
BFPQ Bits	3 (SAR) , 2(Alt)
SAR Modes	
Incidence Angles	20˚-40˚
Polarizations	HH and HV
SAR Swath Width	57 and 20 km
Ground Pixel Size	30 and 10 m
SAR Maximum PRF	3300 Hz
SAR Pulse Length	40 µs
Noise Equivalent σ_o	≤-20 dB
Multiplicative Noise Ratio	≤ -14 dB
Number of SAR Looks	16 and 8
Altimeter Mode	
Altimeter PRF	14800 Hz
Altimeter Presum PRF	426 Hz
Altimeter Vertical Resolution	2.5 m
Altimeter Footprint (Pulse)	3 km
Altimeter Pulse Length	0.5 µs
Radiometer Modes	
Brightness Temp. Accuracy	2.0˚K
Brightness Temp. Precision	1.0˚K

The Solid State Power Amplifier (SSPA) is a single H-polarization stage separated from other RF electronics for thermal reasons, and the GaN SSPA transmitter consists of six power-combined 500 W Sumitomo devices. These parts are pre-packaged; after combining losses and front-end losses they produce 2160 W of peak RF power at a power-added efficiency of 36%.

The Digital Electronics Assembly (DEA) design and implementation draw from recently executed JPL flight radar builds to reduce cost and risk. All of the digital subsystem functionality will reside in a single assembly with a nominal mass of 9.6 kg and power consumption of 45.5 W. Each polarization of the SAR return signal will be digitized by an ADC sampling at 200 MSPS to capture the maximum high-resolution bandwidth mode of 60 MHz. The sampled data will be selectively filtered and decimated based on the operational mode and then compressed and formatted for transfer to mass storage on the spacecraft. The interface to the spacecraft mass storage will be WizardLink. The digital processing for the radiometer sensor application will also reside on the Digital Signal Processing (DSP) FPGA utilizing the same digitized channels as the SAR when no transmit signal is present. The Digital Subsystem will also include the waveform generation, system control and timing, telemetry acquisition and the necessary DC power conversion.

4.2.2. Interfaces and resources requirements

The VenSAR instrument has components mounted both internally and externally to the spacecraft and is designed to operate in the Venus environment.

Mechanical Interfaces and Mass Budget. – The reflectarray and feed are stowed for launch and deployed shortly after launch via damped actuators. Following deployment the reflectarray and feed remain stationary with respect to spacecraft. All electronics (4 assemblies) are mounted to the interior of the spacecraft with SSPA being mounted close to the Feed location and RFES assembly close to the SSPA to reduce RF losses. The ESS also will be mounted in close proximity to the SSPA to reduce cable losses.

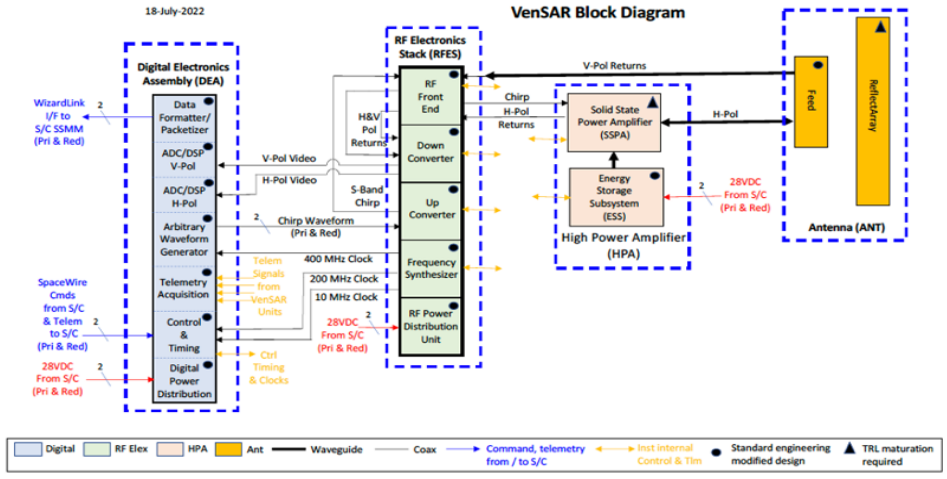

Figure 4.2.2 – *VenSAR instrument block diagram with the major functional elements and their interfaces color coded. The radar consists of three primary subsystems which are the Antenna, RF and Digital Subsystems.*

Thermal Interfaces. – Close proximity of the high power SSPA and ESS presents a thermal challenge and heat pipes are used to dissipate the heat from these units. Thermal analysis of the reflectarray and feed, both during science operations and during aerobraking, show that neither element exceeds its operational or allowed flight temperature limits. Paint, thermal coatings and MLI are employed to protect the exposed antenna assemblies in flight.

Electrical Interfaces and Power Budget. – The DC power bus provided by the spacecraft will be 28V DC. There will be 3 separate DC power bus inputs: one for the RFES, one for the DES, and one for the ESS/SSPA. The VenSAR power converters will provide isolation on the primary side of the DC power bus provided by the spacecraft.

Data Volume and Storage Requirements. – Depending on operational mode the VenSAR instrument has nominal output data rates that vary from 89 Mbs in the 30 m SAR mode, 178 Mbs in the polarimetric SAR mode, 192 Mbs for the 10 m SAR mode, 2.2 Mbs for the altimeter mode and 2 kps for the radiometer modes (nadir, near-nadir and off-nadir). The instrument is designed to operate continuously for up to 13 minutes per orbit in the 30 m SAR mode.

4.2.3. Operation requirements

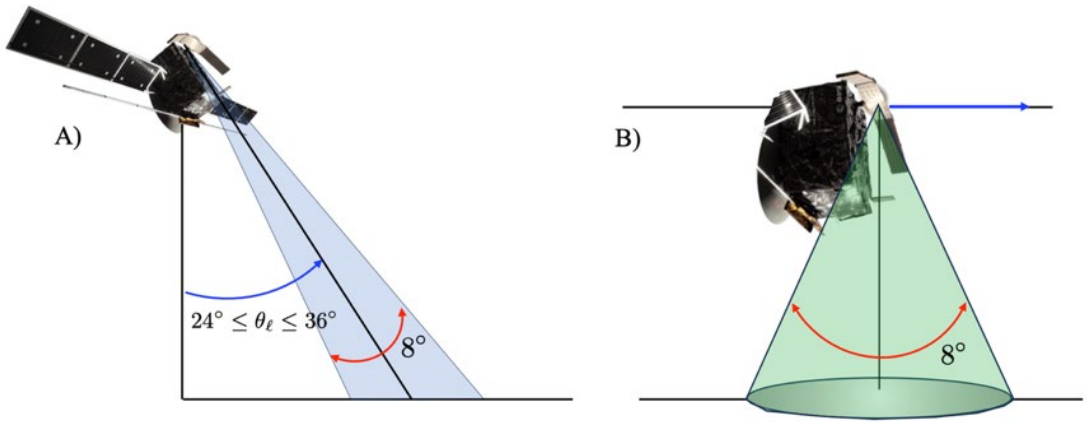

Figure 4.2.3 – *During SAR operations the VenSAR instrument is pointed between 24˚ and 36˚ off-nadir as shown in panel A (velocity vector is perpendicular to the plane of the page, in the direction along the solar panels). During altimeter (and radiometer observations) the VenSAR instrument is pointed to nadir (or 14˚ off-nadir for near-nadir radiometer observations) with the long axis of the antenna perpendicular to the flight track (indicated by the blue arrow) as shown in panel B.*

VenSAR operation is controlled by preplanned command sequences generated on the ground that are regularly uploaded approximately once per week. During SAR acquisition the antenna is oriented to the desired off-nadir look angle whereas during altimeter and nadir looking radiometer observations the antenna is pointed to nadir, or slightly off nadir by 14˚ for certain radiometer only passes, with the long axis of the antenna perpendicular to the flight track as shown in Figure 4.2.3. The command sequences are transferred from the spacecraft to the radar and are executed based on time provided by the radar clock. A timing offset uploaded every couple of days compensates for along-track timing offsets from the time the commands were generated on the ground and uploaded to the spacecraft. Parameters uplinked to control the radar include PRF, timing for the data window,

bandwidth and sampling frequency, pulse-length, polarization channels and the number of BFPQ bits. As the orbit is elliptical the PRF and data window commands can be updated every 100 seconds.

4.2.4. Heritage

VenSAR design is predicated on flight qualified designs and technologies used by JPL on other flight programs like the NASA/ISRO Synthetic Aperture Radar (NISAR) and Surface Water and Ocean Topography (SWOT) missions. The most novel element of the radar is the transmitter which is a solid-state power amplifier undergoing early prototyping risk mitigation activities and testing prior to the Mission Selection Review (MSR, which took place in 2021). Reflectarray panels, feed, hinges, HDRMs, viscous dampers, and boom designs are all based on flight proven or flight qualified designs that will require only engineering modifications for the VenSAR application. JPL has successfully used similar deployable FPR antenna technology on the ISARA (Ka-band, Earth LEO) and MarCO (X-band, Mars) missions, and recently flight qualified a 5 m Ka-band FPR with a similar waveguide feed for SWOT. The SSPA is based on solid-state GaN 500W devices from Sumitomo, screened by the vendor to flight specifications. The ESS design will be based on heritage flight designs, most recently the ESS design qualified for the NISAR T/R Modules. The Digital Electronics Subsystem is based on NISAR designs. Circuit designs previously implemented on REASON and SWOT are added to enable waveform generation and potentially DDR memory for data buffering if required.

4.2.5. Instrument Performance

The VenSAR instrument acquires data in 3 data collection modes which are the 15.5 MHz and 60 MHz bandwidth SAR modes used to generate 30 m/pix and 10 m/pix SAR imagery respectively, a nadir looking altimetry mode used to generate topography measurements and passive receive mode whereby nadir, near-nadir and off-nadir passive microwave radiometry measurements are used to measure surface brightness temperature and emissivity. The VenSAR instrument will also acquire SAR imagery at with incidence angles separated by about 5˚to generate 300 m spatial resolution SAR stereo topographic maps. For each science mode, well established radar performance models and metrics are used to quantify instrument performance and to establish how each mode will meet the requirements for the science objectives it supports. The performance model incorporates a detailed instrument model including RF, digital and antenna subsystems, orbital ephemeris and pointing over the full 6 cycles of the mission, model of the Venus atmosphere and surface scattering and S-band informed by the Magellan mission. For all VenSAR modes of operations, we have adequate performance margin to meet all science objectives (see Section 7.3.1).

4.2.6. VenSAR measurement and instrument requirements

Based on the top-down requirements assessment analysis and earlier Venus's mission payloads, the following set of VenSAR measurement and mission requirements were defined in phase 0 and phase A. These were confirmed to meet the VenSAR product and coverage requirements through bottom-up performance simulations. In phase B1, some requirements were updated based on a further maturing of the instrument and mission design and new bottom-up performance simulations (see Section 4.2.5; and Chapter 7, Section 7.3.1). Finally, the coverage requirements were confirmed through the ESA SORS simulations (Chapter 7, Sections 7.1-2).

Table 4.2.2 – *VenSAR measurements and mission requirements associated to the different VenSAR instrument modes. Beige: radiometry, light red: stereo, light blue: altimetry, light orange: SAR imaging, light green: polarimetry. White: requirements applicable to several modes.*

Requirement number	Parent	Requirement description
R3-MEA-015	R2-A-10	Acquire brightness temperature measurements of the surface (1) at a wavelength of 9.3685 cm (2) in a nadir or near-nadir (~13 off-nadir) viewing geometry (3) with a precision over a radiometry pass of < 1 K (4) and an absolute accuracy of <2 K in the 650-1200 K surface temperature range (5) with spatial resolution of <50 km (the spatial resolution will be met when the altitude is below 350 km).
R3-MEA-050	R2-H-35	Acquire brightness temperature measurements of selected surface areas (1) at 9.3685 cm wavelength in (2) both V and H polarizations (3) in an off-nadir viewing geometry (all radiometry off-nadir angles from nadir to a particular target)

		(4) with a precision over a radiometry pass of < 1 K (5) and absolute accuracy of ≤ 2 K or better in a 650-1200 K surface temperature range (6) with spatial resolution of ≤ 50 km (the spatial resolution is met when the altitude is below 350 km).
R3-MEA-080	R2-H-20	Acquire 30 m SAR observations at two different look angles of ɵ1 and ɵ2 over the selected RoIs, for the generation of stereo-derived topography data. The nominal look angle for the SAR observations is ɵ1= 30˚±2˚, and the stereo pair look angle is ɵ2=ɵ1+Δ, where -4.0≤Δ≤-6.0.
R3-MEA-085	R2-H-30	Acquire nadir-looking radar altimetry with (1) 10 m vertical resolution (intrinsic radar range resolution) and (2) ≤6 km along track resolution.
R3-MEA-090	R2-H-10 R2-H-20	Acquire SAR surface images with (1) 30 m pixel spacing and (2) SNR sensitivity or Noise Equivalent Sigma Zero (NES0) <-20dB (enabling sufficient contrast for feature recognition on the plains).
R3-MEA-100	R2-H-20	Acquire SAR surface images of selected target areas at ≤ 10 m spatial resolution.
R3-MEA-124	R2-H-10 R2-H-20	VenSAR shall operate with a centre frequency of 3.2GHz (wavelength of 9.3685 cm).
R3-MEA-125	R2-H-40	Acquire dual-polarization SAR images (polarized and cross-polarized linear) (1) with a horizontal spatial resolution of 30 m and (2) a NES0 ≤-20 dB and (3) a swath width >54 km.
R3-MEA-126	R2-H-10 R2-H-20	VenSAR shall have a calibrated backscatter accuracy of 3 dB excluding topographic effects for the 30 and 10 m SAR backscatter imagery.
R3-MEA-127	R2-H-10 R2-H-20	VenSAR shall have a 1.0 dB (TBC) relative radiometric accuracy over the swath excluding topographic effects for the 30 m and 10 m SAR backscatter imagery.
R3-MEA-128	R2-H-10 R2-H-20	VenSAR shall have 1.3dB (1-sigma) (TBC) swath averaged radiometric resolution for the 30m resolution SAR products for altitude and look angle range where the MNR requirement (R3-MEA-129) is satisfied.
R3-MEA-129	R2-H-10 R2-H-20	VenSAR shall have a swath averaged Multiplicative Noise Ratio (MNR) which includes ISLR, ambiguities and quantization noise less than -16 dB (TBC).
R3-MIS-020	R2-H-10 R2-H-20	The mission shall (1) Enable Standard SAR imaging at 30 m spatial resolution, with the same look direction, over selected RoIs, (2) at incidence angles between 20° and 40°. (3) The images shall be contiguous within each RoI. (4) The standard SAR observations, over the selected RoIs, shall cover 20% of the Venus surface.
R3-MIS-015	R2-A-10 R2-H-50	For radiometric brightness (1) The mission shall enable microwave radiometric measurements in a nadir or off-nadir (~14°) viewing geometry for 75% of the surface. (2) At least 2 observations of each covered region shall be performed.
R3-MIS-016	R2-A-10 R2-H-50	VenSAR altimeter and radiometer observations shall be acquired while maintaining the pointing of the antenna beam such that the nadir or off-nadir pointing is within ±0.2˚ (TBC) of the nominal desired commanded pointing angle throughout a data take.
R3-MIS-020	R2-H-10 R2-H-20	The mission shall (1) Enable Standard SAR imaging at 30 m spatial resolution, with the same look direction, over selected RoIs, (2) at incidence angles between 20 and 40 deg (3) The images shall be contiguous within each RoI. (4) The standard SAR observations, over the selected RoIs, shall cover 20% of the Venus surface
R3-MIS-021	R2-H-10 R2-H-20	VenSAR (stereo) (polarization) (standard or high resolution) imaging SAR observations shall be acquired with an absolute error between the SAR antenna principle direction and the commanded beam direction better than 1/12th of the radar beamwidth in elevation (TBC), and 1/10th in azimuth (TBC), with a 95% confidence level (2σ) assuming a statistical mixed interpretation (APE).
R3-MIS-025	R2-H-30 R2-A-20	The mission shall accommodate ROIs distributed anywhere in latitude and longitude on the surface of the planet.
R3-MIS-030	R2-A-20	The mission shall enable a third SAR observation at 30 m spatial resolution (1) with the same look direction and over selected RoIs imaged in R3-MIS-020, focusing on volcanic provinces covering >2% of the surface, and (2) at an incidence angle within +-1.5 deg of either of the standard or stereo observations made in R3-MIS-020-(4) or R3-MIS-060.
R3-MIS-035	R2-H-10 R2-H-20	The altitude of the VenSAR science observations in the SAR modes, during the nominal mission lifetime, shall be such that: (1) the maximum altitude is always less than 510 km (2) the minimum altitude should be greater than 220 km (TBC) (3) VenSAR SAR observations shall be acquired with at least 75% of data collected below 350 km in altitude
R3-MIS-040	R2-H-20	The mission shall enable 10 m spatial resolution SAR imagery to be obtained for 2% of the surface.
R3-MIS-060	R2-H-20	The mission shall: (1) Enable Standard SAR to be obtained at a different view angle for stereo at 30m (as defined in R3-MEA-080), with the same look direction (2) Enable the second 30m SAR imaging observation of 18% of the surface (i.e. 90% of the area covered in R3-MIS-020-(4)) for stereo-imaging. The two observations constituting a stereo pair shall overlap over at least 90% of their respective swath, with a 95% (2 sigma) confidence level.

R3-MIS-070	R2-H-40	The mission shall enable the collection of dual-polarization SAR imagery at 30-m resolution for 5% of the surface.
R3-MIS-080	R2-H-30	The mission shall enable the measurement of surface topography with nadir altimetry with an average observation density of 2 per degree of longitude at Equator over at least 65% of the longitudes.
R3-MIS-081	R2-H-10 R2-H-20	VenSAR shall have 300 m (TBC) 1-sigma geolocation accuracy in both azimuth and ground projected range, in average over all VenSAR SAR data.
R3-MIS-210	R2-H-35	The mission shall enable off-nadir dual polarization radiometer imaging for a set of selected target areas totalling 1% (TBC) of the surface during the nominal mission lifetime.

4.3. Subsurface Radar Sounder SRS

4.3.1. Instrument objectives and description

SRS will be the first instrument to profile the subsurface of Venus and thus will acquire fundamental information on subsurface geology by mapping the vertical structure (mechanical and dielectric interfaces) and properties of tesserae and their edges, plains, lava flows and impact craters and debris, thus providing useful data for inferring the genesis of these features. It also provides information on the surface in terms of roughness, composition and permittivity (dielectric) properties at wavelengths much longer than those of VenSAR, thus allowing a better understanding of the surface properties. SRS also obtains altimetry measurements by providing low-resolution profiles of the topography that can be integrated with the altimetric data of VenSAR. It has also the capability to detect lightning when operating in receiving only mode (see Section 8.1.1).

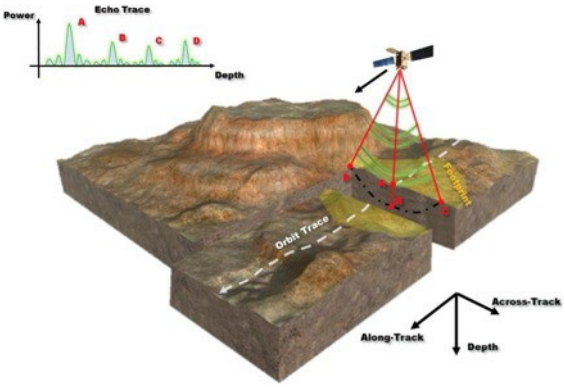

Figure 4.3.1 – *SRS acquisition concept (Carrer and Bruzzone, 2017). Varying reflections are detected by the radar receiver and used to create a depth image of the subsurface (referred to as radargram) and map unexposed subsurface features.*

SRS is a nadir-looking radar sounder instrument which transmits low frequency radio waves with the unique capability to penetrate the subsurface (see Figure 4.3.1). The long-track resolution (after focusing) is between 1.90 and 2.90 km, depending on the spacecraft altitude (220-500 km). The across-track resolution is between 7.2 and 11.0 km (satellite altitude dependant). The track-to-track distance is ~50 km for the low density sounding (global) mode, and ~10 km for the high density sounding mode. As these radio waves travel through the subsurface, their reflected signal varies through interaction with subsurface horizons and structures with different dielectric constants. These varying reflections are detected by the radar receiver and used to create a depth image of the subsurface (referred to as radargram) and so map unexposed subsurface features.

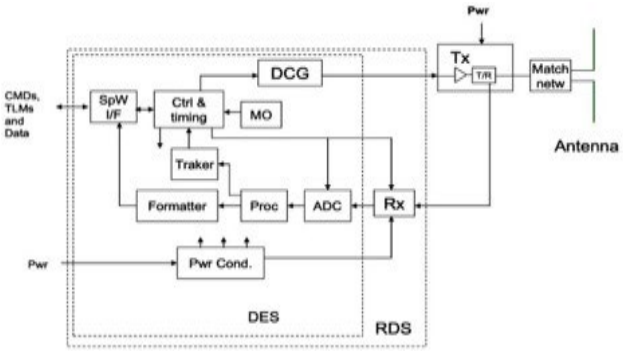

Figure 4.3.2 – *SRS block diagram.*

As discussed in §3.3.4, the scientific requirements call for a subsurface penetration of between few tens and few hundred meters (up to 1000 m in favourable conditions on terrain attenuation), and a vertical resolution of 20 m (summarized in Figure 4.3.1). This drives the selection of SRS central frequency, transmitted bandwidth and power. The penetration depth for SRS sounding has been calculated considering a wide range of dielectric properties at Venus temperature, corresponding to many different possibilities for the composition and the porosity of surface material, such as basaltic (from Lunar, Terrestrial and Martian analogues), granitic and rhyolitic; these calculations are based on dielectric properties of rocks at elevated temperatures (e.g., Bruzzone et al., 2020). The operating frequency also needs to be high enough to minimize interference from the ionosphere. This leads to adopting a central frequency of 9 MHz with 5 MHz bandwidth as the baseline SRS design. The radiated peak power is 200 W, an order of magnitude higher than that of MARSIS and SHARAD to address the expected increase of attenuation on Venus. Figure 4.3.2 shows the SRS overall architecture that includes three main units: the transmitter (TX), the Receiving Digital Subsystem (RDS) including the Digital Electronic subsystem) and the

Matching Network (MN). The deployable dipole antenna with a total length of 16 m will be provided by the spacecraft manufacturer.

4.3.2. Interfaces and resources requirements

The instrument nominal mass is 12.8 kg excluding the antenna. The SRS peak radiated power is 200 W, while the average power consumption is 115 W. The data rate for the main science modes ranges between 3.35 Mbps and 6.69 Mbps. The estimated total data volume collected over the nominal mission is 16 Tbits.

4.3.3. Operation requirements

During operations the SRS antenna shall be parallel to the ground with an absolute pointing error of ±5 degrees. On Venus the maximum plasma frequency on the day side is 5–6 MHz, and below 1 MHz on the nightside. Thus, acquisition of the SRS should be performed at nighttime to limit ionospheric distortions that can be corrected with consolidated techniques (Campbell et al., 2011; Restano et al., 2016). Moreover, to reduce the noise of solar electromagnetic radiation, the instrument itself shall be in eclipse. The instrument is very versatile and can be programmed in different ways. The two main science modes are: 1) SRS high-density mode is optimised for acquiring data on targets of high interest over 10 % of the surface of Venus with average observation density of 10 per degree of longitude at Equator and no compression; 2) SRS low-density mode will perform measurements over 65 % of the surface of Venus with average observation density of 2 per degree of longitude at Equator and lossy data compression. To meet the coverage requirement, the nighttime observations will be distributed over all the nominal mission.

4.3.4. Heritage

SRS benefits from rich heritage in the development of planetary radar sounders. These instruments were extensively used in planetary investigations. Two subsurface radars are currently operating at Mars: 1) the Mars Advanced Radar for Subsurface and Ionosphere Sounding (MARSIS) on-board ESA's Mars Express spacecraft optimised for deep penetration of the Martian subsurface (Picardi et al., 2005); and 2) the SHAllow RADar (SHARAD) on-board NASA's Mars Reconnaissance Orbiter (Seu et al., 2007) optimised for high vertical resolution with shallow penetration. The subsurface of the Moon is explored by the Lunar Radar Sounder (LRS) on-board the SELENE, Kaguya mission (Ono et al., 2009). For the study of the Jovian icy moons, two radar sounders are under development: 1) the Radar for Icy Moons Exploration (RIME) on-board the Jupiter Icy Moons Explorer (JUICE) (Bruzzone et al., 2015); and 2) the Radar for Europa Assessment and Sounding: Ocean to Near-surface (REASON) on-board the Europa Clipper. SRS will be mainly based on the heritage of RIME (which operates at the same central frequency considered as baseline for SRS).

4.3.5. Instrument Performance

The performance of SRS has been derived by considering advanced radar sounder simulation techniques (Gerekos et al., 2018; Thakhur and Bruzzone, 2019) and by realistically modelling different target terrains on Venus. A hierarchical approach to the simulation has been followed by considering all main variables affecting the performance with an increasing level of detail. Simulations of different Venus geological scenarios (e.g., buried craters, lava flows) have been performed for assessing the detectability of subsurface interfaces under different conditions of digital elevation models (clutter) and dielectric contrast, as described in Bruzzone et al. (2020); an example is given in Figure 4.3.3. The results indicate that the baseline design of SRS meets the required detection performance for important Venusian target types. Further details from the SRS end-to-end performance simulations are provided in Section 7.3.2.

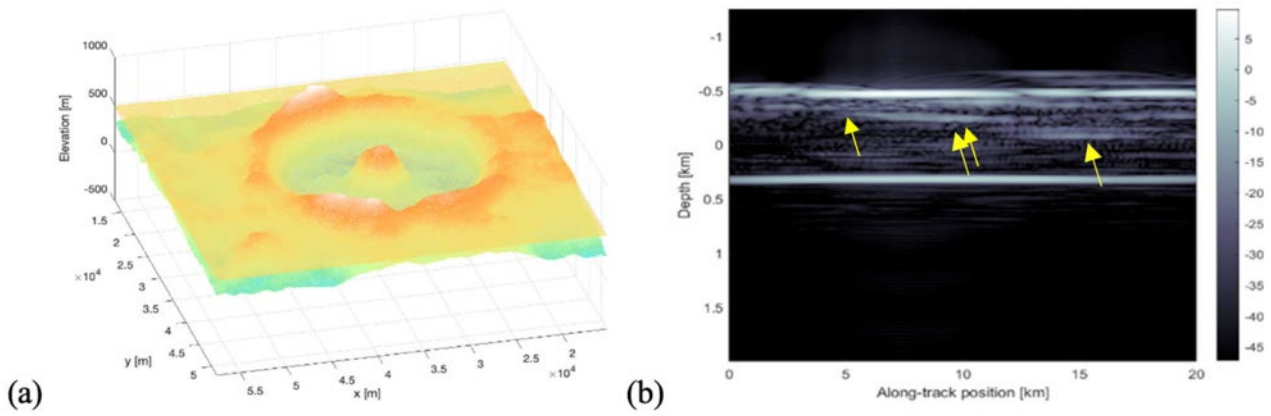

Figure 4.3.3 – *Example of 3D simulation of sounding of a crater partially buried up to a depth of 200-600 m under the plains (and , with the underlying crater material having (a, left): 3D model of the buried crater derived starting form Magellan stereo DEM. (b,right): Simulated radargram with the yellow arrows showing the diffused reflections from the buried crater floor. Further simulations of craters, tesserae and lava flows are described in (Thakur et al.,2020).*

4.3.6. SRS measurement and instrument requirements

Based on the top-down requirements assessment analysis and earlier Venus mission payloads, the following set of SRS measurement and mission requirements were defined in phase 0 and phase A. These were confirmed to meet the SRS product and coverage requirements through bottom-up performance simulations (see Section 4.3.5 and Chapter 7, Section 7.3.2). In phase B1, some requirements were updated based on a further maturing of the instrument and mission design and new bottom-up performance simulations. Finally, the coverage requirements were confirmed through the ESA SORS simulations (Chapter 7, Sections 7.1-2).

Table 4.3.1 – *SRS measurements and mission requirements*

Requirement number	Parent	Requirement description
R3-MEA-130	R2-H-30 R2-H-70	Perform low-density sounding (on-board lossy compression/presumming performed) of the subsurface structure at SRS wavelength with (1) SNR at the surface: ~74 dB (assuming an orbit altitude <350 km); (2) Frequency band width: 5 MHz around the 9 MHz central frequency; (3) Horizontal resolution: ≤ 3 km along-track, ≤ 11 km across-track (the pulse limited footprint is defined as sqrt(altitude * c / bandwidth), assuming an orbit altitude <510 km); (4) Vertical measurement resolution: ~20m
R3-MEA-135	R2-H-70	Perform high-density sounding (no lossy compression/presumming performed) of the subsurface structure at SRS wavelength of the SAR imaging mode RoIs with: (1) SNR at the surface: ~74 dB (assuming an orbit altitude <350 km); (2) Frequency band width: 5 MHz around the 9MHz central frequency; (3) Horizontal measurement resolution: ≤ 3 km along-track, ≤ 11 km across-track (the pulse limited footprint is defined as sqrt(altitude * c / bandwidth), assuming an orbit altitude <510 km); (4) Vertical measurement resolution: ~20m.
R3-MIS-220	R2-H-30 R2-H-70	The mission shall enable low density subsurface sounding with (1) Temporal sampling: nightside observations; (2) Geographical sampling: an average observation density of 2 per degree of longitude at Equator; (3) Geographical coverage: ≥65% of the planet shall be observed, and 75% of the covered area shall be observed from an altitude fulfilling the SNR requirement (R3-MEA-130(1))
R3-MIS-225	R2-H-70	The mission shall enable high density subsurface sounding with: (1) Temporal sampling: nightside observations; (2) Geographical sampling: an average observation density of 10 per degree of longitude at Equator; (3) Geographical coverage: ≥ 35% of the Regions of Interest (ROIs) imaged with the VenSAR 30 m SAR imaging mode.
R3-MIS-226	R2-H-70	The altitude of the SRS observations over the 6 cycles nominal mission lifetime shall be such that: (1) the maximum altitude is always less than 510 km (noting that R3-MEA-130 and -135 are not met at this altitude); (2) the minimum altitude should be greater than 40 km; (3) at least 75% of the data shall be collected below 350 km altitude (allowing R3-MEA-130 and -135 to be met)

4.4. VenSpec suite overview

VenSpec consortium consists of three instruments incorporated scientifically. VenSpec will provide unprecedented insights into the current state of Venus and its past evolution. VenSpec will perform a comprehensive search for volcanic activity by targeting atmospheric signatures, thermal signatures and compositional signatures, as well as a global map of surface composition. The scientific cooperation and shared interface to the spacecraft through a common Central Control Unit (CCU) allows to leverage the synergies between the three instruments and minimize the resources, while at the same time ensuring that each partner can develop their contributions largely independently. The VenSpec suite consists of three instruments: VenSpec-M, VenSpec-H, VenSpec-U, and the Central Control Unit (CCU). All three instruments have their independent optics due to the very different imaging concepts and wavelengths ranges covered. The instruments are all nadir pointing.

4.5. Near-IR Multispectral Imager VenSpec-M

4.5.1. Instrument objectives and description

VenSpec-M (Helbert et al., 2017, 2018; 2019; Smrekar et al. 2018b) is a pushbroom multispectral imaging system which will provide near-global compositional data on rock types, weathering, and crustal evolution by mapping the nightside emission of Venus surface and lower atmosphere in 14 near-IR spectral transparency 'windows' at 0.86-1.18 µm (Figure 4.5.1; Mueller et al., 2008; Meadows and Crisp, 1996; Pollack et al., 1993). A total of six narrow spectral bands (red-brown colour in Figure 4.5.1) sound the surface across five atmospheric windows. The broadest 'window' at 1.02 µm is split by two filters to obtain information on the spectral slope of the surface reflectance across the 'window'. Eight additional channels provide measurements of atmospheric water vapour abundance (two bands in blue in Figure 4.5.1) as well as cloud microphysics and dynamics (three bands in orange) and stray light (three bands in green) permitting an accurate correction of atmospheric interference on the surface data. Continuous observation of Venus' thermal emission in the surface windows will place tight constraints on current day volcanic activity.

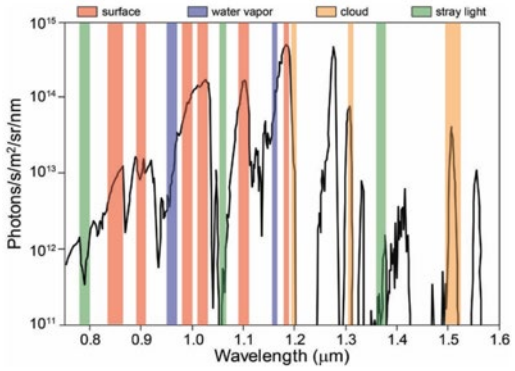

Figure 4.5.1 – *Wavelengths of near-infrared bands used opportunistically around gaps in the CO_2 atmosphere of Venus. Collectively, these offer a comprehensive sampling of surface, water vapour, cloud opacity, and stray light as needed to estimate errors on surface bands. Black line is an observed nightside emission spectrum of Venus. Adapted from Helbert et al. (2018).*

Figure 4.5.2 shows the functional layout and design of VenSpec-M. The instrument consists of two main units mounted together in a mono-block structure to allow for simplified spacecraft interfaces. A telecentric optics images the scene onto a filter array. VenSpec-M uses a multilayered dielectric-coating ultra-narrow-band filter array to split the light into 14 spectral bands. Figure 4.5.1 shows the spectral assignment of each filter and their main objective. The filter array is located at an intermediary focus of the optical path. Each band is imaged by two lens relay optic onto 33×640-pixel rows on the detector. The filter array is used to provide greater wavelength stability than a grating design. VenSpec-M is using a 640×512 pixel Xenics XSW-640 InGaAs detector. The FOV is 30°×45º; each 20-µm-pitch pixel sees a 0.07°×0.07º FOV. An integrated thermo-electric cooler is used to stabilize the working point of the detector. The detector requires no cryogenic cooling, avoiding a single point failure. The frontend electronics use the highly integrated AFE device LM98640QML-SP, a fully qualified (radiation tolerant), 14 bit, 5 MSPS to 40 MSPS, dual channel, complete Analog Front End. Texas Instruments specially designed it for digital imaging applications.

4.5.2. Interfaces and resources requirements

All main interfaces are shown in Figure 4.5.2a. The three units are also the main thermal subunits of VenSpec-M supported by spacecraft interfaces according to their requirements. One Thermal Reference Point (TRP) is the instrument mounting plate, which handles the electronics thermal control in an appropriate operating range with heater maintenance as needed. It also connects the optics/detector section via thermal strap to a stabilized spacecraft interface, which is the second TRP. Thermal interference of both units is controlled by the optics mounting elements to the electronics unit. The instrument's nominal mass is 5.9 kg. Mean and peak power consumption are 11.5 W and 15 W respectively (including 15% margin). Data rate is typically 0.5 Mbps with a

peak of 1 Mbps for calibration observations. Commanding, data link to the spacecraft and power supply will be provided by a dedicated Central Control Unit (CCU).

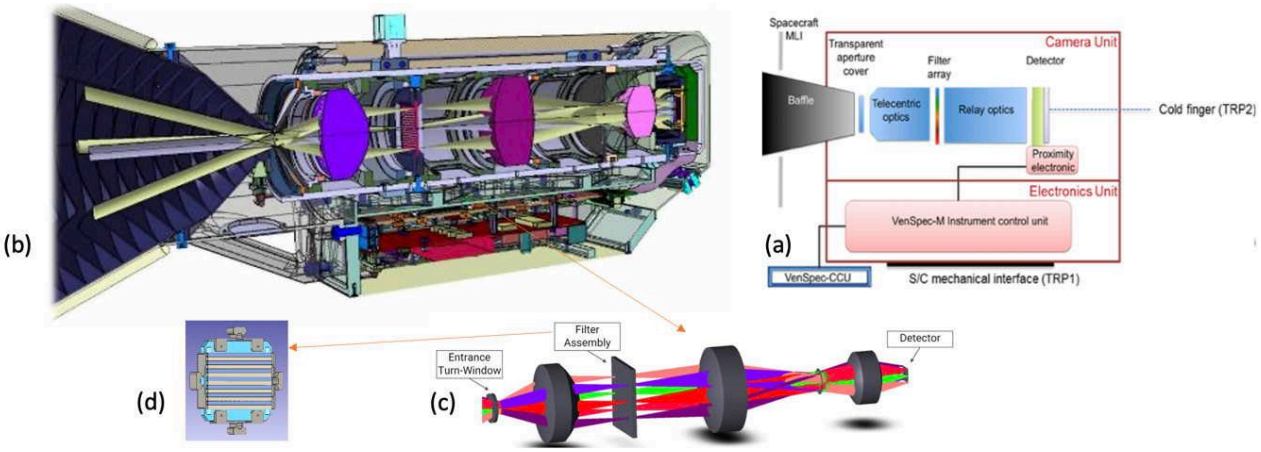

Figure 4.5.2 – *VenSpec-M block diagram (top right, a) and design (left, b). The instrument consists of two main units mounted together in a mono-block structure to allow for simplified spacecraft interfaces. A telecentric optic (c) images the scene onto a filter array (d). VenSpec-M uses a multilayered dielectric-coating ultra-narrow-band filter array to split the light into 14 spectral bands.*

4.5.3. Operation requirements

VenSpec-M is continuously operating on the nightside of Venus to reach 60% coverage with three repeats by the end of the nominal, 6-cycle mission. To search for volcanic activity the instrument will acquire sets of five consecutive orbits, that due to sufficient overlap of orbital swaths, would enable robust detection and avoid false positives. Over the mission duration seven revisits are required to minimize the effect of atmospheric uncertainties not included in the atmospheric model used for emissivity retrieval.

4.5.4. Heritage

VenSpec-M low development risk results from a standard camera optical design, a flight-proven InGaAs detector with a thermo-electric cooler, and flight-qualified support systems from MERTIS (D'Amore et al., 2019; Peter et al., 2013).

4.5.5. Instrument Performance

VenSpec-M has a mature design with an existing laboratory prototype verifying an achievable instrument SNR of well above 1000 as well as a predicted error in the retrieval of relative emissivity of better than 1% (Helbert et al. 2018). By observing through all five windows using the six narrow band filters, ranging from 0.86 to 1.18 µm, VenSpec-M provides a global map of surface composition as well as the redox state of the surface. To assess the performance of the current VenSpec-M design, we derive performance parameters based on the recent laboratory work and the Venus Express data sets in Section 7.3.3.

4.5.6. VenSpec-M measurement and instrument requirements

Based on the top-down requirements assessment analysis and earlier Venus mission payloads, the following set of VenSpec-M measurement and mission requirements were defined in phase 0 and phase A. These were confirmed to meet the VenSpec-M product and coverage requirements through bottom-up performance simulations (see Section 4.5.5 and Chapter 7, Section 7.3.3). In phase B1, some requirements were updated based on a further maturing of the instrument and mission design and new bottom-up performance simulations. Finally, the coverage requirements were confirmed through the ESA SORS simulations (Chapter 7, Sections 7.1-2).

Table 4.5.1 – *VenSpec-M measurements and mission requirements*

Requirement number	Parent	Requirement description
R3-MEA-010	R2-A-10 R2-H-60	Map nightside thermal emission (650-1400 K) in the near-IR spectral channels at the planet surface at the atmospheric diffraction limit: (1) Measurement wavelength: 1.02 microns with

		(2) SNR: >300 (derived from parent relative emissivity accuracy <4%) (3) Horizontal measurement sampling: < 100x100 km^2
R3-MEA-120	R2-H-60 R2-C-10 R2-C-20	Provide nightside spectral mapping of the thermal emission from the surface and lower atmosphere 1) Measurement wavelength: in the near-IR spectral transparency windows at ~1 µm. 2) Spectral windows: Relative emissivity values are required to be measured at (centre/bandwidth) 0.86/0.04, 0.91/0.06, 0.99/0.03, 1.02/0.015, 1.11/0.02, 1.18/0.018 µm 3) SNR: > 300 (derived from accuracy relative emissivity <4%, to discriminate between felsic versus mafic rock types). 4) Horizontal measurement sampling: <100x100 km^2
R3-MEA-200	R2-C-10 R2-C-30	Obtain nightside H_2O partial column densities and Venus cloud variability from spectral observations in the near-IR spectral windows on the nightside: 1) H_2O partial column densities (0-10 km): a. Spectral band central wavelength: 960 and 1150 nm b. SNR: ≥ 100 c. Accuracy: <10% 2) Cloud variability: a. Spectral windows: 1195, 1310, 1510 nm b. SNR: ≥135 (derived from accuracy requirement near-IR surface emissivity product) 3) Horizontal measurement sampling: <100x100 km^2 at the planet surface
R3-MIS-010	R2-A-10 R2-H-60	The mission shall enable nightside measurements of spatial and temporal changes in thermal emission of the surface in the near-IR 1) Measurement sub sampling: 10x10 km (+/- 1 km) (to be downlinked); 2) Temporal sampling: measurements in 4 consecutive orbits per 24 hours, at temporal sampling of less than 3 hours; 3) Temporal coverage: ≥ 3 cycles to observe variations on time scales from hours to years; 4) Geographical observation coverage: ≥ 60% of the planet surface; 5) Nominal observation geometry: nadir; 6) Measurement geographical location knowledge: 10 km (applicable to the down-linked raw data product)
R3-MIS-200	R2-H-60 R2-C-10 R2-C-20	Enable nightside spectral mapping of the thermal emission from the surface and lower atmosphere in the near-IR (R3-MEA-120), with the following mission requirements: 1) Measurement subsampling: 10x10 km (+/- 1 km) (to be downlinked) 2) Temporal sampling: measurements in 4 consecutive orbits per 24 hours, at temporal sampling of less than 3 hours; 3) Temporal coverage: ≥ 3 cycles to observe variations on time scales from hours to years; 4) Geographical observation coverage: ≥ 60% of the planet surface; 5) Nominal observation geometry: nadir; 6) Measurement geographical location knowledge: 10 km (applicable to the down-linked raw data product)
R3-MIS-300	R2-C-10 R2-C-30	The mission shall enable nadir observations on the nightside for monitoring of water vapour column and cloud properties specified in R3-MEA-200, with the following mission requirements: 1) Measurement sub sampling: 10x10 km^2 (+/- 1 km) (to be downlinked); 2) Temporal sampling: 2a. 4 consecutive orbits per 24 hours; 2b. An overlap of >70% (TBC) of the swaths (FoV) between 2 consecutive orbits; 2c. <3 hours between 2 consecutive orbits; 3) Temporal coverage: >3 Venus sideral days allowing multi-season and multi-year observations; 4) Geographical observation coverage: all latitudes and local solar times at > 60% of the planet; 5) Nominal observation geometry: nadir; 6) Measurement geographical location knowledge: 10 km (applicable to the down-linked raw data product); 7) Operation: The VenSpec-M and VenSpec-H instruments shall be operated simultaneously at the nightside of the planet
R3-MIS-315	R2-C-10 R2-C-20	The mission design shall ensure that the VenSpec-U, H and M FoVs are overlapping, with: (1) The VenSpec-H FoV fully included in the transverse extent of the VenSpec-M for the nightside observations, and (2) The VenSpec-H FoV fully included in the transverse extent FoV of VenSpec-U for the day side observations

4.6. High-Resolution Infrared Spectrometer VenSpec-H

4.6.1. Instrument objectives and description

The aim of VenSpec-H (**Ven**us **Spec**trometer with **H**igh resolution) is to monitor the composition of minor species in the lower atmosphere on the nightside, and above the clouds on the day side. These observations will be performed in nadir geometry. More specifically VenSpec-H will focus on the volcanic and cloud forming gases and search for composition anomalies potentially related to the volcanic activity. VenSpec-H will include four spectral bands: 1.16–1.18 µm (Band 1), 2.34–2.48 µm (Band 2), 1.72–1.75 µm (Band 3) and 1.37–1.39 µm (Band 4) that cover the infrared spectral transparency 'windows'. In order to reduce the instrument complexity, B#2 will be further subdivided in two ranges: 2.34–2.42 µm (Band 2a) and 2.45–2.48 µm (Band 2b). Bands 1, 2a, 2b and 3 will be observed on the nightside; Bands 2a, 2b and 4 on the dayside. Figure 4.6.1 illustrates the different bands sounded and which main species will be measured. To separate the signal in Bands 2a and 2b, the detector is divided in two regions using a filter-slit assembly (see Figure 4.6.3).

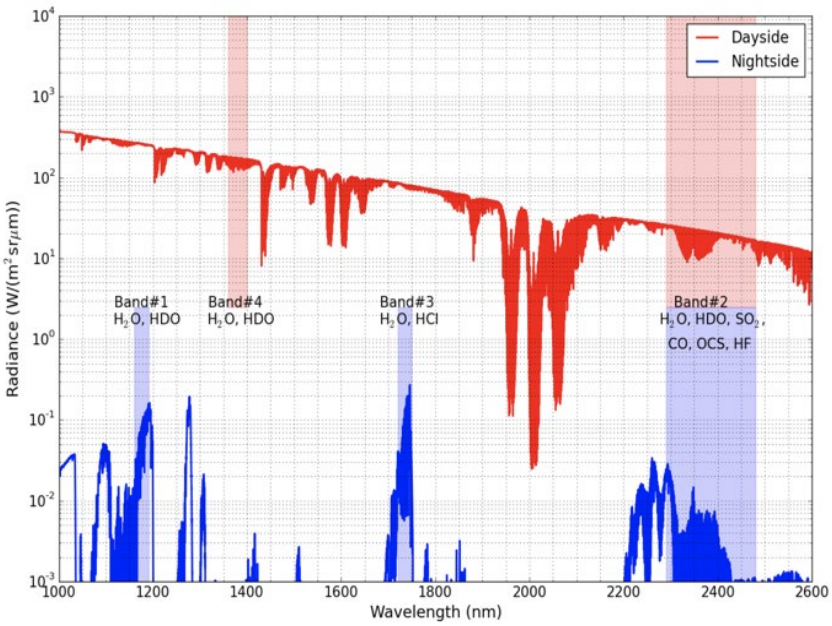

Figure 4.6.1 – *Typical Venus spectra observed by the VenSpec-H for day (red) and night (blue) conditions. The positions of the bands are indicated, as well as which atmospheric species are absorbing.*

VenSpec-H is composed of (1) a cooled optical bench (the 'cold section') with the spectrometer, including the entrance slit; (2) a warmer base plate on which the cold optical bench is mounted, and carrying a shutter mechanism, the filter wheel and the detector; and (3) an electronics unit, separate from the optical bench (Figure 4.6.2). The shutter mechanism (with a transparent window) protects the instrument from the outside environment during cruise and aerobraking. The filter wheel with eight positions harbours the four filters defining the VenSpec-H spectral bands, two polarization filters and an open and a closed positions. The cold section is cooled down to -45°C by means of a dedicated S/C radiator, while the warm baseplate is kept at approximately 0 to 10 °C. The warm baseplate is mounted to the S/C deck with four titanium Λ-shaped bi-pods ensuring mechanical and thermal decoupling from the S/C. The VenSpec-H electronics (mounted directly to the spacecraft deck) contains the channel control unit. The VenSpec-H electronics interface with the Central Control Unit (CCU) of VenSpec.

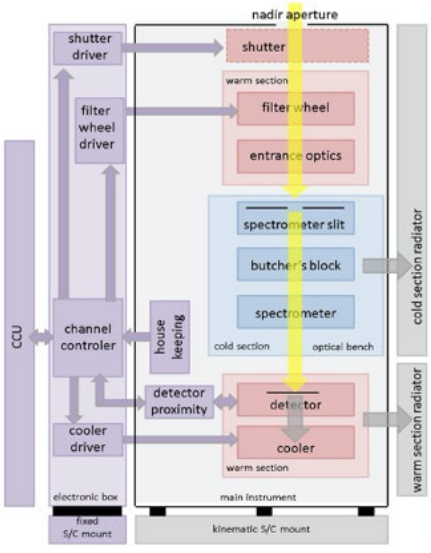

Figure 4.6.2 – *VenSpec-H Functional block diagram.*

The heart of the instrument is the spectrometer section where the incoming uniform light is diffracted into its spectral components, using an echelle grating (Figure 4.6.3). The entrance of the spectrometer section is the spectrometer slit, the image of which is projected on the detector. The output of the spectrometer section is an opening interfacing to the detector assembly. The selection of the spectral band is carried out using filters on a filter wheel situated in front of the slit in the warm section, and a filter-slit assembly with filters deposited to the slit in the cold section. The detector is a Mercury Cadmium Telluride 384 x 288 SWIR detector cooled down to 135 K by a linear Stirling cryocooler. VenSpec-H has a rectangular field of view (defined by the spectrometer slit) of 6°41' (length of slit) by 0.08 (width of slit).

A detailed analysis has shown that the VenSpec-H instrument is sensitive to the polarization state of the incoming radiation, with typical sensitivity of 1 to 4% except at the edge of the Band 2a where it can reach 8%. This effect is only important during day observations during which the incoming radiation gets polarized through its interaction with the cloud particles. Two polarized filters have been added to the filter wheel to help correcting for this effect (see Figure 4.6.3 and also Section 7.3.4). One additional advantage of the presence of these filters is that VenSpec-H will be able to derive important knowledge on the micro-physical properties of the clouds (see Section 8.5.4).

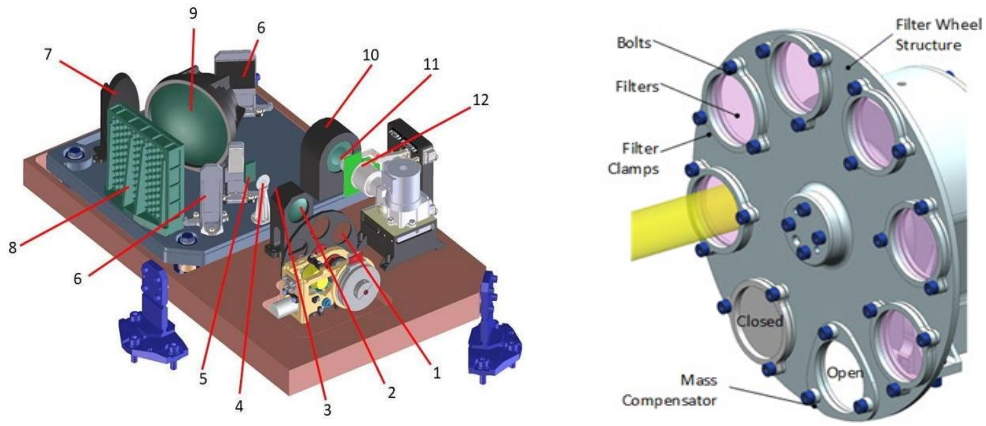

Figure 4.6.3 – *VenSpec-H optical design: (1) filter wheel,(2) warm entrance optics,(3) cold section entrance aperture, (4) filter-slit assembly, (5) free form correction plate, (6) folding mirrors, (7) parabolic mirror, (8) echelle grating, (9) collimating optics, (10) detector optics, (11) cold section exit aperture, (12) detector plane. (right panel): Filter wheel with eight positions.*

4.6.2. Interfaces and resources requirements

The instrument's estimated nominal mass is 18.9 kg (22.5 kg including margins). The estimated nominal mean power (over one orbit) and peak power consumption (during detector precooling) are 24.6 W and 29.7 W respectively (including 15% margin). Data volume can be modulated depending on the available mission resources, by on-board binning, providing 6.5 and 14.2 Mbytes per orbit, for the minimum (binning on 10 lines, 20 min of science) and typical (binning on 16 lines, 30 min science) scenarios respectively, including 20 % margin. VenSpec-H consists of two units (Figure 4.6.2): the main instrument (optical bench) interfaces with four titanium Λ-shaped bi-pods to the spacecraft, and the electronic box which is hard mounted with four mounting points on each long side of the box. The instrument has three Thermal Reference Points (TRPs), one at a foot of the main instrument (warm section), one at a foot of the cold section and one at a mounting point of the electronic box. To achieve the required signal-to-noise ratio the cold section of the instrument that encompasses optics and detector will be cooled down by passive radiator cooling. Commanding, data link to the spacecraft and power supply will be provided by a dedicated Central Control Unit (CCU).

4.6.3. Operation requirements

VenSpec-H will observe in the near-nadir direction on both dayside and nightside. VenSpec-H has an elongated Field of View (FoV) defined by the projection of the spectrometer slit onto the Venusian disk which also corresponds to one detector column, see Figure 4.6.4. To guarantee the spectral resolving power during an observation, the instrument needs always to be oriented such that the velocity vector of the S/C is perpendicular to the long edge of the FoV. The slit size corresponds to an instantaneous Fields of View of 0.32 x 28.27 km² and 0.79 x 69.39 km² for a S/C altitude of 220 km and 540 km respectively. The maximum integration time on the nightside will be 14.29 seconds. The FoV then becomes 28.27 x 99.52 km² and 28.27 x 99.98 km² for 220 km and 540 km altitude respectively.

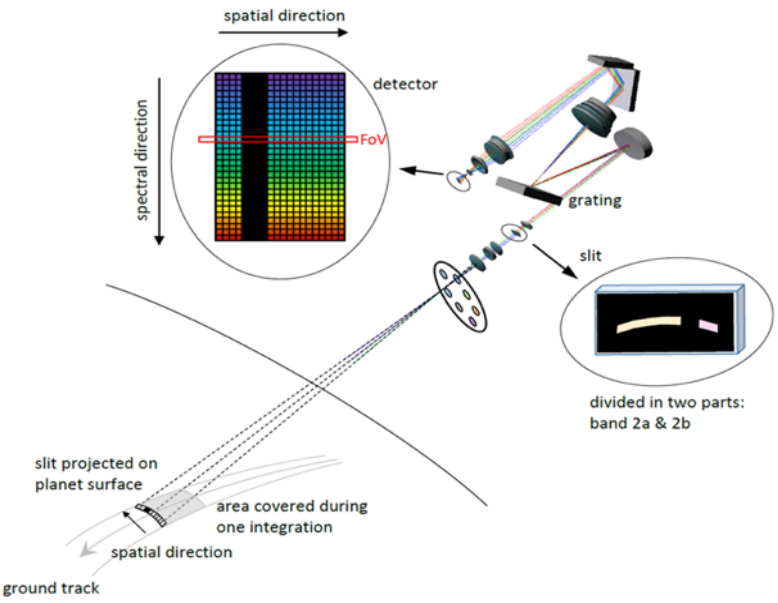

Figure 4.6.4 – *VenSpec-H operational principle. The orientation of the detector and the instrument FoV with respect to the S/C velocity vector are also indicated.*

Good knowledge of the pointing direction is crucial for data interpretation. Regular calibration measurements will be performed using the Sun as a target. These observations will also be used to perform radiometric calibration and straylight verification. Such observations are baselined with a repetition of 112 days and will ensure the stability of the instrument response over time. The requirement on the pointing is as follows: the VenSpec-H instrument shall be pointed towards the centre of Venus with an absolute pointing error (APE) of ≤ 87 mrad (around pointing axis) and ≤ 50.0 mrad (off pointing axis). The relative pointing error (RPE) or drift stability shall be ≤ 87.0 mrad (around pointing axis) and ≤ 35 mrad (off point axis) considered over an interval of an observation. The Absolute Knowledge Error (AKE) in all directions must be smaller than the respective APE values.

While VenSpec-H is capable of measuring continuously, the basic operations scenario foresees periods of four consecutive orbits of observation per cycle. VenSpec-H science operations are timeline controlled. In the standby mode only the central electronics are active. Once the command is received by the instrument it switches to pre-cooling mode. Then, the instrument goes into measurement mode. Pre-cooling mode lasts for 10 minutes. Science mode duration depends on the length of the observation (a duration of 30 minutes is assumed as the typical EnVision case). During the entire period that VenSpec-H is switched on, housekeeping data will be transmitted at a rate of one frame per second.

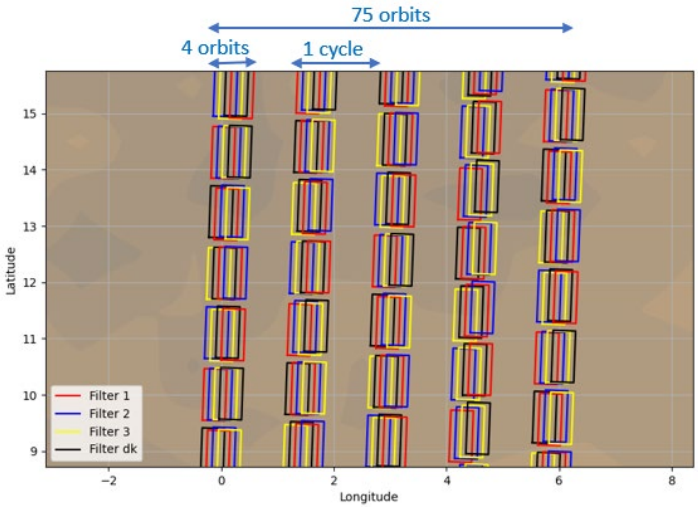

VenSpec-H will be operated during four consecutive orbits (Figure 4.6.5). These are partially overlapping and will allow us to derive vertical information by combining the different spectral bands recorded. This is of high importance on the nightside, where vertical profiles will be reconstructed from Band 1 probing the 0-15 km layer, Band 3 the 20-30 km layer and Bands 2a and 2b, the 30-45 km layer.

Figure 4.6.5 – *Typical ground track and footprint for 75 orbits, in which the blocks of four consecutive orbits are repeated. This example corresponds to a nighttime observation during which 3 filters (Band 1 – red, Band 2 – blue, Band 3 – yellow) are sequentially measured followed by a dark frame measurement (black).*

4.6.4. Heritage

The instrument builds heavily on the LNO channel of NOMAD on board ExoMars Trace Gas Orbiter (Neefs et al. 2015; Vandaele et al. 2018).

4.6.5. Instrument Performance

Instrument performance, i.e., the signal-to-noise ratio (SNR) reached under different observing conditions, is summarized in Table 4.6.1. The integration time is limited by the saturation of the detector on the day side because the signal strength is quite high (solar radiation reflected by the clouds), and on the nightside because thermal emission from the instrument itself is the dominant contribution. The SNR values in Table 4.6.1 are those achieved

when the cold section is at -45°C and the detector is at 135 K. Observations on the dayside are always compliant with the scientific requirements. However, measurements on the nightside are in some cases non-compliant. Mitigation measures (increasing the integration time and co-adding observations) have been considered to recover compliance, as well as the possibility of operating the detector at a lower temperature (see Section 7.3.4).

Table 4.6.1 – *Expected performances of VenSpec-H. The SNR values are given for binned detector regions (288 pixels for Bands 1, 3, 4; 19 pixels for Band 2a, and 181 pixels for Band 2b, for an averaged value of the signal, and considering that the cold section temperature is -45°C and for observations corresponding to a footprint of 50 km on the dayside, 100 km on the nightside, and 200 km for H_2O and HDO for Band 1 on the nightside. (*) Beginning of Life (BOL) and End of Life (BOL) are indicated*

		Spectral range (nm)	Integration time x number of accumulation (s)	Binned SNR BOL/EOL (*)	Targeted molecules	Altitude range probed
DAYSIDE	Band 2a	2340-2420	7.45	5874/4859	H_2O, HDO,OCS, CO	65-80 km
	Band 2b	2450-2480	7.45	14134/11067	H_2O, HDO, OCS, SO_2, HF	65-80 km
	Band 4	1370-1390	7.45	34543/28343	H_2O, HDO	65-80 km
NIGHTSIDE	Band 1	1165-1180	30.08	55/47	H_2O, HDO	0-15 km
	Band 2a	2340-2420	15.04	152/136	H_2O, HDO, CO, OCS	30-45 km
	Band 2b	2450-2480	15.04	105/91	H_2O, HDO, OCS, SO_2, HF	30-45 km
	Band 3	1720-1750	15.04	485/422	H_2O, HCl	20-30 km

4.6.6. VenSpec-H measurement and instrument requirements

Based on the top-down requirements assessment analysis and earlier Venus's mission payloads, the following set of VenSpec-H measurement and mission requirements were defined in phase 0 and phase A. These were confirmed to meet the VenSpec-H product and coverage requirements through bottom-up performance simulations (see Section 4.6.5 and Chapter 7, Section 7.3.4). In phase B1, some requirements were updated based on a further maturing of the instrument and mission design and new bottom-up performance simulations. Finally, the coverage requirements were confirmed through the ESA SORS simulations (Chapter 7, Sections 7.1-2).

Table 4.6.2 – *VenSpec-H measurements and mission requirements*

Requirement number	Parent	Requirement description
R3-MEA-201	R2-C-10	VenSpec-H radiance spectra measurement requirements in the near-IR spectral transparency windows on the **nightside** are defined as follows: (1) H_2O partial column densities (0-15 km, 15-30 km, 30-40 km): a. **Spectral range:** Band 1: 1.16–1.18 µm, Band 3: 1.72-1.75 µm, Band 2a: 2.34–2.42 µm, Band 2b: 2.45 – 2.48 µm b. **Resolving power**[2]: $R=\lambda/\delta\lambda \geq 7000$ c. **SNR(after integration across track and along track)** ≥ **45** at 1.17 µm, **126** at 2.38 and 2.46 µm , **70** at 1.73 µm d. **Altitude range:** Band 1: 0-15 km, Band 3: 15-30 km, Band 2a and b: 30-40 km e. **Bias/stability:** 10% accuracy on absolute radiometric measurements (2) HDO partial column densities (0-15 km, 30-40 km): a. **Spectral range:** Band 1: 1.16–1.18 µm, Band 2a: 2.34–2.42 µm, Band 2b: 2.45 – 2.48 µm b. **Resolving power:** $R=\lambda/\delta\lambda \geq 7000$ c. **SNR (after integration across and along track)** ≥ **48** at 1.17 mm, **70** at 2.38 and 2.47 mm d. **Altitude range**: Band 1: 0-15 km, Band 2a and b: 30-40 km e. **Bias/stability**: **10%** accuracy on absolute radiometric measurements (3) CO partial column densities (30-40 km): a. **Spectral range:** Band 2a: 2.34–2.42 µm b. **Resolving power:** $R=\lambda/\delta\lambda \geq 7000$) c. **SNR (after integration across and along track)** ≥ **70** at 2.38 and 2.47 µm d. **Altitude range:** Band 2a: 30-40 km e. **Bias/stability: 10%** accuracy on absolute radiometric measurements (4) OCS partial column densities (30-40 km): a. **Spectral range:** Band 2a: 2.34–2.42 µm, Band 2b: 2.45 – 2.48 µm b. **Resolving power:** $R=\lambda/\delta\lambda \geq 7000$ c. **SNR (after integration across and along track)** ≥ **70** at 2.38 and 2.47 µm d. **Altitude range:** Band 2a and b: 30-40 km e. **Bias/stability: 10**% accuracy on absolute radiometric measurements near TBC µm (5) SO_2 partial column densities (30-40 km): a. **Spectral range:** Band 2b: 2.45 – 2.48 µm b. **Resolving power:** $R=\lambda/\delta\lambda \geq 7000$ c. **SNR (after integration across and along trac)** ≥ **70** at 2.38 and 2.47 µm

[2] Due to the non-uniformity of the grating angular dispersion, a grating spectrometer will result in a variable spectral resolution as a function of wavelength. Therefore, this requirement is expressed as a resolving power, where the lowest spectral resolution obtained is sufficiently resolving the spectral lines.

		d. **Altitude range:** Band 2b: 30-40 km e. **Bias/stability: 10**% accuracy on absolute radiometric measurements (6) **Horizontal measurement sampling applicable to SNR requirement:** <100 km along-track and across-track (according to FOV illumination on detector) and <200 km along track for Band 1; (7) **Instrument swath width:** FoV > 6.593° (i.e. ~25 km surface swath for an orbit altitude of 210 km, ~59 km surface swath for an orbit altitude of 510 km)
R3-MEA-211	R2-C-20	VenSpec-H radiance spectral measurement requirements in the IR above the clouds on the **dayside** are defined as follows: **(1) H_2O partial column densities (SciO#H1):** a. **Spectral range:** Band 4: 1.37-1.39 µm, Band 2a: 2.34–2.42 µm, Band 2b: 2.45 – 2.48 µm b. **Resolving power**: $R=\lambda/\delta\lambda \geq 7000$ c. **SNR ≥ 100** (in all bands) d. **Altitude range:** Band 4: 65-80 km, Band 2: 65-80 km e. **Bias/stability:** 10% accuracy on absolute radiometric measurements **(2) HDO partial column densities (SciO#H2):** a. **Spectral range:** Band 4: 1.37-1.39 µm, Band 2a: 2.34–2.42 µm , Band 2b: 2.45 – 2.48 µm b. **Resolving power:** $R=\lambda/\delta\lambda \geq 7000$ c. **SNR ≥ 100** (in all bands) d. **Altitude range:** Band 4: 65-80 km, Band 2: 65-80 km e. **Bias/stability:** 10% accuracy on absolute radiometric measurements **(3) CO partial column densities (SciO#H3):** a. **Spectral range:** Band 2a: 2.34–2.42 µm b. **Resolving power:** $R=\lambda/\delta\lambda \geq 7000$ c. **SNR** ≥ 100 (in all bands) d. **Altitude range:** Band 2a and b: 30-40 km e. **Bias/stability:** 10% accuracy on absolute radiometric measurements **(4) OCS partial column densities (SciO#H4):** a. **Spectral range:** Band 2a: 2.34–2.42 µm, Band 2b: 2.45 – 2.48 µm b. **Resolving power:** $R=\lambda/\delta\lambda \geq 7000$ c. **SNR** ≥ 100 (in all bands) d. **Altitude range:** Band 2a and b: 65-80 km e. **Bias/stability:** 10% accuracy on absolute radiometric measurements **(5) SO_2 partial column densities (SciO#H5):** a. **Spectral range:** Band 2b: 2.45 – 2.48 µm b. **Resolving power:** $R=\lambda/\delta\lambda \geq 7000$ c. **SNR** ≥ 100 (in all bands) d. **Altitude range:** Band 2a and b: 65-80 km e. **Bias/stability:** 10% accuracy on absolute radiometric measurements (6) **Horizontal measurement sampling applicable to SNR requirement:** <50 km km along track and across-track (according to FOV illumination on detector) (7) **Instrument swath width**: FoV = 6.593° (i.e. ~17 km at 70 km (cloud top) for an orbit altitude of 210 km, ~51 km at 70 km (cloud top) for an orbit altitude of 510 km)
R3-MIS-301	R2-C-10	The mission shall enable nadir observations on the **nightside** for monitoring of water vapour column and cloud properties specified in R3-MEA-200, with the following mission requirements: (1) **Measurement sub sampling***:* 10x10 km^2 (+/- 1 km) (to be downlinked); (2) **Temporal sampling**: a. 4 consecutive orbits per 24 hours; b. An overlap of >0% of the swaths (FoV) between 2 consecutive orbits; c. <3 hours between 2 consecutive orbits; (3) **Temporal coverage:** >3 Venus sideral days allowing multi-season and multi-year observations; (4) **Geographical observation coverage:** all latitudes and local solar times at > 60% of the planet; (5) **Nominal observation geometry**: nadir; (6) **Measurement geographical location knowledge**: 10 km (applicable to the down-linked raw data product); (7) **Operation**: VenSpec-M and VenSpec-H instruments shall be operated simultaneously on the nightside of the planet
R3-MIS-311	R2-C-20	The mission shall enable **dayside** monitoring of abundance of trace gases and cloud properties (R3-MEA-211) and characterize their variability, with the following sampling, geolocation geometry, and coverage requirements: (1) **Measurement subsampling (measurement sampling to be downlinked):** 50 km along track. The number of detector pixels across track averaged on-board will be adjusted within the available VenSpec data rate budget; (2) **Temporal sampling:** measurements in 4 consecutive orbits per 24 hours, at temporal sampling of less than 3 hours; (3) **Temporal coverage:** During the nominal mission lifetime, allowing multi-season and multi-year observations; (4) **Geographical measurement coverage** applicable to R3-MEA-211: > 60% of the planet (in local time and latitude); (5) **Nominal observation geometry** applicable to R3-MEA-211: Nadir; (6) **Solar zenith angle geometry:** ≥75% (TBC) of the VenSpec-H measurements shall be acquired for solar zenith angles < 70°; (7) **Off-nadir observations (>15° w.r.t. nadir):** <15% of total VenSpec-H observation duration;

		(8) **Operation:** VenSpec-U and VenSpec-H instruments shall be operated simultaneously on the dayside of the planet
R3-MIS-315	R2-C-10 R2-C-20	The mission design shall ensure that the VenSpec-U, H and M FoVs are overlapping, with: (1) The VenSpec-H FoV fully included in the transverse extent FoV of VenSpec-M for the nightside observations, and (2) The VenSpec-H FoV fully included in the transverse extent FoV of VenSpec-U for the dayside observations

4.7. Ultraviolet Spectrometer VenSpec-U

4.7.1. Instrument objectives and description

The VenSpec-U experiment will map distribution and spatial and temporal variations of sulphur bearing gases (SO, SO_2) and unknown particulate absorber at the cloud tops. These measurements will support the search for volcanic activity by constraining variability of the species that can be attributed to atmospheric dynamics.

The VenSpec-U instrument is a dual channel UV spectral imager (low and high spectral resolution channels, 'LR' and 'HR' hereafter). Each channel consists of an entrance baffle, an objective composed of two lenses and a stop diaphragm, and a spectrometer composed of a slit and a spherical holographic grating. It also includes a short-pass filter to reject the wavelengths above the higher limit of both channel bands and a zeroth- order trap to avoid straylight due to internal reflections of the grating zeroth-order. The optical layout is presented in Figure 4.7.1. Both LR and HR slits are parallel and the optical layout is such that both channels have the same instantaneous FoV, allowing simultaneous observations and calibrations. Each slit image is then spectrally dispersed by its respective toroidal holographic grating and is formed on a shared CMOS back-side illuminated detector.

The narrow-slit axis of the detector contains the spectral information, whereas the long-slit axis contains the spatial information along the 20° FOV of each slit. The spectra of LR and HR channels are dispersed one above the other on the focal plane. The remaining spatial direction is provided through orbital scrolling ('pushbroom' strategy). Binning on the spatial axis is performed on the detector. The detector will be controlled such that the integration time and the binning scheme is adjusted independently (and simultaneously) for each channel giving high flexibility and providing parameters for the optimization of each acquisition.

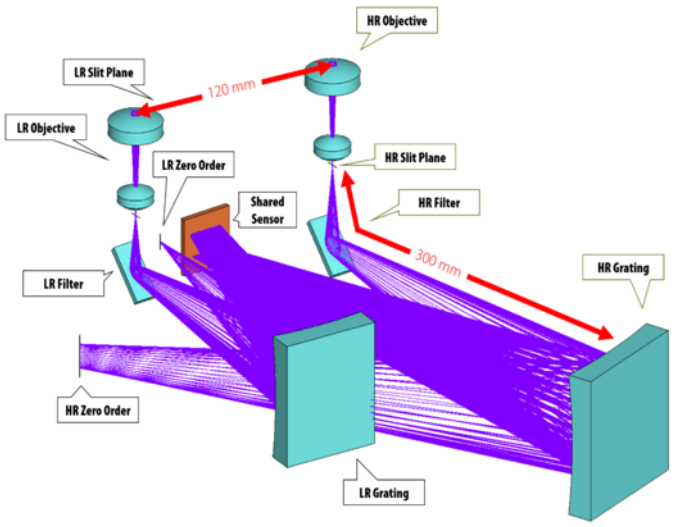

Figure 4.7.1 – *VenSpec-U optical layout overview, with the HR and LR channels respectively on the left and on the right.*

4.7.2. Interfaces and resources requirements

Interfaces between VenSpec-U and the spacecraft are: (1) Thermal interface providing TRP1 (for detector cold finger) and TRP2 (electrical box and optical bench); (2) Power interface (redundant 28 V) to VenSpec-U electronics and spacecraft controlled heaters and (3) Data link (including ground debug EGSE) through SpaceWire. Commanding data link to the spacecraft and power supply will be provided by a dedicated Central Control Unit (CCU).The instrument nominal mass is 9.9 kg. The power resources are 11.3 W in standby, 23.2 W during science operations and 35.3 W for peak power (decontamination mode). The data rate is 174-500 kbit/s depending on the distance to the clouds and spatial sampling mode (medium or high). The maximum data rate is reached during solar calibration (80 Mbps).

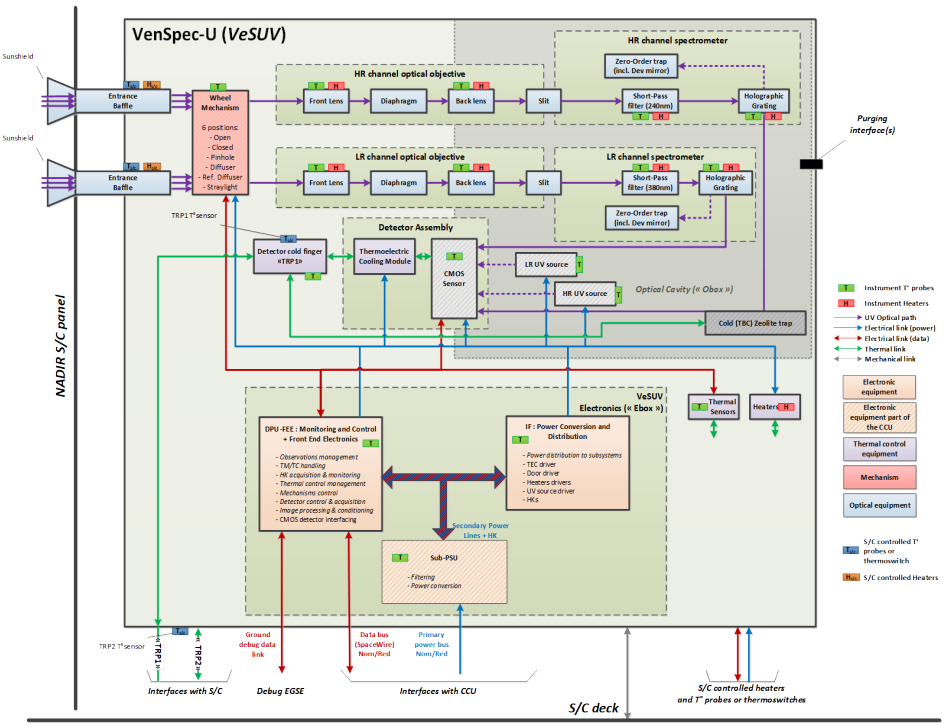

Figure 4.7.2 – *VenSpec-U block diagram.*

4.7.3. Operation requirements

VenSpec-U will operate according to three different calibration modes (dark calibration, internal calibration using an embedded UV source, and solar calibration through pinholes and/or diffusers located on the entrance wheel mechanism), a decontamination mode for optics using internal heaters, and a science operation mode. VenSpec-U nominal science operations will consist of four overlapping measurements of 50 minutes duration per day performed at emission angle < 30° on the dayside, with a ground swath 50-165 km (Figure 4.7.3) sometimes extending cross-terminator up to solar zenith angle of 100° in order to better assess the vertical structure of clouds and hazes, albeit with an extensive binning to compensate for the reduced SNR. The spatial sampling of the data products is reported in the product table in Section 3.1 and Section 4.7.5.

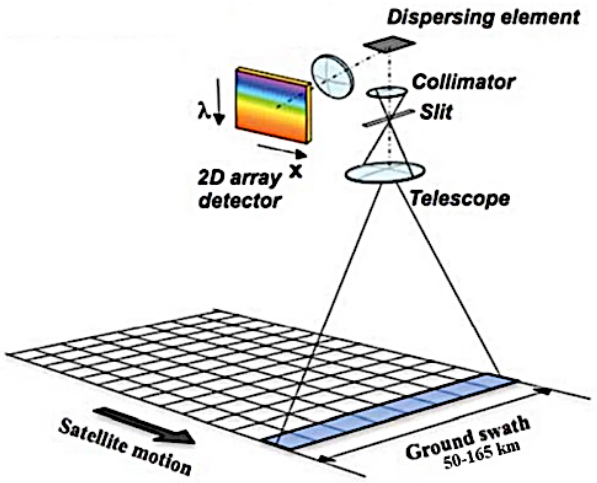

Figure 4.7.3 – *VenSpec-U observation geometry.*

The observations will be interleaved with solar and internal/ dark calibrations performed once every 30-112 days. The required pointing accuracy in Venus observations mode is: Absolute Pointing Error (APE; 3σ) = 60 arcmin, Relative Pointing Error (RPE; 3σ) = 2.2 arcmin over 30 seconds, and Absolute Knowledge Error (AKE) = 22 arcmin (Table 5.3.1). For solar calibration, we have Absolute Pointing Error (ARE; 2σ) = 0.001 deg/s. The mission shall achieve coverage of 60% of the planet in local time, latitude, longitude, with no gap larger than 10%. In case of an instrument or spacecraft anomaly, the wheel mechanism shall be closed in less than 20 seconds before switching off the instrument.

4.7.4. Heritage

VenSpec-U is an instrument based on a strong heritage mainly provided by PHEBUS onboard BepiColombo, a double UV spectrometer covering from 55 nm to 315 nm, Quémerais et al., 2020); and SPICAV-UV onboard Venus Express, an UV spectrometer covering from 118 nm to 320 nm, Bertaux et al., 2007). Both instruments

were assembled and tested in LATMOS as it is expected for VenSpec-U, so the laboratory technical expertise is also a major part of this heritage. The optical scheme of the spectrometer part of VenSpec-U is based on holographic gratings and is therefore very similar to the PHEBUS and SPICAV ones. Due to the quite large field of view required, VenSpec-U is the first ultraviolet spectrometer developed at LATMOS using lens objectives as a telescope, but a strong experience is available within the channel consortium for such optical subsystem.

4.7.5. Instrument Performance

The following specifications are valid for the two VenSpec-U channels:

(1) The HR channel operating at 205-235 nm at 0.3 nm spectral resolution and spatial sampling not coarser than 24 km (12 km as a goal) should reach a SNR (at 220 nm) of at least 100;

(2) the LR channel operating at 190-380 nm at 2-5 nm spectral resolution and spatial sampling not coarser than 5 km (3 km as a goal) should reach a SNR (at 220 nm) of at least 200.

According to our forward model based on SPICAV-UV heritage, this shall be sufficient to measure targeted species with a random accuracy better than 20 % for SO2 column, 25% for the SO:SO2 column ratio, and monitor the UV absorber with a radiometric accuracy better than 10 % at 365 nm. These measurements shall allow characterizing variability on timescales from hours to years (Fig. 4.7.4).

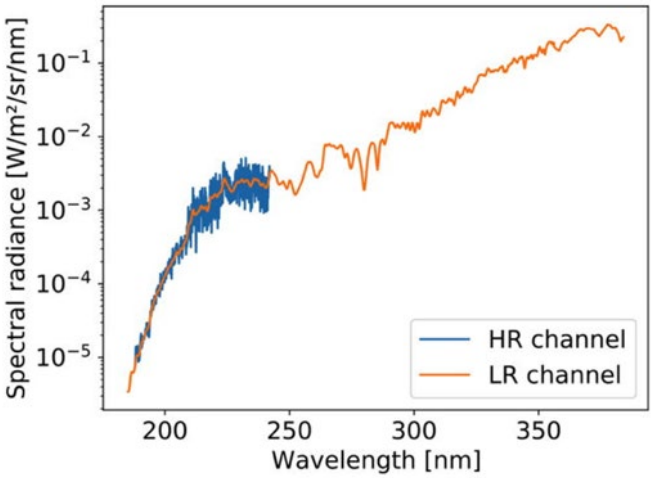

Figure 4.7.4 – *Synthetic radiance factor as measured by VenSpec-U for a 25% SO:SO_2 ratio, 500 ppbv SO_2 abundance, and 0.2 imaginary index of cloud particles at 250 nm for a solar zenith angle of 30° and zero emission angle (nadir viewing). The predicted spectral structure comes from both solar spectrum and absorption by SO, SO_2 and UV absorber at Venus' cloud top.*

4.7.6. VenSpec-U measurement and instrument requirements

Based on the top-down requirements assessment analysis and earlier Venus mission payloads, the following set of VenSpec-U measurement and mission requirements were defined in phase 0 and phase A. These were confirmed to meet the VenSpec-M product and coverage requirements through bottom-up performance simulations (see Section 4.7.5 and Chapter 7, Section 7.3.5). In phase B1, some requirements were updated based on a further maturing of the instrument and mission design and new bottom-up performance simulations. Finally, the coverage requirements were confirmed through the ESA SORS simulations (Chapter 7, Sections 7.1-2).

Table 4.7.1 – *VenSpec-U measurements and mission requirements*

Requirement number	Parent	Requirement description
R3-MEA-210	R2-C-20 R2-C-40	The VenSpec-U spectral measurement requirements in the UV above the clouds on the **dayside** are defined as follows: (1) **Measure the SO_2 column density above the clouds (SciO#U1)** a. **Spectral range:** 190 – 320 nm b. **Spectral resolution:** <2 nm c. **SNR**≥200 (normalized at 220 nm) d. **Effective Spectral Radiometric Accuracy (ESRA)** < 50% (TBC) (2) **Measure the SO:SO_2 column density ratio (SciO#U2)** a. **Spectral range:** 205 – 235 nm b. **Spectral resolution**: < 0.3 nm c. **SNR**≥100 (normalized at 220 nm) d. **Effective Spectral Radiometric Accuracy (ESRA)** < 100% (TBC) (3) **Perform long term monitoring of the UV absorber and clouds (SciO#U3)** a. **Spectral range:** 240-380 nm and includes 365 nm (UV absorber range and peak absorption wavelength) b. **Spectral resolution:** 5 nm c. **SNR**≥100 (normalized at 220 nm)

		d. **Absolute radiometric accuracy** (at 365 nm): < 10% (4) **Horizontal measurement sampling** applicable to SNR requirement and at derived data product level: a. 24x24 km² (HR channel, SciO#U2) b. 5x5 km² (LR channel, SciO#U1) (5) **Instrument swath width:** FoV = 20° (i.e. ~53 km at 70 km (cloud top) for an orbit altitude of 220 km, ~155 km at 70 km (cloud top) for an orbit altitude of 510 km)
R3-MIS-310	R2-C-20 R2-C-40	The mission shall enable monitoring of abundance of trace gases and cloud properties above the clouds (65-80 km) (R3-MEA-210) and characterize their variability on time scales from hours to years and spatial resolution from 24 to ~5 km, with the following mission requirements: (1) **Horizontal measurement sampling** (applicable to the data downlink rate, see T3-MIS-310) a. Between 24x24 km² and 12x12 km² for the HR channel (205-235 nm) b. Between 5x5 km² and 3x3 km² for the LR channel (190-380 nm); (2) **Temporal sampling:** a. 4 consecutive orbits per 24 hours; b. An overlap of >70% (TBC) of the swaths (FoV) between 2 consecutive orbits; c. <3 hours between 2 consecutive orbits; (3) **Temporal coverage**: During the nominal mission lifetime, allowing multi-season and multi-year observations; (4) **Geographical measurement coverage**: > 60% of the planet (in local time, latitude, longitude) with no gaps > 10%; - see Note 2 T3-MIS-310; (5) **Nominal observation geometry** applicable to R3-MEA-210: Nadir; (6) **Solar zenith angle geometry:** ≥75% (TBC) of the VenSpec-U measurements shall be acquired for solar zenith angles < 70°; (7) **Measurement geographical location knowledge**: Better than 100 km relative to the surface latitude and longitude position (i.e. knowledge available during data processing); (8) **Operation**: VenSpec-U and VenSpec-H shall be operated simultaneously at the dayside of the planet.
R3-MIS-315	R2-C-10 R2-C-20	The mission design shall ensure that the VenSpec-U, H and M FoVs are overlapping, with: (1) The VenSpec-H FoV fully included in the transverse extent of the VenSpec-M for the nightside observations, and (2) The VenSpec-H FoV fully included in the transverse extent FoV of VenSpec-U for the dayside observations.

4.8. Radio Science Experiment (RSE)

4.8.1. Experiment objectives and description

The Radio Science Experiment relies on the recording, at ground stations, of the frequency of the radio-signal sent by the spacecraft. The experiment consists of two parts, described below and illustrated on Figure 4.8.1.

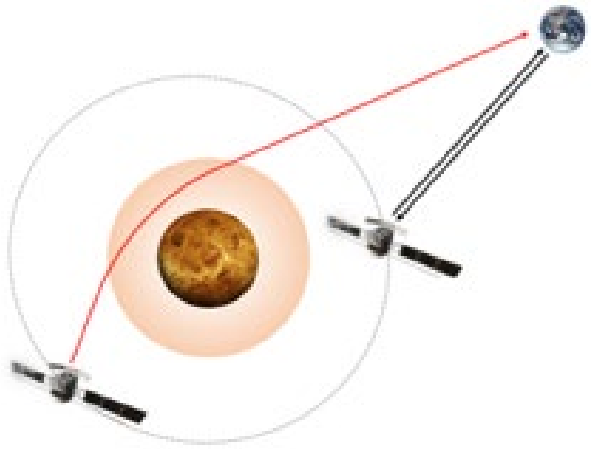

Figure 4.8.1 – *Illustration of the two operation modes corresponding to the two experiments of the RSE (red: Radio-occultation, black: Gravity).*

Gravity experiment. – The gravity experiment aims at mapping of the Venus gravity field with 140-200 km spatial resolution (~95-135 degree strength) and thus constraining interior structure. The experiment will use the 2-way mode with an X-band uplink and a dual X-Ka band frequency downlink in order to reduce the noise on the frequency measured at the ground station resulting from the interplanetary plasma. The Doppler shift of the received frequency with respect to the transmitted frequency will be used to monitor the velocity variations of the spacecraft in order to precisely reconstruct its trajectory around the planet. The orbital velocity perturbations are then inverted to reconstruct the gravity field of Venus (including the tidal component, the k_2 Love number). The space segment of the experiment is the onboard transponder used for telemetry and radio-navigation and the high gain antenna. The ground segment are Earth's based ground stations, which record the phase of the downlink signal and extract the Doppler shift of the received carrier frequency.

Radio-occultation experiment. – The radio-occultation experiment aims at sounding of the temperature and pressure structure of the Venus atmosphere in the altitude range 90-35 km and the abundance of sulfuric acid in

gaseous and particulate phases. The experiment relies on observation of the radio-link propagation (frequency and amplitude) through the atmosphere of Venus during radio-occultation. The experiment is performed in the 1-way mode and therefore requires a Master Reference Oscillator (MRO) onboard the spacecraft to ensure the frequency stability. The radio ray path changes in the ionosphere and neutral atmosphere are induced by a change in the refractivity profile. This leads to a shift in the measured frequency at the ground station. These frequency changes can be used to retrieve the neutral number density, temperature and pressure profiles as a function of the planetary radius at a high vertical resolution. The recording of the absorption of the radio waves at the base of the clouds and below in both X- and Ka-band will allow to estimate sulfuric acid abundance in both gaseous (down to 35 km) and particulate (~50 km) phases, as well as SO_2 at ~50 km (complementing VenSpec-H and VenSpec-U SO_2 measurements, see Section 7.4.4).

4.8.2. MRO interfaces and resources requirements

One-way radio-occultation experiment requires high frequency stability of the radio signal. This is provided by a Master Reference Oscillator (MRO) included in the TT&C system of the spacecraft. The MRO shall provide Allan deviation (ADEV) less than 10^{-12} from 1 to 1000 s. The MRO is designed to perform the function of providing a stable frequency reference to the spacecraft Deep Space Transponder (DST) at the time scales of interest for the atmospheric experiment. The Oscillator generates the base frequency using a high-quality factor quartz crystal oscillator (the Ultra Stable Oscillator manufactured by Rakon, France, and provided by the CNES). The MRO is developed by Bonn Hungary Electronics Ltd.

4.8.3. Operation requirements

Spacecraft radio-tracking will be performed during each slot of communication with the ground station. It will ensure 3 to 3.5 hours of effective tracking of the spacecraft per day during the nominal science mission (6 cycles). Radio-occultations will be performed during two tracking passes within 24 hours (as per requirement R3-MIS-320, see Table 4.8.1) over half of the days within each cycle. Bending of the radio ray path in the atmosphere must be compensated by slewing the spacecraft with appropriate slew rates.

4.8.4. Heritage

Both gravity and radio-occultation experiments exploit well established techniques used on many planetary missions before. The precise reconstruction of the orbit will use state-of-the-art methods and orbitography software to reach a precision of the order of a few meters, which will allow reconstructing the gravity field within the scientific requirements for the gravity investigation. This accuracy in orbit reconstruction is currently reached for Martian spacecraft from which high-resolution gravity field of Mars is obtained (Marty et al., 2009; Genova et al., 2016). The analysis of the radio occultation profiles uses retrieval methods developed for Venus Express radio occultations. These software packages are even capable of correcting measurement difficulties resulting from multipath effects in the cloud layer (Tellmann et al., 2009).

4.8.5. Experiment performance

The gravity field will be obtained with a spatial resolution between 140 and 200 km (~95-135 degree strength) and accuracy better than 20 mGal. The k_2 Love number accuracy will be better than 1%. This performance is due to the very favourable geometry of the Doppler link, the mission duration (the impact of the number of cycles is highlighted on Figure 4.8.2) and the strong gravity field signal in the Doppler measurements. It will significantly improve the current gravity field solution based on Magellan data which has a spatial resolution between 200 and 500 km and a k_2 accuracy of 22%. The Radio-occultations will probe the atmosphere with a much better temporal resolution than performed so far and will perform the first ever measurements of the liquid sulfuric acid content with accuracy of 30 mg m^{-3} at the base of the cloud layer. The end-to-end simulations performed to estimate the performances of both experiments are described in Section 7.3.6.

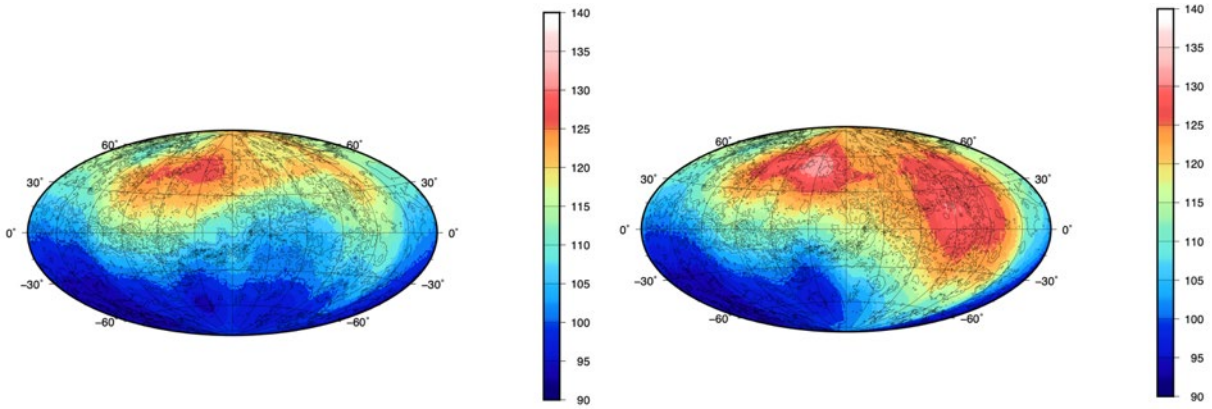

Table 4.8.2 – *Map of the expected degree strength (at 3-sigma) of the gravity field after Cycle 4 (left) and Cycle 6 (right), using a Hammer projection centred at 180°.*

4.8.6. RSE gravity and radio occultation measurement and instrument requirements

Based on the top-down requirements assessment analysis and earlier Venus's mission payloads, the following set of RSE measurement and mission requirements were defined in phase 0 and phase A. These were confirmed to meet the RSE product and coverage requirements through bottom-up performance simulations (see Section 4.8.5 and Chapter 7, Section 7.3.6). In phase B1, some requirements were updated based on a further maturing of the instrument and mission design and new bottom-up performance simulations. Finally, the coverage requirements were confirmed through the ESA SORS simulations (Chapter 7, Section 7.1-2). It should be noted that at the end of EnVision phase A, the ESA Mission Selection Review Board requested that the RSE shall not drive the design of the S/C, nor the cost and schedule of the mission. As a consequence, at the time of writing it has not yet been confirmed whether the current candidate S/C designs fully meet in particular the EIRP variability requirement in R3-MEA-220. This means that the full compliance to the H_2SO_4 and SO_2 product requirements still has to be confirmed (see Table 7.3.3).

Requirement number	Parent	Requirement description
R3-MEA-140	R2-H-80	Gravity science (1) Tracking shall be performed using a 2-way coherent carrier Doppler link, X (up) / X-Ka (down). (2) The end-to-end noise budget @10s count time shall be less than <0.043 mm/s and 0.137 mm/s for Sun-Venus-Earth angle (i.e. the angle between the Venus-Sun and the Venus-Earth position vectors) of 180° (inferior conjunction) and 20°, respectively
R3-MEA-220	R2-C-50 R2-C-60	(1) The radio-occultation experiment shall be performed in a one-way radio link mode, with both X-band and Ka-band downlinks coherent among themselves. (2) The EIRP on the downlink has to be at least 101 dBm with a maximum variability of ±2dB on Ka-band, and 91 dBm with a maximum variability of ±0.3dB on X-band, whatever the size and the power of the HGA and over 10 min (TBC), corresponding to the typical observation duration for an ingress or an egress occultation event[3]. .
R3-MEA-221	R2-C-50 R2-C-60	For the radio occultation experiment (1) An Ultra-Stable Oscillator (USO) shall be developed as part of a Master Reference Oscillator (MRO), for potential implementation and use during the Radio Occultation experiment. (2) The MRO shall have a frequency stability (ADEV) better than 1e-12 between 1s and 1000s integration time.
R3-MIS-230	R2-H-80	The mission shall enable global measurements of the gravity field such that: (1) The altitude is < 520 km (R2-H-80 is not fully met at this altitude); (2) The pericentre altitude is < 260km over ≥40% of the planet (allowing R2-H-80 to be fully met); (3) The measurement altitude is ≥200 km.
R3-MIS-231	R2-H-80	The effective tracking shall be performed at least 3.5 hours per day in average (excluding superior conjunction period) with a minimum of 3 hours per day. Maximum distance between tracked tracks should not be larger than 100 km at the equator over all the tracks of the nominal science operations phase.
R3-MIS-232	R2-H-80	For the gravity field (1) A maximum amount of DV disturbance allowed is 1 mm/s per day. (2) It should take place maximum 1 hour before the tracking passes.
R3-MIS-240	R2-H-80	The mission shall return the received carrier frequency at the receiving ground station recorded in closed-loop mode with a sampling of 1 per 10 seconds in both X-band and Ka-band downlinks as well as the transmitted uplink carrier frequency at the transmitting ground station.

[3] Note: The variability shall be considered with a 68% confidence level, assuming the mixed statistical interpretation

R3-MIS-241	R2-H-80	For the gravity raw data products (1) The mission shall provide the orientation of the spacecraft, the bus and the mobile part wrt the bus (like solar arrays), either predicted or reconstructed, with a sample of 1 per 10 seconds. (2) The error on the s/c orientation knowledge is required to be better than 1 degree around each axis, with confidence level 68% (1 sigma), limiting its contribution to the non-gravitational force error budget at a level of 1%.
R3-MIS-242	R2-H-80	For the gravity raw data products (1) The mission shall provide the macro-model of the spacecraft as flat plates representing the bus, the solar array and the HGA. (2) On-ground measurements of the surface area, and of the optical properties (average value of reflectivity, absorptivity and emissivity coefficients) of the surface of these plates are required to be determined before launch.
R3-MIS-320	R2-C-50 R2-C-60	Radio occultation operations shall be performed during dedicated tracking passes, (1) preferably during radio occultation campaigns consisting of at least 2 passes (where each pass include calibration, ingress, egress and calibration) within 24 hours, (2) on 50% of the days at each cycle. (3) Radio occultation operations shall not be performed if the SUN-Earth-Probe (SEP) angle is less than 10 degrees (superior solar conjunction).
R3-MIS-321	R2-C-50 R2-C-60	The two one-way radio signals shall be recorded in open loop mode at the following A/D conversion rates: (1) ESA European Space Tracking (ESTRACK): 1a. 100,000 samples/second if no atmospheric predict is available for the steering of the local ground station oscillator; 1b. of the order of 5000 samples/second if the local oscillator can be steered by an atmospheric predict during occultation ingress and egress; (2) NASA Deep Space Network (DSN, if applicable): 2a. of the order of 5000 samples/ second if the local oscillator can be steered by an atmospheric predict. (3) The two one-way signals shall also be recorded in closed-loop at 10 samples/second and serve as verification data.
R3-MIS-322	R2-C-50 R2-C-60	The Radio-Occultation experiment (i.e., 1-way communication mode) shall (1) starts/stops when the s/c is at 200 km (as seen from the Earth). (2) The telemetry shall be off and the radio carrier shall not be suppressed when the s/c is below 100 km (as seen from the Earth) during the radio-occultation experiment.

5. Mission and Spacecraft Design

5.1. Mission Design

To meet its science objectives, the EnVision mission needs to return a significant volume of science data to Earth, with a large distance-to-Earth dynamic range (from 0.3 to 1.7 AU), from a low Venus polar orbit, in the hot Venus environment (exacerbated by the operation of highly dissipative units), while operating three spectrometers in an almost cryogenic level environment. This needs to be achieved within constraints on the spacecraft mass due to launcher capability, as well as programmatic boundaries of ESA's 5th M-class call. Achieving the science objectives under these multiple constraints without oversizing the spacecraft calls for a careful planning of science operations, making the science planning strategy a critical driver in the design of the whole mission, against which the spacecraft and ground segment are then sized. In this chapter the main mission requirements and design drivers will be first summarized, the design of the science mission profile explained, before detailing the resulting spacecraft design. It will be shown that the mission and spacecraft design successfully meet the requirements with sufficient margins.

5.1.1. Summary of mission requirements and design drivers

On top of mission design drivers are two top level driving mission requirements: (1) EnVision science orbit requirements (Section 5.1.5); (2) Launcher, debris mitigation and planetary protection requirements (Section 5.1.4). Based on these driving mission requirements, the following mission design drivers were analysed in preparation for the adoption review: ESA's 5th Medium class call design-to-cost strategy (Section 5.1.2); environmental constraints imposed by a deep space mission to Venus orbit (Section 5.1.3); payload accommodation requirements on the spacecraft and observation modes (Section 5.2.5); operational point for data return (a mission-level operational point allows retrieving the required data return while minimizing spacecraft resources and for an acceptable load on the ground segment, Section 5.1.6); design of science mission profile (e.g. surface coverage to be observed by the various experiments and instruments over the six cycles[4] of the mission, Section 5.1.7)

5.1.2. ESA's 5th Medium class call design-to-cost strategy

The mission is designed to achieve all the prime key science objectives with a cost-at-completion compatible with the programmatic boundaries imposed by ESA's 5th Medium class call. This so-called 'design-to-cost' approach is a driver for key design choices for the mission architecture. It leads to: (1) preference for a body-fixed dual band High Gain Antenna rather than a steerable HGA, to limit the on-board solid state mass memory size to 8 Tbits (at End Of Life), and generally speaking to rely on mature, high TRL technologies for all subsystems; (2) discard of electric propulsion solutions which otherwise would also fulfil the mission requirements but at a significantly higher cost; (3) limit the complexity and duration of ground operations, in particular, the mission duration being adjusted to six cycles to confidently fulfil all science requirements. In that context, the use of aerobraking becomes mandatory to reach the desired science orbit, and the science orbit itself can only be coarsely controlled; and (4) limit the complexity and duration of ground operations, in particular, the mission duration being adjusted to six cycles to confidently fulfil all science requirements.

5.1.3. Environmental requirements imposed by a deep space mission to Venus orbit

The thermal fluxes in orbit around Venus are high, the solar flux at Venus distance is twice its value on Earth (around 2600 W/m^2), and the reflected sunlight flux has a similar order of magnitude due to the albedo of 0.75. Besides, during aerobraking, a third thermal flux, the aerothermal flux, needs to be taken into account, with a similar order of magnitude as the two others. These high total thermal fluxes, together with the cold instruments requirements, high power dissipation, and low orbital period, make the thermal environment a design driver for

[4] a Venus cycle is defined as 243.02 Earth days, or 1 Venus sidereal day, the time needed for Venus to spin 360 degrees on its axis in a celestial reference frame, in retrograde motion. This Venus "sidereal day" lasts longer than the revolution of Venus around the Sun (or Venus "year", 224.70 days).

the mission. Avoiding the aerothermal flux to fully add up to the two others thermal fluxes drives the aerobraking strategy.

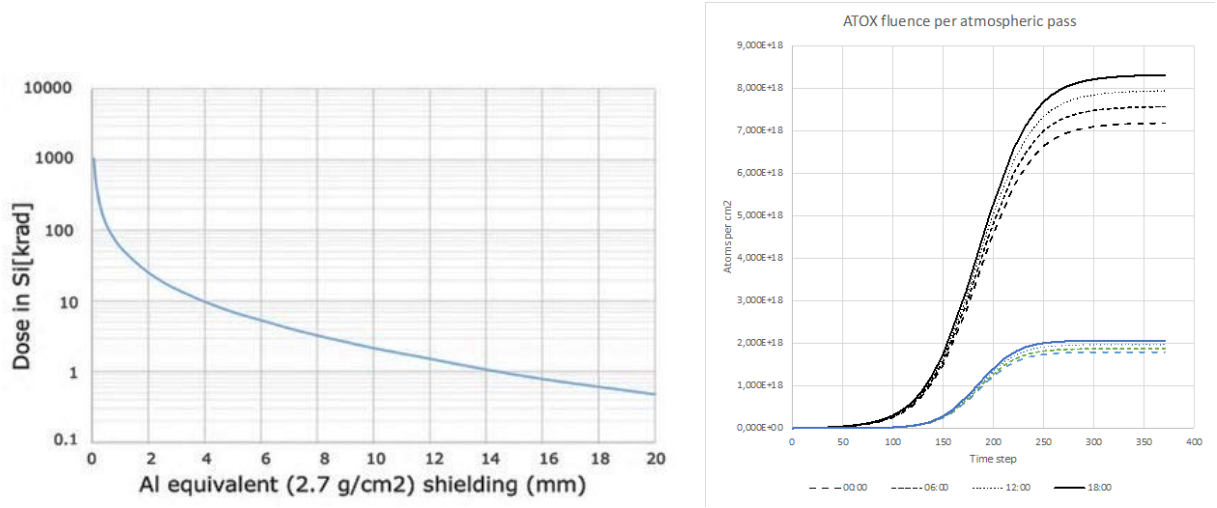

Figure 5.1.1 – *(a) Total Ionizing Dose for EnVision behind Aluminium equivalent spherical shielding, without margins (b) total atomic oxygen fluence per atmospheric pass at the beginning and end of aerobraking, without margins.*

The rather long interplanetary mission leads to total radiation dose requirement for the spacecraft of 37.5 kRad behind 2-mm equivalent Aluminium spherical shielding, assuming a margin of 100%, for a 7.4 years total mission duration (Figure 5.1.1). This is comparable to typical doses encountered for Low Earth Orbit missions.

The atmospheric environment during aerobraking needs also to be taken into account. Atomic oxygen exists in Venus atmospheres at the altitude range foreseen for aerobraking, with densities of up to $8 \cdot 10^{18}$ oxygen atoms per square centimetres at aerobraking altitudes. Though the concentrations are small, their accumulation over up to 3500 atmospheric passes (current mission sizing case) lead to non-negligible total atomic oxygen fluxes on the exposed spacecraft surfaces which are comparable to those encountered on ISS over two years. Combined with the high temperature encountered during passes, this drives the selection of spacecraft materials e.g. Multiple Layers Insulation on the most exposed surfaces.

5.1.4. Launch strategy

EnVision is required to be launched with Ariane 6, the new generation European launcher, in its dual booster configuration (Ariane 6.2, Figure 5.1.2). Ariane 62 maiden flight being scheduled in 2024, the launcher will have reached its mid-life by the time when EnVision is launched, which means a mature launch configuration with proven flight experience.

Figure 5.1.2 – *EnVision is required to be launched with Ariane 6 in its dual booster configuration (Ariane 62). The launcher will have reached its mid-life by the time when EnVision is launched, which means a mature launch configuration with proven flight experience.*

The long aerobraking duration (2 years at the time of the Mission Selection Review in 2021) was highlighted as a significant operational risk and efforts have been implemented since then to reduce this duration from 24 to 15 months nominally. A key driver for the aerobraking duration is the propellant available after insertion which can be used to reduce the apocenter altitude – and therefore to lower the starting point of the aerobraking phase, reducing de facto its duration. With the Ariane 6.2 launcher, the mass in direct escape launch strategy is heavily constrained. A trade-off performed between the end of phase A and the kick-off of phase B1 indicated that an alternative launch strategy resulted in a significantly lower orbit at aerobraking start, despite a larger spacecraft (S/C) design (and therefore an increase in dry mass), and provided more robustness in case of dry mass growth and/or launcher under performance. Such strategy consists in launching the spacecraft into a highly elliptical orbit (HEO) around the Earth with a low inclination to maximise the launcher performance.

Table 5.1.1 – *Indicative comparison of direct escape and HEO scenarios with an Ariane 62 launcher*

	Direct Escape strategy (phase A)	High elliptical orbit (HEO) strategy (Phase B1)
S/C dry mass	~1350 kg	~1675 kg
Tank sizing	2*700 L	2*1100 L
Drag Area	~30 m^2	~45 m^2
Starting aerobraking orbital period	~24 h	~12 h
Aerobraking duration	~24 months	~15 months
Ariane 62 Launch Capability	~2300 kg	~3700 kg

The HEO strategy comes with additional operational risks compared to the direct escape. These risks are discussed in the risk chapter, as well as the implemented mitigations.

5.1.5. Debris mitigation and planetary protection requirements

The mission shall fulfil its nominal science objectives within a maximum duration of 7.4 years from launch to spacecraft disposal. On top of these science-driven requirements, EnVision is a Planetary Protection Category II mission, in accordance with ESA Planetary Protection Requirements. A planetary protection plan will be prepared and maintained as per phase B of the mission, in accordance with the applicable planetary protection requirements. Being operated in Earth orbit (although for a limited portion of time), EnVision needs to comply with Debris Mitigation requirements and regulations. In particular, the capability to perform collision avoidance in that phase of the mission is implemented as a baseline in the mission design, at ground segment and spacecraft levels. A space debris and mitigation plan is therefore also developed and maintained as per phase B.

5.1.6. EnVision science orbit requirements

The choice of science orbit around Venus is mainly driven by the Radio Science gravity Experiment and the operational altitude range for the SAR and SRS instruments. The former requires a low altitude polar orbit, with at least 40% of the time spent below 260 km over at least six cycles to reach a degree strength of 90 over the full Venus surface. The latter requires the observations to be done at altitudes lower than 510 km to achieve sufficient imaging qualities with high incidence angles, and at least 75% of the observations below 350 km to fulfil the SNR requirements. The orbit shall also remain at all points during the science mission above 220 km to keep the atmospheric drag torque controllable by the spacecraft reaction wheels. There is no other imposed constraint on the orbit, and no strict orbit control requirement is derived from the science requirements. In particular the orbital ground track does not need to be repeatable from cycle to cycle, a natural track-to-track shift of around 10 km is sufficient to implement the planned SAR observations. Such a shift is naturally achieved with orbit requirements summarized in Table 5.1.2.

Table 5.1.2 – *Science orbit requirements*

Maximum apocentre altitude	510 km
Minimum pericentre altitude	220 km
Inclination	> 85 degrees

5.1.7. Operational point for science data return

The baseline mission operational point for achieving the required science data return is tuned by design optimization at mission level, combining space and ground segments. It can be summarized as follows:

- At spacecraft level: use of Ka-band RF subsystem for science data downlink, Ka-band travel waveguide tube amplifier (TWTA) with high RF power (120 W), large body-fixed high gain antenna (HGA) diameter (2.5m), and on-board mass memory with 8 Tbits capacity at end of life (EOL);
- At ground segment level: use of cryocooling technology at the deep space antennas ground station receivers to maximize the G/T in Ka-band, and average daily usage of 9.3 hours of ESA's 35 m deep space antennas for Ka-band downlink during the nominal science phase.

This mission-level operational point allows retrieving the required data return while minimizing spacecraft resources and for an acceptable load on the ground segment. The following paragraph (Section 5.1.8) presents the

overall design of the proposed planning and operations strategy. More detailed presentations and a demonstration of its feasibility on a science operations reference scenario is presented in Section 7.1.

5.1.8. Overall design of the science mission profile

The mission design needs to accommodate the operation of the science instruments, namely VenSAR (standard, stereo, polarimetry, HiRes, altimetry, nadir, near-nadir and off-nadir radiometry modes), SRS (high and low density modes), VenSpec-M, VenSpec-H (cooling and nominal), VenSpec-U (Nominal and SNR-limited modes) and Radio Science Experiment (gravity experiment and radio-occultation experiment) such as to achieve the mission objectives in terms of surface coverage and repeated observations, while taking into account the constraints imposed by the spacecraft design (e.g., wheel offloading manoeuvre duration and frequency, slew manoeuvre for pointing, mass memory capacity constraints, thermal and power constraints), the instrument design (e.g. VenSpec-M operates on the nightside, VenSpec-U operates on the dayside, cooling of VenSpec-H is required) and mission boundaries (e.g., the baseline science duration is six Venus cycles).

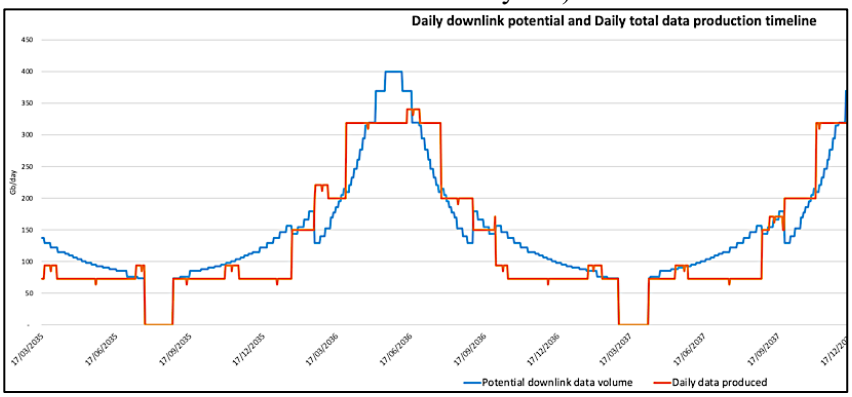

Figure 5.1.3 – *Potential downlink data volume in Gb/day (solid blue). Date and EnVision daily data production (solid orange).*

To cope with the varying downlink capacity and S/C avionics constraints (there is only a limited, discrete number of possible downlink rates due to data handling and transponder limitations), and achieve the science surface coverage requirements, several observation profiles are defined to optimize the data return. They correspond to 15-orbit patterns including observations, slews, and communication slots. They are defined such that the daily science data return is as-close-as possible to the data downlink potential that day, so as to store only for a limited time the science data onboard and avoid embarking a very big SSMM which would have cost and mass implications, not affordable in the context of EnVision.

The adopted observation strategy distinguishes between measurements which need to be performed on a regular, routine basis at each cycle, to meet global coverage requirements (e.g., VenSpec, altimetry, RSE, nadir and near-nadir radiometry, SRS) or contiguous coverage requirements (e.g., VenSAR, SRS), and measurements which can be acquired on an irregular basis, e.g. when the available downlink allows it (SAR dual polarization, SAR 10 m resolution, off-nadir radiometry) and when the given target is in visibility. The first category forms the definition of the basic science operations profile, while the second category forms the intermediate and maximum science operations profiles. Each category is then declined in 'seasonal' versions, to take into account thermal constraints imposed by the S/C configuration (see Section 7.1).

There are eight such science operations profiles defined, created to meet the science requirements, while minimizing the needed on-board mass memory capacity, and considering the variations in data downlink rate and eclipse / occultation durations. These profiles allow to return between 70 and 340 Gbits per day to Earth. The data downlink potential volume profile is depicted in Figure 5.1.3 in blue. The produced data volume is depicted in orange and shows many variations that are due to the transitions between the various science operations profiles.

5.1.9. EnVision payload nominal resources budget

The SAR instrument, due to its size (6 m reflectarray length) and accommodation constraints (2.75 m between reflectarray and feed array), its number of operating modes (standard, polarimetry, high resolution, altimetry, radiometry) and its associated resources (mass, power, data volume), determines the spacecraft configuration. The infrared spectrometers (VenSpec-M and H) drive the design of the spacecraft thermal control subsystem, due to their thermal requirements. VenSpec-H for instance needs to be kept at -45 degree, in its cold section, while VenSpec-M requires thermal stability in the order of a few degrees. This leads to the definition of a 'cold' face on the spacecraft, which needs to be maintained cold whatever the sun elevation with respect to the orbital plane, requiring specific 180 degrees flip-around manoeuvres of the spacecraft twice per Venus year. The Subsurface Radar Sounder requires deployment of a 16 m tip-to-tip antenna composed of two 8 m dipole antennas, driving

in particular the spacecraft configuration and attitude control requirements to avoid exciting the associated flexible modes.

Table 5.1.3 – *EnVision payload nominal resources summary. (*) the nominal mass and power include design maturity margins. (**) the allocated mass corresponds in phase A to a 20% higher mass and the allocated power to 30% higher power. The SRS antenna is under prime responsibility and its mass included in the spacecraft 'mechanisms' budget.*

Unit	VenSAR	Radio Science	VenSpec suite	SRS	Total
Allocated mass [kg] (**)	190	3.5 [MRO]	54	15.34	**262.5**
Nominal peak power (*) [W]	1364	5.2 [MRO]	72.9 [M:15, H:29.7, U:18.7]	Peak: 200	**1400 max.** (sequenced operations)
Allocated power (**) [W]	1773	11.4 [MRO]	66.2	170	**1800 max**
No. of units	Reflectarray, Feeder, ESS, RF electronics, Digital electronics, SSPA	USO	VenSpec-M, VenSpec-H, VenSpec-U, CCU (central control unit)	RDS, TX, MN	**14**
Size (cm)	see Section 4.2.1	9.9 x 8.8 x 5.5	M: 38 x 14.4 x 17.3 H: 65.5 x 46.3 x 27.5 U: 30 x 30 x 30		
Data rate (Mbps)	0.003-197	--	M: 0.5-1, H: 0.030, U: 0.04-0.64	3.25-6.47	
Downlinked data volume (nominal mission) [Tbits]	**160**	--	**12**	**17**	**189**

The need for the spacecraft to follow the changing bending angle of the communication system radio ray path, during radio-occultation experiment leads to specific slew profiles which need to be provided by the spacecraft reaction wheels. The various pointing modes of the spacecraft required for instrument operations and the downlink of their data are also driving the sizing of the spacecraft power and thermal subsystems, and in general the spacecraft configuration (solar array and battery sizing, radiator area).

The various planetary coverage requirements of the payload instruments lead to a total return of 189 Tbits over the nominal science phase, the various SAR modes representing more than 80% of this data volume (Table 5.1.3). Achieving the required science data return drives the concept of operation of the mission, in particular the ground stations usage and the spacecraft communications and data handling subsystems designs, and as a consequence also the power subsystem sizing and therefore the dry mass of the spacecraft.

5.2. Spacecraft design, main operations and payload accommodation

5.2.1. Spacecraft design overview

Two design solutions are studied in the EnVision Definition phase B1, both meeting the applicable mission requirements and compliant with the payload reference operations scenario; the two competing design are developed with ADS and TAS in phase B.

5.2.2. Spacecraft structure and configuration

Mechanical design. – The mechanical design consists of a central tube configuration:

- The Primary Structure is the main stiffness contributor, and is composed of the launcher interface ring (1194 mm diameter), the central tube itself and shear webs;
- The Secondary Structure mounts the platform and instrument units and adds local stiffness.

The total height of the S/C is about 3 m from launcher ring interface to the bottom of the nadir panel (+x panel), for widths and depths of about 2 m for both designs in stowed configuration.

Panel description. – The +x panel (Figure 5.2.1) is dedicated to nadir-looking instruments (spectrometers and SRS). The -x panel includes the ring interface to the launcher, as well as the Main Engine used in particular for the Venus Orbit Insertion manoeuvre. The y and -y panels include the attachment of the two Solar Arrays wings and are mostly covered in Optical Surface Reflectors (OSR) radiators for platform and payload units. The +z panel is where the fixed X/Ka High Gain antenna is located. The -z panel is the so-called cold face where the radiators of thermally sensitive instrument parts are located, in particular VenSpec-H, U and M.

Figure 5.2.1 – *Overview of the EnVision spacecraft design configuration, as studied in phase B1. The figure is an artist impression of the spacecraft, which is relatively similar to the design by both competing consortia. The -z panel of the spacecraft is the so-called cold face of the spacecraft. Specific radiator cavities (notches) are implemented on that face to avoid exposing the most sensitive radiators to the planetary fluxes (mostly albedo) and to minimize direct sun flux during communications around inferior conjunctions. Artwork: VR2Planets.*

Aerobraking configuration. – The S/C aerobraking configuration, with the -x face of the spacecraft facing the aerothermal flux, is fully compatible with the aerobraking phase: the most sensitive elements (e.g. spectrometers) are naturally protected from the flux, being located on the opposite panel of the spacecraft, while the least sensitive elements are directly exposed to the flux (e.g. Main Engine nozzle and ring adapter). The solar arrays longitudinal axis crosses the spacecraft only typically 50 cm below the nadir-panel to ensure the centre of pressure remains behind the centre of mass during aerobraking, guaranteeing a naturally stable aerodynamic configuration. The solar arrays, SAR back-side, the -x face of the spacecraft and the lateral side of the HGA are the main contributors to the drag surface, which totalise about 45 m^2, for a ballistic coefficient close to 20 kg/m^2 at the start of aerobraking.

5.2.3. Main modes of operations

Three main spacecraft pointing modes for instruments operations are identified:

(1) ***default*** pointing mode, with the long direction of the SAR antenna parallel to S/C velocity vector and either (1a) The central part of the SAR antenna aligned with the orbital velocity and the nadir face (+x) nadir pointed for radiometry, VenSpec and SRS observations; (1b) The 30 m, 10 m-resolution and off-nadir SAR observation pointing with the +x face of the spacecraft at an angle between -50 degrees and +20 degrees around the y axis (pointing along the S/C velocity vector) to cover the range of off-nadir look angles for the SAR (Figure 5.2.3);

(2) ***altimeter*** pointing mode, with the long direction of the SAR antenna perpendicular to the S/C velocity vector. This mode is used for altimetry observations. The SAR boresight is nadir-pointed. The +x face is off-pointed by -14 degrees around the S/C y axis (i.e. perpendicular to the S/C velocity vector);

(3) ***communications*** pointing mode, with the fixed High Gain Antenna Earth-pointed (COMMS mode): (3a) in the comms mode the body-mounted HGA, accommodated on the S/C +z panel, needs to be pointed to Earth for several hours. Since communications are required every day, the spacecraft attitude with respect to the Sun and Venus can take any value; (3b) for radio-occultation (at ingress and egress of the atmosphere during seasons of Earth occultation), the spacecraft needs to follow an attitude profile to compensate for the changing bending angle of the RF signal in Venus's atmosphere. This involves S/C angular rates of up to 0.07 deg/s, provided by the reaction wheels.

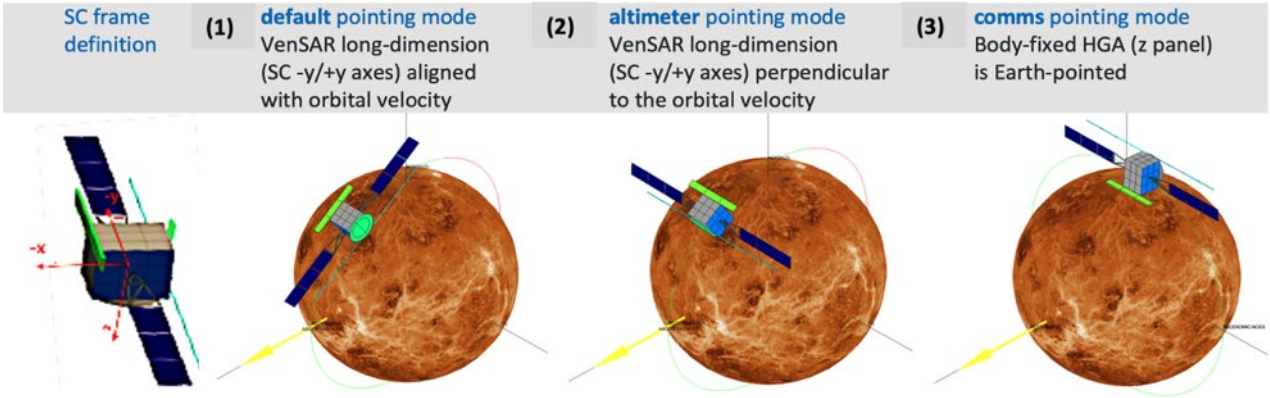

Figure 5.2.2 – *This figure shows the three spacecraft pointing modes required for scientific observations: (1) default pointing mode; (2) altimeter pointing mode; (3) comms pointing mode. The combination of the spacecraft attitude, the Solar aspect angle and the Earth aspect angle need to be considered for the sizing of the spacecraft critical subsystems: power and thermal. Sun calibration and deep space calibration modes are not represented, but would be very similar to comms pointing mode (3).*

The transition between any of these modes is achieved via the reaction wheels assembly, with typical slew times between 10 and 20 minutes, depending on the mode. Outside of the science pointing modes, the main modes required to execute the operational mission and handle any contingency situation are the Cruise Mode, the Thruster Control Mode, the Aerobraking Mode, and the Safe/Survival Mode.

The Safe Mode strategy relies on the star trackers, the Coarse Sun Sensor, and gyroscopes to automatically point the solar arrays to the Sun and the HGA to the Earth to minimize the recovery time. In the unlikely case where the star trackers would not be available, a second level of Safe Mode is activated, relying on the omnidirectional coverage of the two X-band low gain antennas (LGA). The X-band TT&C chain is sized to allow commanding from the ESTRACK ground station at any attitude and any distance from the Earth, and to provide a minimum downlink signal in the form of semaphore tones. In such situations, NASA's DSN stations may be used to minimize the time of S/C unavailability for science operations.

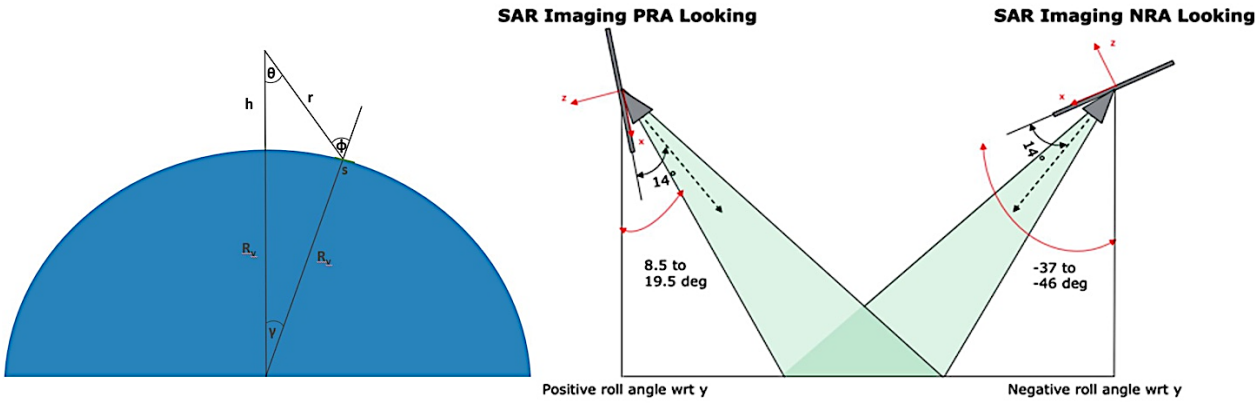

Figure 5.2.3 – *(Left) The look angle ϴ for a SAR observation is the angle between the nadir direction and the direction to which the maximum gain of the antenna is beamed. The incidence angle ϕ is defined as the angle between the local vertical at the target location and the direction of the incidence SAR radiation. (Right) A positive or negative look angle can be provided by the spacecraft corresponding to respectively positive roll angle (PRA) or negative roll angle (NRA). Positive Roll observations are in general preferred as they require smaller amplitude manœuvres and are more favourable from a thermal point of view.*

Table 5.2.1 – *Spacecraft pointing and orientation with respect to the orbital plane, as a function of observation type: targeted observations of Regions of Interest (RoIs, see Figures 3.3.1 and 3.3.3; Figures 7.1.2 and 7.2.1); global observations (Figure 7.2.2). See also Science coverage requirements in Table 3.6.1.*

Spacecraft pointing	Spacecraft orientation with respect to orbital plane	EnVision targeted observations	EnVision global observations
Nadir and near-nadir	Parallel to velocity	SRS High Density	SRS Low Density VenSpec-M VenSpec-U VenSpec-H
	Perpendicular to velocity		VenSAR Altimetry
	Parallel and perpendicular to velocity		VenSAR Nadir Radiometry VenSAR Near-nadir Radiometry
29 degrees incidence **Up to 40 degree incidence**	Parallel to velocity Parallel to velocity	VenSAR off-nadir radiometry • VenSAR Standard (30 m) • VenSAR Stereo (30 m) • VenSAR Polarimetry • VenSAR High-res. (10 m)	
Earth-pointing	Any attitude	RSE Gravity Science (High resolution)	• RSE Gravity Science(Low resolution) • RSE Radio occultation

5.2.4. Thermal design

In the hot environment of Venus, and with the variety of possible spacecraft attitudes, the placement of the radiators on the spacecraft is constrained. Only three faces of the spacecraft are available and can be kept cold enough for the needs of the platform and of the instruments: the two faces where solar panels are attached (y and

-y), and the -z face. Radiators placement for platform / payload are therefore distributed over those panels. The three main thermal design drivers are as follows:

(1) ***180 degree flip-around of the S/C about its x-axis twice a Venus sidereal year*** – The -z face can be maintained cold all year long during science observations, thanks to a 180 degree flip-around of the spacecraft twice per Venus year (every 112 terrestrial days), allowing for a cold and stable thermal environment, as required for the operations of the three spectrometers VenSpec-M, H and U;

(2) ***High radiator area*** – The large dissipation power for the science payload and the communication subsystems lead to a high radiator area which means also high thermal losses in cold cases, therefore requiring significant heating power;

(3) ***Altimetry pointing mode*** – The altimeter pointing mode may lead +y or -y to be fully exposed to the Sun. This drives the choice to perform altimetry observations only when the spacecraft is in eclipse for science operations planning.

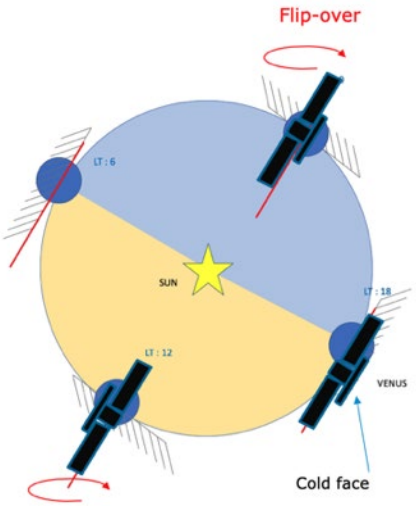

Figure 5.2.4 *– Top view of the orbital geometry w.r.t. sun during 1 Venus year of 224 days. A 180 degree flip-around of the S/C around its x axis is performed twice a Venus sidereal year (or every 112 terrestrial days), when the Sun crosses the orbital plane. This allows to maintain the -z face always in the shadow whenever the instruments are operated in the default pointing mode. This means the S/C will be naturally right looking for half of the year, and left-looking the other half.*

With the help of the spacecraft configuration and its concept of operation, the thermal design is kept simple and based on reliable technology. Heat pipes are used to spread high thermal dissipation evenly on radiators when necessary. Despite the harsh Venus thermal environment, only flight-proven materials are used.

5.2.5. Payload accommodation: VenSAR, SRS, VenSpec-U, -H, and -M

VenSpec-U, -H, and -M – The three spectrometers VenSpec-U, H and M are accommodated on the +x panel (see Figure 5.2.1). This prevents any obstruction of the three spectrometers field of views, and minimize the exposure to the aerobraking environment. Calibration sequences are performed on a regular basis (alternatively sun and deep sky calibration) for the VenSpec instruments.

VenSAR. – VenSAR is composed of two main elements: the reflectarray antenna, accommodated on the -x/-z edge and deployed after launch, and the feedarray which is located on the +x/-z edge, 2.75 m away from the reflectarray centre to reach the required performance. Both elements are rigidly attached to the S/C bus (e.g. no dedicated boom) to minimize thermo-elastic deformations between both elements. The S/C Attitude and Orbit Control Systems (AOCS) and flight dynamics on-ground are designed to meet the VenSAR pointing requirements.

SRS. – The SRS antenna is under the industrial prime responsibility and is composed of two identical 8 m dipole antennas that are held inside a Hold-Down and Release Mechanism (HDRM), and parallel to each other once deployed, providing 16 m tip-to-tip. The SRS antenna is accommodated on the +x panel, parallel to the -z/+x edge, allowing for a safe deployment of the two dipole antennas with sufficient mechanical clearance to the other platform and payload elements. The technology is built on ESA's heritage gained in particular on JUICE (RIME instrument built by the same instrument team, see Section 4.3.4). The SRS antenna is deployed after launch, when the spacecraft is on its escape trajectory to Venus.

5.2.6. Guidance, Navigation and Control system (GNC)

The Guidance, Navigation and Control system relies on a classical design, with Star Tracker as the main attitude sensors, and Inertial Measurement Unit (IMU) which provide 3-axis angular rates and non-gravitational accelerations measurements. Two internally redundant coarse sun sensors are used to acquire and maintain sun pointing in safe mode. The Attitude and Orbit Control Subsystem (AOCS) is completed by a swarm of four reaction wheels which allow to slew the S/C in any required attitude in less than 10 minutes, even in the case of one wheel failure. Wheels are offloaded once per day. The S/C pointing requirements are summarized in Table 5.3.1.

Table 5.3.1 – *Summary of main pointing requirements along spacecraft x, y, z axes (Figure 5.2.1). All values are given in mrad at 2 sigma. Driving Attitude Knowledge Error requirements are VenSAR for S/C axis x and z, and RSE (Gravity) for axis y.*

S/C axis	Absolute Pointing Error (APE)	Relative Pointing Error (RPE)												Attitude Knowledge Error (AKE)
		70 µs	250 µs	40 ms	0.1 s	0.5 s	2 s	5 s	14 s	30 s	240 s	420 s	1000 s (Cal.)	47 min	
x	1.4 VenSAR	0.42 VenSAR	0.14 VenSAR	0.8 VenSpec-M	0.42 VenSAR	0.84 VenSAR	0.28 VenSAR	1 VenSpec-U	-	3.5 VenSpec-U	0.84 VenSAR	1.49 VenSAR	2.5 VenSpec-U	4.19 VenSAR	1.12 VenSAR
y	12.9 VenSAR	3.88 VenSAR	1.29 VenSAR	3 VenSpec-M	3.88 VenSAR	7.8 VenSAR	2.59 VenSAR	1 VenSpec-U	-	0.6 VenSpec-U	7.77 VenSAR	12.95 VenSAR	2.5 VenSpec-U	38.8 VenSAR	1.14 RSE
z	1.49 VenSAR	0.45 VenSAR	0.149 VenSAR	3 VenSpec-M	0.45 VenSAR	0.89 VenSAR	0.30 VenSAR	1 VenSpec-U	16 VenSpec-H	0.6 VenSpec-U	0.89 VenSAR	1.49 VenSAR	0.5 VenSpec-U	4.46 VenSAR	1.19 RSE

5.2.7. Spacecraft propulsion, electric power and data handling systems

Propulsion. – The propulsion system relies on a bi-propellant MON/MMH system, with Helium as a pressurant. It is composed of the LEROS-4 1 kN Large Apogee Engine currently in development, and two redundant sets of eight RCS thrusters of 10 N which are used for wheel offloading and small delta V manoeuvres, e.g., for orbit correction manoeuvres during science or aerobraking phases. The propellant tanks are accommodated in the central tube of the structure and store more than two tons of propellant for the needs of earth escape sequence, interplanetary transfer manoeuvres, Venus Orbit Insertion, aerobraking manoeuvres, orbital control manoeuvres, and wheels offloading. The maximum total delta V required from the system is about 2300 m/s.

Electric power. – The power subsystem relies on a battery-regulated 28V bus. The Li-Ion battery provides about 10000 Wh at end of life, and is sized by the so-called maximum science operations profile in worst case eclipse conditions. The solar arrays are composed of two wings totalling more than 15 m^2 and a yoke per wing. The wings use one degree of freedom Solar Array Drive Mechanism (SADM) to track the Sun for a significant portion of any orbit. Solar Arrays are sized to enable all planned nominal science operations in the worst orbital conditions (e.g., Sun in the orbital plane). The solar arrays are also used as one of the main drag surfaces during aerobraking operations.

Data handling. – The data handling subsystem consists mainly of a Central Data Management Unit (CDMU) including the On-Board Processor and a flash memory, a Remote Interface Unit (RIU), and an external large capacity Mass Memory of 4 to 8 Tbits End-Of-Life. The spacecraft uses file-based protocols for all its operations, simplifying the management of science data and overall spacecraft operations. The main data handling interfaces towards EnVision instruments are through WizardLink and a SpaceWire (SpW).

5.2.8. Spacecraft communications: X-band up/down and Ka band (down) (32 GHz)

The communication system relies on X-band uplink for simultaneous telecommand and ranging reception, on X-band downlink for simultaneous S/C telemetry and ranging transmission, and Ka-band (32 GHz) downlink for high data rate transmission of science data or alternatively for ranging. The communications subsystem relies on a fixed high gain antenna (diameter 2.5m), which is attached on the +Z panel of the Spacecraft (Figure 5.2.1).

The HGA is the primary antenna used for S/C communication in X and Ka-band, and is completed by several Low Gain Antennas (LGA) used for X-band communications only, during LEOP and safe modes. To maximize the data return, the Ka-band communications subsystem relies on a powerful Travel Waveguide Tube Amplifier (TWTA) with an RF power output of at least 120 W. This architecture, together with daily communication passes with 35 m Deep Space Antennas of 9.3 hours on average, allow to downlink the required science data return whatever the Earth to Venus distance.

5.3. Overview of system-level budgets

5.3.1. Margin philosophy

The mission design is currently in phase B1 (definition phase). To cope with unknowns in the future evolution of the project, the current design phase involves significant margins on key resources at various levels:

(1) ***the standard ESA margins*** apply on the dry mass of the spacecraft at payload and platform levels. The margins on dry mass include maturity margins (DMM) and system margins (SMM);

(2) ***a 30% system margin*** is also included on the power budget at payload and platform levels, and a 30% system margin is applied on the instruments data rate; additional margins are applied to the delta V manoeuvres depending on their nature, e.g., 5% for deterministic manoeuvres;

(3) the Spacecraft is designed to be compatible with an aerobraking starting orbit of 36 hours in terms of thermal loads, number of thermo-mechanical fatigue cycles, atomic oxygen fluence, while in nominal conditions the starting aerobraking orbit is 12 hours. This allows the mission to absorb the following degraded cases, with a penalty on the duration of the aerobraking and therefore higher operational cost and risk:
   (a) An increase in S/C dry mass;
   (b) An underperformance of the launcher;
   (c) the use of a less capable but higher TRL main engine.

5.3.2. Mass budget

Table 5.4.1 – *Indicative mass budget for the spacecraft design, including all margins. All values given in kilograms (kg)*

Total dry mass	1675
Communications	94
Power	226
Data Handling	39
Propulsion	200
Mechanisms	25
Structure	355
AOCS	57
Thermal	103
Payload	248
Harness	80
System Margin	248
Propellant including 2% Residuals	1957
Launch Adapter	71
Total Wet Mass including launch adapter	3703
Ariane 62 performance	3889

The margins in the power budget represent more than 50% of the ‘raw’ power budget (when assuming the system margins with design maturity margins at platform and payload levels).

5.4. Definition study conclusions: Mission and S/C Design

The selected mission profile allows to robustly fulfil the science requirements of the mission with significant margins. The preliminary spacecraft design solutions studied in phase A, and further matured in phase B1, demonstrated two feasible solutions, technically and programmatically, meeting the mission requirements and presenting good margins with respect to the launch performance requirements. In both design solutions, a suitable configuration has been found for all instruments, which satisfies the science requirements. The spacecraft designs are both compatible with the described science operations strategy, guaranteeing that the pre-selected regions of science interest can actually be observed as required. Mission-level risks are limited, understood and mitigation strategies have been put in place already in phase A and B1.

6. Mission and Science Operations

ESA will be responsible for the launch and operations/checkout of the spacecraft and the payload. An EnVision ground segment (GS) will be set up to provide the means and resources with which to manage and control the mission via telecommands, to receive and process the telemetry from the satellite, and to produce, disseminate and archive the generated products.

6.1. Ground Segment Overview

Responsibility for, and provision of, the EnVision GS is split between ESA and the EnVision Instrument teams. ESA will be responsible for the Operations Ground Segment (OGS), consisting of (1) ESA tracking station network (ESTRACK) managed in ESOC (Darmstadt, Germany); (2) Envision Mission Operations Centre (MOC) in ESA-ESOC (Darmstadt, Germany); (3) EnVision Science Ground Segment, including the Science Operations Centre (SOC) and Planetary Science Archive (PSA) in ESA-ESAC (Madrid, Spain). A schematic drawing of the top-level operational interfaces of the EnVision mission is shown in Figure 6.1.1.

6.1.1. Envision Mission Operations Centre (MOC)

The EnVision mission will be operated from a single EnVision MOC located at ESA-ESOC, Darmstadt. The MOC includes all facilities, hardware, software, documentation, flight control teams and support engineers needed to conduct the mission operations.

The MOC is responsible for the monitoring and control of EnVision ensuring the spacecraft's safety and health. The MOC executes mission platform and payload operations preparation, planning (using planning inputs from Science Operations Planning (SOC, see Section 6.3.1) and execution. Spacecraft monitoring and performance analysis is routinely performed together with payload health and status monitoring. Flight Dynamics service is provided including determination and control of the satellite’s orbit and attitude.

The MOC performs all communications with the satellite through the ground stations for the upload of the platform and payload telecommand and reception of the downloaded telemetry data. MOC is also responsible for downloading the science data and its distribution to the SOC, along with the required telemetry, housekeeping and auxiliary data. The spacecraft will be primarily controlled via execution of timed activities from an onboard mission timeline. It is foreseen for the majority of the routine ground station pass activities to be automated. Due to the One-Way Light Time (OWLT) and subsequent delay in command and visible response, real time commanding activities are minimized. Any onboard anomalies will normally also be detected with a slight delay. The mission control system monitoring and alert functions support anomaly detection and the Flight Control Team and on-call engineers will respond and intervene to the anomalies as defined in the agreed procedures.

The different mission phases from the Launch and Early Operations Phase (LEOP), near-Earth commissioning, interplanetary cruise phase, the orbit insertion and aerobraking to reach the Venus science orbit, and the science phases follow the same basic concept with adaptation of response times, team coverage, planning cycles and ground station coverage dependent on the criticality of the operations being executed. Detailed operational plans are prepared for all mission phases. All plans for critical phases are verified and validated using simulators. The Flight Control Teams are fully trained to execute both critical and routine operations via simulations training program.

The science phase mission planning consists of two cycles (Section 6.3.3) with science inputs provided by the Science Working Team (SWT) and PS, instrument teams, and SOC. The SOC prepares the planning and sends it to the MOC. The planning interface between SOC and MOC will be designed to avoid iteration loops with respect to resources. Event timelines and reference orbit will be provided by MOC flight dynamics to the SOC allowing independent planning of the science activities.

The mission planning needs to consider specific mission constraints such as the periods of HGA coverage/outage and periodic radio occultations of EnVision behind Venus. These two constraints define the periods when Space-to-Ground links can be established. These periods are considered together with the allocated ground station availability to establish uplink and downlink communication slots. The mission planning adopts a success-oriented approach assuming that the ground station is operational at the requested scheduled time. The start of TC uplink, reception of real time housekeeping telemetry and onboard telemetry dumps slots are shifted to account

for Earth-to-Venus light time delay. Tuning of these margins is nominally executed early in-flight phase to maximize ground station return/usage.

Orbit control manoeuvres for pericentre control are planned to be executed at most once per cycle (243.02 Earth days). Reaction wheel momentum management is planned from ground and scheduled to avoid wheel offloading during science windows. Spacecraft slew manoeuvres to the observable targets are performed based on the SOC science plan targets and executed from the uploaded mission timeline. Orbit event updates are envisaged to be needed up to three times per week based on updated tracking information. This requires a shift of the onboard mission timeline for payload operations avoiding changes to platform activities. This functionality can be met using standard mission timeline control services and slew timing margins. The nominal science phase operations assume a weekly commanding pattern, a cycle which is typically followed for ESA planetary missions.

6.1.2. Ground Stations: ESA/ESTRACK, NASA/DSN

All communications and tracking with EnVision will be done at X-Band for uplink and spacecraft housekeeping telemetry downlink, and Ka-band for science data downlink. The three ESTRACK 35 m ground stations (Malargüe, New Norcia, and Cebreros) are baselined to support the operational needs of the EnVision mission using existing capability in the ground segment. No ground station upgrades are currently needed to support the EnVision mission. The upgraded cryogenic capability has been assumed to be available in all ground stations supporting EnVision in both X and Ka band feeds. This cryogenic capability improves the antenna gain assumed to be available at the different ground stations and has been used in the spacecraft communications subsystem link budget calculations. For the Radio Science Experiment at least one of the three 35 m is assumed to be equipped with a Water Vapour Radiometer facility and/or GPS techniques to correct for tropospheric effects.

The smaller ESTRACK stations, i.e., Kourou (15 m) and NewNorica2 (NNO-2), are considered in addition to the 35 m antennas for support during the LEOP and initial transfer orbit phases. NNO-2 is envisaged to be used for first acquisition (assuming launcher Direct Ascent). Alternatively Maspalomas antenna could be used for early mission phase LEOP support.

The science data downlink will be dumped daily from the on-board mass memory to ESTRACK 35 m stations for a daily duration between 4 and 7 hours depending on the occultation duration and science operation profile being implemented (Sections 7.1 and 7.2). Ground station passes will nominally be scheduled in two slots every day, split across two of the 35 m ground stations. In the case of a missed ground pass, the spacecraft mass memory is sized to store the science data until the next opportunity. Solar conjunctions will interrupt the ground station contact periods with EnVision. The operations will be suspended when the Sun-Earth-Venus angle is within ±5 degrees during superior solar conjunctions (Venus passes behind the Sun) and ±1 degree during inferior solar conjunctions (Venus passes in front of the Sun).

Access to the NASA DSN ground stations as support antennas during emergency phases is achieved by ensuring compatibility of EnVision with both ESTRACK and DSN networks. In case of unforeseen unavailability of the ESTRACK 35 m antennas during the science phase, or to support a critical phase or emergency recovery of the mission, NASA’s 34 m DSN or 70 m equivalent antennas may be used (Figure 6.1.1).

6.1.3. EnVision Science Ground Segment (SGS)

Science Operations Centre (SOC), the Planetary Science Archive (PSA) and the (nationally-funded) Instrument Teams and their mutual interfaces comprise the Science Ground Segment (SGS). The responsibility for the SGS tasks and activities is distributed and shared between the SOC, PSA and instrument teams, taking the Science Activity Plan compiled by the Science Working Team (SWT) and Project Scientist (PS) as input. The SGS comprises the SGS architecture, science operations planning, instrument operations and calibration, data processing, archiving and community support. The software needed for the instrument operations planning, operation commanding, and the data processing is developed by the instrument teams. Software needed for the overall science operations planning, data processing at the SOC, and data archiving is done by the SOC. The SOC and PSA (Section 6.1.5) and the instrument operation teams will work together under guidance of the project scientist and SWT, in the planning of science operations and the co-ordination of the scientific input. The SOC is responsible for providing agreed and coordinated planning inputs to the MOC, limited processing of instrument data and the archiving of science data products together with eth PSA team. The SOC and PSA is located at

ESAC, near Madrid, Spain. The SGS requirements are provided in the Science Implementation Requirements Document (SIRD, ESA 2023b)

6.1.4. Overall SGS architecture

To achieve the mission objectives, science operations is divided into two paths, from the ground segment to the EnVision spacecraft, commonly classified as the uplink path; and from the EnVision spacecraft to the ground segment, commonly classified as the downlink path. To support the uplink, the activities comprise opportunity analysis, observation planning, its validation and the generation of spacecraft pointing and payload operations requests to be converted into telecommands via defined procedures for transmission to the spacecraft.

Following the downlink of data, the SGS activities comprise the reception of the science and housekeeping telemetry (science data, spacecraft and instrument housekeeping data, orbit data, on-board events, spacecraft attitude data, etc.), data transfer to the instrument teams for processing and generation of science data and calibration products, and archiving of the science data in the ESA PSA and NASA PDS archives enabling the general scientific community to access the final mission products..

6.1.5. ESA Science Operations Centre (SOC)

The ESA Science Operations Centre (SOC) is responsible for (1) development and maintenance of the Science Ground Segment (SGS) system; (2) supporting the Project Scientist (PS) and Science Working Team (SWT) in development of the Science Activity Plan (SAP); (3) simulation and validation of the Mission Operations Plan (MOP); (4) coordination, preparation and validation of science operations and submission of planning inputs to the MOC; (5) interfacing with MOC for reception of science and auxiliary data; (6) operation and maintenance of the raw data processing and archiving pipeline; dissemination of the raw data products to the instrument teams.

The SOC is the single interface to the MOC during the science operations phase for commanding. The SWT and PS are responsible for the SAP development, with support by the SOC. The instrument teams are responsible for; Providing inputs for the instrument science and calibration operations; The developing and running of the data processing pipelines; The analysis and monitoring of the instruments health and performance; The delivery of science data products to the ESA PSA (see Section 6.3.3).

6.1.6. Summary of science planning activities

The SOC will coordinate the different phases of science operations planning by interfacing with the MOC, the instrument teams, the science operations working group (SOWG), and the project scientist who is coordinating the Science Working Team (SWT). There are three levels of planning, Mission Level Planning, Long Term Planning and Short-term planning. The resulting operations plans will be validated with respect to science requirements and simulated, and constraint checked at all levels. Commanding and detailed instrument constraints will be checked at short-term planning.

The main science objectives require collecting a nested set of observations on selected regions of interest. The dataset relies on the full set of observations being achieved over the mission lifetime. To achieve this, a basic plan will be built for the whole mission, which will ‘pencil-in’ these observations. This plan is referred to as the ‘Mission Level Plan’.

The plan will be adjusted in segments of 6 months, carried out every 6 months, in reaction to the released ESTRACK ground station schedule and spacecraft events schedule. The ground station schedule is issued every 6 months, covering a 6-month period starting ~6 months after issue. The resulting plan (a block of 6 months) is known as the Long-Term Plan. Given nominal circumstances, no change to the observation strategy is expected during the long-term planning step. Any changes to the strategy (regions of interest, or observation type) may have impact on the final data set and must be assessed and agreed by Science Working Team.

The orbit accuracy is not good enough at the time of long-term planning for the generation of instrument command timelines, and pointing requests. This will be finalised during ‘short term planning’, each short-term plan will

cover a ~1 week block and will carried out ~ 2-3 weeks before execution onboard, using the short term orbit file as a reference. Requirements for the science planning is provided in the SIRD (ESA, 2023b).

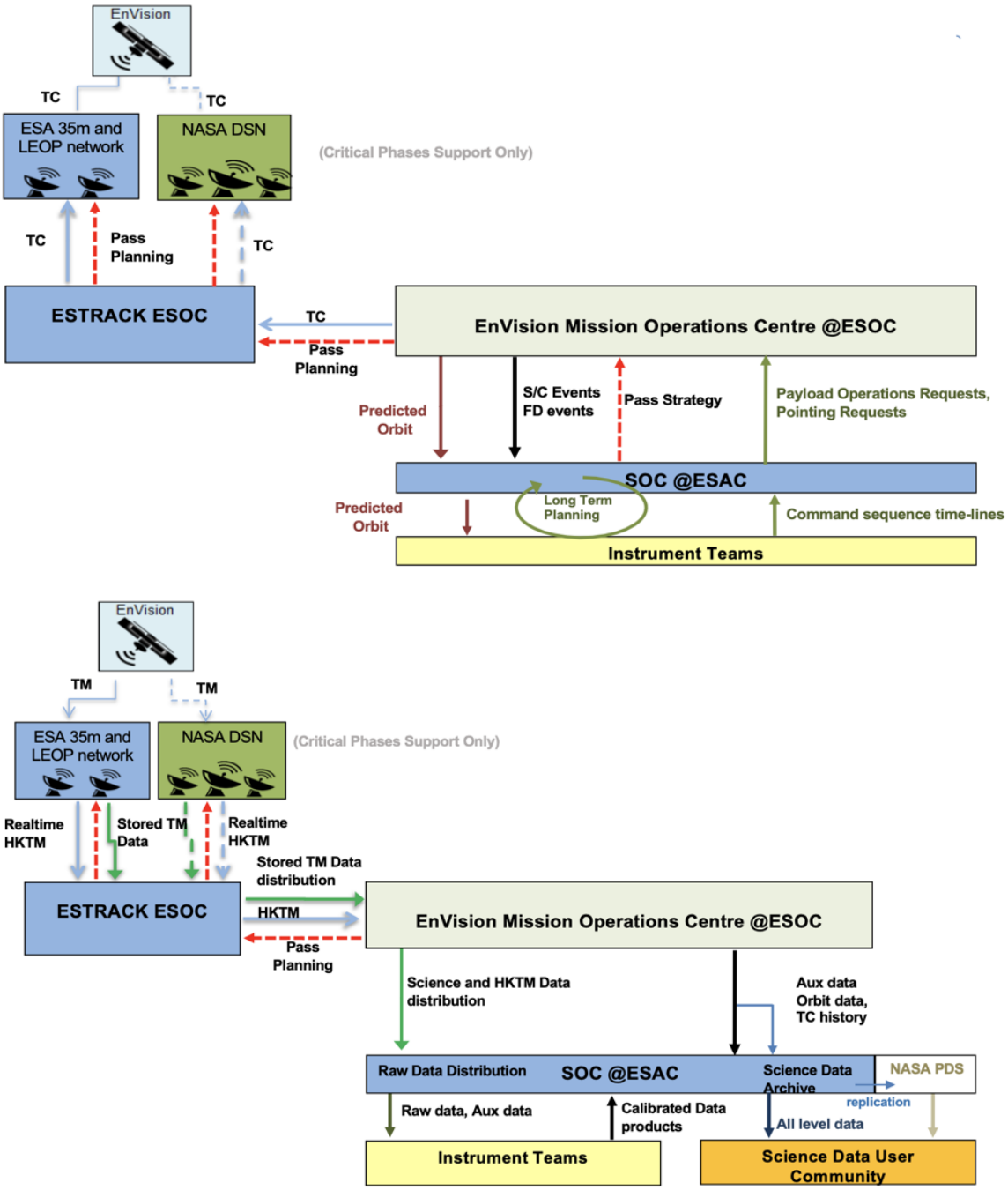

Figure 6.1.1 – *EnVision Ground Segment and operational interfaces for uplink (top) and downlink (bottom).*

6.2. Mission Operations

6.2.1. Baseline Mission Timeline

Table 6.2.1 describes the baseline EnVision nominal mission timeline, starting from opening of the launch period T0 to End of mission at T0+78 months, for a total mission duration of 6.5 years.

Table 6.2.1 – *EnVision mission timeline*

Launch =(T0) (opening of the launch period)	01 Nov 2031
Venus Orbit Insertion (VOI)	06 May 2033
Start of Aerobraking phase	20 June 2033
Science orbit acquisition	21 Sept 2034
Start of nominal science phase	24 Nov 2034
End of mission	7 Dec 2038
Total mission duration	7.4 years

6.2.2. Launch strategy

The baseline launch period opens on 1 November 2031 and closes on 26 November 2031 guaranteeing 21 launch opportunities (one per day, with three days excluded due to the influence of the Moon). The launch trajectory is optimized to allow full visibility from ESA ground stations during the three hours following launcher separation.

EnVision design is fully compatible with a back-up launch opportunity one year later in 2032 (November) with a short direct transfer (type 2, six months duration). In this scenario the required aerobraking duration is slightly longer than for the baseline launch date. An alternative launch date exists also in May 2033, involving a long interplanetary transfer with an Earth swing-by.

6.2.3. Interplanetary transfer phase

Right after separation, the Launch Early Operations Phase (LEOP) will start, marked by the correct deployment of solar arrays, the completion of launcher dispersion trajectory correction, the acquisition of safe attitude and nominal communications with ground. The LEOP is assumed to last no more than three days in the case of EnVision, and is followed by a Near Earth Commissioning Phase (NECP) which extends to up to 2 months depending on the actual launch date. The deployment of the SRS dipole antennas, and VenSAR arrays, will occur during NECP, when the Spacecraft is still in Earth vicinity.

The baseline interplanetary transfer involves a complete revolution around the Sun with an Earth Swing-by, followed by a direct transfer to Venus, and lasts about 18 months. This transfer strategy has been selected as baseline despite its relatively long transfer time, because (1) it maximizes the mass at Venus; and (2) it minimizes the aerobraking phase duration, hence the operational cost of the mission.

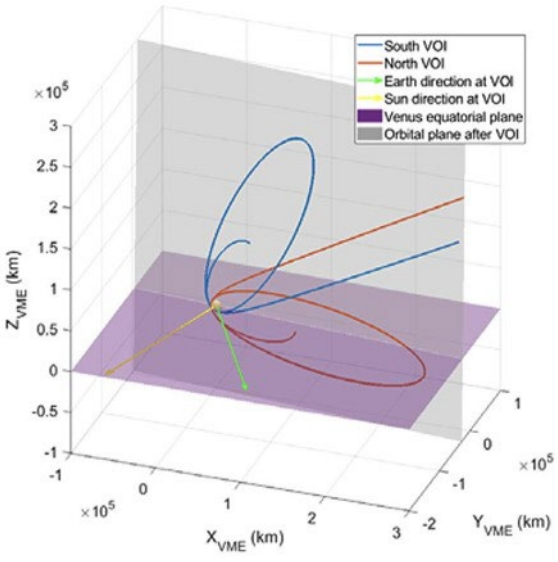

Figure 6.2.1 – *Venus orbit insertion (VOI) approach possibilities for the baseline interplanetary transfer.*

The direction of Venus arrival from the velocity at infinity and the target orbit inclination determine the geometry of the Venus orbit insertion (VOI, Figure 6.2.1), allowing for only two possible solutions: arriving to Venus over either the North or South poles, which determines the location of the VOI manoeuvre and the pericentre of the orbit around Venus. After that, the location of the pericentre remains virtually constant until the end of the aerobraking phase. The approach direction is chosen to place the pericentre at a latitude higher than 60 degrees to minimize the duration of the long eclipses, which would otherwise drive the qualification effort of the various

spacecraft appendages (deep thermal cycles). For the baseline and back-up transfer strategy, this results in performing a North insertion.

6.2.4. Aerobraking (A/B)

Aerobraking consists of a sequence of ~three thousand orbital revolutions during which the orbit dips into the upper atmosphere around each pericentre, resulting in a progressive reduction of the apocentre altitude. The pericentre altitude is controlled to prevent the maximum heat flux, dynamic pressure and the heat load accumulated during a pass from exceeding their specified constraints. The aerobraking strategy relies on the anti-nadir panel of the S/C and the back side of the SAR reflectarray as main drag surface, complemented by specific aerodynamic flaps to minimize the ballistic coefficient of the spacecraft.

The aerobraking sequence is divided as follows:

- An initial walk-in phase, where the pericentre is gradually lowered with a sequence of maneuvres, at low aerodynamic regime.
- A central phase, where the aerodynamic regime is dominated by the peak heat flux/peak dynamic pressure, according to which is dominant. These peak quantities are always achieved close to the pericentre, since the density is mostly dependent on the altitude.
- A final phase, where the prolonged duration of the atmospheric passages makes the heat load the driving quantity for the pericentre control.
- A walk-out phase, where the pericentre is increased up to outside the atmosphere. This phase is not modelled in the current analysis.

The aerobraking central phase is assumed to start roughly 45 days after VOI. This period is dedicated to the execution of apocentre lowering manoeuvres (assumed to be split in two manoeuvres) and the walk-in manoeuvres (7-10 manoeuvres as reference) until the full aerobraking regime is reached.

The selection of the aerobraking strategy is the result of a mission-level trade-off between mission performance (aerobraking duration), mission cost (at ground and space segments levels), and risk. A key guideline for EnVision is to rely on mature technical solutions at spacecraft level to minimize the technical risk. This calls for defining a strategy which allows the spacecraft and its payload to remain within known thermal limits of existing surface materials (MLI and Solar Arrays being the driving elements), with significant margins to cope with the largely unknown atmospheric density variability.

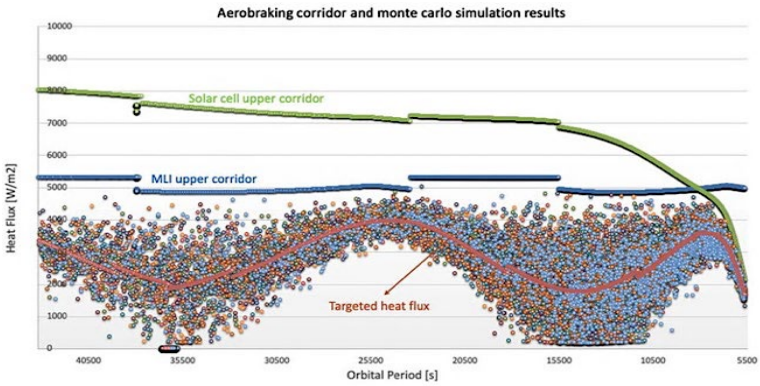

Figure 6.2.2 – *Baseline aerobraking corridor and Monte Carlo (MC) results. Individual point colours correspond to different MC results. The targeted heat flux is the red line, which is dynamically adjusted to the local solar time at pericentre to cope with the expected higher density dispersions at night as observed by previous missions Pioneer Venus Orbiter and Magellan.*

An aerodynamic 'corridor' is defined for the spacecraft based on these considerations, which guarantees that all spacecraft surface materials qualification limits are never exceeded over the aerobraking duration with high probability, considering the known atmosphere density's natural variability (Figure 6.2.2). The aerobraking corridor, defined as a heat flux profile as a function of the orbital period and local solar time at pericentre, is dominated by MLI thermal constraints until orbital periods of few hours, and then by solar arrays thermal constraints toward the end of aerobraking.

In the unlikely case where the materials' thermal limits would be exceeded, the S/C is capable of performing autonomously an emergency pericentre raising manoeuvre (so-called pop-up manoeuvre) before next atmospheric pass. This approach is similar to the one implemented on ESA's Trace Gas Orbiter, which successfully achieved its science orbit around Mars after one year of aerobraking.

The baseline strategy foresees a start of Aerobraking on in June 2033, from a 12 hour orbital period, and stops when the apocentre has reached an altitude of 500 km (similar to NASA's Magellan apocentre altitude at the end of its aerobraking phase). Aerobraking operations are interrupted due to the Superior Solar Conjunction between

14/12/2033 and 24/01/2034, requiring the S/C to be put on a stable orbit by raising its pericentre altitude by 100 km typically. Including this operational interruption, the expected aerobraking duration is about 15 months and is achieved with a total of 2000 passes through Venus' atmosphere.

Aerobraking involves significant ground operations to track the spacecraft, monitor the aerobraking progress, prepare the aerobraking manoeuvres sequences for the next day(s), or update the atmosphere models. In particular 16 hours daily support is required from ESTRACK's 35m Deep Space Antennas for orbital periods above 6 hours, and 24/7 support for orbital periods smaller than six hours.

6.2.5. Transition to science orbit and nominal science phase

The baseline assumption for the science orbit (Table 6.2.2) is that the orbital elements are left untouched at the end of the aerobraking phase, thus driven by the interplanetary transfer, choice of VOI approach, and the actual aerobraking duration. Because of this, the transition to science orbit at the end of aerobraking requires only a pericentre raising manoeuvre, and the apocentre can be left untouched, once aerobraking has reached the target altitude of 500 km. The aerobraking end date (combined with the actual value of right ascension of ascending node) fully defines the initial longitude at the ascending node at the beginning of the science orbit.

A reference orbit example is given in Figure 6.2.3, assuming a start of science on 17/03/2035, which is considered as a worst case in terms of eccentricity among the likely range of starting dates following aerobraking. The resulting science orbit has its pericentre at a latitude of around +60 degrees. The natural evolution of the orbit due to Venus' oblateness implies a secular decrease of eccentricity, i.e. pericentre naturally decreasing and apocentre increasing. Small pericentre lowering manoeuvres are performed once per cycle to avoid a too large decrease in pericentre altitude which would compromise S/C safety. The apocentre altitude is left uncontrolled for the full science phase.

The initial latitude and longitude at pericentre define the orbit evolution. Different initial conditions (e.g. shorter or longer aerobraking) would see similar latitude evolution of the pericentre as in Figure 6.2.3 but shifted up or down by up to 30 deg according to the initial pericentre location. Rather independently of the initial conditions, the overall perturbations in the orbit are expected to be very similar at equal longitudes, therefore this variation would mainly cause a shift in time of the apocenter and pericentre altitude curves but remaining quite close to the examples in terms of altitude versus longitude in Figure 6.2.3. This dispersion in the initial conditions has a non-negligible impact on the orbit maintenance delta V and a conservative (enveloping) delta V allocation has been considered to cope with such dispersion.

Table 6.2.2 – *Example orbit parameters assuming a start of nominal science phase on 15 June 2035*

Pericentre altitude	220-282 km
Apocentre altitude	377-510 km
Semi-major axis	6381-6417 km
Orbital period	93.7 to 94.62 min
Inclination	87.8°-88.6°
Argument of pericentre	-7-118°

6.2.6. Spacecraft disposal

At end of mission, the EnVision spacecraft will be passivated, following ESA's guidelines for spacecraft debris mitigation. The spacecraft will naturally enter the atmosphere and disintegrate in the upper atmosphere of Venus in a few months.

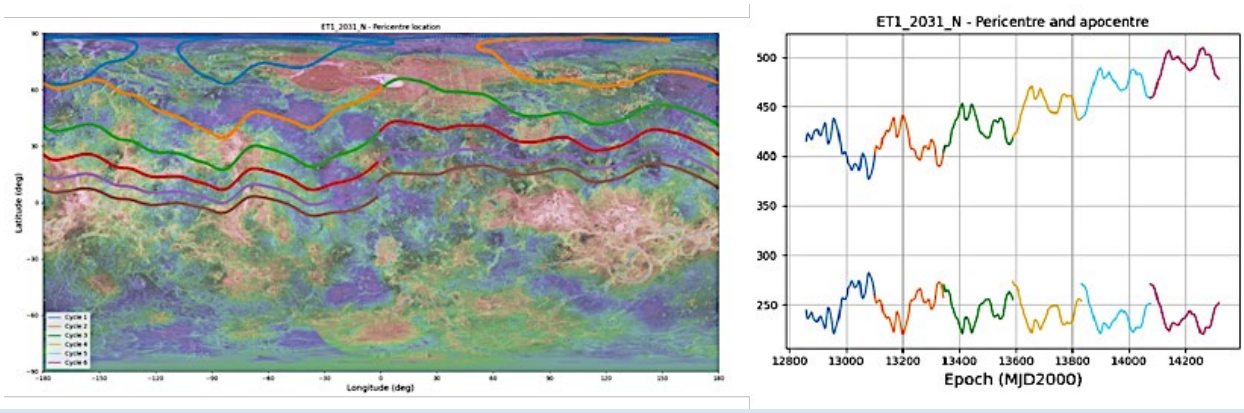

Figure 6.2.3 – *Example orbit evolution assuming a start of science on 17 March 2035 (see Section 6.2.5). The evolution of the pericentre position in Venus' surface coordinates (left), and apocentre / pericentre altitudes (right) along the 6 cycles of the mission. The intra-cycle variations are due to the accumulation of local longitudinal topography effects on the orbit, while the inter-cycle variations are caused by Venus oblateness.*

6.3. Science Operations, Data Handling and Archiving

6.3.1. Sciences Operations Planning

The science objectives of the mission lead to requirements on coverage, swath overlap, frequency and repetition of observations. The mission, spacecraft and instrument design impose constraints on when and how often observations can take place. All science operations will be conducted using an offline planning process coordinated by the SOC. The planning process is split into several phases.

Mission Level Planning (MLP) aims at developing a plan covering the whole mission, which demonstrates the achievability of the science requirements. This is documented in the SAP. The plan incorporates scientific inputs from the SWT and PS, and with support of the SOC it considers data volumes, power and operational constraints. The mission level plan is updated when needed, e.g. following an update to a boundary condition which invalidates the plan. The resulting plan is used as an input into the long-term planning.

Long Term Planning (LTP) covers 6 months of operations and ensures that operations are compatible with the predicted resources (e.g., data and power), the spacecraft and the ground station schedule. A reference trajectory is provided by ESOC Flight Dynamics for this period. The SOC consolidates and validates the payload activities using inputs from the Instrument teams and mission constraints. The spacecraft pointing is frozen at this stage. Requests for calibration activities should also be submitted during this step. Inputs regarding preferred times for communication passes and wheel-off loadings are to be provided to the MOC before the start of the long-term planning, in order to avoid conflicts with the preferred times for science observations. The science strategy is frozen at the end of this planning phase. The LTP plan will remain unchanged, with the exception of the weekly Short Term Planning (STP) cycle when the LTP plan will be refined using the latest orbit information if appropriate. This simplification is possible due to selection of surface Regions of Interest well in advance and the need to cover them with a certain observation pattern and coverage that requires end-to-end planning of the entire nominal mission.

Short Term Planning (STP) is performed on a weekly basis and includes Flight Dynamics update of the orbit using latest tracking data, corrections for deviations from reference trajectory, and refines the timeline of payload operations. At this stage, changes to timing of observations may still be accommodated, as long as they continue to meet spacecraft resource and thermal constraints. For example, this may be used to change the latitude of targeted high-resolution VenSAR imaging. The Instrument teams' requests for payload science operations at command sequence level will be collected by the SOC, validated and checked before being merged into payload operation requests to be submitted to the MOC. The MOC will be in charge of including the requests in the overall mission operations timeline which will be uplinked periodically to the spacecraft. No real time science operations are envisaged.

6.3.2. Data product format, data release and rights

The EnVision data products will be classified according to the Planetary Data System – 4 standard (PDS4 standard) as shown in.(Table 6.3.1).

Table 6.3.1 – *EnVision Mission data level definitions, as defined in the EnVision Science Management Plan (SMP, ESA 2023a), following the Planetary Data System (PDS4) standard.*

Data Level	Definition	Responsibility
Telemetry	Data as downlinked from the spacecraft, byte stream or packets of data from the platform and one or more payloads.	ESA, immediate delivery to instrument teams
Raw Instrument data	Original data from the payloads (depacketized, decompressed, and reformatted instrument data), including instrument housekeeping data, instrument health data, calibration data, instrument sampling information, etc.	ESA, immediate delivery to instrument teams
Raw Spacecraft data	Spacecraft housekeeping data, platform health information, Attitude and Orbit Control System (AOCS) information, orbit reconstruction, satellite tracking data, etc.	ESA, immediate delivery to instrument teams
Calibrated data	Data converted to physical units, which makes values independent of the instrument. E.g. calibrated spectra, calibrated reflectivities, calibrated brightness temperatures, calibrated polarimetric variables, etc.	Instrument teams, delivery to ESA for archiving and public release within 6 months
Derived data	Results that have been distilled from one or more calibrated data products (e.g. surface emissivity maps, atmospheric trace gas concentrations, gravity or magnetic fields, etc.). Supplementary data, such as calibration tables or tables of viewing geometry, used to interpret observational data should be classified as “derived” if not easily matched to one or the other data categories.	Instrument teams, delivery to ESA for archiving and public release

As outlined in the EnVision Science Management Plan (SMP, ESA 2023a), each instrument team will, for scientific purpose, have access to the Telemetry and raw data of their instrument (“Raw Instrument data”) and relevant spacecraft information (“Raw Spacecraft data”), as soon as they become available at ESA. Following in-orbit commissioning, the instrument teams will be responsible to calibrate and validate the data, create the validated and calibrated data products (“Calibrated data”), and deliver them to ESA as soon as possible, at the latest within six months from Raw data reception. At any time, instrument teams will share data among themselves and with the whole Science Working Team (SWT), to allow multi-instrument data analysis and enhance the scientific return from the EnVision mission. Instrument teams and members of the SWT will be asked to deliver the “Derived data” products to ESA as soon as they are available for automatic archival (PDS4 standard) in the ESA-PSA and NASA-PDS databases, to maximise the EnVision mission scientific return. Any use of data for publication before they become publicly available will require agreement by the respective Instrument Lead Scientist(s) (ILSs). Data will be publicly released together with publications.
The ”Raw Instrument data”, “Raw Spacecraft data” and “Calibrate data”, including relevant science and auxiliary data, will be archived, and made publicly available by ESA in the PSA and by NASA in the PDS. Observation geometry data will be provided using the Spacecraft Planet Instrument C-matrix Events (SPICE) information system. Chapter 3, Table 3.1.2 shows a list of notional data products to be provide to the science community.

6.3.3. Overview of science data processing

The EnVision Science Ground Segment science planning, operations, data processing and archiving will be conducted in close coordination between the ESA Science Operations Centre (SOC) in Madrid, the Instrument Lead Scientist (ILS) teams, and ESA Mission Operations Centre (MOC) in Darmstadt. Tool development for processing instrument data will be undertaken by instrument teams, to enhance the scientific exploitation of mission data at the various science data levels described in Section 6.3.2 and Table 6.3.1. The following paragraphs outline plans for each of instrument / experiment teams.

The VenSAR data processing f will be conducted by the NASA Jet Propulsion Laboratory. Data from the radar modes of operation, SAR, altimeter and radiometer will be downlinked to ESA and transferred electronically to JPL along with ancillary ephemeris and telemetry data needed for processing the data.

SAR data products will include 30 m/pixel medium resolution radiometrically calibrated and georeferenced imagery for ROI's, high resolution SAR imagery with 10 m/pixel for selected sites and dual polarization HH and HV imagery with 30 m/pixel resolution. These products will be delivered with ancillary layers, e.g., incidence angle, to facilitate scientific interpretation of the data. Altimetry products will include echo profile data as well elevation and elevation variation estimates with approximately 3 km along-track measurement spacing. Microwave radiometer data collected in nadir, near-nadir and dual polarization off-nadir will be used to generate both surface temperature brightness and surface emissivity maps. High resolution stereo topography measurements will be generated for most of the imaged ROIs with a spatial resolution of 300 m. Along with the elevation measurement an estimate of the elevation precision for each height estimate will also be generated.

Data will normally be delivered to the science team and data archives with 6 months of receipt at the JPL processing centre, and most product will be available on much shorter timescales. All VenSAR data will be archived at the NASA Planetary Data System (PDS) and the ESA Planetary Science Archive (PSA) (see Section 6.1.4 for overall Science Ground Segment (SGS) architecture; and Section 6.3.2 for the data processing and archiving.).

SRS – The data acquired by the SRS instrument (Telemetry product level) will be downlinked from the satellite by ESA. The ESA Science Operation Centre (SOC) will then process the instrument telemetry data to raw data, and distribute the raw data to the SRS instrument team and to the ESA PSA archive. In addition, the SRS team will have access to the telemetry data via ESA-ESOC. The SRS instrument team is responsible for the data processing, the generation of the calibrated, auxiliary, and derived data, and their submission to the ESA PSA archive.
SRS raw data are characterized by a vertical resolution of ~20 meters (depending on the target properties), while the SRS penetration will be between a few tens and a few hundred meters (up to 1000 m). The only on-board processing allowed for SRS is pre-summing. During SRS low-density acquisitions, pre-summing (lossy compression) is allowed, and the track-to-track spacing is >2 tracks per degree at the Equator (i.e. ~50 km track-to-track spacing). During SRS high-density acquisitions, the data are not pre-summed, and the observation density is 10 per degree of longitude (i.e. ~10 km track-to-track spacing). The SRS products will be used to derive both the subsurface features and the surface topography.

The VenSpec instrument teams, together with the SOC, will ensure the long-term archiving and storage of the VenSpec suite raw, calibrated and derived data products as outlined in Section 6.3.2. The data products, SPICE kernel files, software, and other supporting material (e.g., user guides, tutorials, and calibration) will be validated prior to release.

VenSpec data products include rock type maps, H_2O and HDO abundance maps, minor species abundance maps, SO_2 abundance maps, maps of volcanic activity, as listed in Chapter 3. The raw to calibrated data processing will be performed using pipelines that run for each of the channels separately, while the higher-level data products will combine the data sets from all channels.

The RSE team is responsible for the processing and delivery of the raw and calibrated data as well as of the derived data products to the ESA PSA as outlined in Section 6.3.2. The derived data products include s/c precise reconstructed orbit, bending angle and refractivity profiles as well as gravity field, k_2 Love number solution, pressure and temperature atmospheric profiles, profiles of the absorptivity and the sulphuric acid concentration, and (when possible) ionospheric electron density profiles. The raw to calibrated data processing will include troposphere and ionosphere calibrations (for both Gravity and Radio-Occultation experiments), as well as interplanetary plasma and spacecraft macro-model calibrations for the Gravity experiment.

7. Core Science Implementation

7.1. Observation Planning Strategy

Driven by the fixed high gain antenna and requirements to observe short term changes on Venus, the EnVision observation strategy has been designed around a repetitive daily pattern of observations. There are ~15 orbits a day. The operational orbit has a track-to-track separation of ~10km. A typical 15 orbit block comprises 4 sequential orbits dedicated to spectrometer measurements; 3 orbits dedicated to standard SAR or polarimetry imaging of RoIs; 1 full half-orbit of SRS low density observations plus 2 half-orbits with SRS high density observations of RoIs; 3.5 half-orbits of radiometry measurements; half an orbit of altimetry measurements; and 4 to 10 orbits dedicated to communications passes. The requirements on swath overlap, and the size of the VenSAR SAR standard measurement swath (fixed at 57 km, independent of altitude, see Section 4.2, Table 4.2.1) imply that the VenSAR SAR standard or polarimetry observations be performed every 5 orbits to create contiguous swaths over the regions of interest.

There are interoperability constraints. SRS cannot operate during radiometry observations, and due to conflicting attitude requirements, altimetry and active SAR observations cannot be carried out in parallel to SRS or VenSpec observations. The orbit pattern or 'profile' has seasonal dependencies. SRS and altimetry observations are only possible during seasons with long eclipses; additional SAR observations, High-Resolution SAR, and SAR polarimetry observations are added during times of high downlink rates. The High-Resolution SAR observations have a 20 km swath width and require observations on 3 of the 15 orbits, with a separation of 2 tracks (orbits). The required number of hours of dump time depends on the seasonal profile, and the number of orbits required to meet the dump time depends on the occultation duration, which itself is seasonal. In addition to earth occultations, a break in the communications block will be frequently necessary to maintain the VenSAR observation cadence of 5 orbits.

7.1.1. VenSAR observations planning

The VenSAR swath width is 57 km (Table 4.2.1). With a reference orbital ground track shift of 10 km for the reference science orbit, SAR images must be taken every 6th orbit to ensure contiguous coverage of the observed regions of interest. As a consequence, the science observation strategy foresees three SAR 30 m observation slots every day (on 1st, 6th and 11th orbits), as illustrated in Figure 7.1.1 during the full science phase (excluding superior solar conjunction periods). The total duration of the observation per orbit is modulated between 122 s and 488 s as a function of the science operations profile being implemented. SAR observations are performed on the descending arc which optimizes the altitude and therefore maximizes the image quality.

A further constraint in planning arises from the need to perform repeated VenSAR observations of the identified RoIs over two cycles with similar viewing conditions (East-looking) to obtain stereo-topography terrain models (two observations at different incidence angles) or over three cycles with similar viewing direction (all East-looking) to search for surface changes (two observations at same incidence angles and a third one at different incidence angle).

A Venus cycle lasts 243.02 Earth days, and the synodic Earth/Venus period is 578.92 Earth days. The spacecraft will therefore fly over a given science target at the surface of Venus once every ~243 days on the descending branch of the orbit, but the possible downlink data volume over this region will be different from one cycle to another, meaning that the possible VenSAR observation duration at a given longitude will differ from cycle to cycle. Besides, every ~578 Earth days (just over 19 Earth months), superior solar conjunction will occur, lasting for around 2 Earth months, preventing any science observations over a given longitude range. This leads to longitude dependent VenSAR observation time series along the six cycles, that need to be planned carefully to acquire the required number of repeated observations over the desired regions of scientific interest. In practice, bands of longitudes at the surface of Venus are defined (43 bands of longitude for the example observation scenario), with limited latitude extensions within each band, that can be observed once, twice or three times over mission duration, as illustrated in Figure 7.1.1.

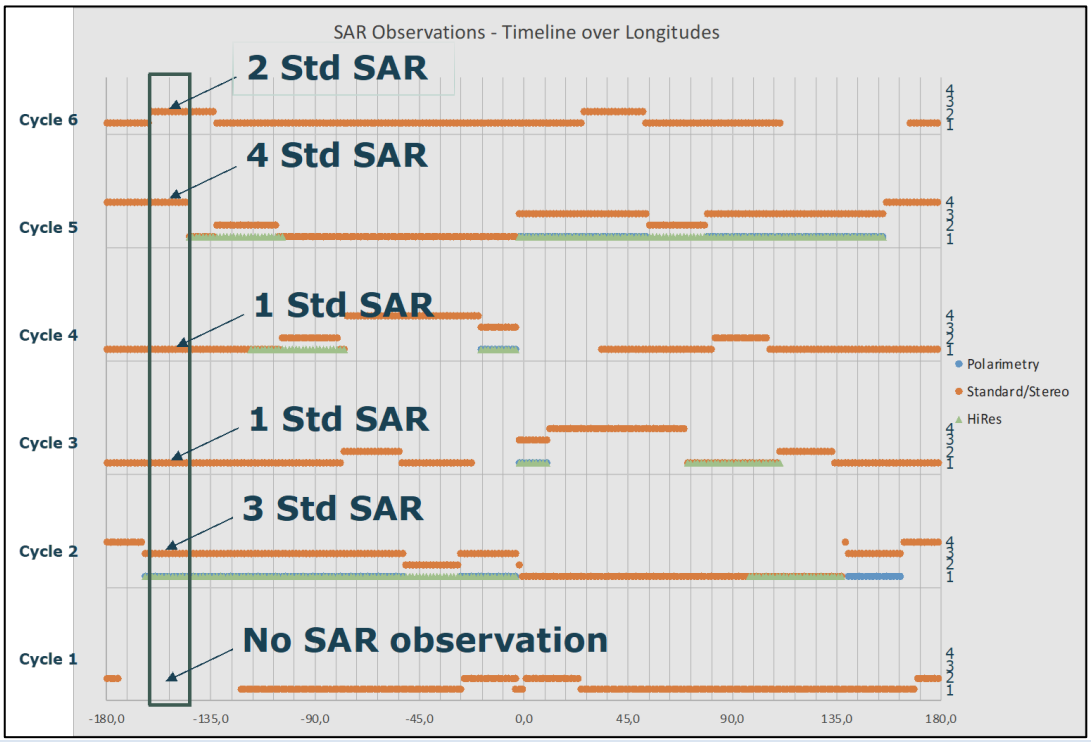

Figure 7.1.1 – *Pattern of repeatable observations (right, Y-axis) numbered 1-4, along the 6 mission cycles (left, Y-axis) resulting from the implementation of the 8 science operation profiles, plotted as a function of longitude at the surface of Venus (bottom, X-axis). For example, on one particular longitude band centred at -150° (highlighted in grey on the left side) it is possible to perform: no standard SAR observations at Cycle 1; 3 standard SAR observations at Cycle 2; 1 SAR observation at Cycle 3 and Cycle 4; 4 standard SAR observations at Cycle 5; and 2 standard observations at Cycle 6.*
One standard SAR observation in this context covers a latitude extension of 8 degrees corresponding to 122 s of continuous observation. The elaboration of the science observation strategy must fulfil the boundaries given by these longitude bands pattern, in particular for the planning of inter-cycle repeated observations. The repeatability pattern is dependent on the starting date of the science phase, and the one provided here corresponds to the science operations reference scenario, assuming a start on 15 June 2035.

With this baseline observation strategy, the mission design allows the following: (1) ***at all longitudes*** where latitude bands of cumulated extension of 21 degrees can be observed at least twice over six cycles. The maximum cumulated latitude extension is 42 degrees and the average 32 degrees; (2) ***at all longitudes*** where latitude bands of cumulated latitude extension of 6.3 degrees can be observed at least three times over six cycles. The maximum cumulated latitude extension is 19 degrees and the average 9 degrees. These bands and the associated latitude extensions can then be used by the science team to pre-select the Regions of Interest (RoIs) to be observed over the mission in an optimal way for a given date of start of science. An example of such RoIs selection based on this approach is provided in Section 3.2.1 and Figure 3.2 assuming a date of start of science on 17/03/2035. This strategy allows to progressively build up, over the nominal mission, the required global and targeted measurements dataset, in particular over all pre-selected RoIs representing a fraction of about 26% of Venus surface. A simulated evolution of the observed RoIs from Cycles 1 to 6 is illustrated in Figure 7.1.2. Any alternative RoI selection fulfilling the conditions above can be accommodated by the mission.

7.1.2. VenSpec observations planning

VenSpec observations require near-global coverage over mission duration, as well as repeatability at short term (hours) and long term (Cycle). The strategy consists of planning VenSpec observations on a daily basis, with observations over half-orbits (on the dayside for VenSpec-U and VenSpec-H for observations at and above the cloud top, on the nightside for VenSpec-M and VenSpec-H for surface and lower atmosphere observations), over four consecutive orbits, and for every cycle. This is reflected in Figure 7.2.2 with a group of four orbits at the beginning of each group of 15 orbits dedicated to VenSpec observations whatever the science operations profile. This strategy allows to fulfil all VenSpec observation requirements in six cycles.

7.1.3. VenSAR altimeter and SRS observations planning

The objective is to cover the majority of the Venus surface with VenSAR altimetry and SRS observations with an average observation density of 2 per degree of longitude at Equator. The science operations planning considers

between 20 and 41 minutes of altimetry per day over the science operations phase. This allows to achieve the required density of 2 per degree of longitude at Equator at the end of the mission, by shifting, from cycle to cycle, within the 15-orbits pattern, the index of the orbit at which altimeter acquisition is planned.

Low density SRS observations need also to be planned such that an average density of 2 per degree of longitude at Equator is achieved over the science phase duration over the whole Venus surface that is accessible on the nightside. This is made possible by scheduling SRS low density observations every day on one orbit for 30 to 41 minutes (when the spacecraft is in eclipse, see Figure 7.2.2b).

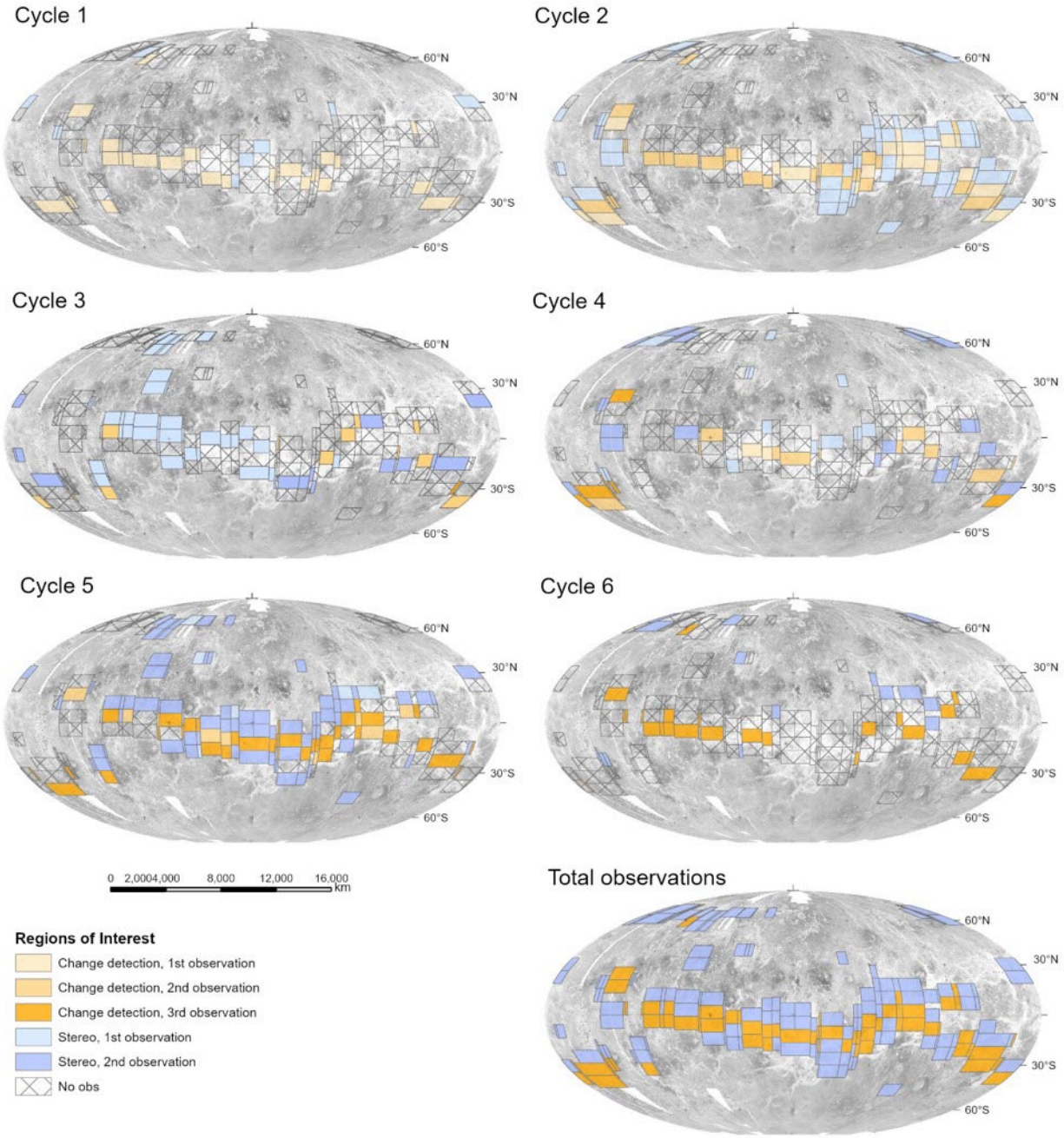

Figure 7.1.2 – *Illustration of the build-up of spatial SAR 30 m RoIs coverage build-up through the cycles. The mission design can accommodate any RoI selection which fulfils the repeatability pattern also described in Figure 7.1.1. Maps are presented here for observations made in Cycles 1 to 6, and total (cumulative) observations at the end of the nominal mission. The mission planning guarantees that all identified RoI can be observed the required number of times over mission duration.*

High density SRS observations are required over a representative fraction of the RoIs observed with the SAR at 30 m resolution, with an average observation density of 10 per degree of longitude at the Equator over the science phase duration. To uniformly distribute SRS HD observations throughout the mission, 244 s of SRS HD observations over the targeted RoIs are planned, performed on three consecutive orbits, and every day of the science mission whenever the spacecraft is in eclipse.

7.1.4. Radio Science observations planning

Within each observation profile, a group of orbits is reserved for data downlink, with an effective downlink duration varying between 3.5 and six hours every day. This strategy naturally fulfils the gravity science requirements in terms of observability and spatial resolution of the whole surface of Venus at low altitude. When downlink periods occur during the Earth radio-occultation season, radio-occultation experiment is performed, providing at least two ingress and two egress observations per day.

7.2. Payload Reference Operations Scenario

To arrive at a realistic sizing of the spacecraft, in particular for its power, data handling (e.g. mass memory), communications, GNC and thermal subsystems, a reference operations scenario for the payload operations has been implemented, based on the mission strategy described in Chapter 3, Section 5.1.8 and Section 7.1 above. This scenario has been simulated by ESA-ESAC with the operational tool GMAPP, taking into account realistic operational constraints (including ground stations availability). The progressive observation maps shown in Figure 7.1.2 have been used for that purpose. The reference scenario assumes a start of science on 17/03/2035 which corresponds to a worst case in terms of orbit stability.

This simulation demonstrates that all identified RoIs can be imaged with VenSAR, with a performance fully compliant with the science requirements, with extra margin (Figures 7.1.2 and 7.2.1; Figure 7.2.3a). The first three cycles allow imaging once 85% of the identified regions of scientific interest with the SAR at 30 m resolution. Most of the requirements are met after 5 cycles, although in some cases with little margin (for instance SRS low density and altimetry). The 6th cycle provides additional robustness to the mission. Dual polarization and high resolution VenSAR observations can be performed at almost all longitudes at least once across the 6 cycles. The strategy shows robustness in the event of an early loss of the mission, a required 20% of Venus surface being imaged at least once at 30 m resolution after three cycles only, while the same coverage in stereo-topography would be met after four cycles.

Due to the limited difference between Venus sidereal day (243 days) and its heliocentric orbital period (224 days), the part of the planet which is visible on the nightside (respectively day side) during each cycle of the mission represents only about half of the Venus surface, with a shift of this zone by about 30 degrees in longitude per cycle. After 6 mission cycles, a small portion representing about 3% of the planet will remain inaccessible for nightside (respectively dayside) observations. This impacts the instruments which have specific diurnal / nocturnal observation constraints such VenSpec-M (nightside), VenSpec-H (nightside and dayside), and VenSpec-U (dayside observations), as can be observed in Figure 7.2.2e (VenSpec-M) and Figure 7.2.2c,d,f (VenSpec-U and H). SRS and VenSAR altimetry operations have the slightly more stringent constraint to be operated only when the spacecraft is in eclipse. After six mission cycles, a larger portion representing about 10% of the planet, will therefore remain inaccessible to such observations (Figure 7.2.2b). Despite these constraints, the accessible coverage during a six-cycle mission is largely sufficient to meet the related science requirements of the mission (Figures 7.2.3b, c and d).

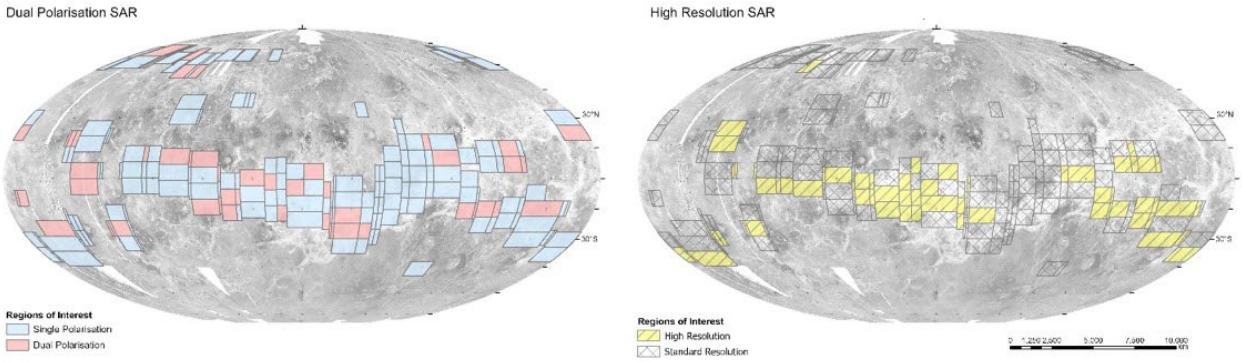

Figure 7.2.1 – *RoIs in which dual polarization 30 m SAR observations (pink, left) and 10 m SAR observations (yellow, right) are achievable over 6 cycles.*

Dual polarization VenSAR observations and 10 m resolution VenSAR observations are performed only when the downlink data rate is sufficiently high (Figure 7.2.1).

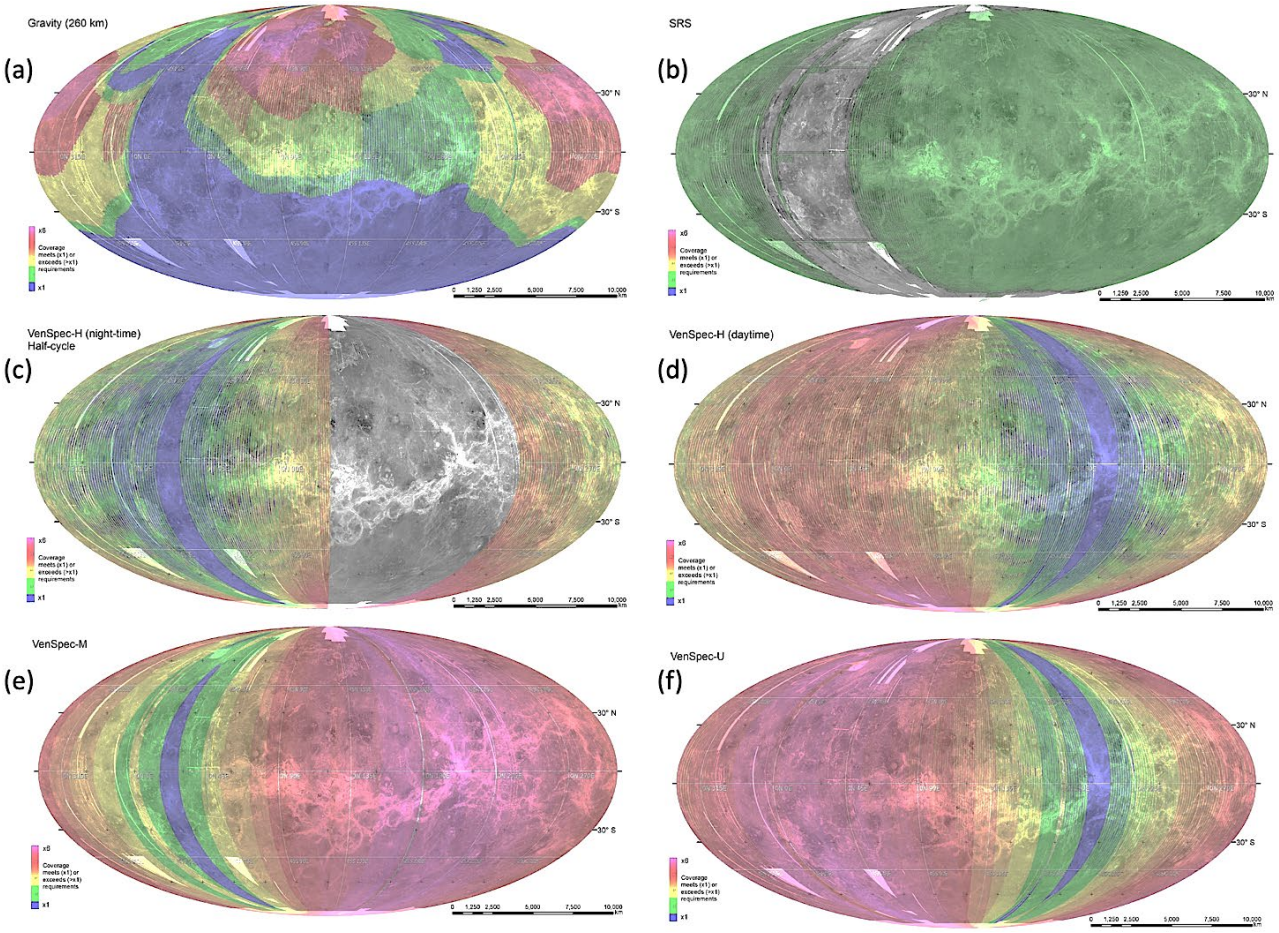

Figure 7.2.2 – *Results of the science operations reference scenario simulation, assuming a starting date on 15/06/2035 (a) Gravity science; (b) SRS LD and altimeter; (c) VenSpec-H, nightside; (d) VenSpec-H, dayside; (e) VenSpec-M, (f) VenSpec-U. For (a) the code indicates (from blue to red) where orbit pericentre altitude requirement < 260 km is met or exceeded over 6 cycles. For (b) the green code represents regions where SRS and altimeter meet or exceed coverage requirements. For (c, d, e, f) colour code indicates the number of observations over 6 cycles, with green representing 1 observation, yellow 2, red 3, 6 or 12 observations. Venus Mollweide surface projection centred on 120°E.*

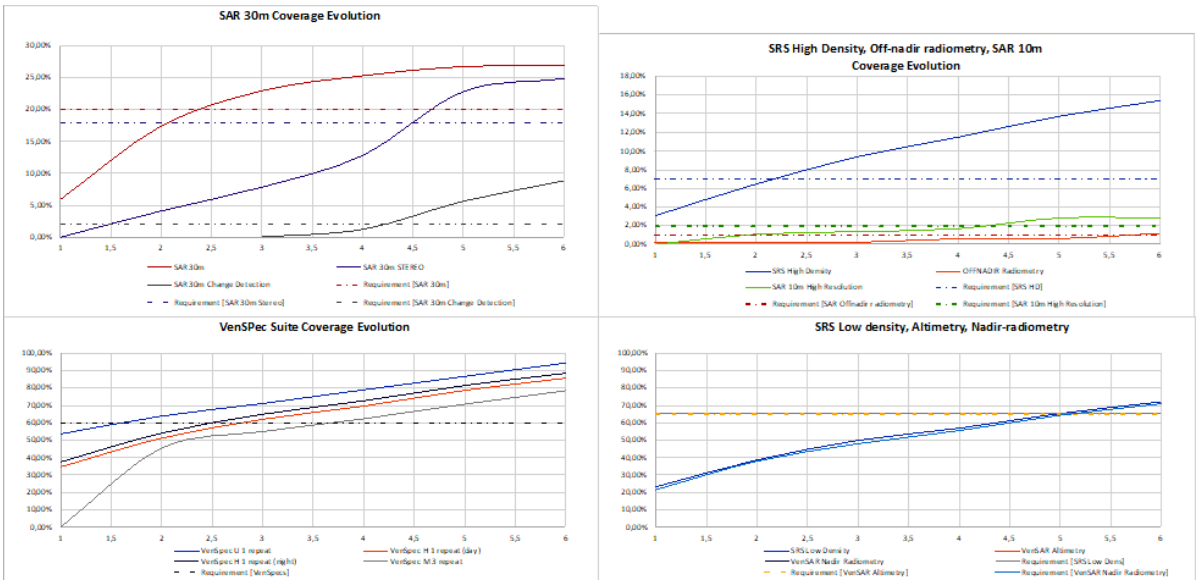

Figure 7.2.3 – *Cumulative science performance metrics based on the science operations reference scenario modeling, assuming a starting date of science on 15/06/2035. Values are provided at the end of each cycle. The linear interpolation between each data point is for illustration only. All values presented are after deduction of a 5% margin for operational contingencies and uncertainty on starting date.*

Radio-occultation performance is also assessed as part of the reference operations scenario (Figure 7.2.4). The requirement of 50% of the days within the mission with more than two radio-occultation events is achieved after five cycles.

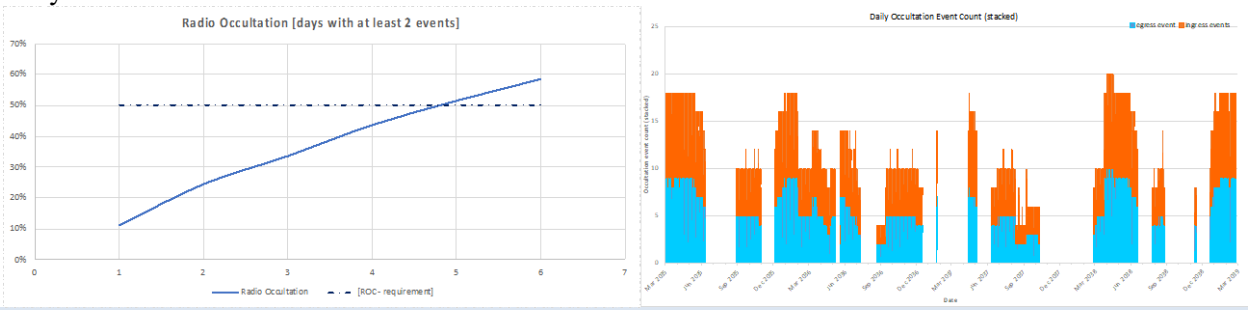

Figure 7.2.4 – *Performance metrics for the radio-occultation experiment. Left: cumulated percentage of days over mission duration with at least 2 radio-occultation events. Right: counts of ROC events (blue: ingress; red: egress) per day from the science operations reference scenario, assuming a start of science on 17 March 2035.*

The simulation of the science operations reference scenario confirms the achievability of all science requirements, with good margin (Table 7.2.1). It validates the overall science observation strategy. The overall science performance is assessed considering a 2% unavailability margin, which means 2% of the duration nominally available for science is assumed not to be available e.g. due to safe mode occurrence or due to uncertainty on the date of start of science.

The Science Operations Scenario presented here is an illustration to demonstrate that all the science observation requirements can be met with ample margins. The mission design offers enough flexibility to adapt the observation plan to potential future changes in the mission objectives. This could include changes in the ratio of different radar modes, for example, or changes of surface targets in response to discoveries made before or during the mission.

Table 7.2.1 – *Science performance synthesis with the science operations reference scenario, assuming a start of science on 17 March 2035, compared to coverage requirement metrics of Table 3.6.1, Table 4.2.2 (VenSAR), Table 4.3.1 (SRS), Table 4.5.1 (VenSpec-M), Table 4.6.2 (VenSpec-H), Table 4.7.1 (VenSpec-U), Table 4.8.1 (RSE). All performance figures are provided after deduction of a 5% availability margin to cover operational contingencies and uncertainty on starting date. The requirements are met with a margin greater than 5% on top of the 5% availability margin.*
(*) VenSpec-M coverage with 3 repeats at long time scales (half-cycles)
(**) VenSpec-U coverage without repeat; (***) VenSpec-H coverage without repeat

Observation mode	Observation type	Science req.	Coverage (nominal mission)
Targeted observations	SAR Standard (30 m)	20%	26.4%
	SAR Stereo (30 m) second pass	18%	24.3%
	SAR Standard (30 m) third pass observations	2%	8.6%
	SAR off-nadir radiometry	1%	2.6%
	SAR Polarimetry (30 m)	5%	6.5%
	SAR High-Resolution (10 m)	2%	2.8%
	SRS High Density	7%	15.1%
	Gravity Science (High resolution; < 260 km)	40% at < 260 km	58.8%
Global observations	SAR Altimetry	65%	69.5%
	SAR Near-nadir and Nadir Radiometry	75%	96.9%
	SRS Low Density	65%	70.7%
	VenSpec-M (*)	60%	76.8%
	VenSpec-U (**)	60%	92.5%
	VenSpec-H nightside (***)	60%	86.7%
	VenSpec-H dayside (***)	60%	83.9%
	Gravity Science (Low resolution; < 520 km)	95% at < 520 km	100%
	Radio Occultation	50%, 2 events/day	58.7%

7.3. Scientific (end-to-end) simulations verifying the expected quality of the derived data products

The EnVision mission, payload and experiment requirements were defined top-down from the science observation requirements (Chapters 2-3), based on knowledge, analysis, and specifications from previous Venus observations from ground and earlier Venus missions. In this section, the results of bottom-up simulations are shown, taking Venus interior, sub-surface, surface, atmosphere and ionosphere reference scenarios and the mission and instrument specifications as an input. The simulations confirm that the required science performance can be met.

7.3.1. VenSAR

VenSAR has four primary data collection modes, 1) a 30 m stripmap imaging mode, 2) a 10 m stripmap mode, 3) a nadir altimetry imaging mode and 4) a passive receive only radiometer mode. The remaining SAR modes use multiple observations from above modes. Each mode of operation meets specific imaging metrics designed to be commensurate with EnVision's science objectives.

The primary metrics used in quantifying SAR imaging performance are:

- **Noise equivalent σ_o (NESZ) –** backscatter value equal to the instrument thermal noise level.
- **Multiplicative noise ratio (MNR) –** which is a function of quantization noise and range and azimuth ambiguities.
- **Radiometric resolution $\delta\sigma$ –** is a measure of the ability to distinguish regions differing in backscatter by this amount in the presence of thermal and speckle noise.

These metrics depend on radar mode, imaging geometry, incidence angle and location in swath.

Altimeter mode performance is characterized by the metrics:

- **Noise equivalent σ_o (NESZ)**
- **Cross-track and along-track resolution** – this can be either beam or pulse limited and depends on whether azimuth SAR processing techniques are employed to improve along-track resolution.
- **Vertical resolution** as determined from the range bandwidth. The represents the achievable resolution for a relatively flat surface, however for rough surfaces the vertical resolution and elevation accuracy are more complex to quantify.

Radiometer performance is specified in terms of the relative and absolute brightness temperatures.

The Venus atmosphere effects radar measurements in two ways: 1) it attenuates the signal with losses strongly dependent on wavelength, and 2) it slows and bends radars waves resulting in range measurements being increased relative to the geometric range. Our performance model accounts for both of these atmospheric effects.

The radar was designed to have a maximum noise equivalent σ_o of better than -20 dB resulting in required SNR and radiometric resolution for the 30 m SAR mode for the Regions of Interest (RoIs). Figure 7.3.1 and Figure 7.3.2 show images and histograms respectively of the SNR on ascending and descending passes or Cycles 1 and 6 that have the highest and lowest mean altitudes during the mission and thus bound the best and worst instrument performance.

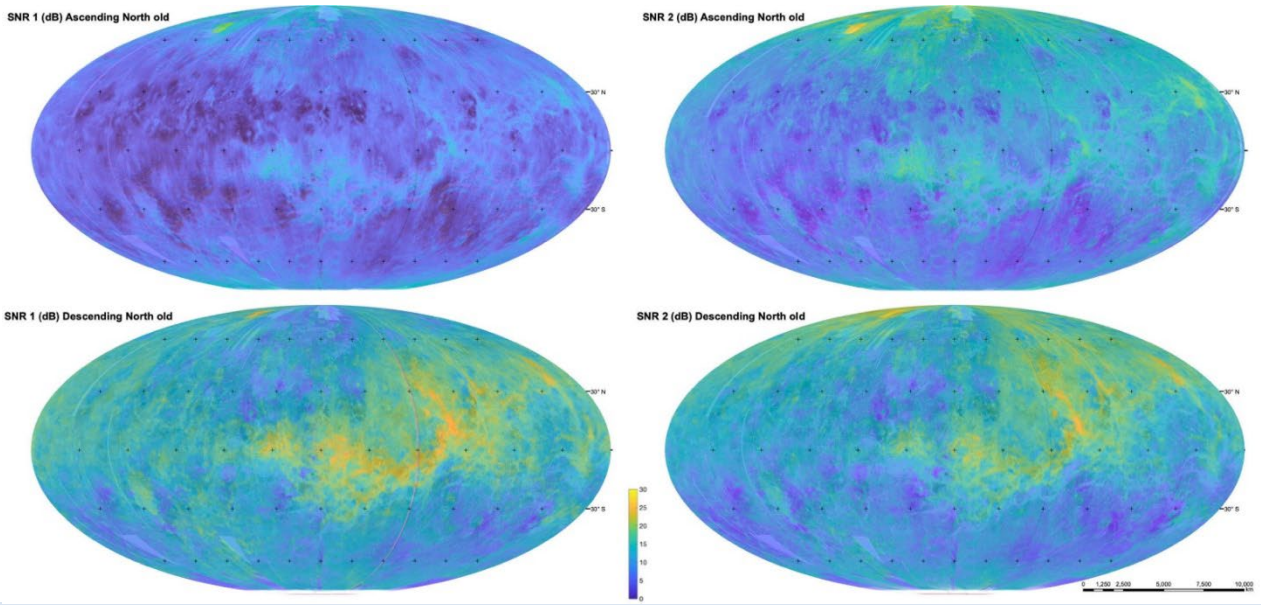

Figure 7.3.1 – *(top): VenSAR 30 m imaging mode SNR for ascending passes on Cycle 1 (left) and Cycle 6 (right) and the corresponding SNR for the descending passes (bottom): Performance is better in Cycle 6 with its lower apoapsis altitude and better on the descending passes containing the periapsis altitude. The mean SNR varies from 8.6 dB on the Cycle 1 ascending orbits to 17 dB on the descending orbits for both Cycles 1 and 6.*

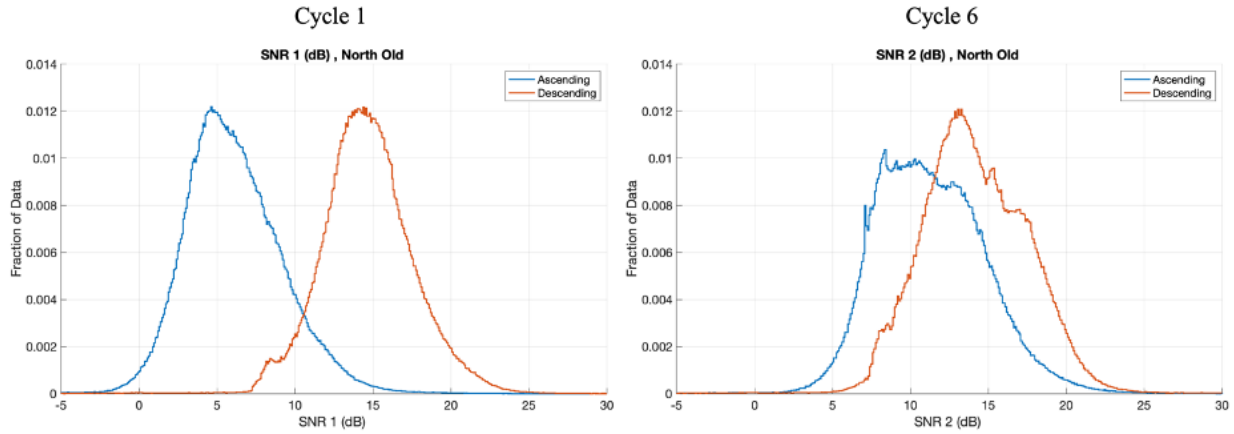

Figure 7.3.2 – *Histograms of the SNR for the ascending and descending passes of Cycles 1 and 6.*

Figure 7.3.3 shows the radiometric resolution for Cycles 1 and 6 for the ascending and descending passes and Figure 7.3.4 shows the associated histograms. The mean radiometric resolution varies from 1.22 dB for Cycle 1 ascending to about 1.1 dB in the other cases. Because of the better SNR and radiometric resolution and more uniform data quality the descending passes are preferred for VenSAR operations.

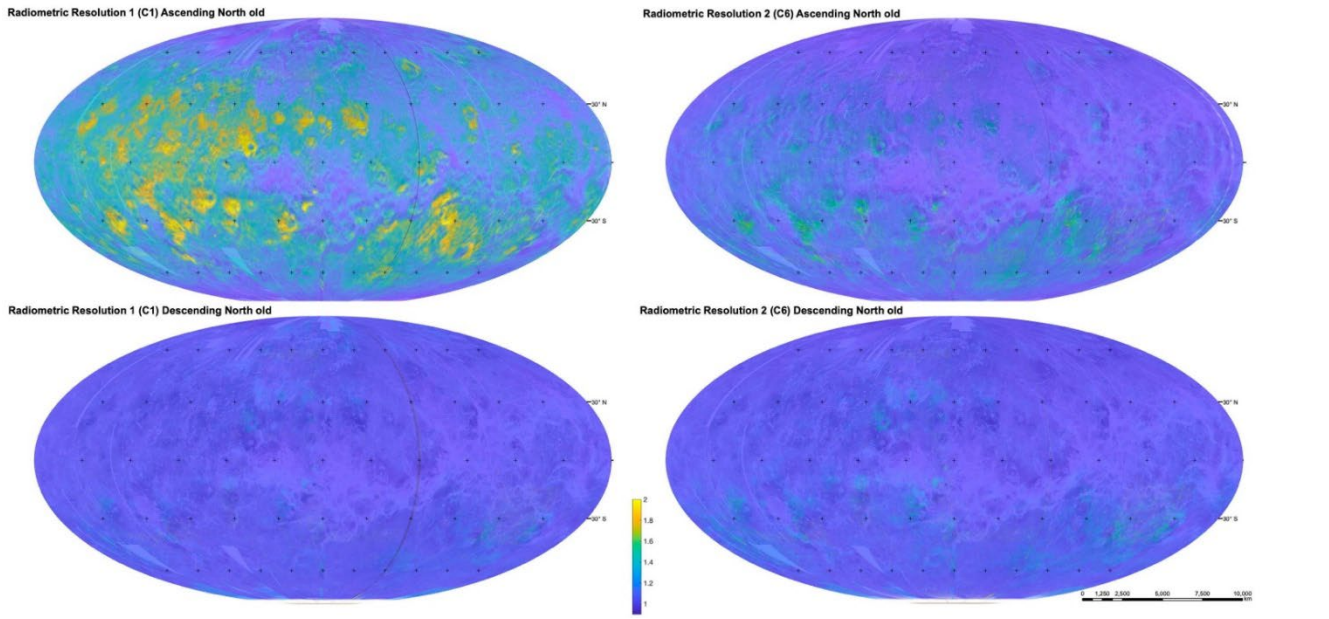

Figure 7.3.3 – *Map of the radiometric resolution as it varies over the surface for Cycles 1 and 6for ascending and descending passes. VensAR radiometric resolution exceeds the Magellan values of 1.5 to 1.75 dB at 120 m resolution, meaning that VenSAR will be more sensitive to features having subtle brightness contrast variations than Magellan.*

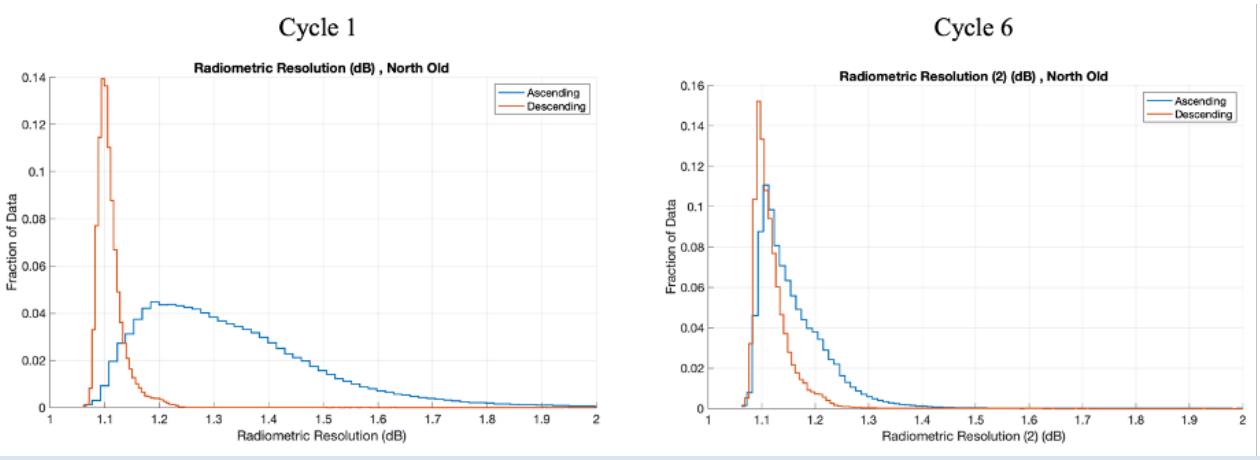

Figure 7.3.4 – *Histograms of the radiometric resolution for the ascending and descending passes of Cycles 1 and 6.*

Altimeter Mode and SAR Stereo Modes. - The altimeter beam limited footprint is 50 km in the along-track direction and 6 km in the cross-track direction. By presumming the data and using SAR azimuth processing techniques a pulse-limited footprint of ~4 km is obtained with the 60 MHz altimeter transmit bandwidth. This results in a vertical resolution of 2.5 m providing a topographic mapping accuracy of ~20-30 m. Using two SAR data acquisitions with incidence angles separated by about 5˚, radar stereo techniques can be employed to generate high resolution topography in regions with sufficient contrast. Because of the 8˚ cross-track beam width incidence angle variation between stereo pairs and stereo elevation accuracy varies across the swath. Figure 7.3.5 and Figure 7.3.6 show the cross-track incidence angle variation and stereo elevation accuracy respectively for three mapping altitudes of 220, 335 and 450 km.

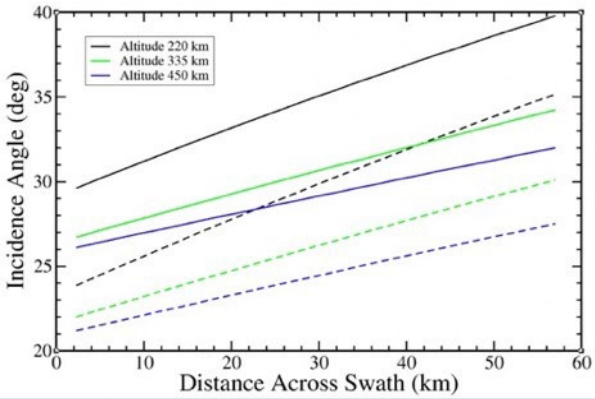

Figure 7.3.5 – *Plot of EnVision radar stereo incidence angle variation across the 57 km swath.*

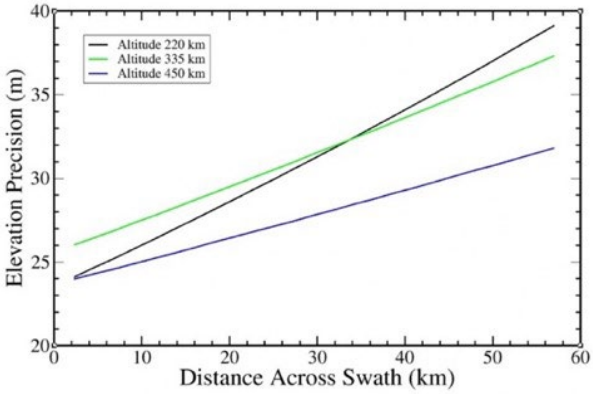

Figure 7.3.6 – *EnVision radar stereo topographic elevation precision as function of ground swath distance for three altitudes spanning the EnVision orbital altitudes. Stereo baselines of roughly 30 km offer the best compromise between stereo acuity and matching accuracy with ~20-40 m height precision after taking in account an additional V2 improvement in elevation precision obtained by over sampling the matches.*

Using a semi-empirical matching model, based on local scene contrast and informed by Magellan stereo match statistics, we estimated the stereo elevation precision using Cycle 3 and 4 stereo pairs. The stereo elevation accuracy used in the images is the swath average stereo mapping accuracy. Topographic maps with 300 m spatial resolution had a mean elevation precision of 33 m with a standard deviation of 22 m as shown in Figure 7.2.8.

Descending tracks have a better predicted stereo elevation than the ascending tracks that have mean values of 27 and 38 m respectively. Histograms of the stereo elevation precisions are shown in Figure 7.3.7.

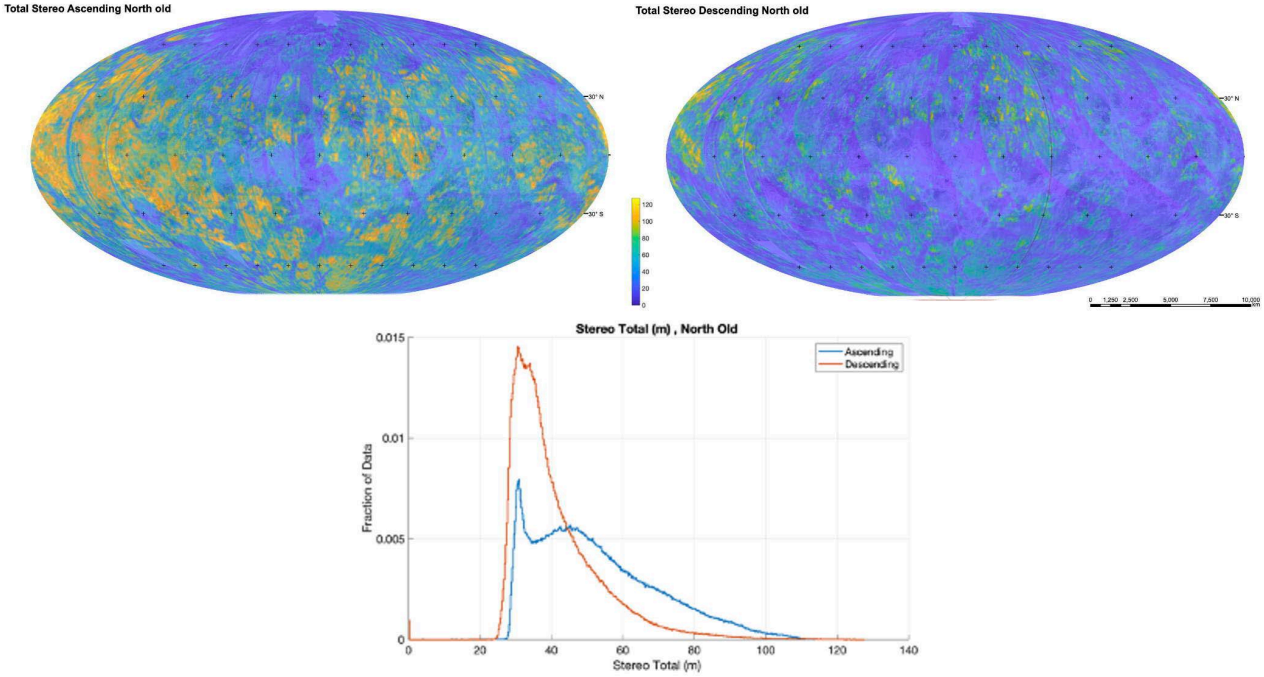

Figure 7.3.7 – *Stereo elevation precision based on the stereo geometry from Cycles 4 and 4 on the ascending and descending passes and associated elevation precision histograms.*

7.3.2. SRS

To verify that the SRS science objectives can be achieved, several end-to-end simulations have been done. The different SRS targets such as tesserae, lava flows, buried craters, sinous rilles, stratigraphy and wrinkle ridges have been modelled from a morphological and geological point of view. 3D models have been generated by considering a realistic geometry of the surface and subsurface dielectric interfaces, and a spatially variable complex dielectric permittivity of the material associated with the interfaces. Each hypothesis corresponds to a set of assumptions on the topographic parameters (RMS height, RMS slope, Hurst exponent), distance between the interfaces, and the dielectric properties (real permittivity ϵ, loss tangent $tan\ \delta$, and contrast $\Delta\epsilon$) of the near-surface material at Venus temperatures.

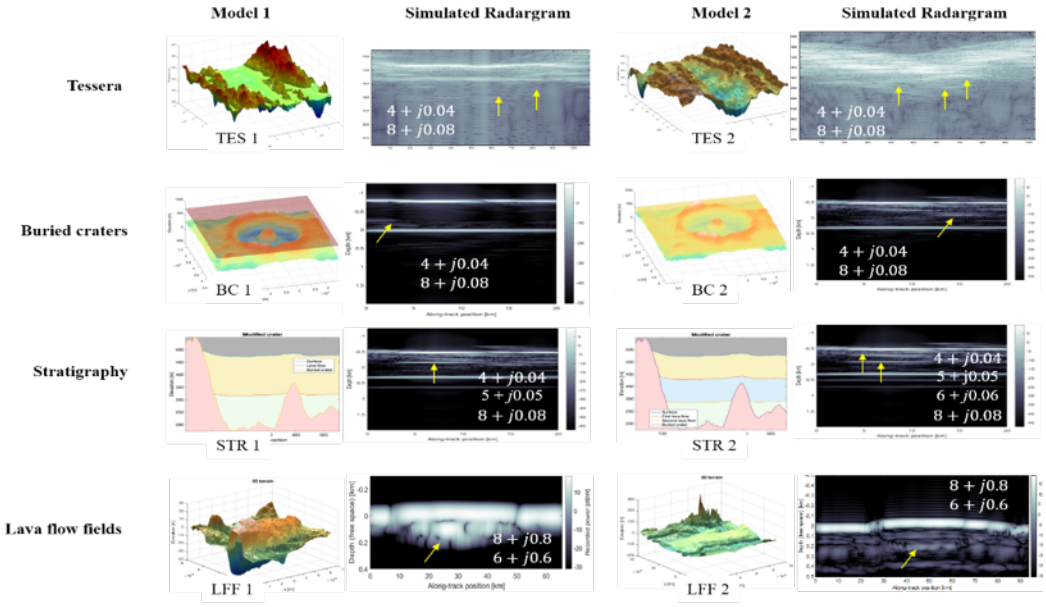

Fig. 7.3.8 – *Examples of simulated SRS radargrams for different target hypotheses: buried craters, tesserae and lava flows. 3D models have been generated by considering a realistic geometry of the surface and subsurface dielectric interfaces, and a spatially variable complex dielectric permittivity of the material associated with the interfaces (see Section 7.3.2)*

Depending on the analysed target and the data available for modelling, a suitable simulator has been used. The main adopted simulation techniques are the multi-layer coherent simulator (MCS) (Gerekos et al., 2018), the methodology based on Finite-Difference Time-Domain (FDTD) (Yee, 1966) and the surface integration simulation technique (Sbalchiero et al., 2021). An example of 3D models and simulation results are reported in Fig. 7.3.8.

7.3.3. VenSpec-M

To assess the performance of the current VenSpec-M design, we derive performance parameters based on the recent laboratory work and the Venus Express data sets.

To distinguish between surface and atmospheric contributions, VenSpec-M uses an updated version of the extensively tested data pipeline developed to process VIRTIS surface data (Mueller et al., 2008), combined with a radiative transfer model (RTM) (Mueller et al., 2008; Haus et al., 2017; Kappel et al., 2012; Kappel 2014; Kappel et al., 2016). Of the VenSpec-M's 14 bands, radiation for the six surface bands at 860, 910, 990, 1020, 1110, 1180 nm (Table 7.3.1) originates at the surface; three bands allow corrections for cloud composition and variability; two measure water abundance, and three compensate for background. Surface emissivity retrieval techniques were developed based on Galileo NIMS observations at 1700 and 2300 nm (Hashimoto et al., 2008). The VenSpec-M cloud bands are at 1195, 1310, and 1510 nm (Erard et al., 2009; Wilson et al., 2009); the first is on the flank of the 1180-nm surface windows. VenSpec-M's cloud bands are close to the surface bands, providing near-optimal correction.

The difference between the retrieved emissivity and the true emissivity (an input to the RTM) represents the plausible impact on uncertainty introduced by atmospheric variability, given as a percentage of emissivity ($\Delta\varepsilon_{atm}$). Based on laboratory measurements, a relative emissivity difference of 4% is sufficient to distinguish between felsic and mafic rock types as well as potentially identify a range of intermediary rock types and weathering products.

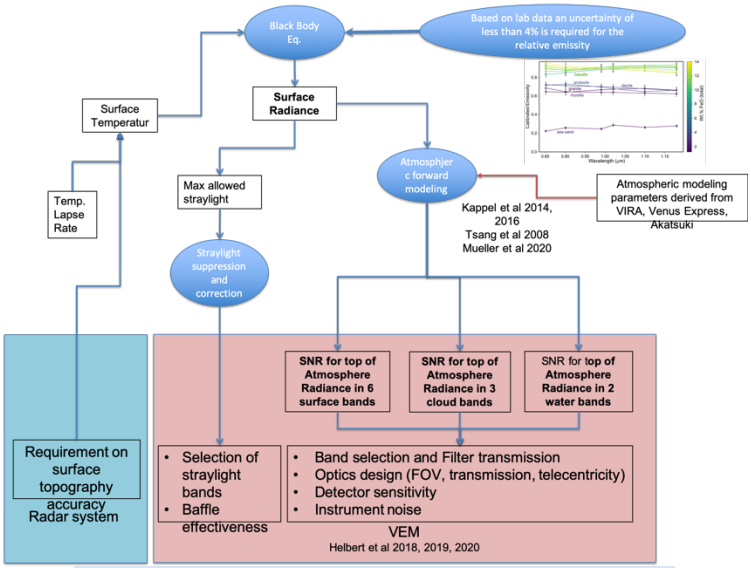

Figure 7.3.9 - Requirement flow-down for the VenSpec-M instrument

From this, we can derive the required Signal-to-Noise-Ratio (SNR) for all our bands as well as the maximum allowed amount of straylight. VenSpec-M has a dedicated two stage baffle to suppress stray light by a factor of at least 10-5 based on a straylight analysis. Residual background signal as for example straylight in the atmosphere of Venus is removed using three of the fourteen bands of VenSpec-M dedicated to measure the residual background. These bands are located at wavelengths of 790 nm, 1060 nm and 1370 nm (Helbert et al., 2018).

Table 7.3.1. - *SNR requirements for all 11 science bands of VenSpec-M. The background bands have by definition an SNR requirement of 0.* .

Purpose	Mineralogy and active volcanism						Clouds			Water	
Wavelength	860	910	990	1020	1110	1180	1195	1310	1510	960	1150
Width	40	60	30	15	20	12	12	30	30	40	30
SNR	53	53	44	43	145	125	134	134	134	100	100

Running the RTM as a forward model, we can derive required SNR values for all 11 bands shown in Table 7.3.1. The background bands which are supposed to have no signal have therefore by definition a SNR requirement of 0. A detailed approach adopted for the evaluation of the VenSpec-M radiometric performance is described in (Helbert et al., 2020; Helbert et al., 2022). It is based on analysis of the corresponding signal chain, including the passage of a simulated radiometric scene signal of the planet Venus through the VEM/VenSpec-M optics, detector, analog and digital electronics subsystems. It has been evaluated based on a theoretical model of the system and of the Venus atmosphere. Radiometric performance is expressed in terms of Signal-to Noise Ratios (SNR) per spectral channel. To verify the overall system performance with respect to the scientific requirements, a set of theoretical considerations is used to prove that the radiometric instrument performance is satisfying the scientific requirements.

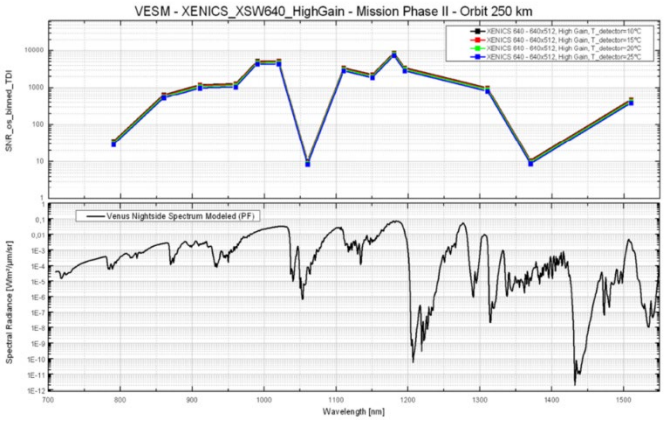

Figure 7.3.10.- *SNR values per spectral channel (shown at CWL). TOP: SNR values are the result of application of all SNR-improvement methods for an orbit at 250 km altitude. Results are shown for different detector temperatures (baseline is 10°C, black curve). BOTTOM: Simulated spectral radiances values for Venus (seen at top of atmosphere).*

Results of the performance evaluation for an orbit altitude of 250-540 km is presented in Figure 7.3.10 using SNR for raw image data and for the image data resulting after the application of the different SNR-improvement methods (Helbert et al., 2020; Helbert et al., 2022). The results represent the current baseline prediction for evaluation of instrument performance. This performance model will be updated over the life of the projects. More detailed modelling will be added for improvement of the predictions and for general support during VEM/VenSpec-M development.

7.3.4. VenSpec-H

The end-to-end chain of VenSpec-H consists of several steps: (1) Radiances (incoming signal at the entrance of the instrument) are calculated with the in-house radiative transfer code, ASIMUT-ALVL (Vandaele et al., 2008); (2) Noise is added to these radiances, in accordance with the Signal to Noise Ratio (SNR) model; (3) These noisy radiances are used as input in a retrieval procedure, also run using ASIMUT-ALVL. The errors obtained from the fit represent the random error to be accounted for in the total error budget.

ASIMUT-ALVL is a radiative transfer code developed and maintained at BIRA-IASB (Vandaele et al., 2006). Inputs (Figure 7.3.11-A) include the atmospheric state (p, T, n), surface description (albedo, temperature), spectroscopic parameters for molecules and aerosols' description (extinction, asymmetry, etc.). ASIMUT-ALVL can be run as a forward model and produce spectra or as a retrieval tool delivering molecular densities with uncertainties, using the Optimal Estimation Method (Rodgers, 2000).

The VenSpec-H SNR model is based on the current design of the instrument (Figure 7.3.11-B). It takes into account various terms such as the analogue to digital conversion noise, the dark current, the thermal background and the read-out noise. Each radiance and its corresponding noise were used to perform retrieval of the abundances of the target species (Figure 7.3.11-C). Column abundances of the molecular species of interest were derived. Convergence was achieved each time after 4 iterations.

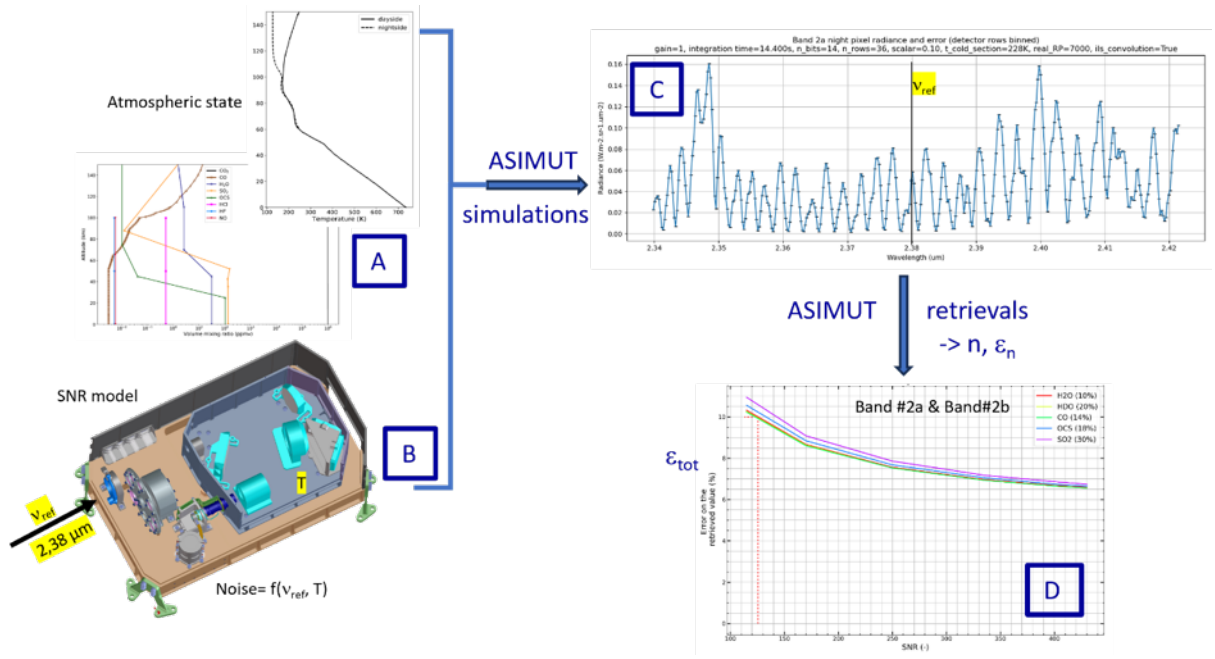

Figure 7.3.11 – *End-to-end simulations and determination of the SNR values in order to reach the required accuracies on the different targeted species.*

This exercise was repeated for various detector temperatures of the cold section of the spectrometer ("T" on Figure 7.3.11-B). This is the most critical instrument parameter which has an impact on the SNR value through the dark current. The SNR value used was chosen at a specific wavelength in each spectral band, i.e., at the continuum level outside of absorption lines due to the atmospheric species (Figure 7.3.11-C). Another critical parameter is the cold section temperature which directly affects the thermal background levels.

The retrievals' configuration was defined as an ideal case. The atmospheric state (pressure, temperature, molecules, aerosols and continuum) was considered as known. This kind of fit gives access to the random error (ε_n) which represents the impact of the noise on the retrieved values. The total error (e_{tot}) on the retrieved abundances is made of the random error (ε_n) and systematic errors for which were considered the accuracy on the cross-sections (3 %), on raytracing (1 %) and on the source term (nightside: 1.2 % - dayside: 3.6 %). This led to the determination of the required SNR to reach the required accuracies (see Section 4.6.6). An example is shown in Figure 7.3.11-D for Band 2b from which H_2O and HDO abundances among others can be derived in the troposphere. One can see that to determine the H_2O abundance with a 10 % accuracy (Requirement R2-C-10, see Table 3.1.1 and Sections 2.3.5, 2.3.7), a SNR value of at least 126 is required (Requirement R3-MEA-201, see Table 4.6.2).

Measurements performed on the dayside are always compliant, as the SNR achieved by the instrument is always at least a factor 50 above the required SNR. Nighttime observations are more challenging, especially the measurements in Band 1 that probe the near-surface layer. As can be seen in Table 7.3.1, VenSpec-H is non-compliant when considering the phase A spatial requirement (footprint ≤ 100 km) when the detector is cooled down at 135 K, which is the current detector temperature baseline. However, different mitigation scenarios were proposed in phase B1, leading to a relaxation of the spatial requirement for band 1 from 100 to 200 km and a relaxation of the lower troposphere H_2O and HDO partial column accuracies as reported in Sections 3.1 and 4.6.6. Moreover, discussions with the detector provider indicate the possibility of reducing the temperature of the detector, down to 120 K, which potentially could restore the dark current to the values studied in phase A. Table 7.3.1 shows that compliance or partial compliance is achieved for all bands following the phase B1 relaxations. In Table 7.3.1, we distinguish compliance and partial compliance: compliance is achieved when the instrument SNR is higher than the requirement at "Beginning of Life" (BOL) and "End of Life" (EOL), while partial compliance corresponds to an SNR value higher than the requirement at BOL but not at EOL. Table 7.3.2 indicates the trace gas partial column accuracies that will be obtained for these scenarios, corresponding to the requirements in R2-C-10 (see Section 3.1).

Table 7.3.1 –*SNR values in the different bands probed during the nightside for different scenarios: baseline 100 km footprint, extended footprint of 200 km, and extended footprint of 200 km considering also two consecutive orbits. The SNR values required to attain the accuracy on the abundances of the targeted species are specified (Requirement R3-MEA-201) with and without margin. The colour code indicates compliance at End of Life (EOL, Green), partial compliance, i.e. compliance at Beginning of Life (BOL) but not at EOL (Orange), and non-compliance at BOL (Red).* See also text and Table 4.6.1.

NIGHT	VenSpec-H	SNR - Detector at T=135 K BOL/EOL			SNR - Detector at T=120 K BOL/EOL		
Band*	Requirement† SNR	100 km	200 km	200 km 2 orbits	100 km	200 km	200km 2 orbits
1	H_2O: 45	39/34	55/47	77/67	75/63	114/99	161/127
	HDO: 48						
2a	H_2O: 126	152/136	215/193	304/273	398/248	358/350	563/495
	HDO, CO, OCS, SO_2: 70						
2b	H_2O: 126	105/91	148/128	209/181	202/171	286/241	405/341
	HDO, CO, OCS, SO_2: 70						
3	H_2O: 70	485/422	685/597	969/845	899/769	1271/1087	1798/1538

*Band: see Table 4.6.1; †SNR requirement: Requirement R3-MEA-201, see Table 4.6.2

Table 7.3.2 *– Accuracy values in the different bands probed during the nightside for different scenarios: baseline 100 km footprint, extended footprint of 200 km, and extended footprint of 200 km considering also two consecutive orbits. Different scenarios are applied as described in the caption of Table 7.3.1.*

NIGHT	VenSpec-H	Expected Accuracy at T=135 K BOL-EOL (%)			Expected Accuracy at T=120 K BOL-EOL (%)		
Band*	Requirement† (R2-A-10)	100 km	200 km	200 km 2 orbits	100 km	200 km	200km 2 orbits
1	H_2O (20 %)	22-23%	17-19%	13-16%	14-16%	11-12%	10-12%
	HDO (30 %)	35-38%	27-30%	20-23%	22-25%	16-18%	15-17%
2a+2b	H_2O (10 %)	11-12%	10-10%	8-8%	9-9%	7-8%	7-7%
	HDO (20 %)	11-12%	10-10%	8-8%	9-9%	7-8%	7-7%
	CO (14 %)	11-12%	10-10%	8-8%	9-9%	7-8%	7-7%
	SO_2 (30%)	12-13%	10-10%	9-9%	9-9%	7-8%	7-7%
	OCS (18%)	11-13%	10-10%	9-9%	9-9%	7-8%	7-7%
3	H_2O (10 %)	7-7%	6-6%	6-6%	< 6%	< 6%	< 6%
	HCl (bonus)	To be done					

†Accuracy requirement: Requirement R2-C-10; see Table 3.1.1

7.3.5. VenSpec-U

The spectral radiance entering the instrument during observations can be simulated using a forward radiative transfer model based on the one described extensively by Marcq et al. (2021). This model has been validated previously on the 190-320 nm spectral range at a moderate spectral resolution (2 nm) against SPICAV-UV/Venus Express nadir observations (Marcq et al., 2019, 2020), and at a spectral resolution of 0.15 nm using STIS/HST data (Jessup et al., 2015). It has since been extended in the 320-380 nm range in order to include the whole VenSpec-U spectral range, through a prescribed parameterization of the unknown UV absorption by matching both SPICAV-UV/Venus Express and MASCS/Messenger constraints (Pérez-Hoyos et al., 2018).

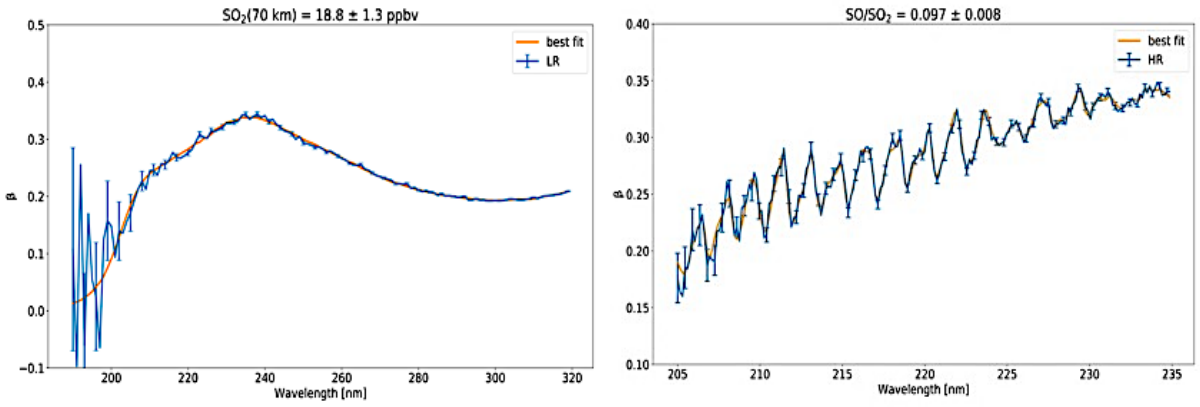

Figure 7.3.10 – *Synthetic radiance factors, including synthetic noise following the SNR(λ) specification (in blue) and their best fit using the inverse model (in orange) for spectral resolutions matching the VenSpec-U LR channel (left) and VenSpec-U HR channel (right).*

Synthetic noise can be added following the signal-to-noise spectrum derived from instrumental constraints, in order to derive the random uncertainties on the retrieved parameters using an inverse model (Figure 7.3.10). Sensitivity to non-random biases is assessed through the use of gain matrices (pseudoinverse of the Jacobian matrix computed using the forward model) in order to check compliance with ESRA target values (Conan et al., in prep.).

7.3.6. RSE

Gravity experiment

The expected Doppler data of the gravity experiment have been simulated based on a Doppler noise budget in 2-way (X-up and X-Ka down). The temporal coverage is 3.5 hours per day as a conservative assumption of the averaged duration of the telemetry slots, repeated each day over the 6 Venusian days (~4 Earth's years) duration of the science phase. A budget of the forces driving the spacecraft orbital motion has been established and perturbed as realistically as possible in order to produce a second set of Doppler data. A least-squares fit on the difference between this set and the simulated noisy Doppler set (see the end-to-end two-way noise budget on Figure 7.3.11) has been performed to check the compliance of the EnVision gravity experiment with the Science goals defined in the Science Requirements of the mission. The estimated performance meets the requirements for the k_2 Love number as well as for the accuracy and spatial resolution of the gravity field solution.

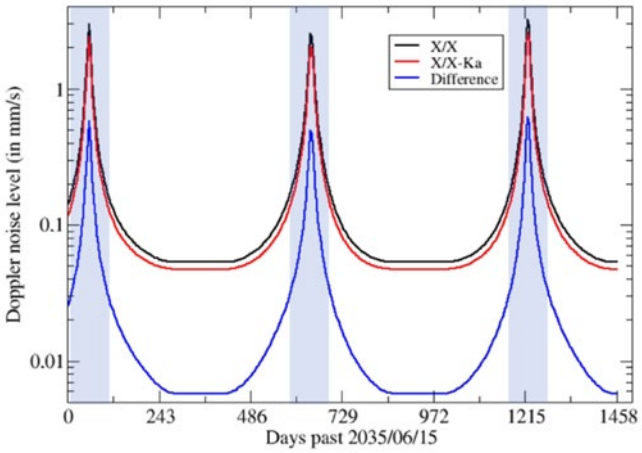

Figure 7.3.11 – *EnVision end-to-end two-way Doppler noise at 10 s count time over the six cycles of the mission for an X/X-Ka vs. X/X radio-link (from Rosenblatt et al., 2021).*

Radio occultation experiment

The atmospheric frequency shift expected during the radio occultations at Venus can be simulated using the Radio Science Simulator (RSS), developed at the University of the German Armed Forces in Munich (Selle, 2005) and already successfully used for the VeRa radio occultations on Venus Express (Häusler et al., 2006). The software has been adapted to simulate EnVision radio occultations, using the planned spacecraft orbit and a realistic spacecraft model. The software uses an atmospheric model to simulate the expected atmospheric frequency shifts. The software also studies the measurement sensitivity at the two different used radio frequencies, X- and Ka-band. Since radio occultation at Venus have never been performed at Ka-band frequencies, no real radio occultation data are available. The software simulates Ka-band measurements and studies their sensitivity based on atmospheric models and laboratory measurements. Synthetic noise are added to the data and the simulated frequency residuals are used to generate refractivity profiles as well as atmospheric and ionospheric profiles. These profiles are used to study the measurement sensitivities.

The radio occultation analysis software used for these purposes has already been successfully used to retrieve atmospheric absorptivity profiles from Venus Express. Synthetic atmospheric profiles are also used to study the absorption sensitivity of the measurements towards H_2SO_4 absorption as well as the accuracy of the sulfuric acid measurements. An example of the impact of the EIRP (Effective Isotropic Radiated Power) variability on the accuracy of the content in H_2SO_4 liquid is shown Table 7.3.3. As reported in Chapter 4.8.6, it should be noted that at the end of EnVision phase A, the ESA Mission Selection Review Board requested that the RSE shall not drive the design of the S/C, nor the cost and schedule of the mission. As a consequence, at the time of writing it has not yet been confirmed whether the current candidate S/C designs fully meet in particular the EIRP variability requirement in R3-MEA-2204. This means that the full compliance to the H_2SO_4 and SO_2 product requirements still has to be confirmed.

Table 7.3.3 – *Influence of X- and Ka-Band small-scale signal variations on the error of the derived cloud density (mg/m3). The estimated uncertainties represent mean values computed in the altitude range between 45 and 55 km altitude.*

		Ka-Band Signal Power Variation (dB)										
		0.01	0.025	0.05	0.075	0.1	0.25	0.5	1	2	3	4
X-Band Signal Power Variation (dB)	0.010	2	2	3	3	3	5	8	15	28	41	53
	0.025	5	6	6	6	6	7	10	16	29	42	57
	0.050	11	11	11	11	11	12	14	20	32	46	59
	0.075	16	16	16	16	16	17	19	23	37	49	60
	0.1	21	22	22	22	22	23	25	29	37	51	65
	0.25	53	53	53	54	54	54	55	61	65	74	86
	0.5	100	102	102	103	103	104	104	112	123	125	135

7.4. Approaches for the synergetic scientific data exploitation to address mission science objectives

In this section we address particular science investigations that will benefit from the combination of EnVision instruments and experiment. The synergistic and holistic way in which the payload instruments collaborate to investigate processes at different altitudes, depths and spatial scales is characteristic of the EnVision mission.

7.4.1. Surface mass movements and slope processes (VenSAR High-Resolution, VenSAR Dual-Polarization, VenSAR Topography, SRS)

Background. – The term "mass movement" encompasses a wide variety of processes that cause the downward and outward motion of slope-forming materials (rock, regolith and soil or a combination of these). These materials may move by falling, toppling, sliding, spreading, or flowing (see Figures 2.2.8, 2.2.9). Figure 7.4.1 shows the generic illustration of a landslide, with the commonly accepted terminology describing its features. Movements or failures may involve rotational or translational sliding, falling, toppling, flowing or spreading motions of materials. Combination of two or more of the above types are referred to as "complex" failures.

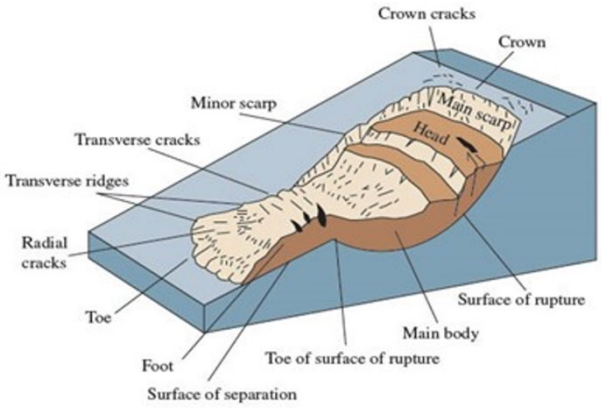

Figure 7.4.1 – *The figure represents the generic morphological features of a landslide (Varnes, 1978). High-resolution VenSAR will enable identification of more and much smaller landslides, and detailed mapping of their internal features. Better topography is vital to understand slope angles and morphology. Dual polarization will help discriminate solid from unconsolidated materials. SRS will help understand material thicknesses and superposition.*

Why slope failure occurs. - On Earth, the various types are also differentiated by the kinds of material involved and the mode of movement, and the key factors are usually slope steepness and water content (increasing bulk density and pore water pressures, and thus reducing friction and cohesion). On Venus, liquid water is absent so the key factors leading to slope instability are reduced to the presence of weak, sensitive, weathered, sheared, jointed, fissured or faulted materials, and the triggering mechanisms and morphological causes are likely to be earthquake shaking, tectonic uplift, basal slope erosion (causing over-steepening). Slope failures occur on a very large range of spatial scales.

How can we better understand slope processes on Venus. – Therefore, key to our better understanding of how mass movements work on Venus are higher resolution imagery, better topographic data (both to visualise the morphology), dual polarization (to resolve the degree of consolidation/disaggregation of materials), and sub-surface profiles (to establish thicknesses of failed materials).

7.4.2. Baltis Vallis: topography of long lava flows (VenSAR Topography, SRS, RSE)

Baltis Vallis is a 6,800-km long lava channel on Venus, the longest channel on the surface of Venus and on any known rocky surface in the Solar System. Following Baker et al. (1992)'s proposed placements of the channel's source at a volcanic construct near the northern end (185°E, 44.5°N) and terminus at the southern end, the canale seemingly flowed uphill over its length, A to A' (Figure 7.4.2). Its apparent uphill flow direction is interpreted as

a consequence of deformation changing topography after flow emplacement. The topography of BV thus retains a record of Venus' convection history, as mantle convection causes time-dependent surface deformation (Conrad and Nimmo, 2023; Gillmann et al., 2023). The observed deformation of Baltis Vallis indicates that mantle convection was active over the past ~400 Myr, and therefore it provides constraints on the length scales and vertical amplitudes involved.

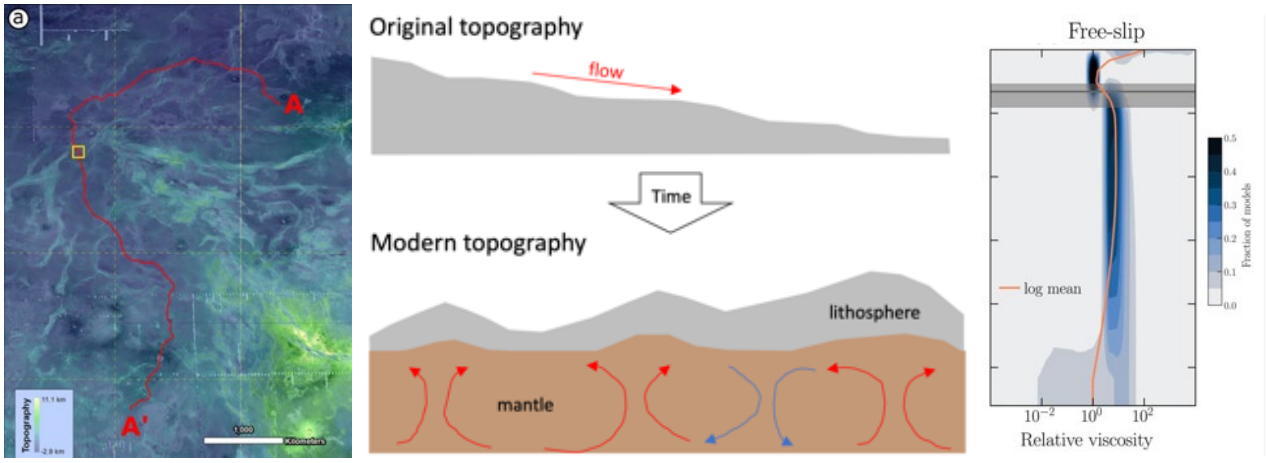

Figure 7.4.2 – *(a) Map of Baltis Vallis in Atla Regio, extending more than 6,800-km long. This puzzling lava channel is the longest on planet Venus and on any known rocky surface in the Solar System. The standard proposed source is at location A, and the end is at A' (Baker et al., 1992). Magellan topography reveals that the lava channel has been deformed and uplifted to the point that little information remains of its original topographic profile (b). This alteration of the features allows us to set a timescale on Venusian crustal deformation processes, and constraints from mantle viscosity (c) (Conrad and Nimmo, 2023; Gillmann et al., 2023; Maia and Wieczorek, 2022).*

Baltis Vallis has been deformed and uplifted to the point that little information remains of its original topographic profile, this alteration of the features allows us to set a timescale on Venusian crustal deformation processes. Understanding the timing and strength of deformation belts and dynamic uplift, on top of constraints on upper mantle viscosity, requires combining VenSAR Topography, SRS altimetry and sub-surface mapping, and RSE mapping of crustal and lithospheric thickness and mantle dynamical properties to model results (Figure 7.4.2).

7.4.3. Sulphur cycles measurements (RSE, VenSpec-H, VenSpec-U)

VenSpec-H nightside observations of trace gas abundance change, over terrain of different compositions and/or elevations, will yield insight into the surface-atmosphere exchanges, horizontal variability of trace species, and coupling between atmospheric dynamics and chemistry. The RSE observations of the main cloud constituent, H_2SO_4, in both vapor and liquid form from the cloud base to middle cloud deck near 55 km, will provide clues to cloud formation, dynamical processes, and chemical and microphysical processes at work in the cloud layer (Section 3.4.2).

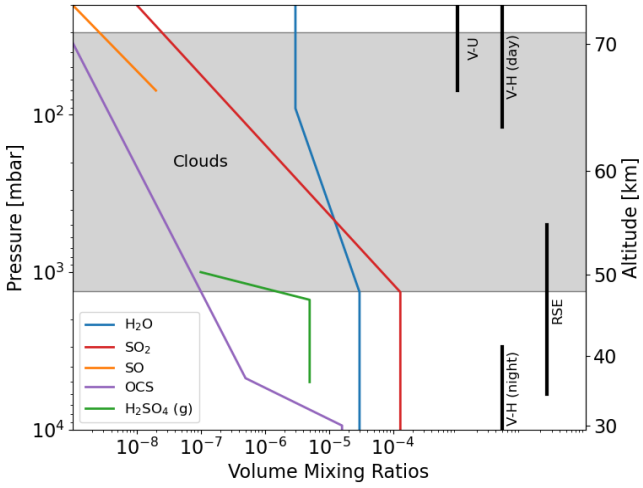

Fig. 7.4.4 – *Minor gaseous species involved in the sulphur cycle and probed altitude ranges for EnVision payload*

Combining RSE, VenSpec-H and VenSpec-U observations will help interpret how the convective cloud layer and topographically generated waves, which cause mixing of momentum, heat, and chemical species in the Venus atmosphere (Kouyama et al., 2017; Hickey et al., 2022; Lefèvre et al., 2022; Fig. 7.4.4 and Table 7.4.1). This variability may be associated with intrinsic atmospheric processes rather than volcanism. The probability that buoyant volcanic plumes, injected in the dense Venus atmosphere, would reach altitudes of 40 – 50 km is very small, and would require a very strong volatile-rich eruption. The atmospheric signature of such plumes would depend on the flux of volcanic gases, and the mixing rate with the air through eddy diffusion

and turbulence (Lefèvre et al. 2020; Morellina and Bellan, 2022; Wilson et al., 2023). On the dayside of the planet, the VenSpec-U and VenSpec-H observed UV and near-IR sunlight, scattered by Venus' cloud top, will allow the simultaneous observations of ($SO+SO_2$) near 215 nm, SO_2 near 280 nm and H_2O, HDO, CO, COS, SO_2 in several near-IR bands between 70 – 90 km altitude. The same species will also be monitored by VenSpec-H below the clouds, using nightside near-IR radiation emitted by the Venus surface and atmosphere (Robert et al., 2022). Repeated observations will provide insight on the local time, vertical, longitudinal, latitudinal and temporal variability of trace gasses essential for the understanding the complex chemical cycles on Venus (Section 3.4.3).

Table 7.4.1 – *Sulphur cycle molecules and their p (g)hysical state probed by RSE, VenSpec-H and VenSpec-U investigations. The species are observed in gas form, whereas H_2SO_4 is observed in gas and liquid (l) form.*

	H_2O	SO_2	SO	OCS	H_2SO_4 (g and l)
RSE		X			X
VenSpec-H	X	X		X	
VenSpec-U		X	X		

7.4.4. Constraint on core's size (VenSAR 10m and 30m imaging, RSE)

The VenSAR experiment will determine the spin state of Venus by using a control point network (tie-points) on its surface. Such accurate data acquired by Envision on Venus can be supported by tie-points determined by Magellan data, see Section 8.3.4. Furthermore, Earth-based radar speckle can be used to obtain longer time series of spin state (see Section 8.4.1). The RSE experiment data will be used to obtain maps of Venus's gravity field, including the degree-2 Stokes coefficients with high accuracy. The accuracies have been estimated to be about 25 times better than those obtained from Magellan data. The EnVision gravity data will be compared with those from Magellan. The combination of the estimation of the spin state (i.e. orientation, precession, length of day (LOD), and nutation (TBC)) from VenSAR high-resolution imaging of key tie-point pairs in Regions of Interest, and the gravity coefficients, will enable a better determination of Venus' moment of inertia (MoI). This quantity is a key geophysical parameter for better constraining the internal distribution of the planet mass and the size of the planet's core.

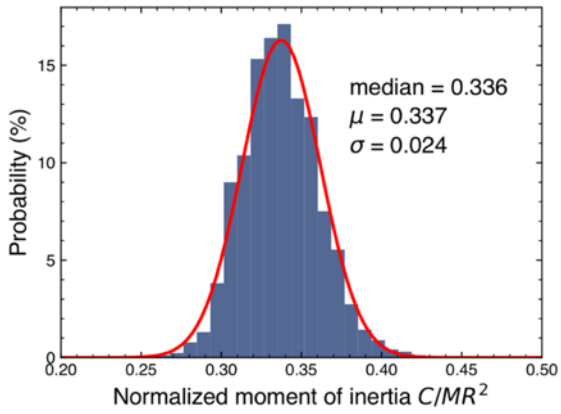

Fig. 7.4.5 – *Distribution of normalized moments of inertia using radar speckle tracking estimates showing the residual uncertainties of 7% on the Moment of Inertia (MoI). Figure from Margot et al. (2021).*

Each tie-point comprises two VenSAR observations of a fixed feature in repeated images, within the same Region of Interest (RoI) over the mission duration (see Chapter 3, Figure 3.3.5 and Chapter 7, Figure 7.1.2). There are two observation times, and two position vectors for each surface point. The position is retrieved relative to the centre of mass of Venus, in an inertial reference frame. Recent Earth-based radar speckle observations allow to determine the precession rate of Venus at 44.58 +/- 3.3 as per year (Margot et al., 2021). Using the Venus gravity field obtained by Magellan (Konopliv et al., 1999), the Venus moment of inertia (MoI) is estimated at 0.337 +/- 0.024, and the size of the core, for a simple two-layer model, is of the order of 3500 +/- 500 km (Margot et al. 2021, see Figure 7.4.5). The synergy between the different instruments and past observations will allow a better determination of the size of the Venus core that is useful to better understand the thermal, magnetic and rotational history of this planet.

7.5. EnVision data return robustness assessment

Two main elements may influence the data return of the mission: (1) the date at which the science actually starts may differ from the assumed one due to aerobraking uncertainties. The initial date influences the data return for a six-cycle fixed science mission duration; (2) the actual available duration of the ground communication slots might not be as anticipated, leading to a shorter communication slot, or no communication slot at all, requiring the spacecraft to store the excess data and the mission to ensure this excess data can be later retrieved without compromising the planned observations. The strategy for science data acquisition needs to show robustness to these events to guarantee the science return of the mission.

7.5.1. Sensitivity to starting date

The mission science performance has been simulated and verified on a reference scenario assuming a notional start of science on 15 March 2035 which provides the most eccentric orbit value over the likely period of start of science following the aerobraking, and from this point of view constitutes a worst case. The actual date of science start is expected to be different, depending on the performance of the aerobraking phase. An uncertainty of +/-3 months is considered conservative for the total aerobraking duration uncertainty. Changing the reference date requires adjusting the definition of the longitude bands as described in Figure 7.1.1, and therefore to adapt the pre-selected list of targets to optimize the coverage criteria. A three month earlier or later date (Figure 7.5.1) would increase the total data volume returned by 4%. The selected date used for the performance assessment constitute a worst case in terms of data return, and the assessed science performance is therefore built on this conservative assumption.

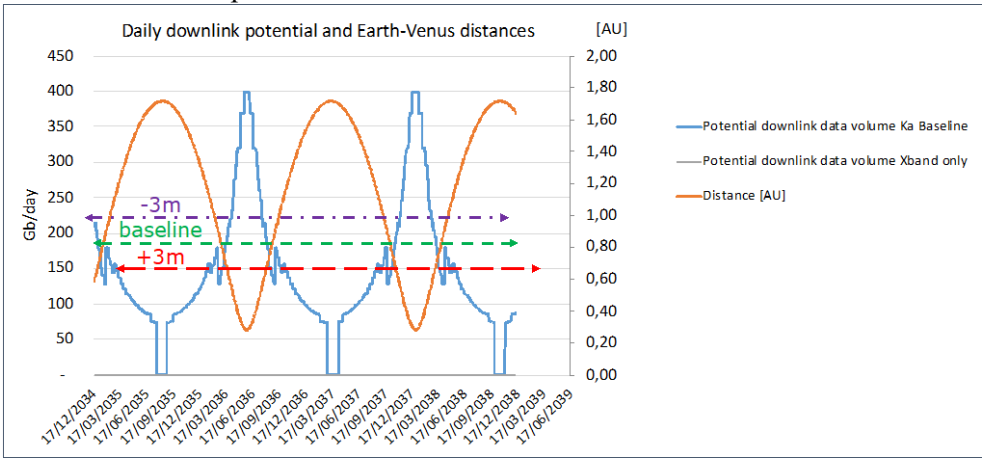

Figure 7.5.1 – *Sensitivity to the start date of the science operations phase. The operations reference scenario assumes a start date close to the minimum data rate (green vertical bar), and only 2 months before a superior conjunction. A start date three-months earlier would provide a similar data return. A start date three-months later would provide higher data return since in that case more than two peaks of high data rate would occur for the six-cycle mission.*

7.5.2. Resilience in degraded communication scenarios

The mass memory is sized for 8 Tbits capacity at end of life (EOL), while the absolute peak requested based on the reference scenario is at 6 Tbits. This represents 2 Tbits of reserve at all times beyond what is required, providing robustness to the data return strategy in case of downlink issue. The reference Solid-State Mass Memory (SSMM) fill state profile is presented in Figure 7.5.2 (orange curve). The mass memory sizing is compatible with two days of science data generation without any ground contact, which could occur at any point of the nominal mission. The SSMM sizing also nominally includes a 30% margin on the instruments data rates. Even with these conservative assumptions, the available free memory space is higher than 80% of the SSMM capacity for 20% of the time, and higher than 20% for 90% of the time. In the worst case the free memory space represents still 6% of the EOL capacity. It needs to be checked if this is sufficient to cope with potentially reduced communication slot durations. The following contingency cases impacting the duration of the communication slot have been identified:

Planning conflict. - If a communication slot is in conflict with a SAR observation, that observation should take priority at the expense of one communication orbit. The data volume which was supposed to be downloaded in that orbit needs to be stored and downlinked later. The SSMM provides flexibility in the planning of observations in such situations. A frequency of one such conflict per month is conservatively assumed;

Missed ground pass. - If a full communication slot is missed, this means in the worst case one full day without ESTRACK ground contact. A frequency of once a year is considered for such events based on station maintenance statistical data from ESOC;

Late ground pass. - A 10 minutes late station acquisition could occur. A frequency of once per week is considered for such events, based on ESOC experience. The SSMM shall absorb such cases.

Any data which has not been downloaded and which is stored on the SSMM needs to be downlinked later, without compromising the plan. This means, in particular, that no additional communication orbit can be placed in lieu of an already planned observation.

In such a case, offline arraying techniques in Ka-band between distant antennas of the ESA's ESTRACK network will be used to regularly offload the on-board mass memory. For Malargue and Cebreros the visibility overlap is

around four hours every day and this pair of stations is therefore assumed as baseline for the arraying technique. During such overlap periods the data rate can be increased by around a factor two with respect to the reception from a single antenna by using the two antennas at the same time. Offline arraying implies a significant delay between reception of the signal at the antennas and delivery of the final products to the user, as well as a channel bandwidth limitation, both due to the need to record and transfer digital raw samples between remote locations across the wide area network. Such a significant delay (days) is acceptable for science data. The maturity of such an offline arraying technique in Ka-band has been subject to a technology development activity during the phase B1 of EnVision, the technology has reached a sufficient maturity (TRL > 5 at adoption) to be baselined for EnVision.

A total of 160 hours of offline arraying (corresponding to 40 slots of four hours) over mission duration, with a distribution between eight and 48 hours per six months period, is sufficient to absorb the worst case accumulated extra data on the on-board mass memory due to the described contingency cases, and is fully compatible with ESTRACK capabilities. To cover the case of loss of contact during one day per year would require between 16 hours and 84 hours of extra offline arraying per year. The data return strategy is therefore fully robust against the identified data return contingencies.

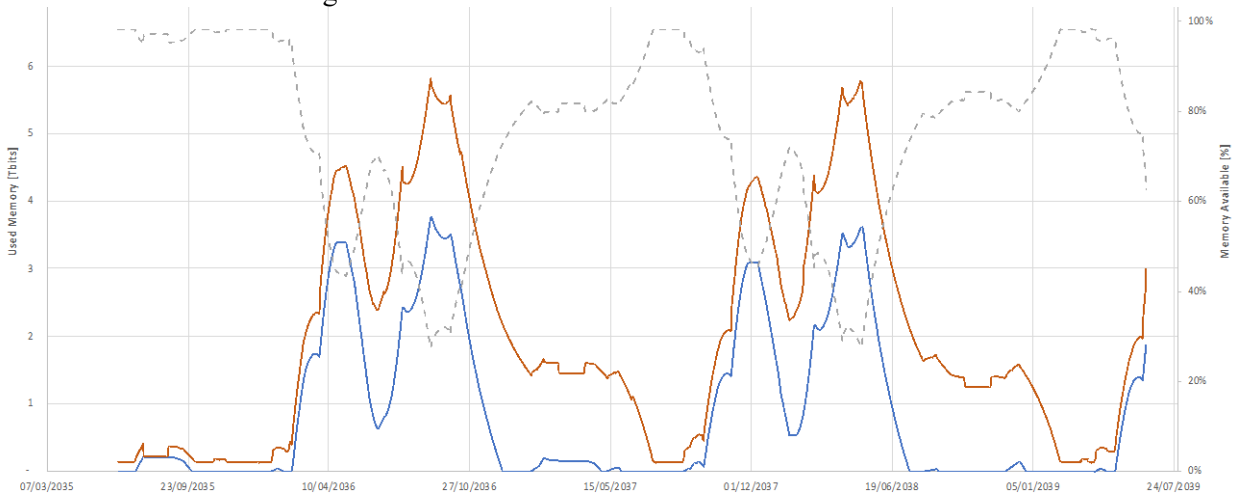

Figure 7.5.2 – *This figure shows the EnVision Solid-State Mass Memory (SSMM) loading profile consistent with the science operations reference scenario, assuming a starting date on 15/06/2035. The blue curve represents the nominal accumulation of science data in the SSMM. The orange corresponds to the blue line with the addition of 2 days accumulation at the current data volume generation rate to preserve the science return at any moment even with a 2 days interruption of ground contact, combined with 60 mins per week of downlink losses, and 1 full downlink loss per cycle. The grey dotted line represents in % the available free memory compared to the EOL SSMM capacity. The free memory ratio is always higher than 30%, and in average at 75%.*

8. Extended Use of EnVision Observations

8.1. Synergistic use of EnVision and DAVINCI observations

The NASA DAVINCI mission to Venus is scheduled to launch in June 2029 (Garvin et al., 2022). After a ~6-month cruise phase, the Carrier Relay Imaging spacecraft (CRIS) makes a Venus fly-by where some of the instruments on-board will be operated. This includes near-UV imaging, to derive cloud top motion, and near-IR surface emissivity observations. When the spacecraft returns for a second science flyby, the in-situ Descent sphere (DS) will be released for a descent to the Venus surface. The DS is a hermetically sealed titanium pressure vessel, with dimensions 1.1 m × 0.85 m and a mass of 250 kg. After the DS atmospheric entry and parachute deployment (~70 km altitude), the heat shield is released and the DS-based instruments begin to collect and transmit altitude-resolved, high-fidelity measurements of noble gasses and their isotopes, trace gasses, isotopic abundances, atmospheric temperature, pressure, and winds. Furthermore, high-resolution broadband and ~1 μm narrow-band images will be made (Figure 8.1.1). DAVINCI will provide highly accurate measurements of the atmosphere composition via noble gas isotopes, isotopes of hydrogen (D/H), and other species in a highly detailed physical context, while also imaging the surface in the near infrared from under the clouds at spatial scales not possible from orbital altitudes.

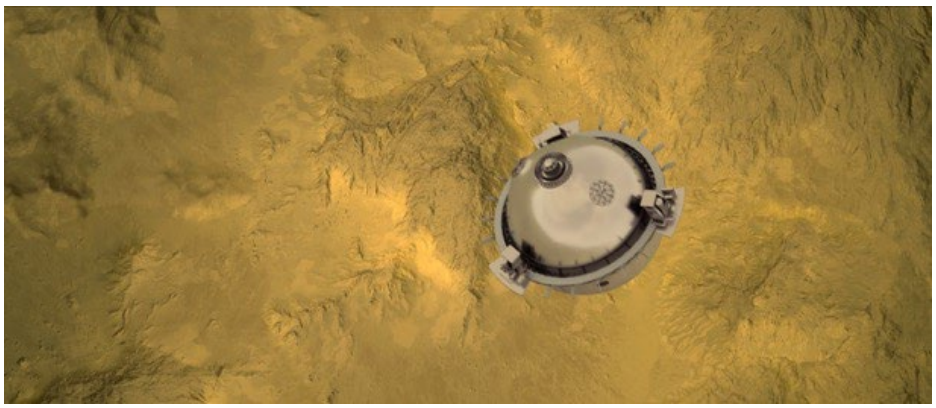

Figure 8.1.1 – *Artist's view of the DAVINCI probe during its ~59 minute long descent from the upper clouds to the surface over an entry-descent-science corridor. The descent is cheduled for June 2031. The landing ellipse is located at the western Alpha Regio, an EnVision Region of Interest (ROI). Credit: NASA GSFC / CI Labs – Michael Lentz.*

8.1.1. High-res topography and imaging of Alpha Regio

DAVINCI's Venus Descent Imager (VenDI) is a near-IR descent-imaging system with a nadir orientation, onboard the descent probe (DS). It will deliver clear, high contrast, high SNR images (>100:1) near-IR reflectance images below the cloud-deck and sub-cloud hazes. Below ~1.5 km altitude, VenSI will produce unblurred images at horizontal scales finer than 1 m (Garvin et al., 2022).

Topography can be derived from the VenDI images using machine-vision algorithms via Structure-from-Motion (SfM), an expansion of the Scale-Invariant Feature Transform (SIFT) algorithm. The Digital Elevation Model (DEM) is constructed from multiple overlapping images, with varying vertical and horizontal baselines (Garvin et al. 2018, 2022; see also review by Widemann et al., 2023, and references therein). The SfM processing of bundles of descent images will produce first 5 - 60 m scale topography of tesserae on Venus, establishing boundary conditions for tectonic and erosional models. The DAVINCI data products will be compared to stereo topography and imaging products from VenSAR over the western Alpha Regio, which is part of one of the EnVision Regions of Interest (Figure 3.3.1).

8.1.2. Surface composition

The VISOR instrument, on-board the DAVINCI Carrier Relay Imaging Stage (CRIS), is an integrated system of four cameras that provides global dayside coverage of Venus in the UV, and nightside coverage in the near-IR (0.93–1.03 μm). Each of the VISOR cameras has a field of view of 11.3° by 8.9°, which can be converted to a spatial sampling scale as a function of distance to the target. Three cameras observe the nightside of Venus in three

discrete near-IR bands, from 930–938 nm, 947–964 nm, and 990–1030 nm, providing surface emissivity measurements. These will be used to derive regional-scale surface composition at ~60 km resolution, during the January 2030 and November 2030 Venus flybys. These observations can later be compared with regional and global maps of surface emissivity and surface composition obtained by EnVision's VenSpec-M. The dataset comparison can be used for validation in non-active regions, and to look for surface activity (Helbert et al., 2019; Chapter 4, Section 4.5; Garvin et al., 2022).

During the descent above western Alpha Regio, the narrow-band near-IR VenDI channel on board the descent probe will acquire 1.02 µm albedo maps with sensitivity to felsic rocks. Alteration products can be obtained when ratioed against broadband images (0.74 to 1.02 µm) at finer spatial scales (<100 m), not accessible from orbit (Garvin et al., 2022). Mineral stability assessments associated with rocks containing iron (Fe), sulphur (S), and other elements will be conducted to infer possible weathering pathways within ~2 km of the surface. This will be directly connected to near-infrared band-ratio descent imaging at 740–1200 nm, at horizontal scales down toa few meters, for potential identification of rock formation requiring the presence of liquid water. These measurements will be highly complementary to the lower horizontal resolution, but larger spatial coverage measurements from EnVision's VenSpec-M.

8.1.3. Deuterium / Hydrogen ratio and atmospheric structure

DAVINCI's Venus Mass Spectrometer (VMS) is a Quadrupole Mass Spectrometer (QMS) with a gas-enrichment and pumping system, which will perform in-situ measurements of Venus atmosphere noble and trace gases, including e.g. H_2SO_4. VMS is mounted on-board the DAVINCI descent probe. VMS will take samples at least every ~200 m below 61 km altitude. Particularly in the lowest 30 km of the atmosphere, it will probe the supercritical CO_2 boundary, and properties of the CO_2/N_2 mixture in temperature and pressure conditions of the deep Venus atmosphere (Garvin et al., 2022; Widemann et al., 2023).
DAVINCI's descent probe's mass spectrometer VMS measurements of sulphuric species can be compared to the EnVision Radio Science Experiment (RSE) radio occultation (RSE-RO) observations of gaseous and liquid phase sulfuric acid between 35 and 55 km altitude. The RSE-RO H_2SO_4 observation accuracy is expected to be 1 mg/m^3 (liquid) and 1 ppm (gaseous) , with vertical resolution of ~100 m.
DAVINCI's Venus Tunable Laser Spectrometer (VTLS) will directly measure trace species at different heights in the clouds, with a sensitivity of ~1 ppbv. In particular, it will perform ten measurements of the D/H ratio in water vapor between 67 km and ~2 km altitude.

VTLS measurements will be compared to EnVision's VenSpec-H capability to map tropospheric H_2O and HDO partial column (Section 2.3.7).

8.1.4. Gaseous sulphur species and UV absorber

The Technology Demonstration Opportunity (TDO) experiment CUVIS (Compact Ultraviolet Imaging System) onboard the DAVINCI S/C carrier, CRIS, will acquire 0.2 nm resolution spectra and images from 0.20 to 0.40 µm. This UV hyperspectral sensor will make upper atmosphere SO_2 and SO observations, and gather spectral information on the unknown UV absorber. Simultaneously, a near-UV frame-imaging camera (VISOR UV), with a field of view of 11.3° by 8.9°, will acquire video imaging to quantify cloud feature motions. Dayside UV imaging (in a single spectral band) will measure cloud dynamics as the spacecraft approaches and recedes from pericentre, allowing ultraviolet feature tracking at 355–375 nm at a sampling rate that exceeds any existing Venus orbital imaging dataset.

Table 8.1.1 – *Comparison of instrumental capabilities of the UV instruments on board EnVision and the DAVINCI Carrier Relay Imaging Stage (CRIS) (Garvin et al., 2022). CUVIS will image the Venus dayside during each of the two DAVINCI mission flybys in January and December 2030.*

	VISOR UV	CUVIS UV	CUVIS UV-VIS	VenSpec-U LR	VenSpec-U HR
Spectral range (nm)	355 – 375 nm	200 – 390 nm	340 – 570 nm	190 – 380 nm	205 – 235 nm
Spectral resolution (nm)	N/A	0.2 nm	1-20 nm	2 – 5 nm	0.3 nm
Instantaneous Field-of-View (IFOV)	11.3 × 8.9 deg ²	0.3 deg x 2 arcsec	1.3 deg x 4 arcsec	20 × 0.9 deg ²	20 × 0.7 deg ²
Spatial sampling (km / pixel)	10 - 20 km	20 – 100 km	10 – 50 km	3 – 5 km	12 – 24 km

The EnVision VenSpec-U instrument (Section 4.7)will observe the same species but over a longer timescale than CUVIS. Amounts others due to the low polar orbit of EnVision, VenSpec-U to perform spectroscopic measurements at horizontal scales of ~10 km at the Venus cloud top (Table 8.1.1). The very similar spectral range

(190–380 nm for VenSpec-U LR channel) and spectral resolution (0.3 nm for VenSpec-U HR channel) between both instruments will allow for synergistic science opportunities. This includes comparisons of the different data-processing software from calibrated reflectance spectra to science products (SO_2 and SO column densities above cloud top, cloud top altitude, UV absorber, etc.), as well as comparisons of the solar UV illumination spectrum and its variations between 2030 and 2035–2038.

8.2. Synergistic use of EnVision and VERITAS observations

The VERITAS mission is an orbiter carrying the X-band Venus Interferometric SAR (VISAR) and the Venus Emissivity Mapper (VEM) instrument to perform global SAR mapping at 30 m resolution; and to acquire topography, gravity, InSAR, and NIR emissivity data. Following it's launch, the VERITAS cruise phase is estimated to take ~7-monthb, which is followed by a Venus Orbit Insertion (VOI), and a manoeuvre to reduce the orbital period from 120 to 13 hrs. Aerobraking is then applied to reach the final science orbit. VERITAS has two planned science phases: Science Phase I (SP1) and Science Phase II (SP2). Science Phase I uses a 6.1-hour, highly elliptical orbit, and Science Phase II has a 91-minute orbital period at a mean orbit altitude of 217 km. Both have an orbit inclination of 85.5° (Smrekar et al., 2022).

The Venus Interferometric Synthetic Aperture Radar (VISAR) X-band measurements will provide: 1) a global digital elevation model (DEM) with 250 m postings, 5 m height accuracy, 2) Synthetic aperture radar (SAR) imaging at 30 m horizontal resolution globally, 3) SAR imaging at 15 m resolution for targeted areas, and 4) surface deformation from Repeat Pass Interferometry (RPI) at 2-centimeter vertical precision for >12 200 × 200 km potentially active area targets. Community input would be solicited for both RPI and high-resolution imaging targets. The VEM instrument is similar to VenSpec-M flying on EnVision (Helbert et al. 2016, 2020), and will produce surface coverage of most of the surface in 6 near-IR bands located within five atmospheric windows, and eight atmospheric bands for calibration and water vapor measurements (Table 7.3.1). VERITAS will also conduct a radio science experiment with its communication system (see Section 8.2.4).

Figure 8.2.1 – *Artist's view of the VERITAS orbiter. The VERITAS mission profile consists of two phases. Science Phase I (SP1) occurs while aerobraking is paused, about 6 months after insertion into a polar elliptical Venus orbit. Science Phase II (SP2) starts after further aerobraking has placed VERITAS in a near-polar, circular, low-altitude orbit, that allows global observations throughout the mission. Over its ~3.5 Earth years mission, VERITAS will return synergistic, global datasets to meet its science goals: high resolution topography, X-band radar imagery, targeted surface deformation, near-IR spectroscopy, and gravity.*

8.2.1. X-band vs. S-band

VERITAS is designed to enable global topographic mapping, which is complementary to EnVision's strategy of regional observations. Whereas VERITAS observations would provide datasets important for comparative planetology, and support science studies requiring global coverage (e.g., obtaining a complete inventory of crater characteristics), EnVision's multi-messenger geophysics strategy uses combinations of observations at wavelengths from the UV to radio-frequency to study the coupling of different processes associated with geological activity.

Two radar wavelengths: The VERITAS X-band (3.8 cm), and the Magellan and EnVision S-band (12 cm) observations will provide surface roughness information at 2 scales, and hence providing increased information content than the individual missions alone. Change detection, using different frequency radar datasets over geologically relevant surfaces, has been successfully demonstrated on Earth (Patrick et al., 2003). If Venus is geologically active on the timescale of decades, many processes could alter surface backscatter, meaning that comparisons of VISAR on VERITAS, VenSAR on EnVision, and Magellan images could be performed to identify active regions.

8.2.2. InSAR DEM topography products

The VERITAS global topography dataset could be of great benefit to the EnVision mission science in several ways. For example. the VISAR global DEM could be used to identify and remove topography-related surface temperature variability seen by VenSpec-M and VenSAR radiometry. Furthermore, the EnVision's ground penetrating radar, SRS, could use the VISAR global DEM for clutter removal outside of ROIs, in addition to its own and VenSAR's global altimetry products. VERITAS' global topography and imaging could potentially also be used to refine the planning of the EnVision VenSAR ROI imaging, in case the VERITAS data would become available on-time for the EnVision long-term planning cycle.

8.2.3. Expanded global coverage

Together, VERITAS and EnVision provide long timeseries of observations to search for signs of active volcanism (e.g. fresh basalt, thermal anomalies and near-surface water vapor), combining VISAR and VenSAR, VEM and VenSpec-M observations (Figure 3.3.1; Table 3.3.1).

8.2.4. Gravity science products

The Doppler tracking data from EnVision and VERITAS will both contribute to an improvement of the accuracy of the derived Venus gravity field. If the missions are temporally separate, their combined gravity data will allow for a better determination of the rotational state of the planet (Section 7.4.6), which in turn will offer stronger constraints on models of the planet's interior structure.

8.3. Synergistic use of EnVision with earlier Venus missions

8.3.1. Surface activity detection (Magellan, VEx)

The synergistic use of EnVision data with earlier Venus missions for surface activity detection include; detection of volcanic activity in repeated SAR images; search for surface and near-surface temperature anomalies or changes; and detection of volcanogenic gas and particulate plumes (see Sections 2.2.5 and 2.3.5). Following recent work by Herrick and Hensley (2023), detection and characterization of relatively large eruptions over the past 40 years will be achieved by searching for new, large, lava flows, as well as large scale changes to the morphology of volcanic areas with repeat SAR imaging. Temperature signatures associated with volcanic activity from both hot lava and hot volatile gasses will be detected and monitored in the infrared (VenSpec-M) and microwave (VenSAR radiometry) domains. Hotspots may be revealed through the detection of temporal changes in the surface IR or microwave brightness temperature, either at decadal (Magellan and EnVision comparison over 40 years) or yearly (EnVision inter-cycle comparison) time scales (Sections 2.2.5; 2.3.5).

8.3.2. Atmospheric variability (VEx, Akatsuki)

Sulphur dioxide and water vapour are found to be highly variable in Venus' atmosphere (Marcq et al., 2013, 2020), but the cause of this variability has not yet been found (Section 2.1.2). As discussed in Sections 2.2.5 and 2.3.7, the most variable atmospheric species on Venus are SO_2, SO, H_2O, CO, COS, and H_2SO_4, which are often associated with volcanic emissions on Earth. The goal of EnVision is to understand the mechanisms behind the intrinsic atmospheric variability, and to establish whether it is linked to surface geological activity.

On the nightside, the only previous orbiter equipped with spectrometers capable of probing atmospheric species in the Venus atmosphere below the cloud deck was Venus Express. Its near-IR observations demonstrated the viability of mapping H_2O, but the relatively low spectral resolution (VIRTIS-M-IR with resolving power $\lambda/\Delta\lambda\sim70$, and SPICAV-IR with resolving power $\lambda/\Delta\lambda\sim1700$) led to low retrieval precision of typically 5 – 10 ppm for water vapour (see Section 2.3.7, and references therein).

On the dayside, EnVision VenSpec-H and VenSpec-U will measure gas abundances in the mesosphere (70-100 km altitude) above the clouds at unprecedented spatial and spectral scale, such as carbon monoxide (CO), sulphur dioxide (SO2), sulphur monoxide (SO), and water (H_2O), which have all been shown to be highly variable.

Observations from the previous Venus orbiters VMC/VEx and UVI/Akatsuki lacked spectroscopic capabilities, whereas VIRTIS-H/VEx and SPICAV-UV/VEx lacked extensive spatial coverage.

Comparison of EnVision RSE radio occultation temperature, pressure and number density observations (from 35-90 km altitude) with past with VEx and Akatsuki will help to understand the processes driving the short and long-term variability of the cloud, mesosphere sulphuric compounds, and atmospheric stability.

8.3.3. Venus' internal structure (Magellan)

The decades-long interval between the Magellan and EnVision missions offers the opportunity to improve the determination of Venus' orientation in space, including small secular (or long-term) orientation changes. A full understanding of the planet's orientation will permit the reduction of biases when determining the planet gravity field coefficients (including the k_2 Love number and the tidal phase lag, see also Section 2.3.4). Furthermore, improvements of the rate of precession (the change of the planet's rotational axis against a fixed reference frame) yield additional vital information on the planet internal structure.

Measurements of the length of the Venus day have shown variations of up to seven minutes on average over 243 terrestrial days, among which three minutes can be explained from our current knowledge of the planet behaviour as explained i.e. by Cottereau et al., 2011. The combination of Magellan and EnVision data will allow for an improved calculation of the length of the Venus day (LOD) and its temporal variations (Figure 8.3.1).

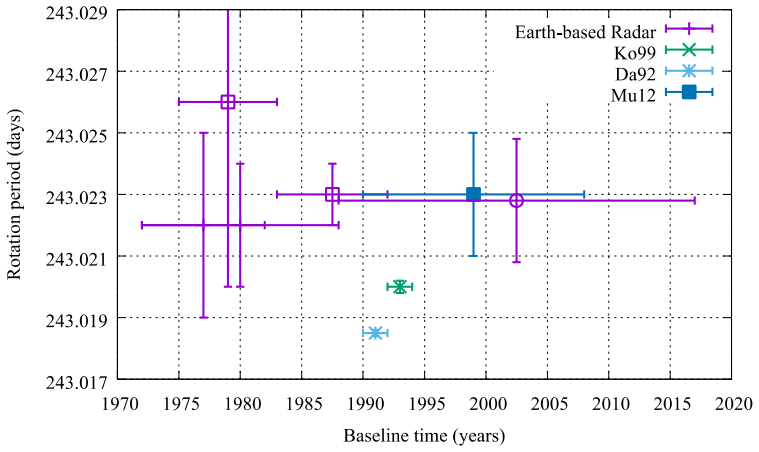

Figure 8.3.1 – *Estimates of Venus' rotation period for different space missions (Ko99: Konopliv et al. 1999, Magellan; Da92: Davies et al. 1992, Magellan; M12: Mueller et al. 2012, VEx) or Earth-based experiments. The horizontal bar at bottom shows the period over which the data have been acquired; the rotation period represents the average during this period. Figure from Rambaux, N., internal team meeting RSE; adapted from Mueller et al (2012).*

8.4. Synergistic use of Envision with ground-based observations

8.4.1. Earth-based radar mapping and speckle tracking

Earth-based radar mapping of the Venus surface can achieve 1–2 km spatial resolution, and can resolve radio echoes in both opposite-sense circular (OC) and same-sense circular (SC) polarization mode. The OC echoes are very similar to the Magellan measurements, and are strongly modulated by slopes facing the radar. The SC echoes are much more sensitive to small-scale surface roughness, rather than the topographic slopes. The capabilities of Earth-based radar measurementwas demonstrated in the mapping of fine debris in the Venus highlands (Campbell and Rogers 1994; Whitten and Campbell 2016). Earth-based polarimetric mapping with the Arecibo radar suggest a correlation between small-scale roughness in Venus lava flows and similar flows on Earth (Campbell and Campbell 1992), and may even reveal deposits formed during recent, volatile-rich eruptions (Campbell et al. 2017).

Fig. 8.4.1 – *The Radar-speckle-tracking technique illustrated as radar echoes sweep over the surface of Earth. the three panels show the trajectory of the speckles one hour before (left), during (center), and one hour after (right) the time of maximum correlation during observations taken on 8 September 2022. The echoes observed at the two receiver stations (Goldstone Solar System Radar and Green Bank Telescope at 8,560 MHz: red triangles) exhibit a strong correlation when the antennas are suitably aligned with the trajectory of the speckles (green dots shown with a 1 s time interval; Margot et al., 2021).*

Earth-based radar can also be used to monitor Venus' spin state and moment of inertia (Margot et al. 2021, see Section 7.4.6). High-precision measurements of the instantaneous spin state of Venus are obtained from radar-speckle-tracking techniques, requiring two telescopes. Margot et al. used the 70-m antenna (DSS-14) at Goldstone, California (35.24°N, 243.11°E), and transmitted a circularly polarized, monochromatic signal at a frequency of 8560 MHz (λ = 3.5 cm), and pa ower of ~200–400 kW. The radar echoes were recorded with the DSS-14 and the 100 m Green Bank Telescope (GBT) in West Virginia (38.24°N, 280.16°E), using fast sampling systems. The results were found to be of sufficient accuracy to classify the Venus interior using interior models (Dumoulin et al. 2017). However, the best-fit value of the moment of inertia factor, combined with knowledge of the bulk density, still enabled a crude estimate of the size of the core of Venus (Margot et al. 2021, see Section 7.4.6).

8.4.2. Millimetre wave, near infrared and visible observations

Ground-based observatory facilities and their instrumentation may perform relevant measurement campaigns of Venus during the EnVision Science Operation phase. Ground-based observations sample a large range of altitudes, using wavelengths and/or spectral resolutions complementary to the EnVision instrumental suite, and may hence trace constituents or motions of the atmosphere in complementary way. Opposed to an orbiter mission, ground-based observations can provide an almost instantaneous large latitude, longitude, and local time coverage, which can be used to observe rapidly variable phenomena. They can also provide decade-long observation time-series, bridging the gap between Venus orbiter or descent missions (Lellouch et al. 2007; Lellouch and Witasse 2008; Widemann et al. 2008). Amongst the Venus atmosphere trace constituents, SO_2 exhibits the most dramatic variations at Venus' cloud top, both spatially and temporally (Esposito 1984; Esposito et al. 1988; Marcq et al. 2013, 2020; Vandaele et al. 2017a,b, Encrenaz et al. 2012, 2016, 2019, 2020, 2023). To understand the causes of this variability, continuous observations and long temporal baselines are needed. This will also improve the understanding of secular climate evolution at Venus. Ground-based observations will, therefore, be highly complementary to the higher precision but shorter time series of SO_2 observations that will be made with EnVisions' VenSpec-U, -H and RSE experiment.

Observing Venus at millimeter and submillimeter wavelengths with heterodyne spectroscopy provides unique means to probe the upper mesosphere (i.e., altitudes of 70–120 km). Heterodyne spectroscopy measurements in the millimetre range of CO, HDO, and H_2O have been performed with single-dish antennae for decades (e.g., Encrenaz et al. 1991, 1995), and in the submillimeter range of CO, SO_2, SO, H_2O, and HDO (e.g., Sandor et al. 2010, 2012) using the James Clerk Maxwell Telescope (JCMT) on Maunakea, Hawaii. The altitude resolution of the observed trace gas concentrations is derived from the shape of pressure-broadened spectroscopic lines and the exponential variation of pressure with altitude (Widemann et al., 2023).

8.5. Additional/Opportunistic science with EnVision

At the 2023 EnVision workshop at DLR, Berlin, Germany, a number of possible science topics and applications that EnVision could potentially address in addition to its baseline science goals were presented and discussed. These science topics and applications are not applicable to the mission requirements and design, and can hence not be guaranteed to be addressed. However, they are mentioned here to illustrate current ideas for potential further mission science output.

8.5.1. VenSAR Repeat-Pass Interferometry (RPI)

The current mission baseline does not include Repeat Pass Interferometry (RPI), due to resource restrictions limits. However the VenSAR instrument is compatible with RPI operations, and there could be a few possible natural instances during the science operations phase where the conditions for RPI would be met. At these times/locations, opportunistic RPI should be achievable. RPI is the only technique that allows the detection of surface changes at centimetre-scales. Even if RPI is only possible at a very small number of locations on the planet, the scientific benefit of doing this would be extremely high. By analogy, with this technique applied to Earth, RPI should reveal a wealth of small-scale activity/change types (comparable to the scale of the radar wavelength) such as volcanic activity, fault movement, and sediment transport. It can achieve such detections through construction of differential interferograms representing measurements of ground motion, and through resolving the degree of interferometric coherence loss between two SAR scenes caused by various surface processes. In the case of a

potential mission extension, it is expected that remaining delta V can be used to conduct RPI in a more targeted way across a variety of regions anticipated to be active. More specifically, for the three types of activity mentioned above, RPI would assist in: (a) detecting cm-scale changes caused by active volcanism; (b) detecting cm-scale crustal motions across jostling blocks and across tectonic boundaries; (c) detecting cm-scale changes caused by aeolian processes and mass wasting as explained below, as follows:

Detecting cm-scale changes caused by active volcanism

We now know that Venus was volcanically active during the course of the Magellan mission (Herrick et al, 2023), and thus we should expect to see plenty of evidence of change between the times of the Magellan and EnVision missions through imaging at 30m and 10 m resolution. RPI offers the chance to detect and measure intra-mission changes and surface activity at scales finer than the SAR imagery. For example, volcanic edifice inflation/deflation in response to subsurface magma movements before or after eruption can be detectable and measurable using RPI (see illustration in Figure 8.5.1a). Volcanic features such as lava flows, pyroclastic flows, or other ash deposits erupting during the mission can reveal themselves as areas of coherence loss.

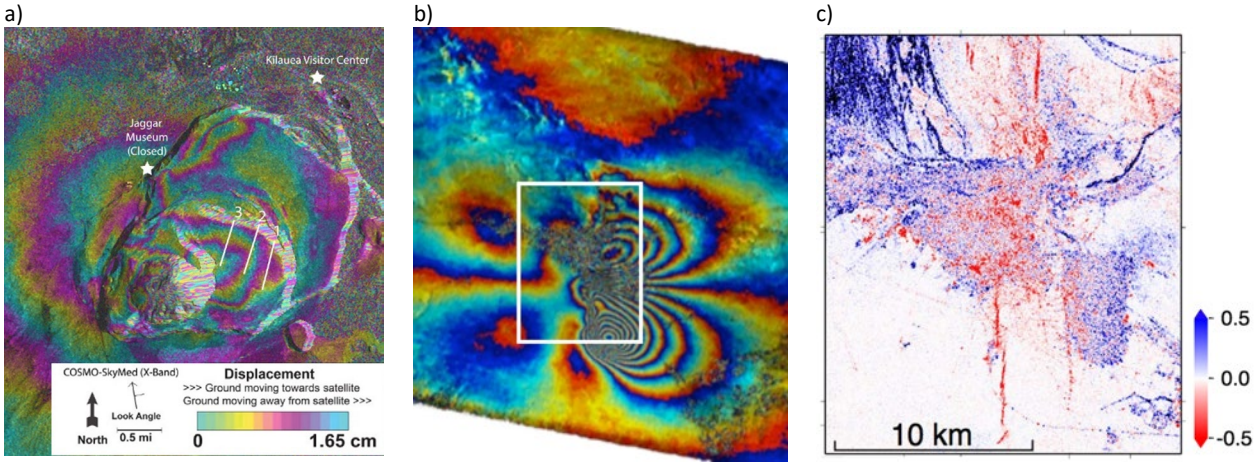

Figure 8.5.1 – *a) Differential Interferogram, from COSMO-SkyMed SAR data (2019.04.06 to 2019.06.02), of the Kīlauea Volcano summit, showing inflation (movement upwards towards the satellite) of a few centimetres (credit: Telespazio). b) Spatial pattern of ground motion, as a differential interferogram, produced from Envisat SAR data acquired before and after the 2003 M_w 6.6 Bam earthquake in Iran. Note the 'butterfly' pattern characteristic of fault-slip- (i.e., earthquake-) induced ground deformation. c) Spatial pattern of co-seismic coherence loss in red (associated directly with the Bam earthquake), as distinct from gradual (pre-seismic) coherence loss in blue, which is interpreted as the result of mass wasting, erosion, fluvial activity, and vegetation growth. Note the distinctive straight-line surface rupture pattern (also red), highlighting the active fault segments that failed during this earthquake (after Fielding et al., 2005).*

Detecting cm-scale crustal motions across jostling blocks and across tectonic boundaries

Most regions of Venus show signs of large-scale tectonic deformation, from extensional features like graben-fissure systems and wrinkle ridges to shortening features like fold mountains and complex tesserae. Although Venus does not exhibit plate tectonics as seen on Earth, there is some evidence for different tectonic regimes under which smaller regional blocks in the planet's lowlands, called 'micro-plates', jostle and rotate (Byrne, 2021). These blocks tend to have heavily deformed margins, with relatively intact interiors. Mass wasting, which is widespread on Venus, is often indicative of active uplift. Tectonic deformation can be studied both by looking for the surface expression of tectonic structures and by measuring cm-scale changes in ground elevation caused by faulting. Deformation rates associated with such motions are expected to be on the order of 10^{-3} to 10^{-1} m/yr, and may be slow and continuous or impulsive with motions of many metres in individual seismic events (see Figure 8.5.1b). Such tectonic changes include motion along faults or regional scale shifts across faulted blocks. RPI would assist in detecting and measuring them.

For such regions, three repeated SAR observations using the same observation geometry (same look angle and direction) are needed. Two observations would be the minimum requirement, but a third observation allows robust confirmation of movement and characterization of whether the change is ongoing. A minimum of two years between the first observation and the last observation is required to allow sufficient change to occur (tectonic movement rates are expected in the mm/yr to cm/yr range).

Detecting cm-scale changes caused by aeolian processes and mass wasting

The significance of aeolian landscape change has only recently been appreciated. Although sediments are likely to be volumetrically small, they may cover a large fraction of the planet, perhaps up to 50% of the plains. Aeolian

erosion is apparently important above ~2 km altitude, and may be linked to a 1.5–1.8 km altitude dust layer detected in Venera 13 and 14 probe data. Mass-wasting can be mapped using repeated imaging. Subtle aeolian processes, including erosion, transport, and accumulation (i.e., sedimentation) even over large areas, would, however, only be detectable at sub-pixel scale by looking at coherence loss between RPI observations. Any coherence loss between observations would point to sudden or gradual changes to the random scatterers on the ground (see Figure 8.5.1c). Such a detection would be hugely important for our understanding of the planet's surface processes, levels of activity, sediment budget, and composition.

8.5.2. Aerobraking science

EnVision will perform a long aerobraking campaign of 15–18 months, following the Venus orbital insertion (see Section 6.2.4 and Figure 6.2.2). This offers a unique opportunity to obtain additional, valuable scientific results on the uppermost layer of the Venus atmosphere (e.g., *in-situ* density, waves, cross track winds), without modifying any of the mission and/or spacecraft requirements.

Previous experiments during aerobraking campaigns at both Venus and Mars were very successful. For example, the VEx Atmospheric Drag Experiments (VExADE) allowed in-situ measurements of mass density and waves using three different techniques: a) Aerobraking down to altitudes below 140 km (AER) utilizing the on-board accelerometers to measure the atmosphere induced drag on the S/C (Muller-Wodarg et al., 2016); b) Precise Orbit Determination (POD) for S/C altitudes on Venus as high as 180 km, where the aerodynamic drag is very small (Rosenblatt et al., 2012); c) The Torque (TRQ) method where the torque on the S/C is measured in response to different orientations of the solar panels in the ram direction. The latter resulted in atmosphere exerting torques on the S/C, which can be measured and included in the platform housekeeping data. This approach worked for S/C altitudes between ~160–200 km.

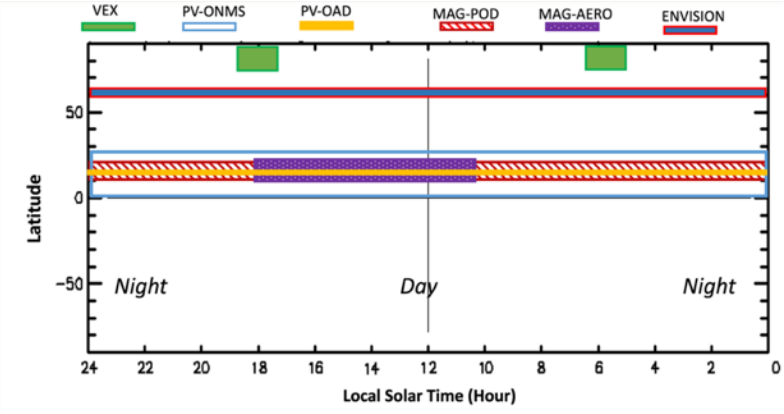

Figure 8.5.2 – *Distribution in local solar time and latitudes of EnVision aerobraking measurements, compared with previous observations from Magellan (Tolson et al. 2013), Pioneer Venus Precise Orbit Determination (PV-POD) (Tolson et al. 2013, Keating et al 1980), PV Orbiter Neutral Mass Gas Spectrometer (PV-ONMG) (Niemann et al. 1980, Kniffin 1993), and the Venus Express Atmospheric Drag Experiments (VExADE-AER) (Muller-Wodarg et al. 2016). EnVision aerobraking is a unique opportunity to infer direct density profiles in the upper atmosphere of Venus between 140 km and 180 km, to fill the gap in the mid-latitude range.*

Before VEx, density measurements were obtained with Magellan (Tolson et al., 2013) and PVO (Keating et al., 1980) during aerobraking in the region 135–150 km and 150–250 km, respectively, covering mostly the equatorial low-latitude region (Figure 8.5.2). Figure 8.5.3 shows the predicted Local Time and latitude coverage of EnVision aerobraking measurements at the pericentre passes. EnVision would offer a unique opportunity to fill the gap of density measurements in the mid-latitude range (about 60ºN), which was not covered by previous missions. Precise Orbit Determination (POD) during pericentre passes would be feasible, depending on the availability of the Low Gain Antenna (LGA) during the aerobraking phase.

Drag acceleration estimation. - The drag acceleration on the spacecraft around the pericentre can be measured with good signal-to-noise ratio (SNR) over a limited altitude range only, with the actual accelerometer specifications. It is estimated as follows:

$$a_{drag} = \frac{1}{2} C_d \frac{A}{M} \rho_{model} v^2$$

with the EnVision drag coefficient C_d (~2), the S/C ram area A= 35 m^2, the S/C mass = 1780 kg, and ν the S/C velocity with respect to the atmosphere (7.3–9.8 km/s, see Table 8.5.1). The modelled density ρ_{model} at pericentre passes is obtained using the ESA atmosphere variability model (Martinez et al., 2023). This model was built specifically for engineering purposes to deal with atmosphere uncertainty and variability during the aerobraking phase and is based on the Venus Climate Database (VCD) (Martinez et al., 2023; Stolzenbach et al., 2023; Gilli et al., 2021).

Two scenarios are considered: 1) a "conservative case" representing the worst atmosphere variability provided by the VCD within the aerobraking altitude range, at the pericentre latitude, for average Extreme UV (EUV) conditions; and 2) a "worst case" taking into account a factor of two underestimation of the VCD densities at the altitudes of the VEx observations (Martinez et al., 2023). Assuming for this exercise a similar Inertial Measurement Unit package onboard EnVision as on VEx[5], the formal read-out accelerometer noise, after processing of velocity increments of 1 sec, is 0.001 m/s^2. With this cut-off threshold, the maximum valid altitude range for density measurements would be approximately 130 to 140 km in the "conservative" case. This range can be extended by increasing the accelerometer precision (Figure 8.5.3). For instance, the TGO/ExoMars SNR values were on average about half of those of VEx (Siddle et al., 2021), and a similar SNR would lead to valid EnVision in-situ densities up to about 145 km. Nevertheless, considering the high atmosphere density variability observed at those thermospheric altitudes, an accelerometer noise lower than 0.0005 m/s^2 is recommended to measure valid densities during the aerobraking phase.

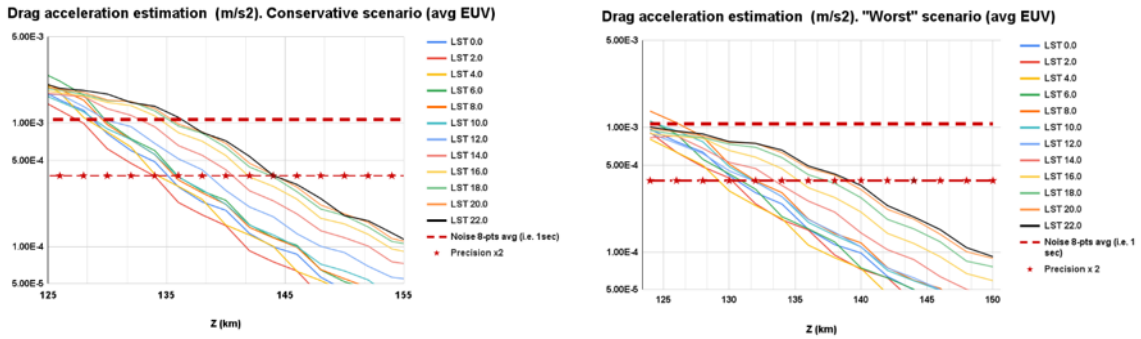

Figure 8.5.3 – *Drag acceleration estimated at the time of the pericentre passes, at latitude 60° N and different local time conditions as indicated, assuming a conservative scenario (left) and a worst-case scenario (e.g., lower densities than predicted) (right). The red dotted line shows the cut-off threshold of in-situ density detection assuming an accelerometer noise similar to that computed during Venus Express aerobraking or a value half that of the VEx computed value (dotted line with stars).*

Additionally, in-situ atmospheric waves could be detected around 130–140 km from density perturbations extracted from background densities using hydrostatic density profiles, as was previously done with VEx aerobraking data (Muller-Wodarg et al., 2016). Similarly, during the aerobraking phases of the Mars Global Surveyor and Mars Odyssey missions (Crowley and Tolson, 2007), cross-track winds (east–west zonal winds) were computed, and the same approach could be followed for Venus' upper atmosphere layers, for the first time by estimating the aerodynamic and the inertia-related torques acting on the spacecraft.

[5] Note that at the time of writing, the Inertial Measurement Unit package on-board EnVision is not knows since there are still two competing S/C industry consortia.

Table 8.5.1 – *Aerobraking phase goal science products.*

G2-C-70	**Aerobraking phase goal science products:** 1) Infer atmospheric density between 130 and 150 km, provided that the spacecraft accelerometer data precision is < 10^{-5} m/s^2; 2) Infer temperature information using the derived scale height H = kT/ mg; 3) Detect waves from density perturbations extracted from background densities using hydrostatic density profiles around 130–140 km; 4) Study seasonal and local time effects on the atmospheric pressure and temperatures; 5) Measure densities at altitude range between 140 and 180 km with POD measurements (i.e., requiring antenna communication); 6) Determine mass density and detect gravity waves at altitudes above 160 km by measuring the torque of the S/C in response to different orientation of the solar panels in the RAM direction; 7) Determine wind from the spacecraft attitude and orbit control system data (provided that the spacecraft is longitudinally and aerodynamically stable in pitch and yaw); 8) Acquire high-resolution local gravity field from frequent track of the spacecraft and the pericentre at the lowest altitude possible.

8.5.3. SRS lightning detection

The possibility to detect lightning on Venus is of high importance, since this phenomenon can be associated with events such as volcanism and atmospheric convection impacting the atmospheric evolution (Lorenz, 2018). Although designed for subsurface analysis, the EnVision SRS has the intrinsic capability to detect lightning by measuring components of lightning-induced electromagnetic signals that are not cut-off by the ionosphere. In this way, SRS could enhance the investigation of Venus atmospheric properties (i.e., physical, chemical, and dynamical processes) that are a product of the present and past climate and activity.

Due to the lack of spatial and temporal coverage, previously potential lightning detections on Venus have not been linked to specific locations, times, atmospheric conditions, or surface phenomena. Given that lightning is a sporadic phenomenon, the long duration of the EnVision mission increases the opportunity of observing the atmosphere and thus the probability of both lightning detection and their triggering mechanisms. SRS should be able to detect lightning when operated in a dedicated receiving only mode, picking up electromagnetic signals induced by this kind of events. SRS could potentially also be able to detect lighting in the standard active mode, mainly exploiting the margins of the receiving window where there are no subsurface echoes. However, this is a less reliable detection scenario.

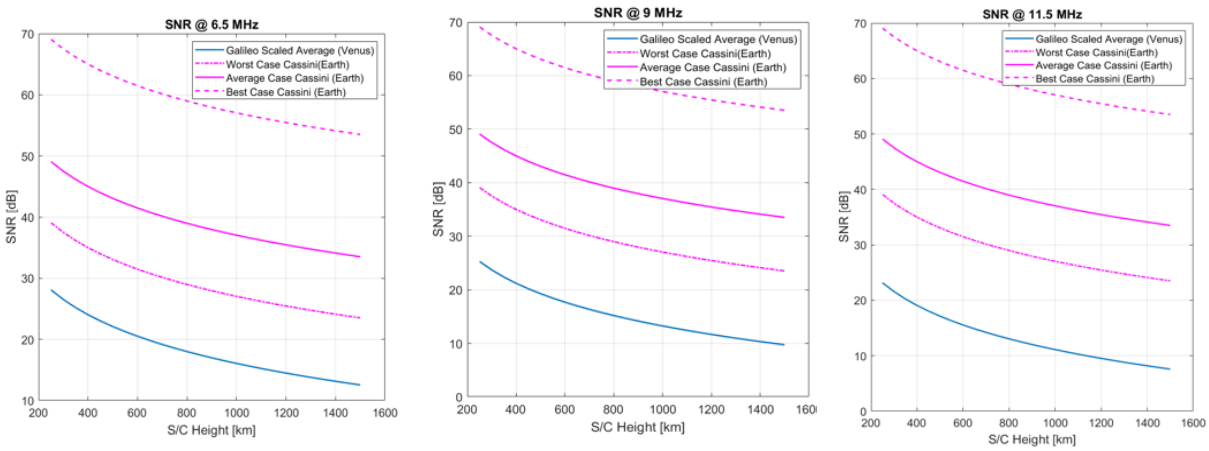

(a) (b) (c)

Figure. 8.5.4 – *Estimated SNR of SRS lightning detection vs EnVision spacecraft. (a) f = 6.5 MHz; (b) f = 9 MHz; (c) f = 11.5 MHz.*

The capability of SRS to detect lightning signals has been studied in detail, defining the requirements on the related instrument parameter values. As reported in the literature (Gurnett et al., 1991; Le Vine, 1986), the strength of the lightning signal depends mainly on the frequency of the measurement (as $1/f^2$), and the range of altitudes at which the lightning signal is generated ($1/R^2$). The analysis method has been applied to observations of radio plasma waves instruments on Galileo and Cassini. Only for the Galileo dataset, potential lightning events during

its Venus flybys were found. Since there is no consensus in the science community whether Venus lighting events have been detected, the analysis also considered the many certain lighting events measured by Cassini in the Earth flyby. From these data, it is possible to derive the expected power spectral density of lightning signal at the SRS receiver by correcting the differences between the SRS and Galileo/Cassini instruments. This analysis shows that the SNR of lightning (with respect to the galactic noise) is about 25 dB (scaled from Galileo) and about 50 dB (scaled from Cassini). The reliability of this analysis depends on the validity of the following assumptions: (1) that Galileo signals were caused by lighting (Lorenz, 2018; Gurnett et al., 2017); and (2) that the Cassini Earth flyby data are representative of the Venus case (Zarka et al., 2004). The SNR analysis shown in Figure 8.5.4 shows that SRS could detect lightning with large SNR across its frequency range and within the spacecraft operational heights.

Another relevant feature of lightning is that the duration of the lightning signal is between hundreds of milliseconds and seconds. Since the sampling time of SRS is $\Delta t \sim 0.08\,\mu s$, potential lightning signal would appear in several range samples and in several consecutive pulses. This makes the detection capability more robust.

Table 8.5.2 – *SRS lightning detection geographical / local time distribution of goal science products.*

G2-C-80	Measure the **occurrence of and geographical distribution of lightning**: 1) Any location at Venus is suitable; 2) Any local time is suitable, since previous claimed detections of lightning detection were made at different locations and times of day, and there is a general lack of spatial and temporal lightning observations.

8.5.4. VenSpec-H polarization

The sunlight reflected from the Venus cloud deck towards the spacecraft will have some degree of polarization due to the scattering by the cloud. In the past, polarization measurements of Venus have been performed at different wavelengths, and a modelling study in support of the VenSpec-H instrument development showed that polarization plays a significant role at the wavelengths observed by VenSpec-H at the Venus dayside. It was therefore decided to included polarization filters to complement the VenSpec-H dayside measurements, both to correct the spectra for potential biases caused by cloud deck polarization, and to enable VenSpec-H cloud aerosol optical properties products, such as aerosol altitude, size, and composition (see also Chapter 2, Section 2.3.8; and Chapter 3, Section 3.5.3).

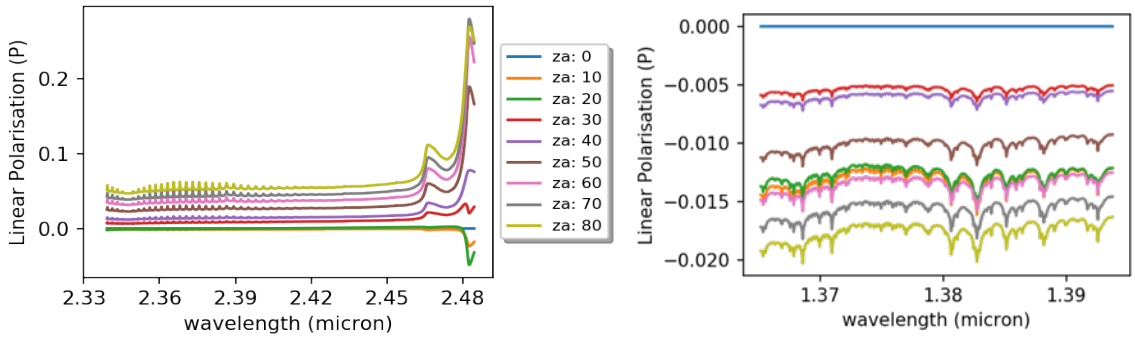

Fig. 8.5.5 – *Simulated degree of linear polarization for Venus nadir dayside observations. Left, VenSpec-H Band 2 and right VenSpec-H Band 4. Color indicates solar zenith angle. Here, in the plane of incidence, the degree of linear polarization is P=-Q/I.*

The simulations of the polarization state in VenSpec-H Bands 2 and 4 are presented in Figure 8.5.5, as a function of the solar zenith angle and wavelength. In addition, this modelling shows that the polarization arriving at the entrance of the instrument is well approximated by just two Stokes components out of four, namely the total radiance and the linear polarization in the scattering plane.

Although the VenSpec-H detector is not sensitive to polarization, the optical elements are. Therefore, the radiance reaching the detector can depend on the radiance and polarization of the light entering the instrument. The Polarization Sensitivity (PS) is the property of the instrument designed used here, to characterize the impact the instrument's performance.

If not accounted for, the correlation between the polarization and molecular absorptions would lead to errors in the retrieved abundance. To keep this bias below 4%, as allocated in the VenSpec-H total error budget, the required PS for the instrument would need to be below 1%. To achieve this, it would have been necessary to add an additional optical element (e.g., a scrambler) in the instrument. This solution was rejected, as it would have added to the instrument complexity and costs.

Alternatively, by combining measurements taken with and without a polarization filter, it is possible to correct the radiance for the degree of polarization. This method takes advantage of the fact that the polarization state is approximated by two Stokes components, and that the angles of the spacecraft/instrument with respect to the orbit and planet are known. By combining the two measurements (with and without a polarization filter), the radiance bias is reduced to near zero and the SNR is only slightly reduced. Since the VenSpec-H dayside SNR is far higher than the science requirement, the reduced SNR as a result of the polarization filters is acceptable, still allowing the trace gas observation accuracies to be compliant. The additional benefit is knowledge of the degree of polarization, which can be used for characterizing atmospheric aerosols, as stated above.

8.5.5. Long-term Observation of the Venus Ionosphere

The photochemical region of the Venus ionosphere consists of two major layers (Figure 8.5.6). The V1 layer at 110 km altitude is formed by photochemical processes driven by solar X-rays and secondary ionization, whereas the main V2 layer at 140 km is formed by solar EUV ionization (e.g., Peter et al. 2014; Girazian et al. 2015). Below the V1 layer, sporadic electron density peaks above the noise level of about 1,000 el/cc (where 1 el/cc = 1 electron / cubic centimetre = 10^6 electrons m^{-3}) occur. These were originally thought to be caused by infalling meteors (Pätzold et al., 2005, 2009), but was later shown to be caused by solar hard X-rays penetrating deep into the atmosphere below 110 km altitude (Peter et al., 2021). Plasma transport becomes the dominant process above approximately 200 km altitude. The formation, location, and appearance of the ionopause, the balance altitude between the dynamic solar wind pressure and the internal pressure of the ionosphere, depends on the individual characteristics of the solar wind and solar radiation flux (Brace and Kliore, 1991; Peter et al., 2021).

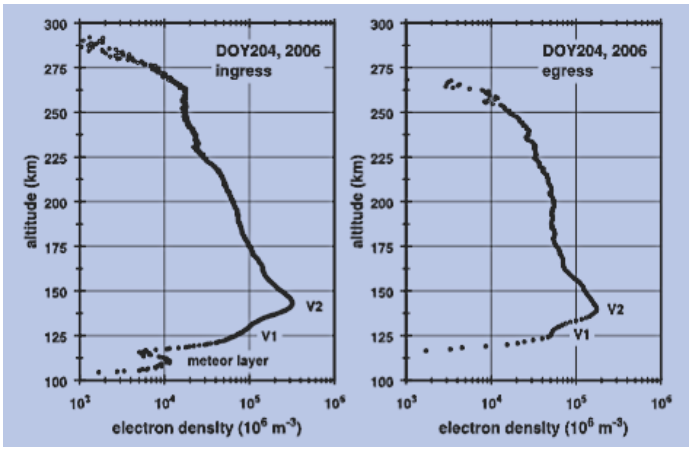

Figure 8.5.6 – *Electorn density profiles in the Venus ionosphere, as observed by the Venus Express VeRa experiment in 2006: The prominent V1 and V2 layers are located in the transport region, and the ionopause is visible as a steep where the density decreases towards the noise level. In the left panel, also another layer is visible below the V1 layer. This was originally thought to be caused by infalling meteors, but it was later concluded that it is most likely is caused by flaring of solar hard X-rays. (from Pätzold et al., 2009).*

The dynamics of the interaction between the Venus plasma system and the solar wind strongly depend on the solar radiation flux, which may vary along the Venus day, year, and solar cycle. Since the first extensive Venus ionosphere observation by Pioneer Venus Orbiter (PVO) during solar cycle 21 (Kliore et al., 1979), the strength of the solar cycles are gradually decreasing. Radio occultation experiments reveal the vertical total electron density distribution representing the proxy of the total vertical plasma density distribution (Pätzold et al., 2007, 2009, 2016; Peter et al., 2014, 2021). Currently, there are three major datasets of the Venus ionosphere: (i) PVO from 1979 to 1990 (Bauer et al., 1985), a dataset of 150 profiles; (ii) the Venus Express VeRa data set of about 900 profiles from solar cycle 23 (2007 to 2014) (Pätzold et al., 2007; 2009); and (iii) the Akatsuki data set of about 100 profiles from solar cycles 24/25 (since 2017 and ongoing) (Imamura et al., 2011). Potential EnVision observations of the ionosphere would extend these long-term observations into solar cycle 26.

PVO and VEx sounded the Venus ionosphere at two frequencies, a measurement that is imperative to extract the true plasma contributions on the downlinked radio signal (Pätzold et al., 2007). EnVision is perfectly equipped to make ionospheric observations by using the two coherent X-band and Ka-band radio frequencies stabilized by an Ultra-stable Oscillator (USO). For proper operations, the observation must start well before the downlink signals propagate through the ionopause at about 300 km. This altitude, however, varies strongly with time due to the varying solar wind/solar radiation flux dynamics, and cannot be predicted.

By starting the ionospheric observations a few minutes earlier than the atmospheric radio occultations, or starting even at 400 km altitude before geometric occultation, the sounding of the ionosphere over its entire structure from the ionopause to the base at 100 km altitude is possible. This would provide: (i) robust information on the electron density distribution in the V1 and V2 layers as a function of Solar Zenith Angle (SZA) over the course of the Venus day, year, and solar cycle, extending the PVO, VEx, and Akatsuki observations from previous solar cycles; (ii) improved statistics on the occurrence of sporadic electron density peaks below V1; (iii) information for the modelling of the Venus ionosphere from the ionopause, through the transport region in the ionospheric topside, to the V2 and V1 layers and below; (iv) the total electron content of the vertical ionosphere; and (v) the lateral electron density content as a direct measurement. It should, however, be noted that the EnVision RO observations are currently limited to altitudes below 200 km.

8.5.6. Solar Corona Sounding

Venus undergoes superior and inferior solar conjunctions with respect to Earth every synodic period of 583.92 Earth days (just over 19 months, Table 8.5.3). During a superior conjunction (Sun–Earth–Planet, or SEP, angle <10°), when Venus appears to be behind the solar disk in the plane-of-sky as seen from Earth, the radio signals from a spacecraft orbiting Venus must propagate through the solar corona. The turbulent coronal plasma induces strong random phase shifts on the radio carrier frequencies, “seen” in the receiver as apparent frequency noise. This noise increases with decreasing SEP angle, or decreasing distance of the radio ray path to the solar limb in the plane-of-sky.

Starting at an SEP angle of <15°, the increasing frequency noise will affect the occultation and gravity observations. The frequency noise increases dramatically within SEP <10°. The capability for dumping telemetry and sending commands is seriously degraded within SEP <3°, which is usually a quiet time for spacecraft operations. However, the time when Venus and EnVision are within SEP <10° could be used for studies of the solar corona, as done since the start of interplanetary spaceflights (Pätzold et al., 2012 and references therein). The MEx, Vex, and the Rosetta missions have performed such observations since 2004, covering almost 1.5 solar cycles in total(Pätzold et al., 2012) and (Pätzold et al., in prep.).

EnVision is perfectly equipped for these observations, which could be performed in a two-way mode at X-band uplink and X- and Ka-band coherent downlinks. The observables would be the received signal power and the range and frequency at both radio carriers. The science objectives of these observations would be to obtain: (i) the mean coronal electron density distribution as a function of distance from the solar limb(s) (Volland et al., 1977; Muhleman and Anderson, 1981; Anderson et al., 1987; Bird et al., 1994; Pätzold et al., 1995, 1997, 2012); (ii) the turbulence level of the coronal plasma (e.g. Efimov et al., 2010a, 2010b); (iii) the solar wind velocity in the acceleration region (e.g. Armstrong and Woo, 1981); and (iv) morphology of coronal mass ejections (CMEs), which can be extracted cleanly from coronal sounding data (Pätzold et al., 2012).

Table 8.5.3 – *EnVision superior and inferior solar conjunctions.*

Superior solar conjunction								Inferior solar conjunction			
Days of Year								Days of Year			
year	ingress			Sup. Conj. day	egress			Year	Ingress	Inf. Conj. day	egress
	<15° SEP	<10° SEP	<3° SEP		>3° SEP	>10° SEP	>15 SEP		<15° SEP		>15° SEP
2035	163	184	210	220	230	257	276	2036	141	151	161
2037	020	042	071	082	093	120	140	2037/2038	360	004	013
2038	235	253	281	290	300	329	350				

9. Management

9.1. Overview of Mission Management and Implementation

The overall EnVision mission management scheme is summarised in Figure 9.1. The overarching responsibility for the EnVision mission rests with ESA's Directorate of Science. ESA responsibilities cover the mission architecture, the development and procurement of the spacecraft, the satellite integration and test activities, the launch services procurement, and the mission and science operations. The ESA ground segment includes the Mission Operation Centre (MOC), the Science Operations Centre (SOC), and the ground stations network. The Science Ground Segment (SGS) is composed of the SOC, which includes the Planetary Science Archive (PSA), and contributions from the instrument teams.

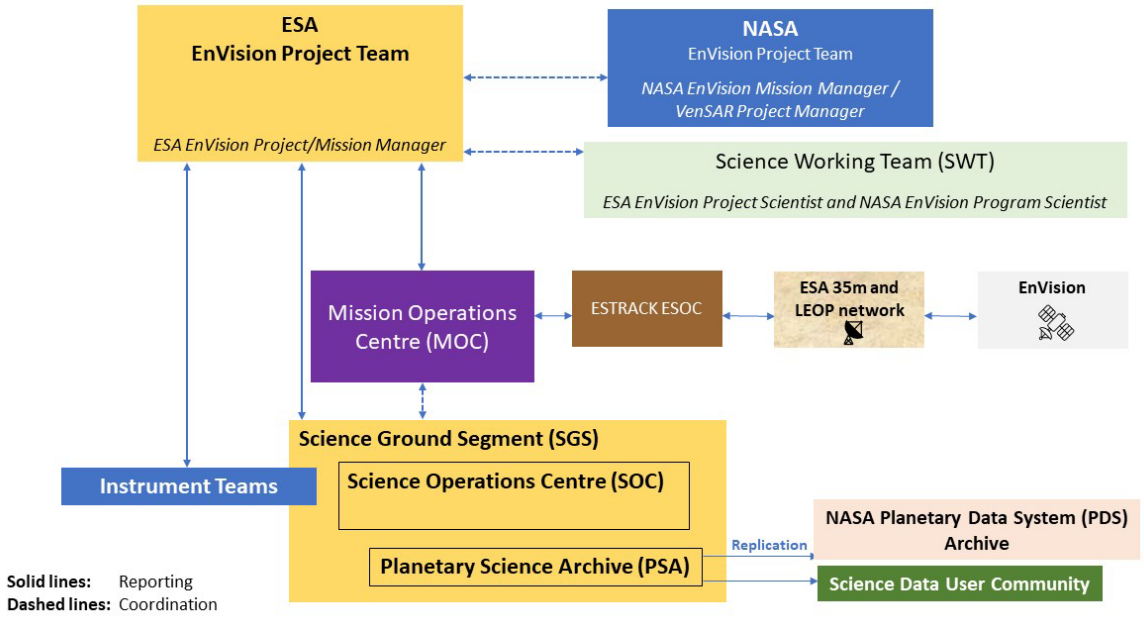

Fig. 9.1 – *Overview of the EnVision mission management scheme.*

During the development and commissioning phases, an ESA-appointed Project Manager (PM) will be responsible for implementing and managing ESA's activities. After a successful commissioning review, a Mission Manager (MM) will take over the responsibility for the mission throughout its nominal and any extended phases.

The scientific instruments are provided by ESA Member States, within the remit of a Multi-Lateral Agreement (MLA), including ESA and the national Funding Agencies. ESA Member States are also responsible to support payload safety, maintenance and operations throughout the mission and to provide contributions to the SGS.

The EnVision mission relies on the partnership with NASA, providing the VenSAR payload, a Ground System for the VenSAR instrument, DSN support for selected mission critical phases and science contribution, within the remit of an ESA-NASA Memorandum of Understanding (MOU).

The EnVision 'Science Management Plan' (SMP, ESA 2023a) describes the approach that will be implemented, including the data policy (see Table 6.3.1) and the opportunities for participation in the mission, up to and including the post operational phase, to achieve the mission's scientific objectives and to optimise its scientific return. An EnVision Science Working Team (SWT) will be appointed by ESA in coordination with NASA after the mission has been adopted. The ESA EnVision Project Scientist and the NASA EnVision Program Scientist will co-chair the SWT. The co-chairs act as the scientific interface to the ESA Project/Mission Manager and NASA EnVision Mission Manager and VenSAR Project Manager in their respective organizations. The SWT will advise ESA and NASA on all aspects of the mission potentially affecting its scientific performance, and will be asked to review top-level requirements (in all areas of the project) that impact science return and assist in potential mission requirements trade-offs. It will assist the ESA EnVision Project Scientist and the NASA

EnVision Program Scientist in maximising the overall scientific return of the mission within the established boundary conditions. It will act as an EnVision mission focal point for the scientific community.

The SWT will consist of the following members:

- Instrument Lead Scientists;
- One Instrument Co-Lead Scientist per instrument team, if relevant;
- Interdisciplinary Scientists.

The SWT may be supported by working groups, which will be established by the SWT as needed. Further details of the EnVision science management and SWT are provided in (ESA, 2023a).

9.1.1. Project Management

Following mission adoption, ESA will issue an invitation to tender (ITT) to the potential industrial contractors for the full implementation phase (called B2/C/D), aiming at the selection of the prime contractor and kick-off of industrial activities by November 2024 to meet the launch date of November 2031. The final industrial organization will be completed in Phase B2, mostly through a process of competitive selection and by taking into account geographical distribution requirements in place at the time. At the start of this phase, the project team in the Project Department of the Science Directorate will take over the overall ESA responsibility for implementing the mission. This team will be led by the Project Manager (PM). The PM will be supported by the Project Scientist (PS) who will have responsibility for science-related aspects of the mission.

Over the course of the implementation phase, the project team will conduct a System Requirements Review (SRR), a Preliminary Design Review (PDR), a Critical Design Review (CDR) and finally a Flight Acceptance Review (FAR). The responsibility for the EnVision mission will transfer from the PM to the Mission Manager (MM), located at ESA-ESAC, following the successful commissioning of the satellite and scientific payload. The PS will continue to support the mission throughout the operations and post-operations phases. Further details of the ESA mission and science operation tasks is provided in chapter 6.

9.2. Development plan

9.2.1. S/C Model Philosophy

The spacecraft development plan is based on a Proto Flight Model (PFM) development approach. A satellite Structural Model (SM) will be developed, aiming at mechanical qualification of the structure and will be refurbished into a Proto-Flight Model (PFM). A functional Avionics Model is foreseen for the functional validation of EnVision, interfacing with the engineering models of the main electronic units at platform and payload levels. All payload teams will deliver instrument models of adequate detail to fully support the system tests with each model. The satellite level thermal and Electromagnetic and Mechanical Compatibility (EMC) qualification will both be achieved on the satellite PFM in line with ESA standards for proto-flight element level testing. Spares would be manufactured depending on criticality and would range from sub-unit to spare kit level.

EnVision relies on fully flight validated thermal hardware in high temperature environments, and all space segment equipment will be fully thermally qualified prior to their integration on the PFM. The spacecraft will therefore proceed through a PFM thermal campaign composed of thermal balance tests and thermal vacuum, with an acceptable level of risk.

9.2.2. Schedule

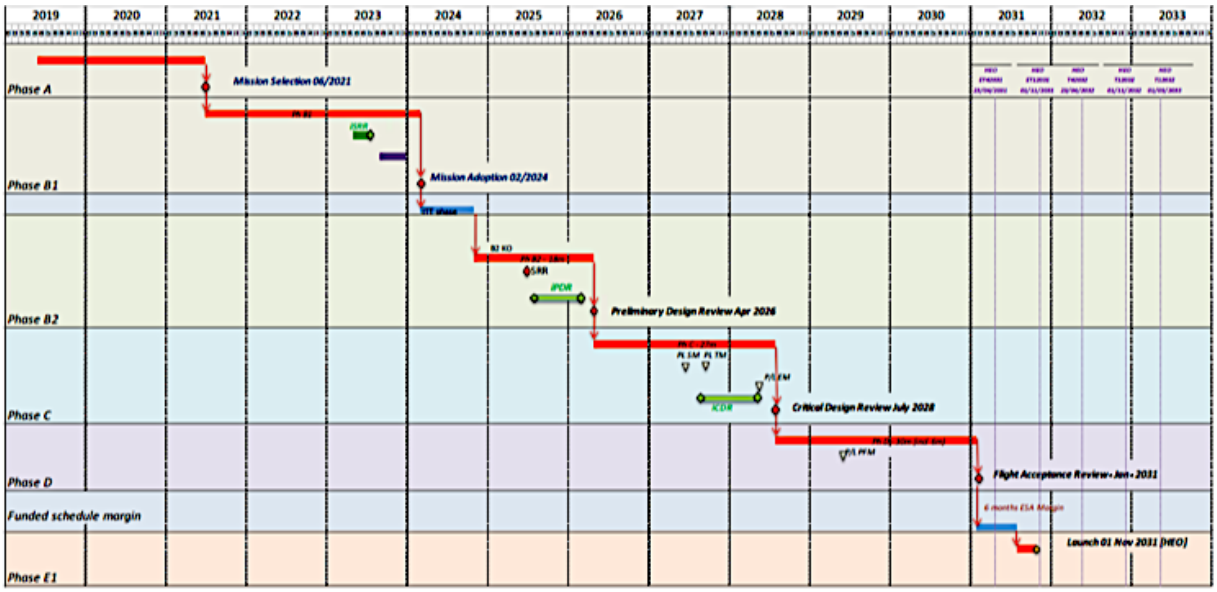

Figure 9.2.1 – *EnVision Master development schedule.*

9.3. Critical Elements and Risk Mitigation

9.3.1. Operational risks linked to the HEO launch strategy

The baseline Highly Elliptical Orbit (HEO) launch strategy comes with a certain number of additional operational risks compared to the direct escape launch strategy envisaged in the earlier feasibility phase of EnVision (Figure 9.3.1).

1. **-** During the first weeks of the mission, the spacecraft has to perform several critical manoeuvres, such as a Pericenter Raising Manoeuvre (PRM) in case of defavourable luni-solar gravitational perturbations, and an Earth Escape Manoeuvre (EEM) to put the spacecraft on its interplanetary course towards Venus. A failure in performing the PRMs or EEM would lead to loss of mission (and loss of spacecraft in the case of the PRM);
2. - Potential occurrences of collision risk events with objects in Earth orbit (space debris or other operating spacecraft) as the spacecraft performs multiple revolutions in Earth orbit;
3. - Multiple crossings of the Earth radiation belts, with the subsequent impact in radiation dose and potential unavailability of critical spacecraft sensors, such as star trackers;
4. - The Main Engine needs to be primed for use in Earth orbit, and re-ignited 15 months after the Escape Manoeuvre for the Venus Orbit Insertion (VOI). This poses some constraints on the main engine operational concept which do not exist in the direct escape case.

To mitigate the risks linked to the inclusion of mission-critical manoeuvres in the post launch phase, the following strategy is implemented :

1. - The mission is designed to be compatible with any two missed PRM slots during HEO phase. In practice this leads to exclude from the launch period the launch opportunities which would require a PRM in the first orbit after launch, and to choose the launch period and HEO orbit such that, in case a PRM is needed to avoid re-entry, two back-up slots are available at the following perigees without leading to re-entry of the S/C;
2. - the mission is designed such as to offer a back-up slot for the Insertion Correction Manoeuvre (ICM) and Earth Escape Manoeuvre (EEM). This means that in case of missed EEM, the mission profile could be adapted to recover the incurred delta V penalty by starting from a higher aerobraking orbit, at a cost of a longer aerobraking duration. The S/C is designed to be compatible with a starting aerobraking orbit with an orbital period of up to 36 hours while in the nominal case only 12 hours is required. This buffer

is sufficient to absorb, in a contingency scenario, an additional delta V incurred by a back-up EEM manoeuvre.

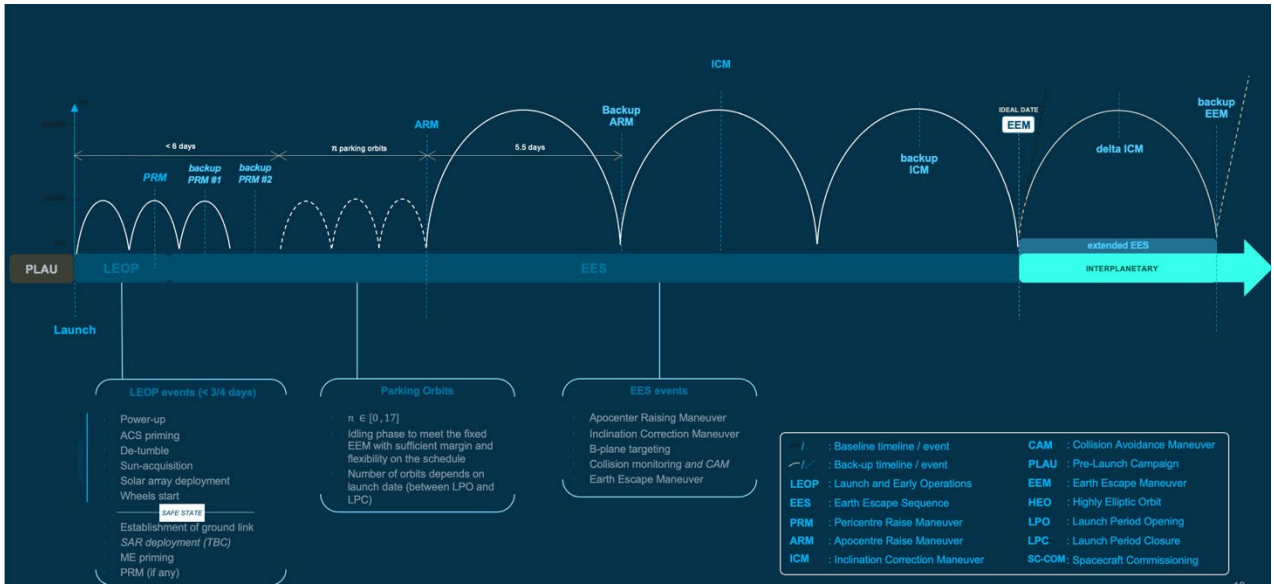

Figure 9.3.1 – *Illustration of the HEO phase timeline, with the sequence of orbital phases and orbital manoeuvres required.*

9.3.2. Risks linked to the Aerobraking environment

The aerobraking technique is well mastered by ESA, as it has been tested experimentally on ESA's Venus Express in 2014, and successfully implemented on the recent ESA's ExoMars Trace Gas Orbiter mission. The knowhow acquired in those missions will directly benefit the EnVision mission, and reduce the operational risks. Early aerobraking risk reduction has already been achieved during phase B1 by specific characterization and testing of the foreseen surface materials (e.g. MLI) and their thermal performance with the planned aerobraking profile in terms of thermal loads and atmospheric conditions (e.g. atomic oxygen). The tests performed, in particular at ESA-ESTEC, have confirmed the existence of materials compatible with such an environment, that there are no showstoppers, and the existence of relevant facilities to provide a representative testing environment (Figure 9.3.2).

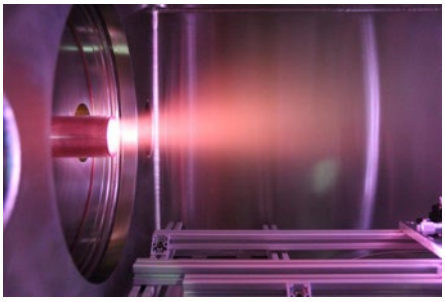

Figure 9.3.2 – *LEOX facility at ESTEC used to generate realistic Atomic Oxygen and high Temperature environment for material de-risking.*

9.3.3. Risks linked to the High Thrust Engine

Given the high gravitational parameter at Venus, the insertion manoeuvre is far from instantaneous, and therefore results in high gravity losses when using standard thrust to mass ratios. Given the mass constraints on EnVision, having a high thrust and high ISP main engine is a must in order to reach the required science orbit within an acceptable aerobraking duration. A 1 kN bipropellant engine, currently in development under ESA funding, is currently at TRL5. Being potentially schedule-critical, and following the EnVision Mission Selection Review recommendations, ESA has placed a technology development activity with the engine manufacturer to qualify this engine to the EnVision environment as early as possible. This is done to avoid this development to be on the critical path of the mission. In the event that this engine would not be ready on time, the spacecraft design is compatible with a back-up main engine from the United States, with a slightly lower thrust (890 N) and ISP. The use of this less capable, but high TRL engine, results in slightly longer aerobraking duration, but still compatible with the aerobraking environmental envelope defined for the spacecraft.

9.3.4. Risks linked to the Launcher

Several risks are linked to the launcher, Ariane 62. One risk is linked to the uncertainty on the Ariane 62 performance, the launcher maiden flight being planned only in 2024. An under-performance of the launcher can be accommodated in the current mission design by targeting a higher aerobraking orbit period than nominally planned, at a cost of a longer aerobraking duration. An additional mitigation at mission level is the possibility to launch the spacecraft on the more powerful Ariane 64 launcher and the spacecraft is designed to be compatible with the environmental loads of the Ariane 64 launcher, and with a direct escape strategy, which would also mitigate the HEO risks mentioned in Section 9.3.1.

9.3.5. Cost risks mitigation

The mission cost is capped by the ESA M5 allocated budget. Maintaining the cost of the mission under control is a critical requirement, and is achieved in particular by relying on mature technologies at ground and space segment levels, with significant heritage from the most recent ESA science missions such as BepiColombo, EUCLID and Solar Orbiter. Technology pre-development activities have been initiated since phase A for critical mission aspects, linked to high data rate deep space communications (at ground segment levels), aerobraking, high thrust main engine, and instruments. The maturity of all critical technologies has been confirmed via a Technology Readiness Assessment performed by ESA ahead of the MAR, confirming TRL of at least 5 for most of them.

In case of cost overrun, a possible mitigation at mission level is the reduction by one cycle of the nominal science mission duration, which would reduce operational costs and still guarantee compliance to all science requirements, however with low margin.

9.3.6. Risks on data return and science performance

The mission needs to return a high data volume to fulfil its science objectives. To achieve this, the mission relies on a regular, daily use of the ESTRACK 35 m ground stations, and on a stable operations planning (long-term planning cycle). Any short-term perturbation to the planning (e.g. non availability of ground station at the planned slot, delayed ground station acquisition, or complete loss of contact due to ground station failure, for example) pose a risk on the science data return. This risk is mitigated at various levels by

(1) oversizing the on-board solid state mass memory to cope with a worst case for such contingency occurring at the period of highest data rate (when Earth is the closest to Venus),
(2) (2) by considering a 30% system margin on the instruments data rates, which result in a de facto margin on the SSMM sizing,
(3) (3) by the introduction of regular SSMM offload sessions based on offline arraying of two of ESA's Deep Space Antennas. This technique allows to absorb extra downlink capacity without modifying the observation plan, and is explained in more details in chapter 5.5
(4) (4) by nominally targeting a significantly higher data return than actually required (e.g. the achieved stereo performance is 26.3% for a requirement of 20%). The robustness of the strategy against various degraded downlink cases is presented in chapter 7.5.

10. Communication and Outreach

EnVision will be an exciting mission, and provides an exceptional opportunity to engage and educate the general public as well as inspire students of all ages in the excitement of scientific discovery and planetary exploration. Venus already has great name recognition among the general public, and is an easy planet to "recognise" as Earth's nearest neighbour being the brightest object in the sky after the Sun and the Moon. The story of how Earth and Venus diverged in their evolution, and discussions of what may or may not trigger a runaway greenhouse effect, are similarly engaging in an era where our own changing climate is of increasing public interest. At the same time, these science questions offer an opportunity to highlight the wider work which ESA and NASA are doing in the Earth and Space Science domains.

As described in the EnVision SMP (ESA, 2023a), ESA, in coordination with NASA, will have responsibility for the science communications, educational and outreach activities related to EnVision. They will be supported by the EnVision instrument teams, and the Science Working Team (SWT).

ESA are hosting several web sites with information about the EnVision mission, such as:

- https://www.esa.int/Science_Exploration/Space_Science/EnVision_factsheet and
- https://www.cosmos.esa.int/web/envision/

The EnVision Science community is also hosting a mission website:

- https://envisionvenus.eu/envision/

EnVision images and videos published by ESA are available on the ESA web pages (see Section 10.2.1), and on the ESA social media channels such as Instagram and X.

The EnVision scientific data will be made publicly available via the

- ESA Planetary Science Archive (PSA) and the
- NASA Planetary Data System (PDS) archive

in-line with the EnVision Science Management Plan (SMP, ESA 2023a) agreements. The ESA EnVision project scientist and the SWT, the EnVision project, and the EnVision instrument and science community also typically support public talks, citizen science projects, art, and educational projects.

Figure 10.1.1 – *Screenshots from films produced for the European Commission* EuroVenus *project (FP7 G.A. 606798, 2013-2016). EnVision public outreach will build on this experience. https://www.whitefoxpictures.com/portfolio-item/eurovenus/.*

11. Reference documents and supplementary material

11.1. List of Acronyms

A/B	Aerobraking (mission phase)
ADEV	Allan Deviation
AER	Aerobraking
AIT/V	Assembly, Integration and Test/Verification
AKE	Absolute Knowledge Error
AOCS	Attitude and Orbit Control System
APE	Absolute Pointing Error
ASI	Agenzia Spaziale Italiana
ASIMUT	[-ALVL] Radiative transfert code at BIRA-IASB
BIRA-IASB	Royal Belgian Institute for Space Aeronomy
BFPQ	Block Floating Point Quantization
BOL	Begin of Life (Component)
CCSDS	Consultative Committee for Space Data Systems
CCU	Central Control Unit
CDMU	Central Data Management Unit
CDR	Critical Design Review
CFDP	CCSDS File Delivery Protocol
CFRP	Carbon Fibre Reinforced Polymer
CMA	Cost Model Accuracy
CME	Coronal Mass Ejection
CNES	Centre National d'Études Spatiales
CP	Chemical Propulsion
CRIS	Carrier Relay Imaging Spacecraft (DAVINCI)
CUVIS	Compact Ultraviolet Imaging System (DAVINCI)
DAVINCI	NASA Deep Atmosphere Venus Investigation Of Noble Gasses, Chemistry, and Imaging
DDR	Double Data Rate (SDRAM memory)
DEM	Digital Elevation Model
DES	Digital Electronics Subsystem
D/H	Deuterium to Hydrogen isotopic ratio
DLR	Deutsches Zentrum für Luft- und Raumfahrt
DMM	Design Maturity Margin
DoF	Degree of Freedom
DS	Descent sphere (DAVINCI)
DSN	Deep Space Network (NASA)
DSP	Digital Signal Processing
DST	Deep Space Transponder
ECM	Eccentricity Control Maneuver
EEM	Earth Escape Manoeuvre
EIRP	Effective Isotropic Radiated Power
EMC	Electromagnetic Compatibility
EOL	End of Life (Component)
ESA	European Space Agency
ESAC	European Space Astronomy Centre
ESOC	European Space Operations Centre
ESS	Extendible Support Structure
ESTRACK	European Space Tracking Network
EUV	Extreme UV radiation
FAR	Flight Acceptance Review
FPR	Fully Polarimetric Radar
FoV	Field of View
gal	1 Gal (symbol) = 1 gal (unit) = 0.01 m s^{-2}
GaAs	Gallium arsenide
GaN	Gallium nitride
GCM	General Circulation Model
GNC	Guidance, Navigation and Control
GS	Ground Segment
GSE	Ground Support Equipment
HDRM	Hold-Down and Release Mechanism
HEO	Highly Elliptical Orbit (or High Earth Orbit)
HF	High Frequency
HGA	High Gain Antenna
HH and HV	Horizontal and Vertical Polarization
HKTM	House-Keeping TeleMetry
ICM	Insertion Correction Manoeuvre
ICRF	International Celestial Reference Frame
IFOV	Instantaneous Field of View
ILS	Instrument Lead Scientist
IMU	Inertial Measurement Unit
InSAR	Interferometric Synthetic Aperture Radar
IR, nIR	Infrared, Near-Infrared
ITP	Interplanetary Transfer Phase
ITT	Invitation To Tender
JPL	Jet Propulsion Laboratory
kN	1 kN = 1 kilonewton = 10^3 N
LEO	Low Earth Orbit
LEOP	Launch and Early Operations (or Orbit) Phase
LOD	Length of Day
LT	Local Time
LTP	Long Term Planning (Operations)
MAR	Mission Adoption Review
MHz	1 MHz = 1 megahertz = 10^6 Hz
MLA	Multi-Lateral Agreement
MLI	Multi-Layer Insulation
MLP	Mission Level Planning (Operations)
MMH	Monomethylhydrazine (Propellant)
MNR	Multiplicative noise ratio
MOC	Mission Operations Centre
MoI	Moment of Inertia
MON	Mixed oxids of nitrogen (Propellant)
MOP	Mission Operations Plan
mrad	1 mrad = 1 milliradian = 10^{-3} rad

MRO	Master Reference Oscillator
MSR	Mission Selection Review (ESA)
NASA	National Aeronautics and Space Administration
Near-IR	Near Infrared radiation
NECP	Near Earth Commissioning Phase
NESZ	Noise equivalent sigma zero (σ_o)
NIMS	Near Infrared Mapping Spectrometer (Galileo)
NIR	Near Infrared radiation
NISAR	NASA/ISRO Synthetic Aperture Radar
OCC	Operations Control Centre
OGS	Operational Ground Segment
OSR	Optical Surface Reflectors
OWLT	One-Way Light time
PDR	Preliminary Design Review
PDS	Planetary Data System
PFM	Proto-Flight Model
PM	Project Manager
POD	Precise Orbit Determination
ppb	parts per billion
ppm	parts per million
PRF	Pulse Repetition Frequency
PRM	Pericenter Raising Manoeuvre
PS	Project Scientist
PSA	Planetary Science Archive
PVO	NASA Pioneer Venus Orbiter
RCS	Reaction Control System
RF	Radio Frequency
RIU (1)	Remote Interface Unit
RIU (2)	Rheinischen Instituts für Umweltforschung
RMS	Root Mean Square
RoI	Region of Interest
RPE	Relative Pointing Error
RTM	Radiative Transfer Model
SADM	Solar Array Drive Mechanism
SAP	Science Activity Plan
SAR	Synthetic Aperture Radar
S/C	Spacecraft
SciRD	Science Requirements Document, ESA 2023c
SEP	Sun-Earth-Planet angle
SfM	Structure for Motion (DAVINCI)
SGS	Science Ground Segment
SIFT	Scale-Invariant Feature Transform
SMM	Shared Memory Model
SMP	Science Management Plan
SNR	Signal to Noise Ratio
SOC	Science Operations Centre
SOM	Spacecraft Operations Manager
SORD	Science Operations Requirements Document
SORS	Science Operations Reference Scenario
SSMM	Solid-State Mass Memory
SSPA	Solid State Power Amplifier
STP	Short Term Planning (Operations)
SWOT	NASA Surface Water and Ocean Topography
SWT	Science Working Team
SZA	Solar zenith angle
TEC	Total Electron Content
TGO	ExoMars ESA/Roscosmos Trace Gas Orbiter
T/R or TR	Transmit/Receive
TRL	Technology Readiness Level
TRP	Thermal Reference Point
TRQ	Torque (measurement technique)
TT&C	Telemetry, Track and Command
TWTA	Travel Waveguide Tube Amplifier
UCS	Unconfined Compressive Stress measurements
UHF	Ultra-High Frequency
USO	Ultra-Stable Oscillator
UV	Ultraviolet
VCD	Venus Climate Database
VCO	JAXA Venus Climate Orbiter (Akatsuki)
VERITAS	NASA Venus Emissivity, Radio Science, InSAR, Topography, and Spectroscopy
VEx	ESA Venus Express
VHF	Very-High Frequency
RSE	Radio Science Experiment
SRS	Subsurface Radar Sounder
VenSAR	Venus Synthetic Aperture Radar
VenSpec	Venus Spectroscopy (suite)
VenSpec-H	Venus Spectroscopy High Resolution
VenSpec-M	Venus Spectroscopy Mapper
VenSpec-U	Venus Spectroscopy Ultraviolet

Abbreviations:

Lat.	Latitude
Long.	Longitude

Molecular species:

CO	Carbon monoxide
CO_2	Carbon dioxide
COS	Carbonyl sulfide
H_2O	Water vapour
H_2SO_4	Sulphuric acid
HCl	Hydrogen chloride

HDO	Deuterated water
HF	Hydrogen fluoride
SO	Sulphur monoxide
SO_2	Sulphur dioxide

11.2. Glossary

Absorber: atmospheric constituent (in a gaseous or condensed phase) which significantly absorbs some incident radiation (e.g. solar, thermal infrared).
Allan Deviation (ADEV): Measurement of stability of the Ultra-Stable-Oscillator frequency for a given count time (square root of the two-sample variance of the signal frequency). After David W. Allan (b. 1936).
Altimetry: a technique for measuring height (here derived from the time taken by a radar pulse to travel from the s/c antenna to the surface and back to the s/c).
Apocenter: the point in a Keplerian orbit farthest from the center of mass, i.e. from the planet.
Basalt: a fine-grained dark basic volcanic rock consisting of plagioclase feldspar, a pyroxene, and olivine.
Block Floating Point Quantization: a form of data compression from 8 bits per sample to 4 bits per sample**.**
Cloud layer: atmospheric layer where condensed particulate matter (aerosols) are present, and contribute significantly to the opacity. On Venus, there are three main cloud layers, located between 48 and 70 km in altitude, straddling the troposphere/mesosphere boundary (tropopause).
Corona/coronae: oval-shaped features interpreted on Venus as the result of upwellings of warm material below the surface forming volcanoes and tectonic structures at the surface.
Cycle: a Venus cycle is defined as 243.023 Earth days, or 1 Venus sidereal day, the time it takes Venus to rotate 360 degrees on its polar axis in a celestial reference frame (ICRF). EnVision's quasi-polar orbit of ~92 min period is in a quasi-fixed celestial reference frame: a cycle of 243.023 Earth days is also the period for the orbit ascending node's equatorial longitude to increase from 0° to 360° in planetocentric coordinates, as the planet rotates westward.
Eccentricity: parameter describing how elliptical an orbit is. Ellipticity of zero denotes a circular orbit.
Emissivity: the ability of a surface to emit radiant energy compared to that of a black body at the same temperature and with the same area.
Extreme UV (EUV): Extreme UV radiation spanning wavelengths shorter than the hydrogen Lyman-alpha line, from 121 nanometers (nm) to the X-ray band of 10 nm.
Fault: a fracture or discontinuity in a volume of rock across which there has been displacement.
Felsic: adjective relating to a rock containing more light-colored minerals than other rocks, including feldspar, feldspathoids, quartz, and muscovite.
Fold: a continuous bent or curved rock resulting from crustal/lithospheric stress.
Granite: a light-colored coarse-grained acid plutonic igneous rock consisting of quartz, feldspars, and such ferromagnesian minerals as biotite or hornblende.
Hadean Period: Geologic eon extending -4.6 to -4 Ga preceding earliest known minerals on Earth.
High Frequency (HF): Range of radio frequencies extending from 3 MHz to 30 MHz i.e., from 10 to 100 m in wavelength.
Highland(s): elevated areas higher than 2 km above the mean radius (5091 km) of the planet. On Venus two large highlands: Ishtar Terra with the highest area (Maxwell Montes with an elevation >10km) near the North pole, and Aphrodite Terra forming a ~15,000 km long equatorial relief belt.
Hurst exponent: a single scalar value that indicates if a time series is purely random, trending, or mean reverting. After Harold Edwin Hurst (1880-1978).
Incidence angle: refers to the angle at which the sun's rays or radar waves strike the surface of the planet with respect to the normal to the surface.
Infrared window: spectral interval where gaseous absorption is small enough so that most of the thermal radiation originates from comparatively deeper atmospheric layers (or even from the surface).
k_2 Love number: gravitational potential modification due to the tidal deformation of the planet. After Augustus E. H. Love (1863-1840).
Ka-band: a nominal frequency range, from 26 to 40 GHz (0.8-1.1 cm in wavelength) within the microwave portion of the electromagnetic spectrum.
Local (solar) time (LT): Hour angle of the Sun as observed from a given point on Venus.
Lowland(s): flat areas at altitude < 0 km beneath the mean radius (5091 km) of the planet, covering ~20% of the planet surface.
Mafic: adjective relative to a rock containing more dark-colored mineral and iron than other rocks, including olivine, pyroxene.
Magma: molten material beneath or within the planetary crust/lithosphere, from which igneous rock is formed.
Magmatic: adjective related rocks derived from molten material beneath or within the planetary crust/lithosphere.
Master Reference Oscillator (MRO): A subsystem of the Telemetry, Track and Command (TT&C) system of the spacecraft, the MRO is designed to provide a stable frequency reference to the spacecraft Deep Space Transponder (DST) at the time scales of interest for the atmospheric experiment. It includes an Ultra Stable Oscillator (USO) that generates the base frequency using a high quality factor quartz crystal oscillator.

Meridian: any great circle joining the North and South poles of a planet.
Mesosphere: atmospheric layer at local thermodynamic equilibrium and where vertical energy transport is performed through thermal radiation only. On Venus, it corresponds to the 60-100 km altitude range.
Microwave: domain of the electromagnetic spectrum extending from 0.3 to 300 GHz i.e. from 1 mm to 1 m in wavelength.
Mineral: a class of naturally solid inorganic substances with a characteristic crystalline form and a homogeneous chemical composition. Their association forms a rock.
(volume) Mixing ratio: amount of an atmospheric constituent (in moles) divided by the total (in moles) of all other atmospheric constituents. For minor species, it is usually expressed in parts per million (ppm) or parts per billion (ppb).
Multiplicative noise ratio (MNR): a function of quantization noise and range and azimuth used in quantifying SAR imaging performance.
Nadir: the direction pointing directly below a particular location. The radar nadir refers to the downward-facing viewing geometry of an orbiting radar.
Near Infrared (Near IR or nIR) **:** Near Infrared radiation, 0.75 – 1.4 μm in wavelength, within the infrared portion of the electromagnetic spectrum (from the approximate end of the response of the human eye to that of silicon)
Noise equivalent σ_0 (NESZ): backscatter value equal to the instrument thermal noise level, used in quantifying SAR imaging performance.
Oxidation: chemical processes by which atoms lose electrons, combining a chemical substance with oxygen, resulting in an oxide.
Pericentre: the point in a Keplerian orbit nearest to the centre of mass, i.e. nearest to the planet
Plutonic: adjective related to rocks derived from magma that has cooled and solidified below the surface of the Earth, consisting of well crystallized minerals.
Polarimetry: an instrumental ability to measure different polarization signatures of every resolution element.
Polarization: orientation of the electric field vector in an electromagnetic wave, frequently 'horizontal' (H) or 'vertical' (V) in conventional imaging radar systems. Polarization is established by the antenna, which may be adjusted to be different on transmit and on receive. Reflectivity of microwaves from an object depends on the relationship between the polarization state and the geometric structure of the object.
Radiometry: a set of techniques to measure electromagnetic radiation. In its passive mode, VenSAR will perform microwave radiometry to record the thermal emission emanating from Venus's surface at 9.5 cm-wavelength.
S-band: a nominal frequency range, from 2 to 4 GHz (7.5-15 cm in wavelength) within the microwave portion of the electromagnetic spectrum.
Sidereal day: 1 Venus sidereal day of 243.23 Earth days is the time needed for Venus to rotate 360 degrees on its polar axis in a celestial reference frame (ICRF). The Venus sidereal day lasts longer than the revolution of Venus around the Sun (or Venus year, 224.667 Earth days).
Sigma nought (or Sigma zero) (σ_0): Scattering coefficient, the conventional measure of the strength of radar signals reflected by a distributed scatterer, usually expressed in dB. It is a normalized dimensionless number, comparing the strength observed to that expected from an area of one square meter. Sigma nought is defined with respect to the nominally horizontal plane, and in general has a significant variation with incidence angle, wavelength, and polarization, as well as with properties of the scattering surface itself.
Silicate: mineral consisting of SiO_2 or SiO_4 groupings and one or more metallic ions, with some forms containing hydrogen. Silicates constitute well over 90 percent of the rock-forming minerals of the earth's crust.
Spatial resolution: minimum distance interval required to detect spatial variations with a given imaging instrument.
Spatial sampling: distance interval between consecutive elements of an image *(pixels)* with a given imaging instrument. Should be at least twice smaller than the spatial resolution to avoid *undersampling*.
Spectral resolution: minimum frequency/ wave-length/ wavenumber interval required to detect spectral variations with a given spectroscopic instrument.
Spectral sampling: frequency/ wavelength/ wave-number interval between consecutive elements of a spectrum *(spectels)* with a given spectroscopic instrument. Should be at least twice smaller than the spectral resolution to avoid *undersampling.*
SPICAV-UV: the UV channel of the SPICAV spectrometer aboard ESA's Venus Express mission.
Stereogrammetry: calculation of 3-D positions by using two or more imaging views obtained using different viewing angles. In the context of EnVision, this is used to calculate a digital elevation model of topography with VenSAR.

Stratigraphy: scientific discipline concerned with the description of rock successions and their interpretation in terms of a general time scale
Tectonic: adjective qualifying a structure resulting from deformation of planetary crust and lithosphere subduction.
Tessera/tesserae: Venusian landforms characterized by high topography and highly deformed terrains.
Topography: relief or three-dimensional quality of the planet surface enabling the identification of specific landforms.
Trace gas: on Venus, any other atmospheric gaseous species than CO_2 (~96.5 %) and N_2 (~3.5%).
Troposphere: atmospheric layer at local thermo-dynamic equilibrium and where vertical energy transport is performed through thermal radiation and fluid convection. On Venus, it corresponds to the 0-60 km altitude range.
Ultra Stable Oscillator: A high quality factor quartz crystal generating the base frequency for the Master Reference Oscillator (MRO) included in the TT&C system of the spacecraft.
VIRTIS-H: the high spectral resolution channel of the Venus Express VIRTIS IR spectrometer aboard ESA's Venus Express mission.
Volume scattering: multiple scattering events occurring inside a medium, generally neither dense nor having a large loss tangent.
X-band: a nominal frequency range, from 8 to 12 GHz (2.5-3.8 cm in wavelength) within the microwave portion of the electromagnetic spectrum

11.3. References

Airey, M., Mather, T.A., Pyle, D.M., Glaze, L.S., Ghail, R.C., Wilson, C.F., Explosive volcanic activity on Venus: The roles of volatile contribution, degassing, and external enviornment, Planet. and Space Sci. Vol. 113, p. 33-48 (2015) doi:10.1016/j.pss.2015.01.009

Anderson, J.D. and 16 colleagues 1987, Radio Range Measurements of Coronal Electron Densities at 13 and 3.6 Centimeter Wavelengths during the 1985 Solar Conjunction of Voyager 2, The Astrophysical Journal 323, L141. doi:10.1086/185074

Antonita, M.T., Das, P.T.D., Kumar, P.K .,(2022) Overview of ISRO's future Venus orbiter mission. In: COSPAR 2022 44th scientific assembly, 16-24 July 2022, Athens, session B4.1 Venus science and exploration

Armann, M., and P. J. Tackley (2012), Simulating the thermochemical magmatic and tectonic evolution of Venus'mantle and lithosphere: Two-dimensional models, J. Geophys. Res., 117, E12003, doi:10.1029/2012JE004231.

Armstrong, J.W., Woo, R, 1981, Solar wind motion within 30 R solar masses - Spacecraft radio scintillation observations.\ Astronomy and Astrophysics 103, 415–421.

Arney, G. et al., J. Geophys. Res. Planets, Volume 119, Issue 8, pp. 1860-1891 (2014) doi:10.1002/2014JE004662

Arvidson, R.E., Brackett, R.A., Shepard, M.K., Izenberg, N.R., Fegley Jr., B., Microwave Signatures and Surface Properties of Ovda Regio and Surroundings, Venus, Icarus 112, 171-186 (1994)

Arvidson, R.E., Greely, R., Malin, M.C., et al., Surface Modification of Venus as Inferred from Magellan

Observation of Plains, J. Geophys. Res., 1992, vol. 97, no. E8, pp. 13 303-13 318.

Anderson, Geological Society of America Special Paper 388 (2005)

Aveline, D.C. et al., LPSC 42, Abstract 2165 (2011)

Baker, V. R., Komatsu, G., Parker, T. J., Gulick, V. C., Kargel, J. S., & Lewis, J. S. (1992). Channels and valleys on Venus: Preliminary analysis of Magellan data. Journal of Geophysical Research, 97(E8), 13421–13444. https://doi.org/10.1029/92JE00927

Barstow, J.K., C.C.C. Tsang, C.F. Wilson, P.G.J. Irwin, F.W. Taylor, K. McGouldrick, P. Drossart, G. Piccioni, S. Tellmann, Icarus, Vol.217, Issue 2, 542-560 (2012) doi:10.1016/j.icarus.2011.05.018

Basilevsky, A.T., Kuzmin, R.O., Nikolaeva, O.V., Pronin, A.A., Ronca, L.B., Avduevsky, V.S., Uspensky, G.R., Cheremukhina, Z.P., Semenchenko, V.V., Ladygin, V.M., The surface of Venus as revealed by the Venera landings, Part II, Geol. Soc. of America Bulletin 96 (1) 137-144 (1985)

Bauer, S.J. and 8 colleagues 1985, The Venus ionosphere, Advances in Space Research 5, 233–267. doi:10.1016/0273-1177(85)90203-0

Bertaux, J.L., et al., SPICAV on Venus Express: Three spectrometers to study the global structure and composition of the Venus atmosphere, Planetary and Space Science 55 (2007), 1673-1700. Planet. and Space Sci. 55, 1673-1700

Bertaux, J.L., Widemann, T., Hauchecorne, A., Moroz, V.I., Ekonomov, A.P. 1996, Vega-1 and Vega-2 Entry Probes: an Investigation of Local UV Absorption (220 – 400 nm) In The Atmosphere of Venus (SO2, Aerosols, Cloud Structure), Journ. Geophys. Research, Vol. 101, N°E5, pp. 12709-12745.

Bézard, B., C. C. C. Tsang, R. W. Carlson, G. Piccioni, E. Marcq, and P. Drossart (2009), Water vapor abundance near the surface of Venus from Venus Express/VIRTIS observations, J. Geophys. Res., 114, E00B39, doi:10.1029/2008JE003251

Bézard, B., C. C. C. Tsang, R. W. Carlson, G. Piccioni, E. Marcq, and P. Drossart (2009), Water vapor abundance near the surface of Venus from Venus Express/VIRTIS observations, J. Geophys. Res., 114, E00B39, doi:10.1029/2008JE003251

Bézard, B., Fedorova, A., Bertaux, J.-L., et al., 2011. The 1.10- and 1.18-μm nightside windows of Venus observed by SPICAV-IR aboard Venus Express. Icarus 216, 173–183.

Bird, M.K., Volland, H., Paetzold, M., Edenhofer, P., Asmar, S.W., Brenkle, J.P., 1994, The Coronal Electron Density Distribution Determined from Dual-Frequency Ranging Measurements during the 1991 Solar Conjunction of the ULYSSES Spacecraft, The Astrophysical Journal 426, 373. doi:10.1086/174073

Bjonnes, E., V. Hansen, B. James, J. Swenson, Equilibrium resurfacing of Venus: results from new Monte Carlo modeling and implications for Venus surface histories. Icarus 217(2), 451–461

Bondarenko, N.V. et al., Geophy. Res. Letters, Vol. 37, Issue 23, CiteID L23202 (2010) doi:10.1029/2010GL045233

Bondarenko, N. & Kreslavsky, M., Icarus, Volume 309, p. 162-176 (2018) doi:10.1016/j.icarus.2018.03.013

Brace, L.H., Kliore, A.J., 1991, The Structure of the Venus Ionosphere, Space Science Reviews 55, 81–163. doi:10.1007/BF00177136

Brackett, R. A., Fegley, B., and Arvidson, R. E. (1995), Volatile transport on Venus and implications for surface geochemistry and geology, J. Geophys.Res., Vol. 100, Issue E1, pp.1553–1563, doi:10.1029/94JE02708.

Breuer, D. und Moore, B. (2015), Dynamics and Thermal History of the Terrestrial Planets, the Moon, and Io. In: Physics of Terrestrial Planets and Moons Treatise on Geophysics (2nd edition), Elsevier, pp.255-305. ISBN 978-0-444-53803-1.

Bridges, N., Ayoub, F., Avouac, J.P., Leprince, S., Lucas, A., Mattson, S., Earth-like sand fluxes on Mars. Nature 485, 339–342 (2012). https://doi.org/10.1038/nature11022

Brossier, J., Gilmore, M. S., Toner, K., & Stein, A. J. (2021). Distinct mineralogy and age of individual lava flows in Atla Regio, Venus derived from Magellan radar emissivity. Journal of Geophysical Research: Planets, 126, e2020JE006722. https://doi.org/10.1029/2020JE006722

Brown, C.D., and Grimm, R.E. (1999), Recent Tectonic and Lithospheric Thermal Evolution of Venus, Icarus Vol. 139, Issue 1, pp. 40-48.

Bruzzone L. et al., IEEE/IGARSS International Geoscience and Remote Sensing Symposium (2020)

Bruzzone, L. et al., "Jupiter Icy Moon Explorer (JUICE): Advances in the design of the Radar for Icy Moons (RIME)," IEEE International Geoscience and Remote Sensing Symposium (IGARSS). IEEE, 2015.

Bullock, M.A., and Grinspoon, D.H. The Recent Evolution of Climate on Venus, Icarus 150, 19-37 (2001).

Byrne, P., The Prospect for Crustal Recycling on Rocky Solar System Worlds, 2021, AASTCS8, Habitable Worlds 2021, id. 1253. Bulletin of the American Astronomical Society, Vol. 53, No. 3 e-id 2021n3i1253

Byrne, P.K., Ghail, R.C., Gilmore, M.S., Celâl Şengör, A.M., Klimczak, C., Senske, D.A., Whitten, J.L., Khawja, S., Ernst, R.E., and Solomon, S.C., Venus tessearaer feature layered, folded, and eroded rocks, Geology (2021) 49 (1): 81–85. doi.org/10.1130/G47940.1

Campbell, L.H., and S.R. Taylor (1983), No water, no granites-no oceans, no continents. Geophys. Res. Lett. 10 (11), 1061–1064.

Campbell, B.A., and D.B. Campbell, Analysis of volcanic surface morphology on Venus from comparison of Arecibo, Magellan, and terrestrial airborne radar data, J. Geophys. Res., 97, 16293-16314, 1992

Campbell, B.A., Merging Magellan emissivity and SAR data for analysis of Venus surface dielectric properties, Icarus, 112, 187-203, 1994.

Campbell, B.A., and P.G. Rogers, Bell Regio, Venus: Integration of remote sensing data and terrestrial analogs for geologic analysis, J. Geophys. Res., 99, 21,153-21,171, 1994.

Campbell, B.A., Putzig, N.E., Carter, L.M. and Phillips, R.J., IEEE Geoscience and Remote Sensing Letters, 8(5), pp.939-942 (2011)

Campbell, B.A., G.A. Morgan, J.L. Whitten, L.M. Carter, D.B. Campbell, and L.S. Glaze (2017), Pyroclastic flow deposits on Venus as indicators of renewed magmatic activity, J. Geophys. Res., 122, 1580-1596, doi:10.1002/2017JE005299.

Carpy et al., EnVision Paris Conference (2020)

Carrer, L. K., F. Zancanella, L. Bruzzone, IEEE Trans. on Geosci. and Remote Sensing, Vol. 59 (2021) doi:10.1109/TGRS.2020.3006586

Carrer, L., L. Bruzzone, “Solving for Ambiguities in radar Geophysical Exploration of Planetary Bodies by Mimicking Bats Echolocation,” Nature Communications, Vol. 8, Article number 2248 (2017), 21 December 2017. DOI 10.1038/s41467-017-02334-1.

Carter, L. M., Campbell, B. A., Holt, J. W., Phillips, R. J., Putzig, N. E., Mattei, S., Seu, R., Okubo, C. H., and Egan, A. F., Geophys. Res. Lett., 36, L23204 (2009) doi:10.1029/2009GL041234. Chamberlain, S., et al., (2020) SOIR/VEx observations of water vapor at the terminator in the Venus mesosphere. Icarus. 346, 113819.

Claudin, P. and B. Andreotti, Earth and Planetary Science Letters 252, 30–44 (2006)

Conrad, J. W., & Nimmo, F. (2023). Constraining characteristic morphological wavelengths for Venus using Baltis Vallis. Geophysical Research Letters, 50, e2022GL101268. https://doi.org/10.1029/2022GL101268

Cottereau, L.; Rambaux, N.; Lebonnois, S. and Souchay, J., The various contributions in Venus rotation rate and LOD, Astronomy and Astrophysics, vol.531, pp.A45 (2011) DOI: 10.1051/0004-6361/201116606

Cottini, V. et al., Plan. Sp. Sci. 113-114, 219-225 (2015) doi:10.1016/j.pss.2015.03.012

Coustenis, A., Taylor, F., & Plainaki, C. in T. Beer, J. Li, & K. Alverson (Eds.), Global Change and Future Earth: The Geoscience Perspective, pp. 40-54. Cambridge University Press (2018) doi:10.1017/9781316761489.006

Crowley, G., and Tolson, R.H. (2007), Mars Thermospheric Winds from Mars Global Surveyor and Mars Odyssey Accelerometers, Journal of Spacecraft and Rockets Vol. 44, N°6. https://doi.org/10.2514/1.28625

Cutler, K.S., Filiberto, J., Treiman, A.H., Trang, D. (2020), Experimental Investigation of Oxidation of Pyroxene and Basalt: Implications for Spectroscopic Analyses of the Surface of Venus and the Ages of Lava Flows, Plan. Science Journal 1:21, https://doi.org/10.3847/PSJ/ab8faf

D'Amore, M., et al., The mercury radiometer and thermal infrared imaging spectrometer (MERTIS) onboard Bepi Colombo: first inflight calibration results, in Infrared Remote Sensing and Instrumentation XXVII. 2019.

Davaille, A., S.E. Smrekar et S. Tomlinson "Experimental and observational evidence for plume-induced subduction on Venus", Nature Geosciences, 10 (2017) 349-355. doi.org/10.1038/ngeo2928

D'Incecco, P. et al. Plan. Sp. Sci., Vol.136, p. 25-33 (2017) doi:10.1016/j.pss.2016.12.002

D'Incecco, P. et al. Earth and Plan. Sci. Let., Vol. 546, article id. 116410 (2020) doi:10.1016/j.epsl.2020.116410

D'incecco, P., Filiberto, J., Lopez, I., Eggers, G.L., Di Achille, G., Komatsu, G., Gorinov, A., Monaco, C., Aveni, S., Mari, N., Blackett, M., Mastrogiuseppe, M., Cardinale, M., El Yazidi, M. (2022), Geologically Recent Areas as One Key Target for Identifying Active Volcanism on Venus, Geophysical Research Letters, 49, e2022GL101813.

Diniega, S. et al., Aeolian Research, Vol. 26, p. 5-27 (2017) doi:10.1016/j.aeolia.2016.10.001

Donahue., T.M., Hoffman, J.H., Hodges Jr., R.R., Watson A.J., Science 07 May 1982, Vol. 216, Issue 4546, pp. 630-633 (1982) doi:10.1126/science.216.4546.630

Dumoulin, C., G. Tobie, O. Verhoeven, P. Rosenblatt, and N. Rambaux (2017), Tidal constraints on the interior of Venus, J. Geophys. Res. Planets, 122, 1338–1352, doi:10.1002/2016JE005249

Duran Vinent, O., Andreotti, B., Claudin, P., and Winter, C. (2019), A unified model of ripples and dunes in water and planetary environments, Nature Geoscience 12, 345-350. https://doi.org/10.1038/s41561-019-0336-4

Dyar, M. D., Helbert, J., Maturilli, A., Müller, N. T., & Kappel, D., Geophys. Res. Lett., 47, e2020GL090497 (2020) doi.org/10.1029/2020GL090497

Efimov, A.I. and 7 colleagues 2010a, Properties of solar wind turbulence from radio occultation experiments with the NOZOMI spacecraft.\ Astronomy Reports 54, 1032–1041. doi:10.1134/S1063772910110089

Efimov, A. and 6 colleagues 2010b, Coronal sounding with three ESA spacecraft during solar conjunction: Radial dependence of radio signal fluctuation spectra, 38th COSPAR Scientific Assembly.

Encrenaz, T., Lellouch, E., Paubert, G., Gulkis, S. (1991) First detection of HDO in the atmosphere of Venus at radio wavelengths: an estimate of the H2O vertical distribution, Astron Astrophys 246:L63–L66

Encrenaz., T., Lellouch, E., Cernicharo, J., Paubert, G., Gulkis, S., Spilker, T. (1995) The thermal profile and water abundance in the Venus mesosphere from H2O and HDO millimeter observations. Icarus 117(1):162–172

Encrenaz, T., Greathouse, T. K., Roe, H., Richter, M., Lacy, J., Bézard, B., Fouchet, T., Widemann, T., HDO and SO2 thermal mapping on Venus: Evidence for strong SO2 variability, Astron. Astrophys. 543, A153 (2012)

Encrenaz, T., Greathouse, T.K., Richter, M.J., DeWitt, C., Widemann, T., Bézard, B., Fouchet, T., Atreya, S.K., and Sagawa, H., Astronomy & Astrophysics, Vol. 595, id.A74, 15 pp. (2016)

Encrenaz, T., Greathouse, T.K., Marcq, E., Sagawa, H., Widemann, T., Bézard, B., Fouchet, T., Lefèvre, F., Lebonnois, S., Atreya, S.K., Lee, Y. J., Giles, R. and Watanabe, S., Astron. Astrophys., Vol. 623, id. A70, 11 pp. (2019)

Encrenaz, T., Greathouse, T.K., Marcq, E., Sagawa, H., Widemann, T., Bézard, B., Fouchet, T., Lefèvre, F., Lebonnois, S., Atreya, S.K., Lee, Y. J., Giles, R., Watanabe, S., Shao, W., Zhang, X., and Bierson, C.J. Astron. Astrophys., Vol.639, A69 (2020) doi:10.1051/0004-6361/202037741

Encrenaz T, Greathouse TK, Giles R, Widemann T, Bézard B, Lefèvre M, Shao W (2023) HDO and SO2 ther- mal mapping on Venus: VI. Anomalous SO2 behavior during late 2021. Astron Astrophys 674:A199. https://doi.org/10.1051/0004-6361/202245831

Erard, S., Drossart, P., Piccioni, G., Multivariate analysis of Visible and Infrared Thermal Imaging Spectrometer (VIRTIS) Venus Express nightside and limb observations, Journal of Geophysical Research-Planets,

vol. 114, Art.n E00b2, Jan 7 2009, doi: 10.1029/2008je003116

ESA, (2018), "CDF Study Report EnVision, Assessment of a Mission to Venus". ESA report CDF-186(A), November 2018, available from ESA. The associated presentation is available here.

ESA (2021), "EnVision, Understanding why Earth's closest neighbour is so different", Assessment Study Report (Yellow Book), ESA document reference ESA/SCI(2021)1, February 2021, 11 pp., https://sci.esa.int/web/cosmic-vision/-/envision-assessment-study-report-yellow-book

ESA (2023a), "EnVision Science Management Plan", ESA document reference ESA/SPC(2023), dated 18 October 2023, 15 pp.

ESA (2023b), "EnVision Science Implementation Requirements Document (SIRD)", ESA document reference ESA-ENVIS-EST-SCI-RS-001, version 1.0, 13/03/2023, 47 pp.

ESA (2023c), "EnVision Science Requirements Document", ESA document reference EnV-EST-SGS-RS-001, version 2.4, 26/04/2023, 220 pp.

ESA BR-247, Cosmic Vision, Space Science for Europe 2015-2025, ESA Publications Division, ESTEC, PO Box 299, 2200 AG Noordwijk, The Netherlands (2005).

Esposito, L., Science, 223, 1072 (1984) doi:10.1126/science.223.4640.1072

Esposito, L. et al., J. Geophys. Res. 93 (D5), 5267-5276 (1988) doi:10.1029/JD093iD05p05267

Fedorova, A. et al., Icarus, 275, 143-162 (2016) doi:10.1016/j.icarus.2016.04.010

Fegley, B., Jr; in Planets, Asteroids, Comets and The Solar System, Vol. 2 of Treatise on Geochemistry (Second Edition). Edited by Andrew M. Davis. Elsevier, p.127-148 (2014)

Fegley, B., Jr, Klingelhofer, G., Lodders, K., Widemann; T. (1997) Geochemistry of surface-atmosphere interactions on Venus. In: Bougher SW, Hunten DM, Phillips RJ (Eds) Venus II. University of Arizona Press, Tucson, pp 591–636

Ferrari, S., Maturilli, A., Carli, C., D'Amore, M., Helbert, J., Nestola, F., Hiesinger, H. (2020), Thermal Infrared emissivity of felsic-rich to mafic-rich analogues of hot planetary regoliths, Earth and Plan. Science Letters 534, 116089. https://doi.org/10.1016/j.epsl.2020.116089

Ferro, A. Pascal, L. Bruzzone, IEEE Transactions on Geoscience and Remote Sensing, Vol. 51, pp. 3037-3055 (2013)

Fielding, E. J., Talebian, M., Rosen, P. A., Nazari, H., Jackson, J. A., Ghorashi, M., and Walker, R. (2005), Surface ruptures and building damage of the 2003 Bam, Iran, earthquake mapped by satellite synthetic aperture radar interferometric correlation, J. Geophys. Res., 110, B03302, doi:10.1029/2004JB003299.

Filiberto, J., Trang, D., Treiman, A. H. and Gilmore, M. S. Sci. Adv., Vol. 6, Issue 1, p. eaax7445 (2020) doi:10.1126/sciadv.aax7445

Fink, J.H., Bridges, N.T. and Grimm, R.E. (1993). Shapes of Venusian "pancake" domes imply episodic emplacement and silicic composition. Geophysical Research Letters 20: doi: 10.1029/92GL03010.

Ford, P. et al., Journ. Geophys. Res. Vol. 97, Issue E8, p. 13103-13114 (1992) doi:10.1029/92JE01085

Gaillard and Scaillet, Earth and Pl. Sci. Let. 403:307-316 (2014)

Ganesh, I.L. M, et al., JVGR, 390, 106748 (2020)

Garvin, J.B., Glaze, L.S., Ravine, M.A. et al (2018) Venus descent imaging for surface topography and geomor- phology. In: 49th lunar and planetary science conference 2018. LPI contrib., vol 2083, LPSC, 49, 2287

Garvin, J.B., Getty, S.A., Arney, G.N., Johnson, N.M., Kohler, E., Schwer, K.O., Sekerak, M., Bartels, A., Saylor, R.S., Elliott ,V.E., Goodloe, C.S., Garrison, M.B., Cottini, V., Izenberg, N., Lorenz, R., Malespin, C.A., Ravine, M., Webster, C.R., Atkinson, D.H., Aslam, S., Atreya, S., Bos, B.J., Brinckerhoff, W.B., Campbell, B., Crisp, D., Filiberto, J.R., Forget, F., Gilmore, M., Gorius, N., Grinspoon, D., Hofmann, A.E., Kane, S.R., Kiefer, W., Lebonnois, S., Mahaffy, P.R., Pavlov, A., Trainer, M., Zahnle, K.J., Zolotov, M. (2022), Revealing the mysteries of Venus: the DAVINCI mission. Planet Sci J 3:117. https://doi.org/10.3847/psj/ac63c2

Genova, A., Goossens, S., Lemoine F.G., Mazarico, E., Neumann G.A., Smith, D.E., et al., Icarus, 272, 228-245 (2016) doi:10.1016/j.icarus.2016.02.050

Gerekos, G., A. Tamponi, L. Carrer, D. Castelletti, M. Santoni, L. Bruzzone, "A Coherent Multilayer Simulator of Radargrams Acquired by Radar Sounder Instruments," IEEE Transactions on Geoscience and Remote Sensing, Vol. 56, No. 12, pp. 7388-7404, 2018.

Gerya, T., Stern, R., Baes, M. et al. Plate tectonics on the Earth triggered by plume-induced subduction

initiation. Nature 527, 221–225 (2015). https://doi.org/10.1038/nature15752

Ghail, R., et al. (2016), "EnVision, Understanding why our most Earth-like neighbour is so different", Proposal submitted to ESA's Cosmic Vision 5th Medium Class mission call, October 2016, https://www2.physics.ox.ac.uk/sites/default/files/2011-07-07/envisionm5_proposal_without_annexes_pdf_12334.pdf

Ghail, R., abstract #2132 LPSC (2019)

Ghail, R.C. & Wilson, L. Geological Society, London, Special Publications, vol. 401, issue 1, pp. 97-106 (2015) doi:10.1144/SP401.1

Gilli, G., Navarro, T., Lebonnois, S., Quirino, D., Silva, V., Stolzenbach, A., Lefèvre, F., Schubert, G., Venus upper atmosphere revealed by a GCM: II. Model validation with temperature and density measurements,Icarus, Volume 366 (2021),114432, https://doi.org/10.1016/j.icarus.2021.114432

Gillmann, C., Chassefière, E., and Lognonné, P. (2009), A consistent picture of early hydrodynamic escape of Venus atmosphere explaining present Ne and Ar isotopic ratios and low oxygen atmospheric content. Earth and Plant. Sci. Lett., Vol. 286, Issues 3–4, pp. 503–513.

Gillmann, C., and P. Tackley (2014), Atmosphere/ mantle coupling andfeedbacks on Venus, J. Geophys. Res.Planets, 119, 1189–1217, doi:10.1002/2013JE004505

Gillmann, C., Golabek, G.J., Raymond, S.N., Schönbächler, M., Tackley, P., Dehant, V., Debaille, V. (2020), Dry late accretion inferred from Venus's coupled atmosphere and internal evolution. Nat. Geosci. 13, 265–269.

Gillmann, C., Way, M.J., Avice, G., Breuer, D., Golabek, G.J., Höning, D., Krissansen-Totton, J., Lammer, H., O'Rourke, J.G., Persson, M., Plesa, A.-C., Salvador, A., Scherf, M., Zolotov, M. (2022) The long-term evolution of the atmosphere of Venus: processes and feedback mechanisms. Space Sci Rev 218:56. https://doi.org/10.1007/s11214-022-00924-0

Gillmann, C., McGregor, N., Nimmo, F., Golabek, G., Plattner, A., Conrad, J. (2023), Constraining Venus' convection regime from Baltis Vallis topography, DPS-EPSC Abstract, San Antonio, TX, Oct. 2023.

Gilmore, M.S., Mueller, N., Helbert, J. (2015)n VIRTIS emissivity of Alpha Regio, Venus, with implications for tessera composition. Icarus 254:350–361. https://doi.org/10.1016/j.icarus.2015.04.008

Girazian, Z., Withers, P., Häusler, B., Pätzold, M., Tellmann, S., Peter, K., 2015, Characterization of the lower layer in the dayside Venus ionosphere and comparisons with Mars. Planetary and Space Science 117, 146–158. doi:10.1016/j.pss.2015.06.007

Greeley, R., Marshall, J.R., Leach, R.N., Icarus 60, 152–160 (1984)

Greeley, R., Arvidson, R.E., Elachi, C., Geringer, M.A., Plaut, J.J., Saunders, R.S., Schubert, G., Stofan, E.R., Thouvenot, E.J.P., Wall, S.D., Weitz, C.M. (1992) Aeolian features on Venus: preliminary Magellan results. J Geophys Res 97:13319–13345. https://doi.org/10.1029/92JE00980

Greeley, R., Bender, K., Thomas, P.E., Schubert, G., Limonadi, D., Weitz, C. (1995) Wind-related features and processes on Venus: summary of Magellan results. Icarus 115:399

Grieger, B., et al., IPPW meeting, Lisbon (2003)

Gülcher, A. J. P, Gerya, T.V., Montési, L. G. J., & Munch, J., Nature Geoscience 13, 547-554 (2020) doi.org/10.1038/s41561-020-0606-1

Hahn, R.M., and Byrne, P.K. (2023), A Morphological and Spatial Analysis of Volcanoes on Venus, Journ. Geophys. Res. Planets, Vol. 128, Issue 4, e2023JE007753. https://doi.org/10.1029/2023JE007753

Hamano, K., Abe, Y. & Genda, H., (2013) Emergence of two types of terrestrial planet on solidification of magma ocean. Nature 497:607–610. https://doi.org/10.1038/nature12163

Hansen, V.L., Willis, J.J. (1996), Structural analysis of sampling of tesserae: implications for Venus geodynamics. Icarus 123:296–312

Haus, R., Kappel, D., and Arnold, G., Radiative energy balance of Venus: An approach to parameterize thermal cooling and solar heating rates, Icarus, vol. 284, pp. 216-232, 2017, doi: 10.1016/j.icarus.2016.11.025.

Hashimoto, G.L., Abe, Y. (2005) Climate control on Venus: comparison of the carbonate and pyrite models. Planet Space Sci 53(8):839–848. https://doi.org/10.1016/j.pss.2005.01.005

Hashimoto, G.L., Roos-Serote, M., Sugita, S., Gilmore, M.S., Kamp, L.W., Carlson, R.W., Baines, K.H. (2008) Felsic highland crust on Venus suggested by Galileo near-infrared mapping spectrometer data. J Geophys Res, Planets 113(E5):E00B24. https://doi.org/10.1029/2008JE003134

Helbert, J., et al., in Infrared Remote Sensing and Instrumentation XXV (2017)

Helbert, J., Dyar, M., Walter, I., Wendler, D., Widemann, T., Marcq, E., Guignan, G., Ferrari, S., Maturilli, A., Mueller, N., Kappel, D. (2018) The Venus emissivity mapper (VEM): obtaining global mineralogy of Venus from orbit. In: Infrared remote sensing and instrumentation XXVI, San Diego, United States, Aug 2018, 107650D. https://doi.org/10.1117/12.2320112

Helbert, J., et al., The VenSpec suite on the ESA EnVision mission to Venus, in Infrared Remote Sensing and Instrumentation XXVII. 2019.

Helbert. J., Säuberlich. T., Dyar, M., Ryan, C., Walter, I., Reess, J.-M., Rosas-Ortiz, Y., Peter, G., Maturilli, A., Arnold, G. (2020) The Venus emissivity mapper (VEM): advanced development status and performance evaluation. In: Proc. SPIE 11502, Infrared remote sensing and instrumentation XXVIII, 20 August 2020, 1150208

Helbert J., et al. The Venus Emissivity Mapper: implementation for flight on the NASA VERITAS mission. In Infrared Remote Sensing and Instrumentation XXX. (2022). San Diego, CA: SPIE

Herrick, R.R., Hensley, S. (2023) Surface changes observed on a Venusian volcano during the Magellan mission. Science 379(6638):1205–1208. https://doi.org/10.1126/science.abm7735

Herrick, R.R., Rumpf, M.E. (2011) Postimpact modification by volcanic or tectonic processes as the rule, not the exception, for Venusian craters. J Geophys Res, Planets 116(E2):E02004

Herrick, R.R., Sharpton, V.L. (2000) Implications from stereo-derived topography of Venusian impact craters. J Geophys Res, Planets 105(E8):20245–20262

Hensley, S. et al., IEEE Radarcon (2020)

Hickey, M.P., Navarro, T., Schubert, G., Walterscheid, R.L. (2022), Venus mountain waves in the upper atmosphere simulated by a time-invariant linear full-wave spectral model, Icarus Vol. 377, 114922. https://doi.org/10.1016/j.icarus.2022.114922

Horinouchi et al. 2020, How waves and turbulence maintain the super-rotation of Venus's atmosphere, Science, DOI: 10.1126/science.aaz4439

Ignatiev, N., Moroz, V.I., Zasova, L., Khatuntsev, I., 1999. Venera 15: water vapour in the middle atmosphere of Venus. Adv. Space Sci. 23 (9), 1549–1558.

Ignatiev, I., Moroz, V.I., Moshkin, B.E., Ekonomov, A.P., Gnedykh, V.I., Grigoriev, A.V., Khatuntsev, I.V. (1997) Water vapour in the lower atmosphere of Venus: a new analysis of optical spectra measured by entry probes. Planet Space Sci 45:427–438. https://doi.org/10.1016/S0032-0633(96)00143-2

Imamura, T. & Hashimoto, G., Adv. Space Res. Vol. 29, No. 2, pp. 249-254 (2002) doi:10.1016/S0273-1177(01) 00575-0

Imamura, T. & Hashimoto, G., J. Geophys. Res. 103 (E13) (1998) doi:10.1029/1998JE900010

Imamura, T. and 14 colleagues 2011, Radio occultation experiment of the Venus atmosphere and ionosphere with the Venus orbiter Akatsuki, Earth, Planets and Space 63, 493–501. doi:10.5047/eps.2011.03.009

Ivanov, M. A., and J. W. Head III, Planet. Space Sci., 113-114, 10-32 (2015) doi:10.1016/j.pss.2015.03.016.

Ivanov, M. A., and J. W. Head III, Planet. Space Sci., 59, 1559-1600 (2011) doi:10.1016/j.pss.2011.07.008.

Izenberg et al., Geophys. Res. Lett. 21, 289-292 (1994)

James, E.P. et al., Icarus 129, 147–171 (1997) doi:10.1006/icar.1997.5763

Jessup, K.L., Marcq, E., Mills, F., Mahieux, A., Limaye, S., Wilson, C., Allen, M., Bertaux, J.-L., Markiewicz, W., Roman, T., Vandaele, A.C., Wilquet., V., Yung, Y. (2015) Coordinated Hubble space telescope and Venus Express observations of Venus' upper cloud deck. Icarus 258:309–336 doi:10.1016/j.icarus.2015.05.027.

Kappel, D., Arnold, G., Haus, R., Piccioni, G., and Drossart, P., Refinements in the data analysis of VIRTIS-M-IR Venus nightside spectra, Advances in Space Research, vol. 50, no. 2, pp. 228-255 (2012) doi: 10.1016/j.asr.2012.03.029.

Kappel, D., MSR, a multi-spectrum retrieval technique for spatially-temporally correlated or common Venus surface and atmosphere parameters, Journal of Quantitative Spectroscopy and Radiative Transfer, vol. 133, pp. 153-176 (2014) doi: 10.1016/j.jqsrt.2013.07.025

Kappel, D., Arnold, G., and Haus,R., Multi-spectrum retrieval of Venus IR surface emissivity maps from VIRTIS/VEX nightside measurements at Themis Regio, Icarus, vol. 265, pp. 42-62, 2016, doi: 10.1016/j.icarus.2015.10.014

Kane, S., G. Arney, D. Crisp, S. Domagal-Goldman, L. Glaze, C. Goldblatt, D. Grinspoon, J. Head, A. Lenardic, C. Unterborn, M. Way, and K. Zahnle, J. Geophys. Res. Planets, 124, p.2015-2028 (2019)

Kane S.R., Kopparapu R. K, Domagal-Goldman S.D, (2014) On the frequency of potential Venus analogs from Kepler data. Astrophys J Lett 794:L5. https://doi.org/10.1088/2041-8205/794/1/L5

Kane, S.R., G. Arney, D. Crisp, S. Domagal-Goldman, L.S. Glaze, C. Goldblatt, D. Grinspoon, J.W. Head, A.

Lenardic, C. Unterborn, M.J. Way, and K.J. Zahnle, 2019: Venus as a laboratory for exoplanetary science. J. Geophys. Res. Planets, 124, no. 8, 2015-2028, doi:10.1029/2019JE005939.

Kasting, J.F. (1988), Runaway and moist greenhouse atmospheres and the evolution of Earth and Venus, Icarus 74, 472–494.

Keating, G.M., Nicholson III, J.Y., Lake, L.R. (1980), Venus upper atmosphere structure, Journ. Geophys. Res. Space Physics, Vol. 85, Issue A13, p. 7941-7956. https://doi.org/10.1029/JA085iA13p07941

Khawja, S., Ernst, R.E., Samson, C., Byrne, P.K., Ghail, R.C., MacLellan, L.M., Nat. Commun. 11, 5789 (2020) doi:10.1038/s41467-020-19336-1

Kiefer, W., & Swafford, L.C. (2006), Topographic analysis od Devana Chasma, Venus: implications for rift system segmentation and propagation, Journal of Structural Geology, Vol. 28, issue 12, pp. 2144-2155.

Kitahara T, Imamura T, Sato TM, Yamazaki A, Lee Y-J, Yamada M, Watanabe S, Taguchi M, Fukuhara T, Kouyama T, Murakami S, Hashimoto GL, Ogohara K, Kashimura H, Horinouchi T, Takagi M (2019) Stationary features at the cloud top of Venus observed by Ultraviolet Imager onboard Akatsuki. J Geo- phys Res, Planets 124:1266–1281. https://doi.org/10.1029/2018JE005842

Kleine, T., Münker, C., Mezger, K., Palme, H. (2002), Rapid accretion and early core formation on asteroids and the terrestrial planets from Hf-W chronometry. Nature. 2002 Aug 29; 418(6901):952-5. doi: 10.1038/nature00982.

Klidaras, A., Mason, P. J., abstract #1893, LPSC (2022)

Kliore, A.J., Patel, I.R., Nagy, A.F., Cravens, T.E., Gombosi, T.I, 1979, Initial Observations of the Nightside Ionosphere of Venus from Pioneer Venus Orbiter Radio Occultations, Science 205, 99–102. doi:10.1126/science.205.4401.99

Klose et al., J. Geophys. Res. Planets 97, 16353-16370 (1992)

Kniffin, M. (1993) PVO Venus SC position VSO COORDS 12 Sec VER1.0, NASA Planetary data System, DOI:10.17189/1519830

Kobayashi, T., Lee, S. R., Kumamoto, A., & Ono, T., In L. Pajewski, C. Craeye, A. Giannopoulos, F. Andre, S. Lambot, & E. Slob (Eds.), Proc. of the 15th International Conference on Ground Penetrating Radar GPR 2014, pp. 1037-1041 (2014)

Komatsu, G., Baker, V.R., Gulick, V.C., Parker, T.J.(1993) Venusian channels and valleys: Distribution and volcanological implications, Icarus 102, issue 1, p. 1-24.

Konopliv, A.S., Yoder, C.F. (1996) Venusian k2 tidal love number from Magellan and PVO tracking data. Geophys Res Lett 23(14):1857–1860 doi:10.1029/96GL0158

Konopliv, A. S., Banerdt, W. B. & Sjogren, W. L. Venus Gravity: 180th Degree & Order Model. Icarus 139, 3–18 (1999)

Kouyama, T., Imamura, T., Taguchi, M.,Fukuhara, T., Sato, T. M., Yamazaki, A.,...Nakamura, M.(2017) Topographical and local time dependence of large stationary gravity waves observed at the cloud top of Venus. Geophysical Research Letters,44, 12,098–12,105 https://doi.org/10.1002/2017GL075792

Korablev, O., et al., SPICAV IR acousto-optic spectrometer experiment on Venus Express. Planetary and Space Science, 2012. 65(1): p. 38-57.

Krasnopolsky et al. 2013, Observations of D/H ratios in H_2O, HCl, and HF on Venus and new Dcl and DF line strenghts? https://doi.org/10.1016/j.icarus.2013.02.010

Kreslavsky, M., and Bondarenko, N.V., Aeolian Res. 26, 29 (2017) doi: 10.1016/j.aeolia.2016.06.001

Lammer, H., Zerkle, A.L., Gebauer, S. et al. Origin and evolution of the atmospheres of early Venus, Earth and Mars. Astron Astrophys Rev 26, 2 (2018). doi.org/10.1007/s00159-018-0108-y

Lebonnois, S., J. Geophys. Res.115, E6 (2010) doi:10.1029/2009JE003458

Lebonnois et al. 2015, JGR (Planets), Analysis of the radiative budget of the Venusian atmosphere based on infrared Net Exchange Rate formalism, doi.org/10.1002/2015JE004794

Lee, C. et al., J. Geophys. Res., 112, E04S11 (2007) doi:10.1029/2006JE002874

Lefèvre, M., Spiga, A., Lebonnois, S., Mesoscale modeling of Venus' bow-shape waves, Icarus 335, 113376 (2020)

Lefèvre, M., Marcq, E., Lefèvre, F. (2022) The impact of turbulent vertical mixing in the Venus clouds on chemical tracers. Icarus 386:115148. doi.org/10.1016/j.icarus.2022.115148

Lellouch E, Widemann T, Luz D, Moreno R (2007) ESA Support Investigation to the Venus Express Mission, European Space Agency

Lellouch E, Witasse O (2008) A coordinated campaign of Venus ground-based observations and Venus Express measurements. Planetary and Space Science 56(10):1317–1319. https://doi.org/10.1016/j.pss. 2008.07.001

Lorenz, R.D., Probabilistic constraints from existing and future radar imaging on volcanic activity on Venus.

Planetary and Space Science (2015), http://dx.doi.org/10.1016/j.pss.2015.07.009i

Lorenz, R.D., Le Gall, A., Janssen, M. A., Detecting volcanism on Titan and Venus with microwave radiometry, Icarus, 270, 30-36 (2016)

Lorenz, R.D., Surface winds on Venus: Probability distribution from in-situ measurements, Icarus, 264, 311 (2016)

Lorenz, R. D., Lightning detection on Venus: a critical review, Progress in Earth and Planetary Science 5, 34 (2018). doi.org/10.1186/s40645-018-0181-x

Lourenço, D.L., Rozel, A.B., Ballmer, M.D., Tackley, P.J. (2020). "Plutonic-Squishy Lid: A New Global Tectonic Regime Generated by Intrusive Magmatism on Earth-Like Planets." Geochemistry, Geophysics, Geosystems, 21, e2019GC008756, doi:10.1029/2019gc008756.

Lucas, A., O. Aharonson, C-A. Deledalle, A. Hayes, R. Kirk, E. Howington-Kraus and the CRST, Insights into Titan's geology and hydrology based on enhanced image processing of Cassini RADAR data, J. Geophys. Res., Vol. 119, Issue 10, pp. 2149-2166 (2014) doi:10.1002/2013JE004584

Määttänen, A. et al., J. Geophys. Res., Vol. 123, Issue 2, pp. 1269-1296 (2018) doi:10.1002/2017JD027429

Maia, J. S., & Wieczorek, M. A. (2022). Lithospheric structure of Venusian crustal plateaus. Journal of Geophysical Research: Planets, 127, e2021JE007004. https://doi.org/10.1029/2021JE007004

Mahieux, A., S. Robert, F. P. Mills, K. L. Jessup, L. Trompet, S. Aoki, A. Piccialli, J. Peralta and A. C. Vandaele (2023a), Update on SO_2, detection of OCS, CS, CS_2, and SO_3, and upper limits of H_2S and HOCl in the Venus mesosphere using SOIR on board Venus Express, Icarus 399: 115556, DOI: 10.1016/j.icarus.2023.115556

Mahieux, A., S. Robert, A. Piccialli, L. Trompet and A. C. Vandaele (2023b), The SOIR/Venus Express species concentration and temperature database: CO_2, CO, H_2O, HDO, $H^{35}Cl$, $H^{37}Cl$, HF individual and mean profiles, Icarus, Vol. 405, A115713, DOI: 10.1016/j.icarus.2023.115713.

Mahieux, A., R. V. Yelle, N. Yoshida, S. Robert, A. Piccialli, H. Nakagawa, Y. Kasaba, F. P. Mills and A. C. Vandaele (2021), Determination of the Venus eddy diffusion profile from CO and CO_2 profiles using SOIR/Venus Express observations, Icarus 361: 114388, DOI: 10.1016/j.icarus.2021.114388

Malin, M. C. Mass movements on Venus: Preliminary results from Magellan cycle 1observations. Journal of Geophysical Research: Planets 97, 16337-16352, doi:10.1029/92je01343 (1992).

Marchi, S., Rufu, R., Korenaga, J., Long-lived volcanic resurfacing of Venus driven by early collisions, Nat Astron (2023), https://doi.org/10.1038/s41550-023-02037-2

Marcq, E., Bertaux, JL., Montmessin, F. et al. Variations of sulphur dioxide at the cloud top of Venus's dynamic atmosphere. Nature Geosci 6, 25–28 (2013). https://doi.org/10.1038/ngeo1650

Marcq, E. et al., J. Geophys. Res., Volume 113, CiteID E00B07 (2008) doi:10.1029/2008JE003074

Marcq et al., Composition and Chemistry of the neutral Atmosphere of Venus, Space Sci Rev. 214, 10 (2018) https://doi.org/10.1007/s11214-017-0438-5

Marcq, E., Jessup, K.L., Baggio, L., Encrenaz, T., Lee, Y.J., Montmessin, F., Belyaev, D., Oleg Korablev, O., Bertaux, J.-L. (2020), Climatology of SO_2 and UV absorber at Venus' cloud top from SPICAV-UV nadir dataset, Icarus, Volume 335, 113368,doi.org/10.1016/j.icarus.2019.07.002.

Marcq, E., Minor species in Venus' night side troposphere as observed by VIRTIS-H/Venus Express, Icarus, vol. 405 (2023) doi:10.1016/j.icarus.2023.115714.

Margot, J. L., Hauck, S.A., Mazarico, E., Padovan, S., Peale, S.J. (2018) Mercury's internal structure. In: Salomon SC, Nittler LR, Anderson BJ (eds) Mercury - the view after MESSENGER. Cambridge University Press, Cambridge. https://doi.org/10.1017/9781316650684

Margot, J.L., Campbell, DB, Giorgini J.D., Jao, J.S., Snedeker, L.G., Ghigo, F.D., Bonsall, A. (2021) Spin state and moment of inertia of Venus. Nat Astron 5:676–683. https://doi.org/10.1038/s41550-021-01339-7

Markiewicz, M. et al., Nature 450, 29 Nov. 2007, 633–636 (2007) doi:10.1038/nature06320

Marov, M. Y., and D. H. Grinspoon, The planet Venus, Yale University Press (1998)

Marshall, J.R. and Greeley, J. Geophys. Res. 97, 1007-1016 (1992)

Marshall, J.R., Fogleman, G., Greeley, R., Hixon, R., Tucker, D., J. Geophys. Res., 96, B2, 1931 (1991)

Martinez, A., Lebonnois, S., Millour, E., Pierron, T., Moisan, E., Gilli, G, Lefèvre, F. (2023), Exploring the variability of the Venusian thermosphere with the IPSL Venus GCM, Icarus 389, 115272. DOI: 10.1016/j.icarus.2022.115272

Marty, J.C., Balmino, G., Duron, J., Rosenblatt, P., Le Maistre, S., Rivoldini, A., et al., Planet. Space Sci., 57(3), 350-363 (2009) doi:10.1016/j.pss.2009.01.004

Massol, H., K. Hamano, F. Tian, M. Ikoma, Y. Abe, E. Chassefière, A. Davaille, H. Genda, M. Gudel, Y. Hori, F. Leblanc, E. Marcq, P. Sarda, V.I. Shematovich, A. Stökl, H. Lammer (2016), Formation and Evolution of Protoatmospheres, Space Science Reviews, DOI 10.1007/s11214-016-0280-1.

McGouldrick, T. & Toon, O.B., Planet. Space Sci., Vol. 56, Issue 8, p. 1112-1131 (2008a) doi:10.1016/j.pss.2008.02.010

McGouldrick, T. & Toon, O.B., Icarus, Vol. 196, Issue 1, p. 35-48 (2008b) doi:10.1016/j.icarus.2008.02.020

McGouldrick, T. & Toon, O.B., Icarus, Vol.191, Issue 1, p. 1-24 (2007) doi:10.1016/j.icarus.2007.04.007

McKinnon, W.B., K.J. Zahnle, B.A. Ivanov and H.J. Melosh (1997) in Venus II : Geology, Geophysics, Atmosphere, and Solar Wind Environment. Edited by Stephen W. Bougher, D.M. Hunten, and R.J. Philips. Tucson, AZ: University of Arizona Press, p.969.

McNutt, M. K. (1984). Lithospheric flexure and thermal anomalies. Journal of Geophysical Research, 89, pp 11180-11194.

Meadows, V.S. and D. Crisp, Ground-based NIR observations of Venus. Journal of Geophysical Research, 1996. 101(E2).

Mikhail, S., and Heap, M.J. (2017), Hot climate inhibits volcanism on Venus: Constraints from rock deformation experiments and argon isotope geochemistry, Physics of the Earth and Planetary Interiors, Volume 268, p. 18-34. doi: 10.1016/j.pepi.2017.05.007

Morellina, S., Bellan, J. (2022) Turbulent chemical-species mixing in the Venus lower atmosphere at differ- ent altitudes: a direct numerical simulation study relevant to understanding species spatial distribution. Icarus 371:114686.https://doi.org/10.1016/j.icarus.2021.114686

Moruzzi, S. A., Kiefer, W. S., and Andrews-Hanna, J. C. (2023) Thrust faulting on Venus: Tectonic modeling of the Vedma Dorsa Ridge Belt, Icarus 392, article 115378, 11 pages.

Mueller et al., Venus surface thermal emission at 1μm in VIRTIS imaging observations: Evidence for variation of crust and mantle differentiation conditions, Journal of Geophysical Research, vol. 113 (2008) doi: 10.1029/2008je003118

Mueller, N.T., J. Helbert, S. Erard, G. Piccioni, P. Drossart (2012). Rotation period of Venus estimated from Venus Express VIRTIS images and Magellan altimetry, Icarus, Volume 217, pp.474-483,doi:10.1016/j.icarus.2011.09.026.

Mueller, N. T., S. Smrekar, J. Helbert, E. Stofan, G. Piccioni, and P. Drossart, Journal of Geophysical Research-Planets, 122(5): p.1021-1045 (2017) doi:10.1002/2016JE005211

Mueller, N.T., S.E. Smrekar, and C.C.C. Tsang, Multispectral surface emissivity from VIRTIS on Venus Express, Icarus, 335, 113400 (2020) doi: 10.1016/j.icarus.2019.113400

Muhleman, D.O., Anderson, J.D, 1981, Solar wind electron densities from Viking dual-frequency radio measurements, The Astrophysical Journal 247, 1093–1101. doi:10.1086/159119

Müller-Wodarg, I., Bruinsma, S., Marty, JC., Svedem, H. (2016), In situ observations of waves in Venus's polar lower thermosphere with Venus Express aerobraking. Nature Phys 12, 767–771. https://doi.org/10.1038/nphys3733

Namiki, N., and S.C. Solomon, Volcanic degassing of argon and helium and the history of crustal production on Venus, *J. Geophys. Res.: Planets,* 103 (1998), pp. 3655-3677

Neakrase, L.D.V., Klose, M., Titus, T.N. (2017) Terrestrial subaqueous seafloor dunes: possible analogs for Venus. Aeolian Res 26:47–56. https://doi.org/10.1016/j.aeolia.2017.03.002

Nealley et al., LPSC XLVIII, Abstract #2498 (2017)

Neefs, E., A.C. Vandaele , R. Drummond, I.R. Thomas, S. Berkenbosch, R. Clairquin, S. Delanoye, B. Ristic, J. Maes, S. Bonnewijn, G. Pieck, E. Equeter, C. Depiesse, F. Daerden, E. Van Ransbeeck, D. Nevejans, J. Rodriguez, J.-J. Lopez-Moreno, R. Sanz, R. Morales, G.P. Candini, C. Pastor, B. Aparicio del Moral, J.M. Jeronimo, J. Gomez, I. Perez, F. Navarro, J. Cubas, G. Alonso, A. Gomez, T. Thibert, M.R. Patel, G. Belucci, L. De Vos, S. Lesschaeve, N. Van Vooren, W. Moelans, L. Aballea, S. Glorieux, A. Baeke, D. Kendall, J. De Neef, A. Soenen, P.Y. Puech, J. Ward, J.F. Jamoye, D. Diez, A. Vicario, and M. Jankowski, Applied Optics, 54(28): p. 8494-8520 (2015)

Niemann, H. B., Kasprzak, W. T., Hedin, A. E., Hunten, D. M. & Spencer, N. W. (1980), Mass spectrometric measurements of the neutral gas composition of the thermosphere and exosphere of Venus. J. Geophys. Res. 85, 7817–7827.

Noack, L., Breuer, D. & Spohn, T. 2012, Coupling the atmosphere with interior dynamics: Implications for the resurfacing of Venus, Icarus Vol. 217, Issue 2, pp. 484-498.

O'Neill, C., A.M. Jellinek, A. Lenardic, Earth and Planetary Science Letters,Vol. 261, Issues 1–2, pp. 20-32. doi.org/10.1016/j.epsl.2007.05.038 (2007)

Ono, T. et al., Lunar radar sounder observations of subsurface layers under the nearside maria of the Moon, Science 13 Feb 2009:Vol. 323, Issue 5916, pp. 849 (2009) doi:10.1126/science.323.5916.849d

O'Rourke, J.G., J. Korenaga, Thermal evolution of Venus with argon degassing, Icarus 260, 128–140 (2014)

Oschlisniok, J., Häuser, B., Pätzold, M., Tyler, G.L., Bird, M.K., Tellmann, S., Remus, S., Andert, T., Icarus 221, Issue 2, p. 940-948 (2012)

Oschlisniok, J., Häusler, B., Pätzold, M., Tellmann, S., Bird, M., Sufuric acid vapor and sulfur dioxide in the atmosphere of Venus as observed by VeRa, 14th Europllanet Science Congress 2020, EPSC2020-139, Sept. 2020

Oschlisniok, J., Häusler, B., Pätzold, M., Tellmann, S., Bird, M. K., Peter, K., Andert, T.P. (2021), Sulfuric acid vapor and sulfur dioxide in the atmosphere of Venus as observed by the Venus Express radio science experiment VeRa, Icarus,Vol. 362, 114405, https://doi.org/10.1016/j.icarus.2021.114405

Parmentier, E.M. and Hess, P.C. (1992). Chemical differentiation of a convecting planetary interior: Consequences for a one plate planet such as Venus. Geophysical Research Letters 19: doi: 10.1029/92GL01862. issn: 0094-8276.

Patrick, M.R., Dehn, J., Papp, K.R., Lu, Z., Dean, K., Moxey, L., Izbekov, P., Guritz, R (2003), The 1997 eruption of Okmok Volcano, Alaska: a synthesis of remotely sensed imagery, Journal of Volcanology and Geothermal Research, Volume 127, Issues 1–2, Pages 87-105.

Pätzold, M., Bird, M.~K., Edenhofer, P., Asmar, S.W., McElrath, T.~P., 1995, Dual-frequency radio sounding of the solar corona during the 1995 conjunction of the Ulysses spacecraft, Geophysical Research Letters 22, 3313–3316. doi:10.1029/95GL03184

Pätzold, M., Tsurutani, B.T., Bird, M.K., 1997., An estimate of large-scale solar wind density and velocity profiles in a coronal hole and the coronal streamer belt., Journal of Geophysical Research 102, 24151–24160. doi:10.1029/97JA01868

Pätzold, M., Tellmann, S., Häusler, B., Hinson, D., Schaa, R., Tyler, G.L., 2005, A Sporadic Third Layer in the Ionosphere of Mars, Science 310, 837–839. doi:10.1126/science.1117755

Pätzold, M. and 6 colleagues 2009, A sporadic layer in the Venus lower ionosphere of meteoric origin, Geophysical Research Letters 36. doi:10.1029/2008GL035875

Pätzold, M. and 7 colleagues 2012, Coronal Density Structures and CMEs: Superior Solar Conjunctions of Mars Express, Venus Express, and Rosetta: 2004, 2006, and 2008, Solar Physics 279, 127–152. doi:10.1007/s11207-012-9991-y

Pätzold, M. and 19 colleagues 2016, Mars Express 10 years at Mars: Observations by the Mars Express Radio Science Experiment (MaRS), Planetary and Space Science 127, 44–90. doi:10.1016/j.pss.2016.02.013

Peter, G., et al., Developing of MERTIS as an advanced process from the study up to the flight model, Proceedings Volume 8867, Infrared Remote Sensing and Instrumentation XXI; 886707 (2013) doi:10.1117/12.2024375

Peter, K. and 10 colleagues 2014, The dayside ionospheres of Mars and Venus: Comparing a one-dimensional photochemical model with MaRS (Mars Express) and VeRa (Venus Express) observations, Icarus 233, 66–82. doi:10.1016/j.icarus.2014.01.028

Peter, K. and 7 colleagues 2021, The lower dayside ionosphere of Mars from 14 years of MaRS radio science observations, Icarus 359. doi:10.1016/j.icarus.2020.114213

Pettengill, G.H., Ford, P.G., Simpson, R.A. (1996) Electrical properties of the Venus surface from bistatic radar observations. Science 272:1628–1631

Pettengill, G.H., Ford, P.G., Wilt, R.J. (1992), Venus surface radiothermal emission as observed by Magellan. J Geophys Res 97(E8):13067–13090.

Pettengill, G.H. P. G. Ford, W. T. K. Johnson, R. K. Raney and L. A. Soderblom, Science, New Series, Vol. 252, No. 5003, Apr. 12, 1991, pp. 260-265 (1991)

Phillips, R.J., R.F. Raubertas, R.E. Arvidson, I.C. Sarkar, R.R. Herrick, N. Izenberg, R.E. Grimm, Impact craters and Venus resurfacing history. J. Geophys. Res. 97, 15,923–15,948 (1992)

Picardi, G. et al., Radar soundings of the subsurface of Mars, Science 310.5756 (2005): 1925-1928.

Piccialli, A., Montmessin, F., Belyaev, D., Mahieux, A., Fedorova, A., Marcq, E., Bertaux, J.L., Tellmann, S., Vandaele, A.C., Korablev, O., 2015. Thermal Structure of Venus Nightside Upper Atmosphere Measured by Stellar Occultations with SPICAV/ Venus Express, Planet. Space. Sci. 113(144), 321-335 (2015) doi:10.1016/j.pss.2014.12.009

Plesa, A.-C., Padovan, S., Tosi, N. et al. (2018) The thermal state and interior structure of Mars. Geophys Res Lett 45(22):12198–12209

Pollack, J.B., et al., Near-Infrared Light from Venus' Nightside: A Spectroscopic Analysis. Icarus, 1993. 103(1): p. 1-42.

Port, S.T., et al., LPSC, 2083 (2018)

Port, S.T., et al., LPSC, 2132 (2019)

Port, S.T., Chevrier, V.F., Kohler, E., Investigation into the radar anomaly on Venus: The effect of Venus conditions on bismuth, tellurium, and sulfur mixtures, Icarus 336, 113432 (2020).

Pruppacher, H. R. and Klett, J. D., Atmospheric and Oceanographic Sciences Library, Kluwer Academic Publishers, Dordrecht, The Netherlands (1997)

Quanz, S.P. et al. (2022), Large Interferometer for Exoplanets (LIFE), Ast. Astrophys. Vol. 664, A21 - https://doi.org/10.1051/0004-6361/202140366

Quirino D., Gilli G., Kaltenegger L., Navarro T., Fauchez T. J, Turbet M., Leconte J., Lebonnois S., Gonzalez-Galindo F., MNRAS, Letters, (2023) Vol. 523, Issue 1, https://doi.org/10.1093/mnrasl/slad045

Quémerais, E., Chaufray, JY., Koutroumpa, D. et al., Space Sci. Rev. 216, 67 (2020) doi: 10.1007/s11214-020-00695-6

Realmuto, V.J., Worden, H.M. (2000), The impact of atmospheric water vapor on the thermal infrared remote sensing of volcanic sulfur dioxide emissions: a case study from the Pu'u 'O'o vent of Kilauea Volcano, Hawaii. Journal of Geophysical Research 105, 21497–21508.

Restano, M., Seu, R. and Picardi, G., IEEE Geoscience and Remote Sensing Letters, 13(6), pp.806-810 (2016)

Rivoldini A, Van Hoolst T, Verhoeven O, Mocquet A, Dehant V (2011) Geodesy constraints on the interior structure and composition of Mars. Icarus 213(2):451–472

Robert, S., A.C. Vandaele , E. Neefs, L. Jacobs, S. Berkenbosch, I.R. Thomas, J.T. Erwin, V. Wilquet, W. Moelans, S. Lesschaeve, A. Algoedt, L. De Vos, B. Bézard, E. Marcq, and C. Wilson, Planet. Space Sci., under review, (2021)

Roberts, K.M., Guest, J.E., Head, J.W., Lancaster, M.G. (1992), Mylitta Fluctus, Venus: Rift-related, centralzed volcanism and the emplacement of large-volume flow units, Journ. Geophys. Res. Planets, Vol. 97, issue E10, p. 15991-16015, https://doi.org/10.1029/92JE01245

Rodgers, C.D., 2000, Inverse Methods for Atmospheric Sounding - Theory and Practice; Series: Series on Atmospheric Oceanic and Planetary Physics, ISBN: 9789812813718. World Scientific Publishing Co. Pte. Ltd., Edited by Clive D. Rodgers, vol. 2; doi:10.1142/9789812813718

Rolf, T., Weller, M., Gülcher, A., Byrne, P., O'Rourke, J. G., Herrick, R., Bjonnes, E., Davaille, A., Ghail, R., Gillmann, C., Plesa, A.-C., Smrekar, S.E., Dynamics and Evolution of Venus' Mantle Through Time. Space Sci Rev 218, 70 (2022). https://doi.org/10.1007/s11214-022-00937-9

Rosenblatt, P., Bruinsma, S.L., Müller-Wodarg, I.C.F., Hausler, B., Svedhem, H., Marty, J. C., 2012., First ever in situ observations of Venus' polar upper atmosphere density using the tracking data of the Venus express atmospheric drag experiment (VExADE). Icarus 217 (2), 831–838. https://doi.org/10.1016/j.icarus.2011.06.019.Rosenblatt P., Dumoulin C., Marty J.-C., Genova A. (2021) Determination of Venus' interior structure with EnVision, Remote Sens., 13, 1624. Doi:10.3390/rs13091624

Salvador, A., Massol, H., Davaille, A., Marcq, E., Sarda, P., Chassefière, E. (2017) The relative influence of H_2O and CO_2 on the primitive surface conditions and evolution of rocky planets. J Geophys Res, Planets 122(7):1458–1486. https://doi.org/10.1002/2017JE005286

Salvador, A., Avice, G., Breuer, D., Gillmann, C., Lammer, H., Marcq, E., Raymond, S.N., Sakuraba, H., Scherf, M. Way, M.J. (2023), Magma Ocean, Water, and the Early Atmosphere of Venus. Space Sci Rev 219, 51 (2023). https://doi.org/10.1007/s11214-023-00995-7

Sandor, B.J., Clancy, R.T., Moriarty-Schieven, G., Mills, F.P. (2010) Sulfur chemistry in the Venus mesosphere from SO_2 and SO microwave spectra. Icarus 208:49–60

Sandor, B.J., Clancy, R.T., Moriarty-Schieven, G. (2012) Upper limits for H_2SO_4 in the mesosphere of Venus. Icarus 217(2):839–844

Santos, A.R., Gilmore, M.S., Greenwood, J.P., Nakley, L.M., Phillips, K., Kremic, T., Lopez, X. (2023) Experimental weathering of rocks and minerals at Venus conditions in the Glenn extreme environments rig (GEER). J Geophys Res, Planets 128:e2022JE007423

Seiff, A. et al., Adv. in Space Res., Vol. 5, Issue 11, p. 3-58 (1985) doi:10.1016/0273-1177(85)90197-8

Seu, R. et al., SHARAD sounding radar on the Mars Reconnaissance Orbiter, J. Geophys. Res. Planets 112.E5 (2007) doi:10.1029/2006JE002745

Shalygin, E. V., W. J. Markiewicz, A. T. Basilevsky, D. V. Titov, N. I. Ignatiev, and J. W. Head, Active volcanism on Venus in the Ganiki Chasma rift zone, Geophys. Res. Lett. Vol. 42, Issue 12, pp.4762-4769 (2015) doi:10.1002/2015GL064088

Shao, W. D., Zhang, X., Bierson, C. J., & Encrenaz, T., Revisiting the sulfur-water chemical system in the middle atmosphere of Venus, J. Geophys. Res.: Planets, 125, e2019JE006195 (2020) doi:10.1029/2019JE006195

Shepard, M.K., Arvidson, R.E., Brackett, R.A., and Fegley Jr., B., A ferroelectric model for the low emissivity highlands on Venus, Geophys. Res. Lett. Vol 21, Issue 6, pp. 469-472 (1994) doi:10.1029/94GL00392

Shields, A.L., Ballard, S., and Johnson, J.A., The habitability of planets orbiting M-dwarf stars, Physics Reports, Vol. 663, 5 Dec 2016, pp.1-38 (2016) doi: 10.1016/j.physrep.2016.10.003.

Siddle, A.G., I.C.F. Mueller-Wodarg, S. Bruinsma, J.-C. Marty (2021), Density structures in the martian lower thermosphere as inferred by Trace Gas Orbiter accelerometer measurements, Icarus,Volume 357, 114109, https://doi.org/10.1016/j.icarus.2020.114109.

Sioris, C.E., Malo, A., McLinden, C.A., D'Amours, R. (2016), Direct injection ofwater vapor into the stratosphere byvolcanic eruptions,Geophys. Res. Lett.,43, 7694–7700, doi:10.1002/2016GL069918

Smrekar, S.E., Davaille, A. and Sotin, C., Venus Interior Structure and Dynamics, Space Sci. Rev. 214, 88 (2018a) doi:10.1007/s11214-018-0518-1

Smrekar, S.E., Hensely, S., Wallace, M.S., Lisano, M.E., Darrach, M.R., Sotin, C., Lehman, D., Dyar, M.D., Helbert, J., Venus Origins Explorer (VOX) concept: A proposed New Frontiers Mission (2018b) IEEE Aerospace Conference, pp. 1-19 (2018b) doi: 10.1109/AERO.2018.8396625.

Smrekar, S.E., Stofan, E.R., Mueller, N., Treiman, A., Elkins-Tanton, L., Helbert, J., Piccioni, G., Drossart, P. (201a) Recent hotspot volcanism on Venus from VIRTIS emissivity data. Science 328:605–608. https://doi.org/10.1126/science.1186785

Smrekar, S.E., Evidence for active hotspots on Venus from analysis of Magellan gravity data, Icarus 112, 2-26 (1994)

Smrekar, S.E., and Phillips, R.J., Earth and Planetary Science Letters, Vol. 107, Issues 3–4, 582-597 (1991) doi:10.1016/0012-821X(91)90103-O

Smrekar, S.E, Hensley, S., Nybakken, R., Wallace, M.S., Perkovic-Martin, D., You, T.-H., Nunes, D., Brophy, J., Ely, T., Burst, E., Dyar, M.D., Helbert, J., Miller, B., Hartley, J., Kallemeyn, P., Whitte, J., Iess, L., Mastrogiuseppe, M., Younis, M., Prts, P., Rodriguez, M., Mazarico, R. (2022) VERITAS (Venus emissivity, radio science, InSAR, topography, and spectroscopy): a discovery mission. In: 2022 institute for electrical and elec- tronics engineers/IEEE aerospace conference (AERO), pp 1–20. https://doi.org/10.1109/AERO53065.2022.9843269

Solomon, S.C., Smrekar, S.E., Bindschadler, D.L., Grimm, R.E., Kaula, W.M., McGill, G.E., Phillips, R.J., Saunders, R.S., Schubert, G., Squyres, S.W., Stofan, E.R. (1992), Venus tectonics: An overview of Magellan observations, J. Geophys. Res. Planets 97, 13199-13255.

Spohn, T., Icarus, Vol. 90, Issue 2, p. 222-236 (1991) doi:10.1016/0019-1035(91)90103-Z

Steinberger B, Werner S, Torsvik TH (2010) Deep versus shallow origin of gravity anomalies, topography and volcanism on Earth, Venus and Mars. Icarus 207(2):564–577

Stevenson, D.J., Earth Planet. Sci. Lett. 208, 1-11 (2003)

Stoddard, P.R., & Jurdy, D.M., Topographic comparisons of uplift features on Venus and Earth: Implications for Venus tectonics, Icarus, Vo. 217, pp. 524-533 (2012) doi:10.1016/j.icarus.2011.09.003

Stofan, E.R., Sharpton, V.L., Schubert, G., Baer, G., Bindschadler, D.L., Janes, D.M., Squyres, S.W. (1992). "Global Distribution and Characteristics of Coronae and Related Features on Venus: Implications for Origin and Relation to Mantle Processes." Journal of Geophysical Research, 97, 13347-13378, doi:10.1029/92je01314.

Stofan, E.R., Smrekar, S.E., Mueller, N., Helbert, J., Icarus, Vol. 271, p. 375-386 (2016) doi:10.1016/j.icarus.2016.01.034

Stolzenbach A., Lefèvre F., Lebonnois S., Määttänen A. , Icarus, Vol. 395, p, 115447 (2023) https://doi.org/10.1016/j.icarus.2023.115447

Strom, R.G., Schaber, G.G., & Dawson, D.D., J. Geophys. Res., Vol. 99, Issue E5 (1994) doi.org/10.1029/94JE00388.

Tellmann S., Pätzold M., Häusler B., Bird M. K., Tyler G.L., J. Geophys. Res. Planets, Vol. 114, Issue E9 (2009) doi:10.1029/2008JE003204

Thakur, S., L. Bruzzone, IEEE Transactions on Geoscience and Remote Sensing, Vol. 57, No.8, pp. 5266-5284 (2019)

Thakur, S., Sbalchiero, E., Paolaz, E., Bovolo, F., and Bruzzone, L.: Venus subsurface targets: assessment of detectability using radar sounder simulations, Europlanet Science Congress 2020, 21 September–9 Oct 2020, EPSC2020-374, https://doi.org/10.5194/epsc2020-374

Thakur, S., E. Sbalchiero, L. Bruzzone, Planetary and Space Science, Vol. 225 (2023) doi: 10.1016/j.pss.2022.105620

Titov, D.V. et al., Icarus, Vol. 217, Issue 2, p. 682-701 (2012) doi:10.1016/j.icarus.2011.06.020

Titov, D.V., Ignatiev, N. I./, McGouldrick, K., Wilquet, V., Wilson, C.F., Clouds and Hazes of Venus, Space Sci Rev. 214:126 (2018) https://doi.org/10.1007/s11214-018-0552-z

Tolson, R.H., Prince, J., Konopliv, A., 2013. An atmospheric variability model for Venus aerobraking missions. AAIA. https://doi.org/10.2514/6.2013-4830.

Travis, L.D., On the Origin of Ultraviolet Contrasts on Venus, Journ. Atmos. Sci. Vol. 32, p. 1190 (1975).

Treiman, A., Harrington, E., & Sharpton, V., Icarus, Vol. 280, pp.172-182 (2016)

Treiman, A.H., et Schwenzer, S.P., Venus Geochemistry, Progress, Prospects, and New Missions, Abstract #2011 (2009)

Treiman, A.H., Exploring Venus as a Terrestrial Planet, Vol. 176, AGU Monograph Series, L.W. Esposito, E.R. Stofan, T.E. Cravens Eds, pp. 7-22 (2007) doi.org/10.1029/176GM03

Tsang C. C. C., Irwin P. G. J., Wilson C. F., et al. Tropospheric carbon monoxide concentrations and variability on Venus from Venus Express/VIRTIS-M observations JGRE 113, E00B08 (2008) https://doi.org/10.1029/2008JE003089

Tsang, C.C.C., Wilson, C.F., Barstow, J.K., Irwin, P.G.J.,Taylor, F.W., McGouldrick, K., Piccioni, G., Drossart, P., Svedhem, H., Geophys. Res. Lett. 37, 2202 (2010) doi:10:1029/2009GL041770.

Turbet, M., Bolmont, E., Chaverot, G., Ehrenreich, D., Leconte,. J., Marcq., E. (2021) Day-night cloud asymmetry prevents early oceans on Venus but not on Earth. Nature 598:276–280. https://doi.org/10.1038/s41586- 021-03873-w

Turcotte, D.L., J. Geophys. Res. Planets Vol 100, issue E8, pp. 16931-16940 (1995) doi:10.1029/95JE01621

Turcotte, D.L., J. Geophys. Res. Planets Vol.98, Issue E9, p.17061-17068 (1993) doi.org/10.1029/93JE01775

Turcotte, D.L., J. Geophys. Res., Vol. 94, p. 2779-2785 (1989) doi:10.1029/JB094iB03p02779

Vandaele, A. C., M. De Mazière, R. Drummond, A. Mahieux, E. Neefs, V. Wilquet, O. Korablev, A. Fedorova, D. Belyaev, F. Montmessin and J. L. Bertaux (2008). "Composition of the Venus mesosphere measured by SOIR on board Venus Express." J. Geophys. Res. 113: doi:10.1029/2008JE003140.

Vandaele, A.C., J.-J. Lopez-Moreno, M .R. Patel, G. Bellucci, F. Daerden, B. Ristic, S. Robert, I.R. Thomas, V. Wilquet, M. Allen, G. Alonso-Rodrigo, F. Altieri, S. Aoki, D. Bolsée, T. Clancy, E. Cloutis, C. Depiesse, R. Drummond, A. Fedorova, V. Formisano, B. Funke, F. González-Galindo, A. Geminale, J.-C. Gérard, M. Giuranna, L. Hetey, N. Ignatiev, J. Kaminski, O. Karatekin, Y. Kasaba, M. Leese, F. Lefèvre, S.R. Lewis, M. López-Puertas, M. López-Valverde, A. Mahieux, J. Mason, J. McConnell, M. Mumma, L. Neary, E. Neefs, E. Renotte, J. Rodriguez-Gomez, G. Sindoni, M. Smith, A. Stiepen, A. Trokhimovsky, J.V. Auwera, G. Villanueva, S. Viscardy, J. Whiteway, Y. Willame, and M. Wolff, Space Sci. Rev., 214:article number:80 (2018) doi.org/10.1007/s11214-018-0517-2

Vandaele, A.C., Korablev, O., Belyaev, D., Chamberlain, S., Evdokimova, D., Encrenaz, T., Esposito, L., Jessup, KL., Lefèvre, F., Limaye, S., Mahieux, A., Marcq, E., Mills, F.P., Montmessin, F., Parkinson, C.D., Robert, S., Roman, T., Sandor, B., Stolzenbach, A., Wilson, C., & Wilquet, V., Icarus, 295, 1-15 (2017a) doi.org/10.1016/j.icarus.2017.05.001

Vandaele, A.C., Korablev, O., Belyaev, D., Chamberlain, S., Evdokimova, D., Encrenaz, T., Esposito, L., Jessup, KL., Lefèvre, F., Limaye, S., Mahieux, A., Marcq, E., Mills, F.P., Montmessin, F., Parkinson, C.D., Robert, S., Roman, T., Sandor, B., Stolzenbach, A., Wilson, C., & Wilquet, V., Icarus, 295, 16-33 (2017b) doi.org/10.1016/j.icarus.2017.05.003

Vandaele, A.C., Mahieux, A., Chamberlain, S., Ristic, B., Robert, S., Thomas, I.R., Trompet, L., Wilquet, V., & Bertaux, J.L., Icarus, 272, 48-59 (2016) doi.org/10.1016/j.icarus.2016.02.025

Vandaele, A.C., Mahieux, A., Robert, S., Drummond, R.,Wilquet, V., & Bertaux, J.L., Planet. Space Sci., 113-114, 237-255 (2015) doi.org/10.1016/j.pss.2014.12.012

Varnes, D.J. (1978), Slope movement types and processes, In: Schuster R.L., Krizek R.J. (Eds) Landslides, analysis and control, special report 176: Transportation research board, National Academy of Sciences, Washington, DC, pp. 11-33.

Venera-D Joint Science Definition Team, Venera-D: 174 p. (2019) URL: https://www.lpi.usra.edu/vexag reports/VeneraD_2019Wkshp_techRp_cover_21July20_v12Final.pdf

Volland, H., Bird, M.K., Levy, G.~S., Stelzried, C.T., Seidel, B., 1977, Helios-1 Faraday rotation experiment: results and interpretations of the solar occultations in 1975, Journal of Geophysics Zeitschrift Geophysik 42, 659–672.

Waltham et al., J. Geophys. Res., 113, EO2012 (2008)

Watters, T.R. et al., Nature, 444, 905 (2006)

Way, M.J., A.D. Del Genio, N.Y. Kiang, L.E. Sohl, D.H. Grinspoon, I. Aleinov, M. Kelley, and T. Clune, 2016: Was Venus the first habitable world of our solar system? *Geophys. Res. Lett.*, **43**, no. 16, 8376-8383, doi:10.1002/2016GL069790

Way, M.J. & A.D. Del Genio, 2020: Venusian habitable climate scenarios: Modeling Venus through time and applications to slowly rotating Venus-like exoplanets. *J.*

Geophys. Res. Planets, **125**, no. 5, e2019JE006276, doi:10.1029/2019JE006276.

Weitz, C.M. et al. (1994), Dunes and microdunes on Venus: Why were so few found in the Magellan Data? Icarus 112, 282–285

Weller, M. B., and Lenardic, A. (1017), On the evolution of terrestrial planets: Bi-stability, stochastic effects, and the non-uniqueness of tectonic states, Geoscience Frontiers 9 (2018), 91-102.

Weller, M.B. and Kiefer, W.S. (2020), The Physics of Changing Tectonic Regimes: Implications for the Temporal Evolution of Mantle Convection and the Thermal History of Venus, Journal of Geophysical Research: Planets, 10.1029/2019JE005960, 125, 1.

Wendlandt, R. F., Baldridge, W. S. and Neumann, E.-R. 1991, Modification of lower crust by continental rift magmatism, Geophys. Res. Let. 18, 9, 1759-1762. doi.org/10.1029/91GL01881

Widemann, T., Lellouch, E., Donati, J.F. (2008) Venus Doppler winds at cloud tops observed with ESPaDOnS at CFHT. Planet Space Sci 56:1320–1334

Widemann, T., Smrekar, S., Garvin, J., Straume-Lindner, A.G., Schulte, M., Ocampo, A., Voirin, T., Hensley, S., Dyar, M. D., Whitten, J., Nunes, D., Getty, S., Arney, G., Johnson, N., Kohler, E., Spohn, T., O'Rourke, J., Wilson, C., Way, M., Ostberg, C., Westall, F., Höning, D., Jacobson, S., Salvador, A., Avice, G., Breuer, D., Carter, L., Gilmore, M., Ghail, R., Helbert, J., Byrne, P., Santos, A., Herrick, R., Izenberg, N., Marcq, E., Rolf, T., Weller, M., Gillmann, C., Korablev, O., Zelenyi, L., Zasova, L., Gorinov, D., Seth, G., Narasimha Rao, Ch. V., Desai, N. (2023),Venus Evolution Through Time: Key Science Questions, Selected Mission Concepts and Future Investigations, Space Sci Rev 219, https://doi.org/10.1007/s11214-023-00992-w

Whitten, J.L., Campbell, B.A. (2016) Recent volcanic resurfacing of Venusian craters. Geology 44:519–522. https://doi.org/10.1130/G37681.1

Williams, J.G., Konopliv, A.S., Boggs, D.H., Park, R.S., Yuan, D.N., Lemoine, F.G., Goossens, S., Mazarico, E., Nimmo, F., Weber, R.C. and Asmar, S.W., J. Geophys. Res. Planets 119(7), pp.1546-1578 (2014)

Wilson, C.F., et al., Analysis of thermal emission from the nightside of Venus at 1.51 and 1.55 μm, Icarus, vol. 201, no. 2, pp. 814-817 (2009) doi: 10.1016/j.icarus.2009.03.010.

Wilson, C.F., & Lefèvre, F., EnVision Science Conference, Feb. 2020, CNES, Paris (2020).

Wilson, C.F;, Marcq, E., Gillmann, C., Widemann, T., Korablev, O., Mueller, N., Lefevre, M., Rimmer, P., Robert, S., Zolotov, M. (2023) Possible effects of volcanic eruptions on the modern atmosphere of Venus. Space Sci Rev, in revision.

Yoder, C.F., Konopliv, A.S., Yuan, D.N., et al. (2003), Fluid core size of Mars from detection of the solar tide, Science 300(5617):299–303

Young, E.F. et al., 13th Europlanet Science Congress Sept. 2019, EPSC (2019)